PHOTOELECTRIC PROCESSES IN CALCIUM OXIDE COATED CATHODES

a Thesis on

Some photoelectric properties of calcium oxide, and their relations with electrical and thermionic properties and with band structure

presented for the Degree of Ph.D.
at the University of Birmingham

by

C.H.B. MEE, B.A., M.Sc., Grad. Inst. P.

Department of Physics,
University College of
North Staffordshire.
September, 1960.

SYNOPSIS

Photoconductivity and photoelectric emission in calcium oxide coated probe diodes have been investigated in the near infra-red, visible and near ultra-violet regions of the spectrum (i.e. for incident photon energies of from 1.4 to 3.2 eV). The experimental evidence suggests that the apparent photoconductivity current in the porous cathode material is, in fact, a photoemissive effect through the pores rather than a true volume or surface photoconductive effect. The process is somewhat similar to that observed in the high-temperature region of dark conductivity determinations with cathodes coated with the alkaline earth oxides. This hypothesis has been confirmed by experiments involving the comparison of the recovery of photoemission and photoconductivity after oxygen poisoning, and the comparison of the magnetoresistive effect for dark conductivity in the high-temperature region with that for photoconductivity at room temperature.

The spectral sensitivity of photoelectric emission and photoconductivity in calcium oxide cathodes shows a general increase with increasing photon energy. A rapid rise to about 2.2 eV is followed by a more gradual rise to about 3.0 eV, with an indication of a slightly steeper

rise beyond 3.0 eV. In many cases some structure is detected in the curve at about 2.6 eV. There is no correlation between the structure observed and thermal activation energies obtained from studies of thermionic emission and dark conductivity, but an arbitrary photoelectric threshold (which has no relation to the optical activation energy of the semiconducting cathode coating) can be defined by considering a minimum measurable photocurrent, and this shows a rough correlation with the Richardson thermionic work function of the cathode.

Preliminary results on optical absorption, photoelectric emission and photoconductivity in thin films of calcium oxide evaporated on to glass in vacuo are also reported. The spectral sensitivity of optical absorption shows structure which may be correlated tentatively with that observed in photoelectric measurements of calcium oxide as a cathode material. There is some evidence to suggest that intense illumination of the film causes a modification of its electrical properties, possibly due to changes in the surface equilibrium. Photoelectric emission from materials evaporated on to the anode of the experimental diodes has also been studied.

Measurements of thermionic emission and dark conductivity in calcium oxide cathodes suggest the presence of an

impurity level about 1.4 eV below the bottom of the conduction band and give a value of 0.8 eV for the external work function. These values are in reasonable agreement with a recent determination in which the values of 1.6 and 0.8 eV were quoted. Preliminary measurements of the thermoelectric power of calcium oxide are reported.

CONTENTS

Chapter 4 (cont.)

Introduction

The activities of a research group working in this laboratory under the general direction of Professor F.A. Vick have been directed towards an understanding of the basic physics of the oxide-coated cathode. Among the problems of general interest is the reason why a mixture of the oxides of barium, strontium and calcium should have a much greater electron emission than any of the oxides singly - a fact which was discovered early in the commercial development of radio valves. An extension of this problem is the investigation of the role played by calcium oxide, which itself has a very small electron emission. The investigations by the group have taken the form of determinations of the thermionic emission and electrical conductivity of the single and mixed oxides, and the formulation of energy level schemes for each oxide in accordance with a semiconductor model (83, 87, 88).

Studies of the variation of photoconductivity and photoelectric emission with photon energy afford a means for the determination of the optical activation energies for a semiconductor. The present work was undertaken in an attempt to discover the optical energy level scheme for calcium oxide, whose thermal energy scheme has only recently been

determined in this laboratory (88), and to compare the optical and thermal activation energies. Techniques for these determinations have previously been developed by the present author, using barium oxide as the substance under investigation (116), and these methods are improved upon in the course of the work. The literature on the photo-effects in BaO and (BaSr)O cathodes shows certain difficulties in interpretation if conventional solid-state methods are applied, and these difficulties are also apparent in the present work on CaO. In an attempt to clarify the situation, a study of the physical processes involved in the passage of photoelectrons through the oxide cathode matrix has been undertaken, and as a result of this work a hypothesis of the photoelectric processes is put forward which finds an analogy in the theory of electrical conductivity through the matrix in the dark. Photoelectric emission from the anodes of the experimental tubes has also been investigated: in most cases the thin evaporated film of CaO is much more photosensitive than the cathode. To extend the work on evaporated films, photoconductivity and optical absorption are also studied.

Studies of the oxide cathode which give basic information about its processes of operation are of particular interest at the present time. The direct conversion of heat into

electricity utilising thermionic emission, long recognised as being possible in theory (160), has recently been demonstrated in practice by a number of workers (76, 126, 190). One type of transducer utilises the oxide cathode as a source of electrons, and takes advantage of material evaporated from the cathode during operation to keep the anode work function low, a necessary condition of efficiency. The present work, and in particular those sections which deal with the properties of thin evaporated films, has an obvious application to this new technological development.

The first part of this thesis gives a general survey of the preparation and properties of the oxide-coated cathode and of theories of its operation. The second part deals with the action of light on semiconductors, and reviews the literature on photoeffects in the alkaline earth oxides. The third part describes the experimental work attempted and discusses the results obtained in the present investigation.

PART I

Chapter 1 The oxide-coated cathode: preparation and general properties

1.1. Historical introduction

In 1903 Wehnelt, who was investigating the potential distribution in a gas discharge, observed that cathode rays were emitted strongly from certain areas of the platinum wire he was using as a cathode at much lower temperatures than were to be expected from a knowledge of the thermionic properties of pure platinum. He traced these areas of high emission to impurities on the wire, and it seemed that the impurities might originate in metallic oxides from the grease used on the stopcocks of his system. An investigation of the thermionic properties of a large number of oxides followed. Although the values obtained by Wehnelt (188) and his collaborator Jentzsch (99) would no longer be accepted quantitatively, on account of the very poor vacuum conditions attainable at that time, their conclusion that the alkaline earth oxides provide a copious source of thermionic electrons is not in dispute. Thus a chance discovery led to a development of extreme technical and commercial importance: for the last forty years the oxide-coated cathode has been used in vacuum tubes of all types,

and it is perhaps true to say that few recent scientific discoveries have had such a direct impact on the general public.

In spite of the introduction of solid-state devices such as transistors, it is expected that tubes employing oxide-coated cathodes will continue to be used for many years in applications where long life and stability during operation are of importance. Cathodes showing these properties to a remarkable degree have been developed by the G.P.O. Research Station and are used in submarine repeater stations in preference to transistors. Another technical application of great importance is the possibility of the direct conversion of heat to electricity using thermionic emission from an oxide-coated cathode.

To keep pace with the commercial interest in vacuum tubes using the oxide cathode many investigations of the physics of the operation of the cathode have been made, but the mechanism is still not completely understood. Unfortunately many of the earlier investigations were carried out under inadequate vacuum conditions and without a knowledge of the many variables to be controlled, and the results were often misleading. Until the introduction of the band theory of solids no unified interpretation of results could be made.

1.2. Preparation of the oxide cathode

Basically the oxide-coated cathode consists of a metal substrate which supports a thin (~50 μ) layer of one of the alkaline earth oxides, or of a mixture of the oxides. The operating temperature of commercial cathodes is about 1100 °K: the substrate can be heated directly by passing a current through it, or indirectly by an electrical heater insulated from it. Directly heated tungsten or platinum cathodes have largely been superseded by indirectly heated nickel bases. Pure nickel is soft, and an early commercial development was to use harder nickel alloys. It was found that the addition of certain reducing impurities to the nickel assisted in the activation of the cathode as well as in hardening the nickel. The pre-treatment of the metal cathode base, e.g. cleaning by hydrogen furnacing, has also been found to have important effects on cathode behaviour.

At the same temperature the oxides of barium, strontium and calcium show electron emission currents approximately in the ratio 100 : 10 : 1. It is also found that greater electron emission at the same temperature is obtained when a mixed oxide is used instead of the single oxide. The mixed oxide of barium and strontium will be designated by the formula (BaSr)O: this represents not a mechanical

mixture of the oxides, but a mixed crystal in which both Ba^{++} and Sr^{++} ions are present in the same crystal lattice. A trace of calcium oxide increases the emission further and one commercial cathode mixture has a composition BaO : SrO : CaO of 49 : 44 : 7. Why calcium oxide, with its low electron emission, should have this enhancing effect is still not known, although it has been suggested that its inclusion affects the crystal size of the mixed oxide, a fact which was demonstrated by the X-ray diffraction studies of Kawamura (101) and Yamaka (198).

The alkaline earth oxides are unstable in air, forming the hydroxides and carbonates by the action of atmospheric water vapour and carbon dioxide. An oxide cathode must thus be prepared in vacuo from more stable alkaline earth compounds. Although a number of compounds are suitable, the reaction used almost exclusively is the pyrolysis of the carbonate:

$$BaCO_3 = BaO + CO_2$$

The carbon dioxide produced must be pumped away, but is unlikely to react detrimentally with the materials used in the construction of the valve. If a mixed oxide cathode is required, mixed carbonate crystals of the desired proportions are applied to the cathode base: on breakdown by heat, a mixed oxide of the same relative concentrations

is obtained.

The carbonate is usually applied to the cathode in suspension in a suitable organic liquid, such as a mixture of amyl acetate and methyl alcohol. Nitrocellulose is frequently added to the suspension as a binder to promote adhesion between the coating and the base. Several methods of application of the carbonate suspension to the base can be employed: the selection of any particular method depends upon the type of cathode. Directly heated metal ribbons or wires can be coated by dipping or dragging through the suspension; indirectly heated cathodes are most frequently sprayed with the suspension. It is important to note that these methods, and in particular the spraying method, where the distance of the spray gun from the cathode and the proportion of air in the spray must be carefully controlled, lead to cathodes of considerable porosity whose density may be as little as 20 % of that of the bulk carbonate. This porosity is often increased during the breakdown of the carbonate by the evolution of gas in the coating, and has a most important effect on the electrical properties of the cathode. Smooth, less porous cathodes can be prepared by the process of cataphoresis.

The carbonate-coated cathode base and the other electrodes required by the design of the tube are enclosed

in a glass envelope and attached to a pumping system. The carbonate is broken down by raising the temperature of the cathode to about 1100 °K, the carbon dioxide and carbon monoxide formed by the reaction of carbon dioxide with the carbon of the binder being pumped away as rapidly as possible. The possibility of the adsorption of gas on to glass or metal surfaces in the tube and its subsequent desorption when the tube is sealed off demands rigorous outgassing treatment, including baking of the glass and r.f. heating of metal parts. The tube may be sealed off after breakdown and outgassing. Active barium is evaporated on to the glass envelope from getters to take up residual gas.

1.3. Activation processes

A cathode prepared in this way, and subjected to no further treatment than thermal breakdown at 1100 °K, has an extremely low thermionic emission. The level of emission can be increased by the application of a treatment known as activation, of which the essential effect is the formation of a stoichiometric excess of barium in the crystal lattice.

Activation methods in common use include:

1. Thermal activation

At a sufficiently high temperature (~1300 °K) the reducing impurities in the nickel cathode base react with

the alkaline earth oxide to form the metal. Thermal activation may, however, take place to a certain extent even with inert cathode bases such as platinum, and a study of the mechanism of the thermal activation process has been initiated in this laboratory. Possible reducing actions have been studied by Huber (92), Herrmann (82) and Heinze and Wagener (77).

2. Activation by drawing current

If a potential is applied to the anode of a tube containing an unactivated oxide cathode, it is found that the emission current, initially very small, increases over a period of time, often by a factor as great as 10^3 or 10^4. It is supposed that barium is produced by electrolysis of the cathode matrix by the ionic component of the emission current.

3. Activation by reduction with external agents

A method more often employed in research than in commercial manufacture is to heat the cathode in an atmosphere of a reducing gas, e.g. methane at a pressure of 10^{-5} mm Hg (75, 195).

4. Activation by barium evaporation

The excess of barium required to activate the cathode may be evaporated on to the unactivated cathode from another electrode (101, 134, 196). The efficacy of this

method depends on the temperature of the cathode during evaporation. At low cathode temperatures the barium may subsequently re-evaporate from the cathode without any activating effect being accomplished, but at high cathode temperatures the barium diffuses into the pores of the matrix (101).

As with so many other aspects of the oxide-coated cathode, there is much more difficulty in explaining the activation process than in carrying it out. Rittner (152) gives a comprehensive review of possible activation reactions, but Metson (120) suggests that neither the theories of chemical reduction nor of electrolysis are sufficient to explain the very considerable increase in emission produced by activation.

1.4. Composition of the activated coating

Indirect evidence for the presence of excess barium in the cathode coating is presented by experiments which show that, during operation, barium is evaporated from the cathode. Becker (20) observed the emission from a tungsten ribbon placed adjacent to a (BaSr)O cathode during the operation of the cathode at a high temperature, and found temporal changes in the thermionic emission from the tungsten very similar to those observed in the activation

of a W-Ba cathode. Gehrts (67) found the lines of the barium spectrum in a spectroscopic examination of a green glow appearing between the cathode and anode of an experimental tube.

More direct evidence has been given by chemical analysis of the cathode coating. A considerable spread of compositions has been reported, but the best of the more recent determinations, by Moore, Wooten and Morrison (124), gave a value of about 1 atom of excess Ba in 10^6 molecules of (BaSr)O. The presence of a stoichiometric excess of barium is undoubtedly essential for the active state of the cathode, but it is surprising that there does not appear to be a direct relation between the quantity of excess barium and the thermionic emission from the cathode.

The position of this excess barium was a subject of much controversy in early studies of the oxide cathode (Sec. 2.1). The modern theory of the nature of the solid state suggests that at least a proportion of the excess is built into the oxide crystal lattice. A study of the lattice constants of the BaO lattice suggests that the introduction of excess barium in interstitial positions would cause a greatly strained lattice, and it seems very probable that the stoichiometric excess of barium is, in fact, caused by oxygen vacancies, which would have all the

FIG. 1.1. FUNCTIONAL STRUCTURE OF A DIODE

ANODE
SURFACE LAYER

RESIDUAL GAS

SURFACE LAYER
POROUS OXIDE COATING
INTERFACE LAYER
CATHODE BASE

electrical properties ascribed to interstitial barium without straining the lattice.

The evolution of oxygen during activation has been confirmed by chemical means (96), by spectroscopic examination of an electrical discharge in the gas pumped away during the activation process (45) and by mass spectrometer experiments (18, 19, 27, 72, 159, 167, 184). Becker's early work (22) also suggested the presence of oxygen, as the emission from the subsidiary tungsten cathode was poisoned during the activation process of the main cathode.

1.5. Functional structure of a diode

It is important to realise that the properties of the cathode coating itself are seldom separable from the influence of the state of other regions of the tube in which the cathode is mounted. An idealised diode is shown in Fig. 1.1: the seven regions shown there are interdependent, and the emission current obtained at any temperature and at any applied anode voltage is a function of all these regions, rather than of the cathode coating alone.

A region of much importance during the activation process is the interface between the cathode base and the porous cathode matrix. It is found that the emission from an activated cathode depends to a certain extent on the base

metal employed. It has been suggested that this may be due to the formation of interface compounds in competition with the primary process of activation by the reduction of barium oxide to barium. These compounds not only reduce the efficiency of activation, but may also have an electrical resistance higher than that of the matrix itself, and thus have a marked effect on the electrical properties of the combination of cathode base and matrix. The formation of barium orthosilicate, Ba_2SiO_4, as an interface during the activation of a cathode on a base metal containing 5 % Si has been demonstrated by the X-ray diffraction studies of Rooksby (153) and Eisenstein (55), and the electrical properties of the interface have been studied by Fineman and Eisenstein (63), Eisenstein (54) and Mutter (131). The combination of the cathode base, interface layer and cathode matrix may act as a rectifier. According to the Mott blocking-layer theory (126), the flow of electrons from the base to the coating will be impeded, an effect often observed in practice.

Interface layers of this nature should not be formed with cathodes based on chemically inert metals, although Schottky (163) has shown on the basis of semiconductor theory that a rectifying effect would be expected between a metal and a semiconductor if the semiconductor contains

less than 10^{17} defects or impurity atoms per cm^3.

Metson (122) suggests that during the process of activation of an oxide cathode supported on an inert base an interface consisting of a thin film emitter of the alkaline earth oxide is formed. A consideration of this hypothesis is best left to the general discussion of theories of emission in Chapter 2.

1.6. Life of a cathode

A consideration of the factors affecting the life of a cathode illustrates the importance of the concept of the treatment of the diode as a whole. Metson (121) has analysed some of the causes of cathode failure and suggests that they include the effect of the pressure integral of the residual gas, the growth of the interface layer and the evaporation of barium from the coating. It would appear that the integral of the pressure of the residual gas over all stages of the processing of the tube is a life-limiting factor rather than the absolute value of the final, stable pressure in the gettered tube, which may be as low as 10^{-9} mm Hg. Although the alkaline earth oxides evaporate only slowly from a cathode at normal operating temperatures (for BaO the rate of evaporation is about 2.5×10^{-13} g cm^{-2} sec^{-1} at 1000 ^{o}K, and for SrO and CaO the rate is

much less) the free metal is lost at a much greater rate. The products of evaporation of BaO from a number of metallic bases have been studied by Aldrich (12) and by Wooten, Ruehle and Moore (192), who found that for commercial cathodes the evaporant contained less than 2 % of the alkaline earth oxides, the balance being the free metals. These figures were found to be markedly dependent on the metal on to which the cathode material was evaporated, but neither the magnitude of the emission current nor the thermionic activity for individual cathodes could be correlated to evaporation rates. The third life-determining factor is the formation of interface compounds. As barium orthosilicate is itself a semiconductor when activated by excess barium (152), the loss of barium by evaporation causes an increase in the resistance both of the interface layer and of the cathode matrix.

Chapter 2 The thermionic and electrical properties of the oxide-coated cathode

2.1. Early theories of emission

Prior to the introduction of the Fowler-Wilson theory of semiconductors (66, 189) and the recognition of the oxide cathode as an excess impurity semiconductor, it was natural that an explanation of thermionic emission from the oxide cathode should be sought in an analogy to the mechanism of emission from metals and from the thoriated tungsten cathode. Both Becker (20) and Lowry (113) supposed that the electron emission was due to a lowering of the surface work function of the base metal by a monolayer of free alkaline earth metal. Becker thought this layer was at or near the cathode surface, while Lowry held the view that the monolayer was at the core-cathode interface. The former theory required the coating to be a good electrical conductor, but on Lowry's theory the electrons emitted at the base metal diffused through the poorly-conducting coating. Over a period of some years, a considerable quantity of evidence was built up in favour of each theory. Becker and Sears (21) removed the coating from a cathode in vacuo and observed that the emission fell by four orders of magnitude; but the dependence of emission, to a certain extent, on the choice of core metal

favoured Lowry's theory. Electron diffraction experiments by Darbyshire (40) and by Huber and Wagener (93) found no evidence for the presence of a surface layer of barium: in fact, near the surface, a mixed oxide cathode was found to consist of nearly pure SrO.

Order-of-magnitude calculations, using the values for the concentration of excess Ba in the cathode coating obtained by chemical analysis, suggest that if the barium exists as a surface layer, as in Becker's theory, it would have a thickness of the order of 100 atomic layers and would not be a monolayer as the theory requires. A layer as thick as this might be expected to have the properties of bulk barium and the vapour pressure of barium at the operating temperature of the cathode (about 10^{-2} mm Hg) is too high for the layer to be stable. If, instead of assuming that the excess barium is located at the surface of the cathode, it is supposed to cover the surfaces of the crystallites which form the porous cathode, then the layer would be only a few atomic layers in thickness. But both these estimates appear to allow the presence of unrealistically large concentrations of barium on the emitting surfaces of the cathode; the more modern theory supposes that at least a proportion of the stoichiometric excess of metal is accounted for in the crystal lattice of

the crystallites by vacancies at oxygen sites. The crystallites thus contain an excess of the electropositive constituent and behave as typical N-type impurity semiconductor crystals.

2.2. Semiconductors; properties of an N-type impurity semiconductor

A model of a solid may be constructed by taking a collection of infinitely spaced atoms of the solid in question and placing them at a number of regularly-spaced lattice sites. Each atom, on the quantum theory, has a series of allowed energy levels. The effect of the interaction of the levels of all the atoms is to form bands of closely spaced groups of levels, as, by the Pauli exclusion principle, more than two electrons cannot occupy the same state. The bands of closely spaced but still discrete levels are separated by forbidden regions. In addition, there will be levels due to excited states of higher energy: these levels form the conduction band, and if the energy gap between the top of the uppermost filled band and the conduction band is not too large, electrons may be thermally excited across the gap into the conduction band. The larger the energy gap, the fewer the electrons excited across the forbidden band for any given temperature,

and the smaller will be the electrical conductivity of the solid at that temperature. For a forbidden band width of about 10 eV, the solid is effectively an insulator at normal temperatures; but if the forbidden band width is only about 1 eV, sufficient excitation to cause measurable conductivity may take place at temperatures of a few hundred degrees above room temperature, and the crystal is said to be an intrinsic semiconductor. A most important class of semiconductors, and the type which will be of most interest in the present application, is one in which the addition of impurity atoms to the crystal causes the presence of impurity levels in the forbidden band. The impurity levels may provide a very large contribution to the conductivity of the crystal, as the energy required for excitation to the conduction band is much less than that required to excite electrons from the filled band.

Two types of impurity semiconductor are possible. One containing an excess of the electropositive constituent (N-type) has impurity levels known as donor levels in the forbidden zone just below the conduction band, and electrons can be excited into the conduction band from these levels to cause electrical conductivity. A P-type semiconductor, on the other hand, contains an excess of the electronegative constituent (or a deficiency of the electropositive

FIG. 2.1. ENERGY LEVEL DIAGRAM FOR AN EXCESS IMPURITY SEMICONDUCTOR

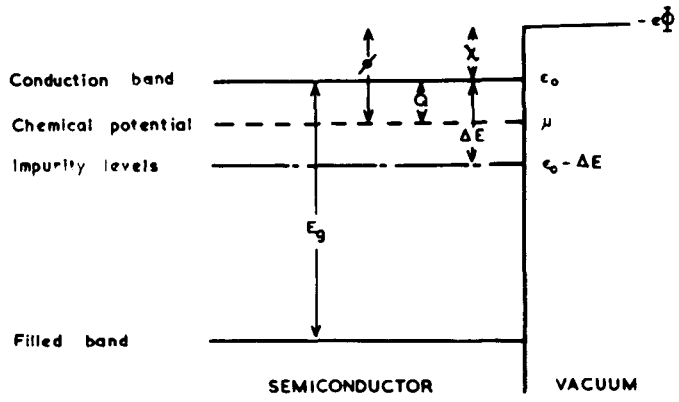

FIG. 2.2. ENERGY LEVEL DIAGRAM FOR AN INTERFACELESS OXIDE CATHODE COATING

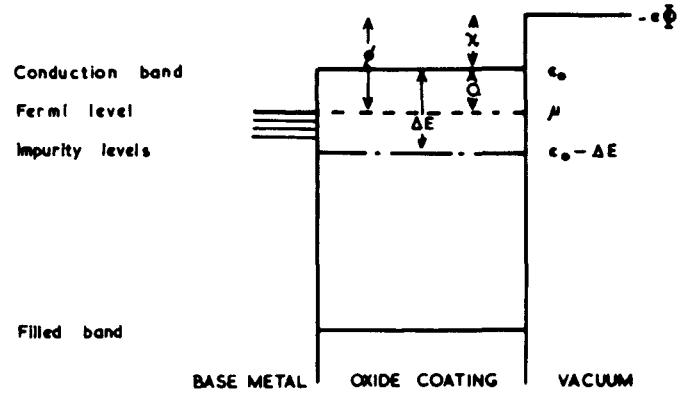

constituent) and the impurity levels, located just above the filled band, are called acceptor levels. Thermal excitation of electrons from the filled band to these levels leaves positive holes in the filled band; the motion of these holes under an applied field again gives rise to electrical conductivity.

The oxide cathode has been shown to contain a stoichiometric excess of barium, the electropositive constituent of the barium oxide lattice (Sec. 1.4). It might thus be expected to show the characteristics of an N-type semiconductor. Measurements of the sign of the Hall coefficient by Wright (196) and Forman (64) have shown that it is normally an N-type semiconductor, although in some cases impurities in the coating have given a Hall coefficient with a sign corresponding to P-type semiconduction.

Fig. 2.1 shows an energy level scheme for an excess impurity semiconductor. The electrostatic energy within the crystal is taken as the zero of the potential scale: the energy of an electron just outside the crystal is $-e\Phi$. The energy at the bottom of the conduction band is E_0, and the energy of the single impurity level shown is $(E_0 - \Delta E)$. The chemical potential level μ (called the Fermi level by analogy with the theory of electrons in metals) represents the partial molar free energy of the electrons. It will

lie between the impurity level and the bottom of the conduction band, its actual position depending on the relative concentrations of available electrons and impurity levels.

If an electron is to be removed from the crystal into vacuum, it must be given first of all sufficient energy to lift it into the conduction band against the difference in potential Q, and then sufficient energy to surmount the potential barrier χ at the surface of the semiconductor. The total energy $Q + \chi$ is known as the total thermionic work function ϕ ; Q is the internal work function and χ the surface work function or electron affinity. The value of Q depends, of course, on the position of the Fermi level, which can in turn be related to the position of the impurity level or levels (66).

Dealing with the simple case for a single sharp impurity level, the following assumptions are made:

1. At 0 ^{o}K the conduction band is empty, and the impurity levels, of density n_b cm^{-3}, are completely filled.
2. The separation between the top of the uppermost filled band and the bottom of the conduction band is sufficiently large to neglect thermal transitions from the filled band. The separation ΔE of the impurity level from the conduction band is large compared with kT.

3. The number of impurities is constant, and does not depend on temperature, time or space.

The location of the Fermi level is given by

$$\mu = E_o - \frac{\Delta E}{2} + \frac{kT}{2} \log_e \left\{ \frac{n_b h^3}{w (2\pi m^* kT)^{3/2}} \right\} \qquad 2.1.$$

using the energy levels defined in Fig. 2.1, and where k is Boltzmann's constant, T is the absolute temperature, w is the statistical weight of states in the conduction band and m^* is the effective mass of an electron in the conduction band.

If the numerator of the logarithmic term is small compared with the denominator, the last term in eqn. 2.1 is practically zero and

$$\mu = E_o - \Delta E/2 \quad , \text{ approximately;}$$

$$\text{i.e.} \quad E_o - \mu = Q \doteq \Delta E/2 \qquad 2.2.$$

The density n_f of electrons in the conduction band will depend on the density of impurity levels n_b and on a Boltzmann factor:

$$n_f = w^{1/2} n_b^{1/2} \frac{(2\pi m^* kT)^{3/4}}{h^{3/2}} \exp\left\{ -\Delta E/2kT \right\} \qquad 2.3.$$

The assumptions on which these general equations are based are unlikely to hold in the case of the crystallites in an oxide cathode coating. The processes of diffusion and ionic conduction will certainly change the number of

excess metal atoms, and hence the concentration of impurities, as a function of temperature, time of operation and position in the cathode. The importance of the porous structure of the cathode matrix cannot be included in this simple general treatment, but will be discussed in a later section (Sec. 2.4).

2.3. Thermionic emission from an oxide-coated cathode

The combination of a semiconducting crystal with a metallic contact (e.g. the simple case where the oxide cathode and base is considered to be a single crystal in contact with a metal) causes the energy level diagram of Fig. 2.1 to be slightly modified, as shown in Fig. 2.2. The simplest case, where no interface compound is formed, is considered.

In equilibrium, the Fermi level W_i of the base metal will coincide with the chemical potential of the semiconducting oxide. Thus

$$W_i = \mu$$

The thermionic emission from such a metal-semiconductor combination has been investigated theoretically by Schottky (162), who showed that the emission current density j_o is given by an equation analogous to that derived by Richardson (150) for emission from metals:

$$j_o = A(1-\rho)\,T^2 \exp\{-e\phi/kT\} \qquad 2.4.$$

where A is a constant given by

$$A = \frac{4\pi m^* k^2 e}{h^3} = 120 \text{ amp cm}^{-2} \text{ deg}^{-2} \qquad 2.5.$$

ρ is the mean reflection coefficient for electrons at the emitting surface of the cathode, and

ϕ is the total work function: (Fig. 2.2)

Substituting the value for $E_o - \mu$ obtained from eqn. 2.1, the Fowler emission equation (66) is obtained:

$$j_o = B(1-\rho)\,n_b^{1/2}\,T^{5/4} \exp - \left\{\frac{\chi + \Delta E/2}{kT}\right\} \qquad 2.6.$$

where B is another constant given by

$$B = w^{1/2} e\, \frac{2\pi m^* k}{h^{3/2}} \qquad 2.7.$$

If it is assumed that ϕ and $\chi + \Delta E/2$ are independent of temperature, ϕ and $\chi + \Delta E/2$ may be obtained by plotting, respectively, $\log_e j_o/T^2$ versus $1/T$ (eqn. 2.4) and $\log_e j_o/T^{5/4}$ versus $1/T$ (eqn. 2.6). The former graph is usually referred to as a Richardson plot; the latter, as a Fowler plot (not to be confused with a Fowler plot for photoelectric emission (65), which will be discussed in Sec. 3.4). In the case of measurements on oxide cathodes, except in the most careful and accurate determinations, it is not practicable to attempt to determine the difference between ϕ and $\chi + \Delta E/2$ by a

comparison of the gradients of the Richardson and Fowler plots, and most workers prefer to use the Richardson plot, as the computational labour involved is rather less.

Not only can a value of $-e\phi/k$ be obtained from the gradient of a Richardson plot, but the intercept on the vertical axis gives $\log_e A^*$ where $A^* = A(1 - \rho)$. An estimate of the value of the transmission coefficient $(1 - \rho)$ can be obtained by combining emission measurements with approximate values for n_b, the concentration of impurity levels, in eqn. 2.6. Eisenstein (1) has used the data of Prescott and Morrison (147) and of Wooten (191) to show that wide variations in $(1 - \rho)$ are possible: if $n_b = 10^{20}$ cm^{-3}, $(1 - \rho) = 0.05$; but if $n_b = 10^{18}$ cm^{-3}, then $(1 - \rho) = 0.5$. Even this wide range in values of $(1 - \rho)$ is insufficient to account for the very wide variation in the values of A^* which is obtained from cathode to cathode; as A is theoretically a universal constant, the variation in the intercepts should only be due to the variation in $(1 - \rho)$. There is an apparent relation between ϕ and $\log A(1 - \rho)$ (183) and an investigation of this relation has recently been undertaken in this laboratory (48). An obvious source of error in the calculation of A^* arises from the difficulty in assessing the effective emitting area of the porous cathode.

An alternative way of displaying the discrepancy between theory and experiment is to assume reasonable values for ϕ , n_b and $(1 - \rho)$, and to calculate the emission current density to be expected at any temperature. This is usually found to be much greater than the values actually obtained under d.c. conditions, but better agreement with the predicted values has been obtained by workers who have used microsecond pulse techniques (37, 171, 193).

It must be pointed out that all the information referred to above has been deduced on the assumption that the total thermionic work function is independent of temperature. If emission measurements are made over a sufficiently wide range of temperature, it is often possible to detect a curvature of the Richardson line, and this curvature can be related to the temperature coefficient of the work function. A method which has been used to determine the temperature coefficient is to assume the value of the reflection coefficient ρ to be zero, and to calculate values of ϕ for a series of temperatures by substituting the emission current density at those temperatures in eqn. 2.4 using the theoretical value for A (98); it is felt that this method is hardly satisfactory because of the doubts which are still held as to the

significance of the constant A. It has been suggested by Nottingham (9) that Richardson plots for semiconductors such as the oxide cathode are most profitably used merely as a means of demonstrating the emissive properties of a cathode under certain conditions, and the constants obtained from the intercept and gradient of the graph should be considered as being more of empirical than of theoretical value. However, a suitable analysis can be applied to these empirical constants which may yield the theoretical values if corrections are applied for the deviations from the assumptions on which the theory is based: an analysis of the results obtained by Hung (94) yielded a value for A of 112 amp cm^{-2} deg^{-2}, instead of 120 amp cm^{-2} deg^{-2}, the theoretical value. But only in a few determinations can the conditions be defined sufficiently accurately to make the necessary corrections.

Richardson work functions will be dependent on the state of the surface from which thermionic emission takes place. It has been supposed by some workers (77, 94, 115) that the surface of the oxide cathode consists of a number of patches of slightly differing work functions. The variation in the distribution of patches of a given work function over the surface may well be temperature-dependent, and may explain some of the discrepancies

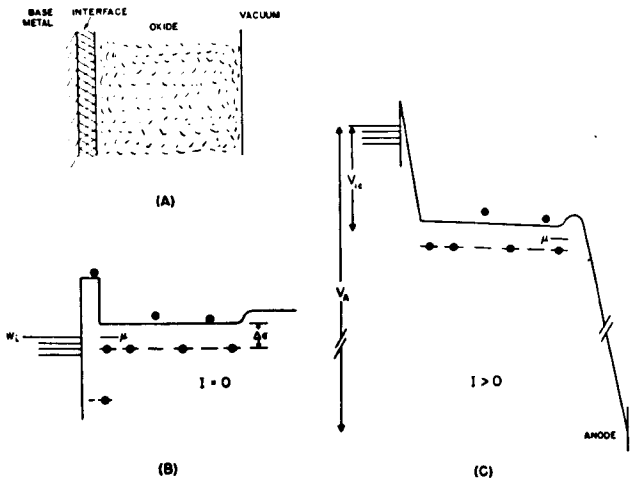

Cross section of interface type cathode; (B) energy levels with no emission; (C) energy levels when emission current is drawn.

Fig.2.3

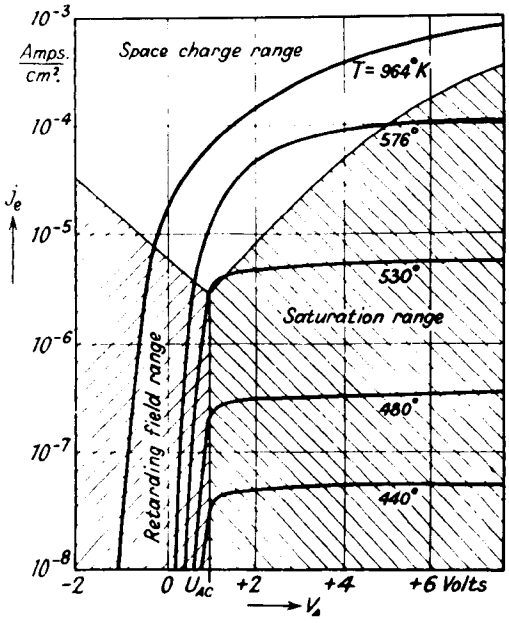

Emission Density j_e as a Function of Anode Voltage V_A for Different Cathode Temperatures.

Fig.2.4

associated with the Richardson line method of measurement. Mahlman (115) showed that the photoelectric work function varied by as much as 0.2 eV over the cathode surface, and a similar type of variation might be expected in the thermionic work function. It has been suggested by Heinze and Wagener (77), who examined the surfaces of oxide cathodes with an electron microscope, that patches of different work function may be due to differences in the alignment of individual crystallites or groups of crystallites. The faces of a barium oxide crystal may exhibit work functions which differ by as much as 0.4 eV.

An interface layer between core and cathode modifies the energy level scheme as shown in Fig. 2.3. Fig. 2.3.B shows that in the equilibrium state, when no current is flowing, the Fermi levels of core and cathode are, as before, at the same potential, but the interface produces a potential barrier over which the electrons must be excited thermally. When an anode voltage V_a is applied, current flow through the interface and coating produces a potential drop V_{ic}. The effect of drawing current is also to distort the energy levels; the extent to which this occurs depends on the electrical properties of the coating. Although the presence of an interface layer will reduce the emission current for a given anode

potential, it should not affect the saturated value unless the impurity concentration n_b has been reduced by the formation of the interface. The possibility of rectification by the interface layer, or by a potential barrier due to the metal-semiconductor contact even if an actual interface compound is not formed, has been mentioned in Sec. 1.5.

The form of thermionic emission current versus anode voltage curves for different cathode temperatures may be considered in detail. A typical family of curves is shown in Fig. 2.4, where the logarithm of the emission current density has been plotted against the anode voltage.

It is observed that in the retarding field region a considerable increase in emission is obtained for only small increases in the anode voltage. The only electrons which can reach the anode are those which have sufficient energy to overcome the total potential barrier between cathode and anode, made up of the applied retarding potential together with any contact potential between the cathode and anode. For a plane-parallel diode, the current density j_r collected at the anode at a retarding potential V such that the barrier height is greater than ϕ is (4)

$$j_r = A(1-\rho)T^2 C \exp\left\{\frac{e(V-\phi_a)}{kT}\right\} \qquad 2.8.$$

where C is a factor to account for electrons which are

reflected at the anode and re-enter the cathode, and ϕ_a is the anode work function.

At low cathode temperatures the emission current density is sufficiently low to neglect space-charge effects and the retarding field characteristic changes abruptly to the accelerating field characteristic. Behaviour in this range has been investigated by Schottky (161) for emission from a clean metal surface: the presence of an electric field intensity E at the surface reduces the work function by an amount $\Delta\phi$ given by

$$\Delta\phi = \sqrt{eE} \qquad 2.9.$$

and the emission current density j_a obtained in this region is given by

$$j_a = c \exp\left\{e^{3/2}E^{1/2}/kT\right\} \qquad 2.10.$$

where c is a constant.

At higher cathode temperatures, the space-charge-limited region intervenes: emission in this range obeys the Langmuir-Child law (36, 107)

$$j_{sp} = \beta V^{3/2} \qquad 2.11.$$

where β is a constant depending on the electrode arrangement and V is the anode potential.

It is convenient to plot emission characteristics in

the form of a graph of log j versus V. In the retarding potential region the graph should be linear, and its gradient may be used to evaluate the cathode temperature. If no space-charge region intervenes, the graph should suffer a sharp discontinuity at $V = \phi_a - \phi$ and become nearly horizontal for low values of the applied electric field.

Experimentally, it is extremely difficult to satisfy the theoretical conditions upon which these equations are based. Fan (59), indeed, found that the actual cathode temperature agreed with that obtained from the gradient, and also that there was a sharp break between the retarding and accelerating field characteristics: he deduced from the agreement with theory that the distribution of thermionic electrons is Maxwellian. However, it is felt that the particularly careful experiments of Hung (94) should be regarded as having more weight. Hung found that the change from the retarding to the accelerating characteristic was not as sharp as would be expected theoretically, and interpreted this in terms of a deficiency of slow electrons. This deficiency can be accounted for in terms of a patch theory of varying cathode work function, or of a high reflection coefficient.

In an experimental examination of emission in the

Schottky region (eqn. 2.10) log j is plotted against $V^{\frac{1}{2}}$. Good agreement is normally found as to the linearity of the plot, although the gradient is usually several times that predicted from the equation. This discrepancy with theory has been discussed by Wright and Woods (197), who extended the theory of Morgulis (125) dealing with the distortion of the energy levels at the cathode surface by the applied field. Periodic deviations have been observed by Champeix (35) and can be explained in terms of the wave mechanical treatment of the flow of electrons over a potential barrier.

For a determination of the Richardson work function ϕ the zero-field current density j_o may be found either from the point of intersection of retarding and accelerating field characteristics, or by extrapolating a Schottky plot to zero voltage.

It is often observed that, for a fixed cathode temperature and anode potential, the emission current decays with time. At low temperatures the rate of decay may be extremely low, but it increases with increasing temperature. Theories of the effect are divided between whether the fundamental process is a property of the cathode or of the anode. Sproull (171) suggested that the effect might be due to the electrolytic removal of

barium from or the deposition of oxygen at the cathode surface; and Wright (193), who found that the electrical conductivity of the coating decays in the same way as the emission, interpreted the process in terms of the electrolytic flow of ions to the interface. Other workers (42, 62) suggest that changes in the anode work function, due to material evaporated from the cathode, provide a sufficient explanation. Metson (119) has examined the influence of substances such as BaO, $BaCl_2$ and $BaSO_4$, evaporated on to the anode during the valve processing: as the anode potential was increased during current activation, the emission current showed decreases at anode potentials of about 5, 10 and 16 V, which may well correspond with the dissociation energies of 5.6, 10 and 16 eV of BaO, $BaCl_2$ and $BaSO_4$ respectively. Decomposition of these substances by electron bombardment may cause poisoning of the cathode by the negative ions formed.

Nergaard (134) has proposed a theory in which a number of the discrepancies between theory and experiment in thermionic emission may be at least qualitatively resolved, although it is felt that the theory has not yet been sufficiently tested by experiment. Nergaard supposes that the donors, which have been suggested by Plumlee (145) to be OH^-.e radicals, are mobile. When emission current is

drawn, the equilibrium distribution of donors throughout the cathode matrix is disturbed, and the donors electrolyse towards the core, leaving a layer at the surface depleted of donors. A process of back diffusion prevents a tendency for the donors to discharge at the metal core. The mobility of the donors requires the position of the Fermi level to be a function of the emission current. On this theory, emission decay is said to be due to changes in donor distribution.

2.4. Electrical conductivity of the cathode coating

The electrical conductivity σ of a semiconductor at a given temperature depends upon the number of electrons n_f in the conduction band (eqn. 2.3) and on their mean mobility u: the relation is

$$\sigma = n_f \, e \, u \qquad 2.12.$$

σ can also be expressed in terms of the electron mean free path l_o (assumed constant at a given temperature T):

$$\sigma = \frac{4 n_f l_o e^2}{3(2\pi m^* k T)^{1/2}} \qquad 2.13.$$

and, substituting for n_f in terms of n_b, the density of impurity levels, and the depth of the impurity level ΔE (eqn. 2.3)

$$\sigma = \frac{4}{3} W^{1/2} n_b^{1/2} \frac{e^2 l_o}{h^{3/2}} (2\pi m^* k T)^{1/4} \exp\{-\Delta E/kT\} \qquad 2.14.$$

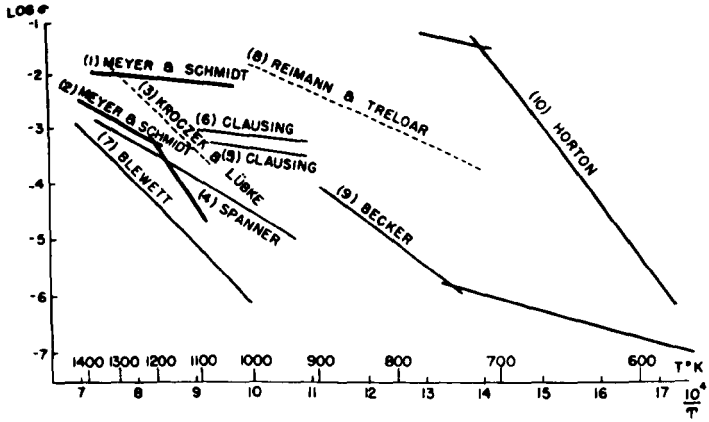

Fig. 2.5

Early conductivity determinations

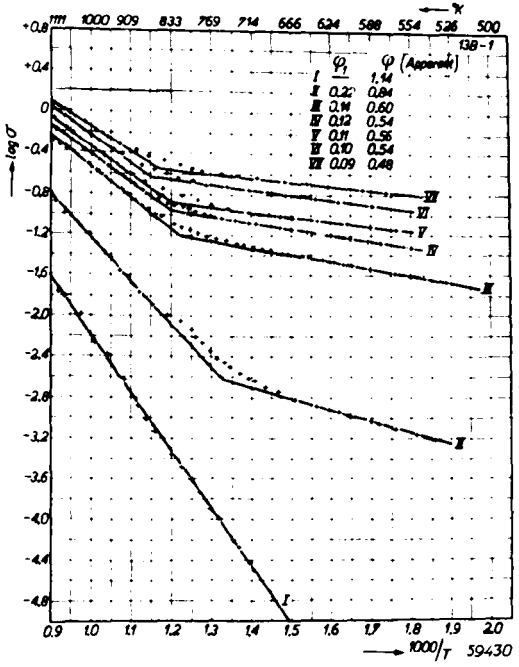

Log σ-1/T curves for succeeding stages of activation (I → VIII), σ being the specific conductivity in $\Omega^{-1}m^{-1}$. Tube 13 B-1.

Fig. 2.6

For values of T such that $\Delta E/2 >> kT$, the temperature variation of σ will depend mainly on the exponential rather than on the $T^{\frac{1}{2}}$ term. Thus, approximately,

$$\sigma = \sigma_o \exp(-Q/kT) \qquad 2.15.$$

where σ_o is practically independent of temperature and Q, the activation energy, is given by

$$Q = \Delta E/2$$

Thus, if the oxide cathode is a semiconductor of the type under discussion, a graph of $\log_e \sigma$ versus $1/T$ should be linear, with slope $-\Delta E/2k$. A linear conductivity plot is a necessary but not sufficient condition for semiconductor behaviour; for ionic as well as electronic conductivity obeys an exponential relationship of this form.

A large number of workers have attempted measurements of the conductivity of the cathode coating as a function of temperature; a graph showing the collected results of early workers (up to 1939) is given in Fig. 2.5. Most of these measurements were restricted to the high-temperature region ($T > 1000\ ^oK$) and most workers found a linear relation between $\log \sigma$ and $1/T$. Some found that the results could best be represented by two linear regions

of different gradient meeting in a sharp break, and Eisenstein (1), who studied the high-temperature conductivity in detail, observed that in all activation states the gradient above this break was less than that below it.

In more recent years attention has shifted from the high-temperature region to lower temperatures. Becker (22), whose results are displayed on Fig. 2.5 (curve 9), Vink (185) and Loosjes and Vink (111) (Fig. 2.6) found another break in the conductivity plot occurring at about 800 ^{o}K for a mixed oxide cathode: the activation energies for temperatures below the break are always less than those above the break. A theory advanced by Loosjes and Vink to account for the form of this curve suggests that two conduction mechanisms operate in parallel, and is a direct consequence of the porous nature of the cathode. If the cathode matrix is considered as an assembly of semiconducting crystallites of the alkaline earth oxide, separated by vacuum interstices, conduction is possible first of all by a true semiconduction process through or over the surface of the individual crystallites and secondly by thermionic emission across the vacuum pores. Although the surface or bulk conductivity of a single crystallite may well be high, the total conduction current carried across the matrix by the first process will be limited

by the area of contact of the crystallites. At low temperatures, the greater part of the conduction current will be due to the true semiconduction component: the lower part of the conductivity plot, below the break, thus refers to true semiconduction, obeying a temperature relation of the form

$$\sigma_c \propto \exp \{ - \Delta E/2kT \} \qquad 2.16.$$

and the gradient may be related to the activation energy $\Delta E/2$. As the temperature is increased, the density of the electron gas in the pores becomes greater and the pore emission component eventually masks the true semiconduction component. For a particular cathode material and state of activation, the temperature at which the break appears will depend on the area of contact between crystallites, i.e. on the porosity of the coating.

The process of conductivity in the pore conduction (high-temperature) region has been examined theoretically by Loosjes and Vink (111), Hensley (78) and Forman (64). The magnitude of the conductivity current for any applied potential and at any cathode temperature in this region depends on the mean free path of the electrons and on the average pore size, the space charge in the pores, and a Schottky effect at the pore surfaces produced by the

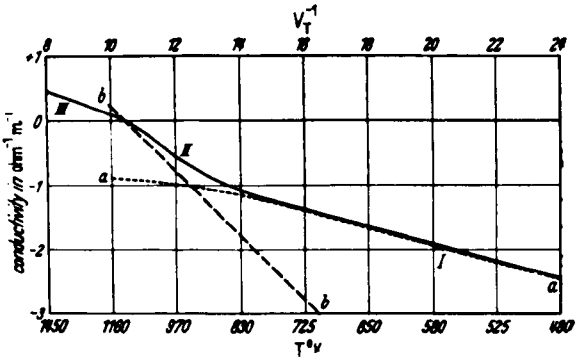

... Range I, semiconductor conductivity within crystals. ...ge II, pore conductivity becomes more important than crystal conductivity. Range III pore conductivity inhibited by space charge. Curve *aa*, semiconductor conduction alone, Curve *bb*, pore conduction alone without space charge.

Fig. 2.7

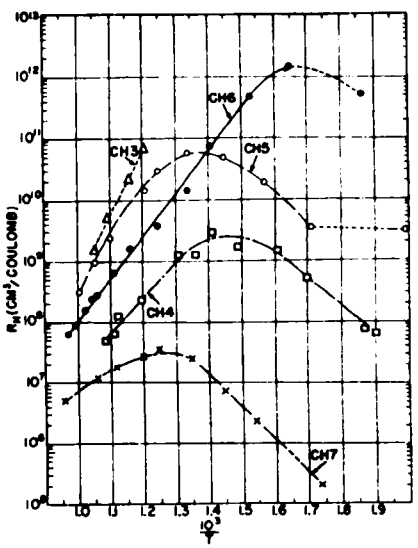

Hall coefficient of the oxide cathode as a function of the inverse absolute temperature.

Fig. 2.8

applied field. It can be shown that all three factors vary as exp (1/T), and the conductivity in this range, neglecting any solid semiconduction component, can be represented by a relation of the form

$$\sigma_p \propto \exp\{-\phi_1/kT\} \qquad 2.17.$$

where ϕ_1 is a work function which, from the similarity of the process to external thermionic emission, has been identified by Loosjes and Vink as the Richardson work function.

The combination of the two conduction mechanisms in parallel can be represented by the equation

$$\sigma = \alpha\sigma_p + \beta\sigma_c = \gamma \exp\{-\phi_1/kT\} + \delta \exp\{-\Delta E/2kT\} \qquad 2.18.$$

where α, β, γ and δ are constants.

If ϕ_1 is taken as the Richardson work function,

$$\phi_1 \doteq \chi + \Delta E/2 \qquad \text{and thus} \qquad \phi_1 > \Delta E/2$$

and at low temperatures the second exponential term in eqn. 2.18, due to true semiconduction, will predominate. A plot of $\log_e \sigma$ versus 1/T thus produces a curve which can be resolved into two linear portions (Fig. 2.7) the gradients of which can be related to ϕ_1 and $\Delta E/2$. It is important to note that the slope of the portion II of the plot of Fig. 2.7 does not give the value of ϕ_1, but it

must be corrected by allowing for the parallel mechanism I to give the line bb. Strictly speaking, the gradients of both high- and low-temperature regions should be corrected for the mechanism acting in parallel; in fact, the correction of the high-temperature region is more important than that of the low-temperature region.

Fig. 2.7 also shows the high-temperature break in the conductivity plot, between ranges II and III, discussed by Eisenstein (1) and observed in many subsequent determinations. On the Loosjes-Vink hypothesis, this can be explained by considering the inhibiting effect of space-charge on the conduction current at high conduction current densities.

Higginson (85) has observed a further change in the gradient of the conductivity plot, taking place at temperatures as low as 400 ^{o}K, and yielding a value of the order of 0.1 eV for the activation energy of the conduction process. He suggests that conductivity in this low-temperature region may be due to the movement of Ba^{++} ions over crystallite faces. Metson (122), however, suggests that the effect may be due to the migration of negative ions of residual gas: the type of tube in which Higginson observed the effect was one in

which the poisoning effect of oxygen on the cathode was studied. The low-temperature conductivity region of the Loosjes-Vink hypothesis, however, may well be one in which conductivity is largely a surface phenomenon (122).

It is important to realise that the form of conductivity plot obtained could formally be explained on the basis of a semiconductor model containing two, instead of only one, impurity levels: the two regions might be due to the thermal excitation of electrons from the different levels. This hypothesis may well seem attractive, particularly in view of the fact that photoelectric studies, to be discussed in Chap. 4, have shown that several impurity levels do exist in BaO. However, a corresponding bend would be expected to occur in the Richardson line for thermionic emission, and only Kestelyn-Loebenstein (102) claims to have observed such a break.

A number of workers have carried out experiments to investigate the fundamental assumption of pore emission in the Loosjes-Vink hypothesis. A consideration of the methods employed is of value, as a number of the principles have been applied in the present work to determine the processes operating in photoconductivity.

Loosjes and Vink (111) and Nakai, Inuishi and Tsung-Che (132) have reported that the values of ϕ_i obtained

from the high-temperature region of the conductivity plot agree with values of the Richardson work function ϕ for thermionic emission from the cathode in the same activation state. These results must be assessed somewhat critically: Loosjes and Vink measured the conductivity between two similar oxide-coated button cathodes, pressed into contact, and separated the cathodes to insert an anode to which emission current was drawn. The process of separation could hardly fail to modify the state of the oxide coating. The Japanese workers did not, apparently, correct the high-temperature conductivity characteristic for the parallel low-temperature mechanism, and agreement with the Richardson work function can have little significance. Many workers, however, have found rough agreement between Richardson work functions and the corrected high-temperature activation energies to within about 20 %: in view of the fact that the emitting surfaces for the two processes may well be different, this agreement is considered to be reasonable.

Forman (64) and Hensley (78) have considered theoretically the Hall e.m.f. and the thermoelectric power to be expected in a porous semiconductor specimen. When the effects are studied experimentally (64, 199) agreement with theory in the pore conduction range is good; between this range and the low-temperature region, at temperatures

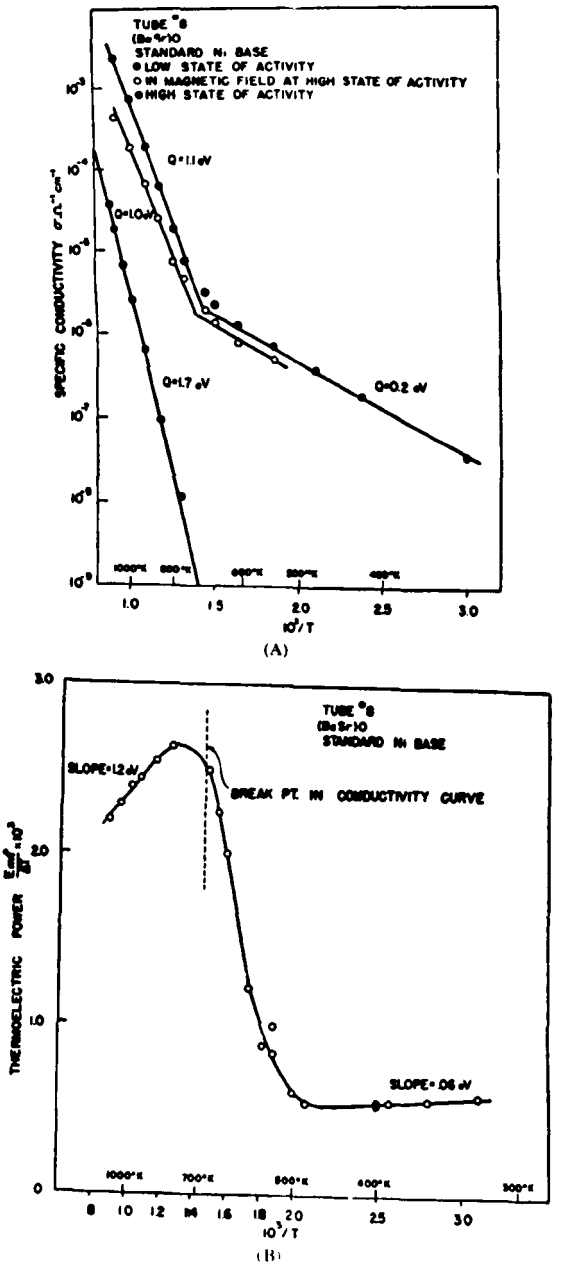

Fig. 2.9 Electrical conductivity (A) and thermoelectric power (B) as functions of reciprocal temperature

roughly corresponding to the break in the conductivity plot, graphs of both Hall e.m.f. and thermoelectric power against 1/T (Figs. 2.8, 2.9) show changes in character, which can be related to a change to orthodox semiconduction in the low-temperature range.

Associated with the Hall effect is a magnetoresistive effect, which has been discussed and investigated by Forman (64) and Metson (122). The application of a magnetic field transverse to the direction of flow of the conductivity current through the porous semiconductor superimposes a transverse drift velocity on the motion of the conduction electrons. On an elementary picture it might be thought that the magnetic field applied would have to be sufficiently strong to make the radius of curvature of the path of the electron of the same order of magnitude as the dimensions of the pores, so that the electron setting out from one side of a pore could be turned round in the pore without reaching the other side, on the magnetron principle. In fact the field required to produce a transverse drift velocity sufficient to increase the longitudinal resistance by an appreciable amount is much smaller than this. The important experimental result obtained was that although a large magnetoresistive effect is obtained in the pore conduction region,

and the magnitude of the effect is within order-of-magnitude agreement with Forman's theory, the magnetic field has a negligible effect on the conductivity current at temperatures in the true semiconduction range.

Another method of investigation of the conduction processes has been employed by Shepherd (166) and by Higginson (84), who examined the recovery of the conductivity current and the external thermionic emission current after poisoning attacks by oxygen and sulphur. At temperatures in the pore conduction range, the recovery of conductivity and thermionic emission follows the same pattern, but at low temperatures recovery is quite different: after an attack thermionic emission recovers very gradually, while conductivity continues to decay.

Hensley (80) observed the effect of mechanical pressure on two parallel planar cathodes with an oxide matrix sandwiched between them. Above about 700 °K, i.e. in the pore conduction region, the conductance of the system does not depend on physical contact between the cathodes, direct evidence in favour of the Loosjes-Vink hypothesis.

Again, if the Loosjes-Vink hypothesis is correct, it should be possible to suppress the pore emission

component of the conductivity current by the introduction of an inert gas which would fill the pores and reduce the direct emission current without influencing any solid conduction mechanism. Hannay, Macnair and White (75) found that helium at a pressure of 1 atmosphere failed to produce any effect on the supposed pore conductivity component, and hence regarded the Loosjes-Vink hypothesis as dubious; but Loosjes and Vink (111) point out that at this gas pressure the electron mean free path is still of the order of the pore diameter. Only at higher pressures, and thus shorter mean free paths, would a suppressing effect be expected. As predicted, xenon at a pressure of 25 atmospheres reduced the conductivity in the high-temperature range.

Loosjes and Vink also predicted a difference in the curvature of the conductivity current - voltage characteristics in the two temperature ranges, and this is observed experimentally in most d.c. determinations. Tomlinson (179) used an a.c. technique which allowed a rapid determination of the complete current - voltage characteristic at any temperature: in the high-temperature region no curvature of the characteristic was observed. Tomlinson's results can be accounted for by a slight modification of the Loosjes-Vink theory.

Rather less experimental evidence is available on the nature of the low-temperature conduction mechanism. Sproull (172) and Dolloff (50) have measured the electrical conductivity of single crystals of barium oxide containing excess barium as a function of temperature. It is found that activation energies are generally greater than those for the low-temperature conductivity region of a polycrystalline BaO cathode, and this suggests that the cathode low-temperature conductivity process may not be one of solid semiconduction. Experiments carried out by Metson and Macartney (122) can be interpreted in favour of a surface conduction process, in spite of the fact that there are likely to be far fewer excess Ba atoms lying on pore surfaces than are built into the lattice of the crystallites: Metson suggests the figure of 1 surface atom for every 10^4 atoms built into the lattice.

There is thus ample experimental evidence for the adoption of the view that the conductivity of the oxide cathode matrix can be considered to be due to two or more conduction processes acting in parallel. In the temperature range from about 700 °K upwards, there is little doubt that the predominant process is one of electron emission across the pores of the matrix; below this temperature there is more doubt as to the nature of the process, but

it may be due to solid semiconduction within the crystallites, limited by grain boundaries, or to surface conduction. The fact that the characteristic break in the log σ versus 1/T curve is obtained with a variety of experimental arrangements - button cathodes in contact (80, 111, 122, 199), cylindrical cathodes with helical probes wound within the coating (166, 84, 85, 88, 116, 48) and retarding potential methods (170)-shows that the effect cannot merely be the result of the choice of one particular method of measurement.

A theory due to Metson (122) suggests the existence of a thin film of semiconducting BaO at the cathode base as the seat of emission, protected from contamination by the porous cathode matrix. Following Loosjes and Vink, two temperature-dependent conductivity processes are possible.

2.5. Deduction of the energy level scheme from emission and conductivity measurements

Measurements of the zero-field emission current density j_o as a function of temperature can be used to construct a Richardson plot: the gradient of this graph can be used to obtain a value of the total thermionic work function, ϕ .

If the Loosjes-Vink hypothesis is accepted, it should be possible to obtain another value of ϕ from the gradient of the high-temperature region of the conductivity plot, corrected for the low-temperature process. It has already been pointed out (Sec. 2.4) that a comparison of the Richardson and conductivity values seldom yields exact agreement, work functions obtained from conductivity measurements usually being up to 20 % less than those from emission measurements.

The slope of the low-temperature region of the conductivity plot has been interpreted as $\Delta E/2$ (Sec. 2.4), which is approximately the separation of the Fermi level from the conduction band: the separation of the impurity level from the conduction band is ΔE.

Since $$\phi \pm \chi + \Delta E/2$$

the external work function can be obtained by direct subtraction of $\Delta E/2$ from ϕ obtained either from the high-temperature region of the conductivity plot or from a Richardson plot. Another method which has been used to obtain a value of χ is to combine measurements of thermionic emission and conductivity. From eqns. 2.6 and 2.14,

$$\frac{j_o}{\sigma} = \frac{3(1-\rho)\,kT}{4L_o e} \exp\left\{-\chi/kT\right\} \qquad 2.19.$$

and a graph of $\log_e j_o/\sigma T$ versus $1/T$ should be linear, with slope $-\chi/k$. It is important to note, however, that for the value of χ obtained in this manner to have any significance, measurements must be made in the temperature region in which eqn. 2.14 is expected to be valid, i.e. in the low-temperature conductivity region. In the pore conductivity region the primary conduction process is one of thermionic emission, rather than of solid or surface semiconduction, and although there should certainly be a relation between j_o and σ at any given temperature, it cannot yield a significant value of χ. This point would appear to have been overlooked by some workers who have used the method (75, 87, 132).

In a typical activated barium oxide cathode, values of ϕ might be expected to lie between about 1.0 and 1.4 eV. Values of $\Delta E/2$, obtained from the low-temperature region of the conductivity plot, vary from 0.2 to 0.4 eV. χ usually takes values between 0.5 and 1.0 eV; a value of 0.7 eV is often quoted.

2.6. Thermal activation energies for calcium oxide coated cathodes

Although the general introduction to the electrical properties of the oxide cathode given in the preceding

sections has frequently referred to mixed oxide or barium oxide coated cathodes, most of the experimental work carried out in the present programme of research has been on calcium oxide coated cathodes. The previous work carried out on such cathodes will now be briefly summarised.

Most of the early work on calcium oxide was in connection with its effect as an additive in mixed oxide cathodes, but a number of determinations were made of the emission from pure CaO cathodes, and these yielded a wide range of values for the work function ϕ. The early results are tabulated in Table 2.1.

Table 2.1. Thermionic work function ϕ of CaO

Date	Worker	Method	ϕ, eV
1924	Spanner (169)	Richardson line	2.4
1926	Espe (56)	Richardson line	1.8
1935	Becker (23)	Review articles: quoted as typical values	3.2
1939	Blewett (29)		1.9
1941	Huber (92)	Retarding potential against electrode of known work function	2.4

There is no doubt that this variation in ϕ can be traced first of all to inadequate vacuum techniques, and secondly to difficulties inherent in the measurement of

such small emission currents as are obtained with calcium oxide cathodes.

The measurement of the electrical conductivity of calcium oxide is also difficult, as the conductivity is much less than that of barium oxide: to obtain measurable conductivity, early determinations were made at very high temperatures. In 1906 Horton (91) measured the conductivity of lime in air in the temperature range 1000 - 1500 ^{o}K. Although his results yield a linear plot of log σ versus 1/T with a gradient corresponding to an activation energy of 1.7 eV (87), this has little significance in comparison with vacuum determinations. The same criticism must be applied to the work of Spanner (169), who determined the conductivity of compressed discs of the alkaline earth oxides in air over the temperature range 900 - 1300 ^{o}K.

Only three recent determinations under adequate vacuum conditions have been reported. The first of these was by Glascock and Hensley (70), who attempted to measure the thermoelectric power and electrical power of a sample of CaO compressed between planar nickel cathodes, in an arrangement very similar to that used by Young (199) in his measurements on BaO and (BaSr)O. They were unable, due to current measuring difficulties, to do more than deduce that calcium oxide was a pore conductor at high

FIG. 2.10. ENERGY LEVEL SCHEME FOR CoO ACCORDING TO HOPKINS (87)

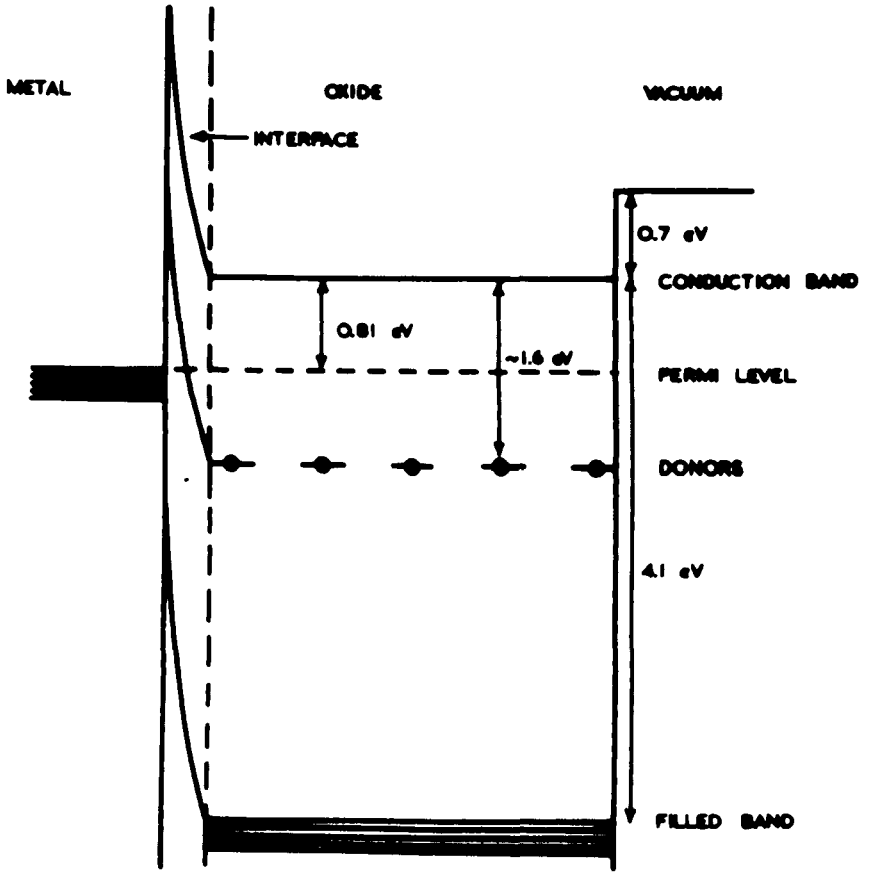

temperatures by the qualitative similarity of the curves obtained with CaO to those obtained with (BaSr)O, and no activation energies or work functions were quoted.

Paulisch (142) included CaO in investigations of the high-temperature conductivity of a number of oxides, the samples being in polycrystalline form, and deduced that it was a pore conductor in the high-temperature range.

Hopkins and Vick (88) reported a much more comprehensive study of the properties of the calcium oxide coated cathode. Probe diodes were used to measure both thermionic emission and electrical conductivity, and it was confirmed that the conduction process could again be explained by the Loosjes-Vink hypothesis. The mean Richardson work function for the fully activated states of five cathodes was 1.7 eV, although unactivated states gave values as high as 2.4 eV (87). Conductivity plots gave rather lower values of the work function in the pore emission range, the average being about 1.3 eV. The mean low-temperature activation energy, $\Delta E/2$, was about 0.8 eV. The energy level scheme deduced by Hopkins (87) from his results is reproduced in Fig. 2.10. The value of 4.1 eV for the separation of the filled band from the conduction band is based on a calculation by Wright (194) of the energy required to lift an electron from the

filled 2p band in the alkaline earth oxides to vacuum: for CaO, it is 4.8 eV.

PART II

Chapter 3 The effects of light on semiconductors

3.1. Introduction

In the most general terms, a beam of monochromatic radiation incident on the surface of a semiconducting crystal will be partially reflected and partially absorbed. The fractions reflected and absorbed, r and a respectively, are related by the equation

$$a + r = 1$$

The fraction of radiation absorbed may interact with the electrons in the semiconductor to raise them to excited states: if $\Delta E'$ is the excitation energy of an electron, the minimum photon energy required to raise the electron to its excited state is $h\nu_0$ where $h\nu_0 = \Delta E'$. For an intrinsic semiconductor, electrons must be excited across the forbidden zone from the filled band to one of the energy levels in the conduction band. For a semiconductor with impurity levels in the forbidden zone, alternative excitation processes are possible: electrons can also be excited from an impurity level to the conduction band, or from the filled band to a vacant impurity level. For a semiconductor model which assumes the existence of sharp impurity levels (the model employed in the discussion of the electrical and thermionic properties

FIG. 3.I. OPTICAL ENERGY LEVEL SCHEME FOR AN EXCESS IMPURITY SEMICONDUCTOR

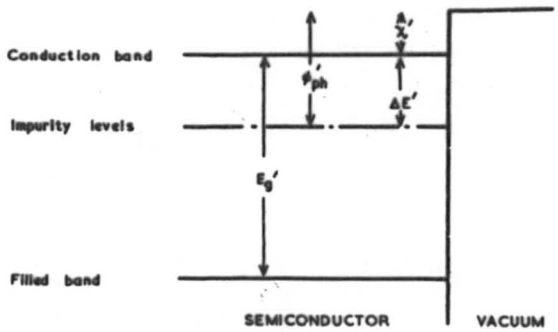

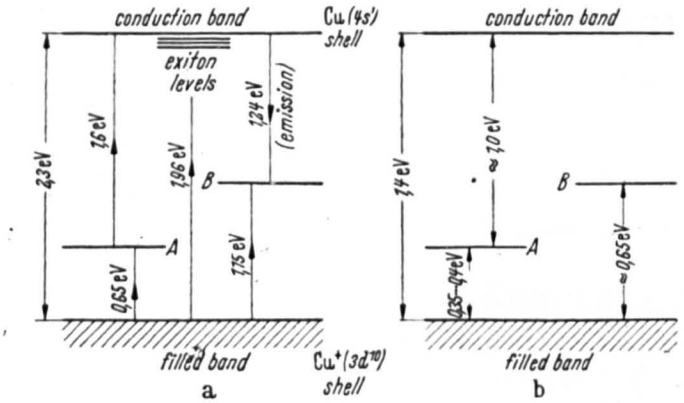

. Energy band scheme for cuprous oxide. a) Optical transition energies. b) Thermal transition energies.

Fig. 3.2

had one such level) each excitation process will have associated with it a sharp low-frequency threshold, ν_0, given by $h\nu_0 = \Delta E'$. A study of the thresholds corresponding to the various possible excitations may lead to a determination of the energy level scheme of the semiconductor.

An optical energy level diagram for the simple case of a semiconductor with a single sharp impurity level is given in Fig. 3.1. It is necessary to distinguish at this stage between optical and thermal activation energies: optical energies are marked with a prime. The distinction is due to the Franck-Condon principle. When an electron is removed from an atom by a photon-absorptive process, neighbouring ions do not have time to move during the process, and thus the optical activation energy is the energy required to remove the electron with the ions stationary. After absorption and removal of the electron, the lattice ions move to new equilibrium positions, lowering the energy of the crystal; the difference between this final equilibrium energy state and the initial one is the thermal activation energy. Thus, in general, the thermal activation energy will be less than the optical activation energy.

Mott and Gurney (8) have made an estimate of the

relation between optical and thermal activation energies due to this principle. They suggest that the ratio of the thermal to the optical activation energy is approximately the ratio of the optical to the static dielectric constant, i.e. ϵ/ϵ_o . Thus for semiconductors which have $\epsilon = \epsilon_o$, e.g. elementary semiconductors (6, 7), optical and thermal activation energies are approximately the same; and in some cases where $\epsilon \neq \epsilon_o$, reasonable agreement between thermal and optical information has been obtained using the ratio ϵ/ϵ_o as a conversion factor. Thus Garlick (3) has successfully correlated optical and thermal results for cuprous oxide (Fig. 3.2): the refractive index of Cu_2O is about 2.75, so the optical dielectric constant ϵ is about $2.75^2 = 7.56$; the static dielectric constant ϵ_o is about 12, and the ratio ϵ/ϵ_o is thus approximately 0.6. A comparison of the transition energies in the thermal and optical schemes shows that they are approximately in this ratio. This type of comparison has not, however, been successful with all oxide semiconductors: there is a discrepancy in the case of zinc oxide (3) which is still not completely resolved, and the case of the alkaline earth oxides will be discussed in Sec. 4.6.

Later sections of this chapter will discuss the

details of the various photon-absorptive processes in a semiconductor, and describe methods of determination of the optical activation energies.

3.2. Optical absorption

The absorption spectrum of a semiconducting crystal in the region of intrinsic absorption will be considered. That is, we consider frequencies of radiation ν such that $h\nu$ is of the order of E_g', the optical forbidden bandwidth. In this region absorption is generally very strong. In the general case, the absorption spectrum might consist of a series of one or more sharp lines leading to a continuous spectrum at greater photon energies. The discrete lines correspond to exciton absorption: an exciton is an electron raised to an excited state in the field of the hole from which it came. Excitons can move through the lattice and may combine with positive holes before sufficient thermal energy has been gained from the lattice to lift the electron into the conduction band. Thus photoconductivity will not necessarily be associated with absorption in the exciton bands, but if we consider absorption in the continuous spectrum at rather greater photon energies, electrons may be excited directly into the conduction band from the filled band, leaving a

positive hole in the filled band. Under the influence of an applied field, a photoconductivity current will flow (Sec. 3.3.1).

It is thus apparent that a determination of the optical absorption spectrum in the intrinsic region gives information about exciton levels and an estimate of the width of the forbidden zone, E_g'. Although the exciton levels should theoretically be discrete, sharp lines, they may well be broadened by interaction with phonons (quanta of lattice vibrations) and may be indistinguishable from the intrinsic absorption edge. A measurement of the frequency corresponding to the absorption edge may not give the exact band separation, as the selection rules forbid optical transitions from the top of the filled band to the bottom of the conduction band. In fact, the selection rules apply only to perfect crystals and in most semiconductors strong intrinsic absorption begins at $h\nu = E_g'$, the selection rules being violated. It should be noted that measurements in the intrinsic absorption region often give information only of the energy levels near the surface of the crystal: absorption is so strong that most photons are absorbed within a short distance of the surface.

An intrinsic semiconductor may show some structure in

the long-wavelength tail of the absorption, due to absorption by any electrons which may be in the conduction band. Although theoretically the absorption of radiation by carriers moving in a perfectly periodic field is forbidden, the periodicity of the field may be impaired by lattice vibrations and impurities, and absorption results.

If now an impurity semiconductor is considered, further structure on the long-wavelength side of the absorption edge would be expected, corresponding to the excitation of electrons from and to the impurity levels, and photoconductivity should accompany this absorption. A theoretical treatment of the dependence of the absorption coefficient on the frequency of the incident radiation is difficult: discussions have been given by Fan (61) and by Koster and Slater (104).

For completeness, two further types of optical absorption should be mentioned. If an energy band is degenerate, optical transitions may be possible between individual levels. Secondly, in ionic crystals, structure in the absorption spectrum at very long wavelengths may be ascribed to displacement of the ions due to lattice vibrations: this absorption is very strong in purely ionic crystals, and may also occur when the crystal is

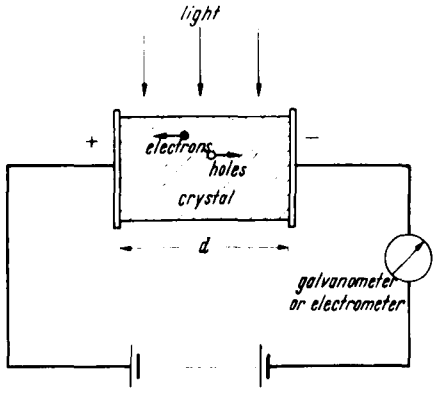

Schematic experimental arrangement for measurement of photoconductivity.

Fig. 3.3

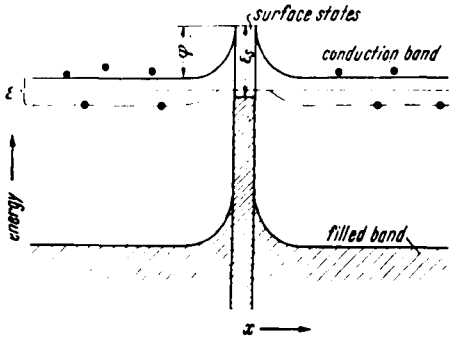

Potential barrier between two N-type crystallites showing surface states for trapping electrons.

Fig. 3.4

only partly ionic in character.

The practical correlation of structure in the absorption spectrum to the energy level scheme is difficult unless the nature of the transitions associated with the absorption is determined: transitions from the filled band or from impurity levels to the conduction band, or from the filled band to impurity levels, result in photoconductivity, and optical absorption and photoconductivity are frequently studied together.

3.3. Internal photoeffects

In the present work, discussions of photoconductivity and of the photovoltaic effect (Secs. 3.3.1 and 3.3.2) will be of most importance. The remaining photoeffects are mentioned merely for completeness, and are only briefly referred to in discussions of the results of the present work.

3.3.1. Photoconductivity

Consider a perfect crystal of a semiconductor mounted between ohmic contacts and connected to a battery via a current measuring instrument (Fig. 3.3). It is assumed that the temperature of the crystal is sufficiently low for a negligible number of electrons to be thermally excited to the conduction band; the dark conductivity

can thus be neglected. As described in Sec. 3.2, illumination of the whole crystal by light of such a frequency ν that $h\nu > E_g$' causes excitation of electrons to the conduction band, leaving free holes in the filled band, and the crystal becomes photoconducting, both electrons and holes contributing to the conduction current. As long as the carriers remain free, a current will flow; but immediately the illumination is cut off and excitation ceases, recombination processes (which are also operative in the illuminated state) reduce the carrier density and the current decays to zero. If a constant intensity of radiation is maintained, the excitation and recombination processes adjust themselves to a state of dynamic equilibrium.

A number of different recombination processes are possible. If direct recombination of holes and electrons takes place, so that electrons return to the filled band from the conduction band, radiation of frequency corresponding to the forbidden band separation is emitted ("edge emission"). Recombination can also take place due to the presence of recombination centres with vacant levels in the forbidden gap. If radiation is emitted it is of lower frequency than that for edge emission, as the transition energies must always be less; but photon

emission does not always result, the transition energy being transferred as phonons of lattice vibration or being used to excite another free charge carrier in a secondary process. Centres at which carriers of one sign are removed are known as traps.

The growth and decay of photocurrents in a crystal when radiation is applied and cut off depend upon the number and position of the various recombination centres. Garlick (3) and Wright (11) have reviewed various treatments of the problem; Rose (154, 155), Fan (60) and other workers have discussed recombination processes in further detail.

The variation of photocurrent with exciting light intensity depends upon the distribution of traps. For example, it can be shown (3) that for deep trapping states the photocurrent is directly proportional to the intensity of irradiation J for weak intensities, changing to a proportionality to $J^{\frac{1}{2}}$ at higher intensities, the break point depending on the temperature of the specimen. For a uniform distribution of traps to a depth of about 1 eV below the conduction band, the photocurrent is again proportional to J, but is insensitive to temperature. If the distribution is exponential below the conduction band, the photocurrent is proportional to J^m where

$0.5 < m < 1.0$ below a certain temperature; above that temperature, $m = 0.5$ (154). A study of the relationship between the photocurrent and the intensity of illumination can thus provide some information on the distribution of trapping states, although interpretation may well be difficult.

The treatment thus far has dealt with a consideration of photoconductive effects to be expected in a single semiconducting crystal. In a large class of photoconducting materials, the specimen consists of a number of crystallites, and trapping of charge carriers may take place at the barrier layers between the crystallites as well as at trapping levels within them. This class is obviously of great importance in the present context. Electrical conductivity studies (Sec. 2.4) have shown that the oxide cathode may be considered as a porous structure of crystallites, with the crystallite boundaries playing an important part in the limitation of the true semiconduction current.

The barrier modulation theory of photoconductivity has been developed by Gibson (69) and by other workers (151, 165, 168) to apply to polycrystalline specimens. The crystallite boundaries give rise to potential barriers which may cause fluctuations in the impurity levels, and

possibly even transitions from N- to P-type semiconduction. Such a potential barrier, rather like a double Schottky barrier, is shown in Fig. 3.4. The absorption of light near a barrier causes a separation of electron-hole pairs so rapid that the effect of recombination is negligible. The effective barrier height is lowered by this separation effect and conduction across the barrier is increased. On the other hand, in the interior of the crystallite recombination may be rapid and effectively limits the photoconductivity. The variation of photocurrent with intensity on this model is one of direct proportionality, and thus in certain cases there might be confusion with the single-crystal process previously described. The processes can be distinguished, however, by significant differences between expressions for the response time and quantum equivalence of the photocurrent derived for the two models.

In some cases, the irradiation of a photoconducting crystal with photons of high energy has been found to enhance the sensitivity at longer wavelengths: this may well be due to the excitation of carriers from the filled band to vacant, low-lying traps. The absorption of radiation of lower energy is then sufficient to cause excitation into the conduction band. The converse effect

FIG. 3.5. HYPOTHETICAL EXPERIMENT TO DETECT A PHOTOVOLTAIC E.M.F.

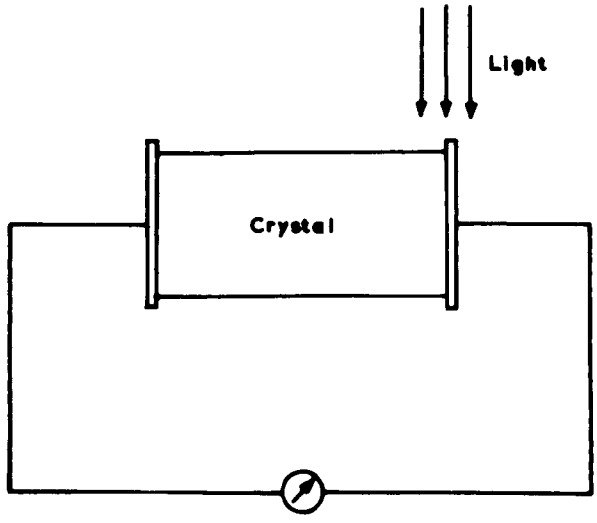

may also be observed. Simultaneous irradiation of a photoconductor with photons of sufficient energy to produce photoconductivity and with infra-red radiation may cause a quenching of the photocurrent. This process can be represented by the liberation of positive holes, trapped at recombination sites, by the low energy photons. The holes then combine with trapped electrons, leaving a number of empty traps available to reduce the number of free charge carriers.

As mentioned in Sec. 3.2, the spectral sensitivity of photoconductivity may be related to the optical absorption spectrum to derive an optical energy level scheme.

3.3.2. Photovoltaic effect

If a semiconducting crystal is mounted between metallic contacts and connected to a galvanometer (Fig. 3.5) uniform illumination of the whole crystal produces no effect. If, however, one electrode and its contact with the crystal are illuminated, a current will be registered on the galvanometer: a photovoltaic e.m.f. has been set up. In general, it is found that illumination of a potential barrier produces a photo-e.m.f.; the barrier may be an external one, as in the hypothetical

experiment described above, or an internal one, e.g. at a crystallite boundary. The photovoltage set up by the illumination is effectively the difference in energy between the Fermi level at the illuminated barrier and the true Fermi level at a distant, unilluminated part of the specimen.

It can be shown that the sign of the photovoltage depends on the sign of the charge carriers which are excited. The magnitude of the voltage, measured under open circuit conditions, is directly proportional to the absolute temperature and to $\log_e (1 + \beta J)$ where J is the exciting light intensity and β is a constant (3, 6).

3.3.3. Dember or photo-diffusion effect

An effect in which non-uniform illumination of a single semiconducting crystal may produce a photovoltage without illumination of a potential barrier was first observed by Dember (44) and has since been discussed by Moss (7). If the surface of the crystal is illuminated by radiation lying in a region of strong absorption, most of the photons will be absorbed within a short distance of the surface, and a high concentration of electron-hole pairs will be produced there. The concentration gradient causes the carriers to diffuse away from the

surface of the specimen towards the unilluminated back surface. Normally the electrons will diffuse faster than the holes; they reach the back surface first, setting up a negative charge there, and the effect of the field due to this charge is to assist the diffusion of holes. In equilibrium, a photodiffusion voltage may be measured between the illuminated and dark surfaces of the specimen.

3.3.4. Photoelectro-magnetic effect

Consider the application of a magnetic field perpendicular to the direction of diffusion of the electrons and holes in the experiment described in the last section. Under the influence of the magnetic field, electrons and holes separate and travel towards opposite ends of the crystal. A voltage difference between the ends of the specimen builds up until it is sufficient to prevent current flow. The effect may be described as the setting up of a photodiffusion Hall e.m.f., and has been discussed by Moss (7) and others.

3.4. External photoelectric emission

The study of external photoelectric emission from a semiconductor yields rather less fundamental information than that of the various internal effects. However, it has been very widely used in investigations on the oxide

cathode and thus deserves attention at this stage.

The basic information which can be obtained from the spectral sensitivity curve for photoelectric emission is the energy required to lift electrons from the filled band and from impurity levels to vacuum potential. The curve should show a sharp increase at photon energies corresponding to the separation between the filled band and vacuum potential, and structure in the long-wavelength tail may be due to emission from impurity levels. Because the electrons are removed from the semiconductor, recombination processes do not enter into the effect and the photocurrent should be proportional to the light intensity J over all values of J, a fundamental relation of photoelectric emission (63).

For excitation from an impurity level at a depth $\Delta E'$ below the conduction band, the photoelectric work function ϕ_{ph} obtained from a study of the spectral sensitivity is (Fig. 3.2)

$$\phi_{ph} = \chi' + \Delta E'$$

which must be distinguished from the total thermionic work function ϕ (Sec. 2.2):

$$\phi \simeq \chi + \Delta E/2$$

The interpretation of spectral sensitivity information

to yield values for ϕ_{ph} is not easy, and suffers from the legacy of methods which were originally developed for the determination of the photoelectric work function of metals. For a metal there is a sharp low-frequency cut-off, below which it is impossible to obtain photoemission; but a semiconductor at temperatures above absolute zero will always have some electrons in the conduction band as well as those in impurity levels and at least a very small photoelectric current can be obtained for radiation of low frequency, corresponding to excitation from the conduction band. Thus there can be no true photoelectric threshold for semiconductors in the sense that there is for metals: it is often found, in fact, that as the wavelength of incident radiation increases, the photo-current per unit incident intensity decreases nearly exponentially (Sec. 4.2). Although a linear plot of photocurrent versus photon energy indicates an apparent threshold, this can be shifted to lower photon energies merely by the use either of more intense radiation or of a more sensitive detector for the photocurrent. Under fixed conditions of light intensity and detector sensitivity these classical methods can be used to give a purely arbitrary value of the photoelectric threshold which may, however, be of use in defining the photosensitivity

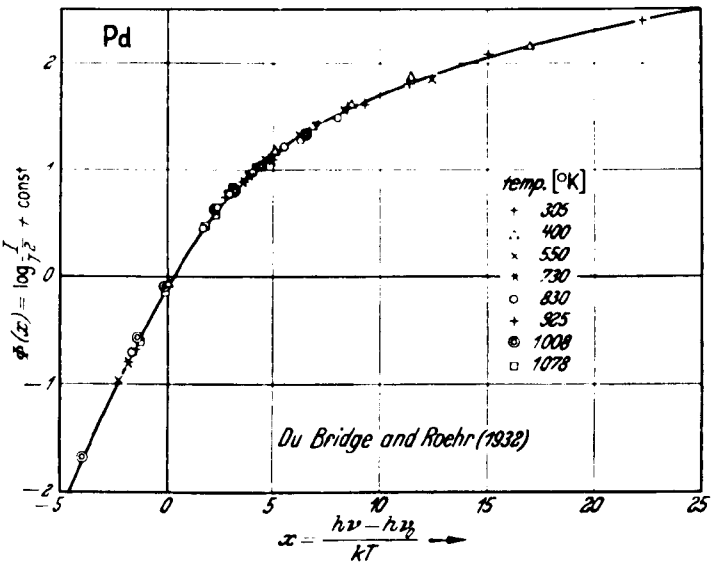

Photoelectric emission from Pd at 8 different temperatures fitted to a FOWLER curve.

Fig. 3.6

of the specimen. A method commonly used for metals, and one which has been applied to the oxide cathode, is due to Fowler (65) and involves the fitting of photoelectric sensitivity results near the threshold to a general theoretical curve. Fig. 3.6 shows results for photoelectric emission from Pd at a number of temperatures fitted to the curve.

Carroll (33) has extended Fowler's theory by applying the mirror-image lowering of the work function to the Fowler equation. For photoelectric emission from a metal caused by monochromatic illumination of frequency ν, the photoelectric current i_{ph} in an accelerating field E is given by

$$i_{ph} \propto \frac{4\pi m}{h^3} \left\{ \frac{[h(\nu-\nu_0)]^2}{2} + h(\nu-\nu_0)e^{3/2}E^{1/2} + \dots \right\} \qquad 3.1.$$

where ν_0 is the photoelectric threshold. The equation is valid at temperatures not very high above room temperature, and at frequencies ν a few tenths of an eV above ν_0. In a plot of i_{ph} versus $E^{\frac{1}{2}}$, both the slope $S = di/dE^{\frac{1}{2}}$ and the zero-field intercept i_0 are proportional to the light intensity: by taking the ratio of these two quantities, it is found that

$$i_0/S = \tfrac{1}{2} h (\nu - \nu_0) e^{-3/2} \qquad 3.2.$$

and thus a plot of i_0/S versus ν cuts the ν-axis at ν_0.

Apker, Taft and Dickey (15) have suggested that an empirical relation

$$i_{ph} \propto (h\nu - \phi)^{m+2} \qquad 3.3.$$

applies to semiconductors, where ϕ is the work function of the semiconductor and m is a constant; Carroll has shown that his treatment will also apply to a semiconductor which obeys this relation.

Another method which has been applied to a determination of the photoelectric work function is that of complete photoelectric emission, derived independently by Suhrmann (176) and Hoy (156), which involves a determination of the photoelectric emission obtained from the specimen when illuminated by blackbody radiation at a number of blackbody temperatures. Herring and Nichols (81) point out that although the method may well give reasonable values for the photoelectric work functions of metals, the thermodynamical assumptions made in the derivation of the theory are most unlikely to be even approximately true in the case of semiconductors.

In the case where a definite peak is obtained in the spectral sensitivity curve it is customary to relate the peak to an energy level at a distance below vacuum potential corresponding to the photon energy at the peak

(46). Moss (6), however, in the case of peaks or plateaux in spectral sensitivity curves occurring at wavelength λ, defines the threshold wavelength $\lambda_{1/2}$ as the wavelength where the sensitivity has fallen to half the value at the peak.

Weissler (10) and Moss (7) have pointed out that a study of the energy distribution of photoelectrons emitted by a semiconductor on irradiation with photons of known energy is required to complete the information which can be gained as to the location and distribution of impurity levels.

3.5. Luminescence

Excitation of a semiconductor by bombardment with electrons or ions, or irradiation with X-rays or the ultra-violet, may lead to the phenomenon of luminescence, a process by which the material dissipates the energy it has absorbed and returns to its original state. The effect includes the emission of radiation during irradiation or bombardment (edge emission has been mentioned in Sec. 3.3.1), and a phosphorescent afterglow which may be observed after the excitation has been removed. The effect is generally associated with the presence of impurity levels, and analysis of the

luminescence spectra of the semiconductor can yield information as to the position of the impurity levels. It may be supposed that an electron excited from the filled band recombines with a hole at an impurity centre (or the impurity centre itself) and the excess energy may be radiated from the centre. This process does not always take the form of the emission of visible radiation; the excess energy may be disposed of by being transferred to the thermal vibrations of surrounding atoms.

If a luminescent material is excited by irradiation or bombardment at a low temperature, and is subsequently heated at a steady rate, the electrons trapped at the various trapping states by the initial excitation will be released by thermal excitation to the conduction band, the electrons in shallow traps being removed at lower temperatures. The transition may be accompanied by the emission of visible radiation, and from the peaks occurring in the light emission versus temperature curve, the distribution of trapping levels can be deduced (149). The study of the thermal quenching of luminescence can be used to correlate optical and thermal activation energies (3).

3.6. Exo-electron emission

An effect related to luminescence is that of exo-

electron emission, first observed by Kramer (106); the subject has recently been reviewed by Grunberg (73). The phenomenon is that of electron emission from substances after a wide variety of treatments, e.g. mechanical deformation, X-ray or ultra-violet irradiation, or electron bombardment. It has been shown that the emission is dependent on the formation of crystal imperfections, and hence donor levels, by the various treatments. Studies of the simultaneous variation of exo-electron emission and luminescence with temperature after low-temperature excitation yield peaks at corresponding temperatures (108), showing a close parallel between the processes.

A somewhat similar effect is obtained in photo-conductivity, and has been briefly mentioned in the previous section. If the semiconductor is excited by photons of a suitable energy at low temperatures, warming the sample in the dark causes the release of trapped electrons, and a conduction current, which varies with temperature in the same way as the luminescence curve, may be observed due to thermal excitation of the electrons into the conduction band. The effect has been treated theoretically by Broser and Broser-Warminsky (30).

Chapter 4 Previous work on photoeffects in the alkaline earth oxides

4.1. Introduction

In this chapter a survey of some of the determinations of the various photoeffects in barium oxide is given, with a view to tracing the historical development of interest in photo-induced effects in the oxide cathode. Not all the published results are quoted: a full discussion has been given in a previous thesis by the present author (116), and here it is only necessary to quote some of the more important experiments and discuss the way in which the workers have made deductions from their results. The way in which an optical energy level scheme for barium oxide can be deduced from an amalgamation of the results of many workers is reviewed in Sec. 4.6, and the published work on calcium oxide is discussed in Sec. 4.7.

4.2. Photoelectric emission

More studies of photoelectric emission from the oxide-coated cathode have been reported than of the other photoeffects, and although less fundamental information can be obtained from them, they will be considered first.

Many of the experiments carried out before 1945 are of little quantitative value: poor vacuum conditions led to much variation in the state of the cathode, and

insensitive instrumentation led to inaccuracy in the measurement of small photocurrents, producing doubtful spectral sensitivity curves. Again, before this date most interpretations of the photoelectric effect were by analogy with the theory of photoelectric emission from metals (cf. Sec. 3.4) and thus figures quoted for the work functions are probably merely arbitrary, depending on the intensity of the illumination and the sensitivity of the instruments used by the observer.

In 1921 Merritt (118) observed that commercial oxide-coated cathode tubes gave an increased emission under illumination, the photoelectric sensitivity increasing towards the violet and ultra-violet. Curves of photo-electric current versus anode potential were found to saturate for potentials both positive and negative with respect to the cathode, i.e. the anode was found to be photosensitive as well as the cathode. Although Case (34) could not detect any photoelectric emission when an oxide cathode was exposed to visible radiation, he found that material evaporated from the cathode on to the anode was photosensitive. A rough determination of spectral sensitivities showed that evaporated BaO had a maximum sensitivity in the light red and orange, SrO in the green and CaO in the far blue: but it should be noted

that these results do not agree with later and more accurate determinations. Photocurrents again showed voltage saturation, and increased over three orders of magnitude when the temperature of the plate bearing the evaporated material was increased from 300 to 700 ^{o}K. Crew (38) confirmed that the photoelectric emission from barium oxide coated filaments was due to the oxide rather than to the base metal: oxide-coated and clean platinum and tungsten filaments were irradiated with light from a mercury arc, and only the oxide-coated filaments gave an appreciable emission. Crew found that the photocurrent - voltage characteristic did not saturate but showed a maximum at an anode potential which apparently depended on the thickness of the oxide coating, but it has been suggested that this effect might have been due to poor vacuum conditions. A rough estimate of the threshold wavelength could be made. Light of wavelength less than 3000 Å (photon energies greater than 4.1 eV) was most effective in causing photoemission, but Crew suggested that longer wavelengths would also produce some photo-emission. It will be observed that later measurements do in fact show a pronounced increase in photoemission at about 4.0 eV.

Newbury (135) and Newbury and Lemery (136) found that

the photocurrent from barium oxide coated filaments saturated, the anode voltage required for saturation depending on the thickness of the coating: no evidence was found for the maximum observed by Crew. The spectral sensitivity of photoemission was determined for a number of lines of the mercury spectrum: a long-wavelength limit to photoemission was estimated at 4000 Å (3.1 eV) with a peak at 3400 Å (3.7 eV) and a sharp rise for wavelengths less than 2500 Å (5.0 eV). The structure near 3.7 and 5.0 eV has been observed by more recent workers, and is undoubtedly a feature of the spectral sensitivity curve; but the threshold at 3.1 eV is, of course, quite arbitrary. Huxford (95) found that the apparent threshold frequency ν depended on the magnitude of the applied electric field E: the relation is of the form

$$\nu = \nu_0 - bE^{1/2} \qquad 4.1.$$

where ν_0 is the zero-field threshold frequency and b is a constant. The effect may be explained in terms of a Schottky lowering of the work function in an electric field. Huxford quotes thresholds in the far red and infra-red ($\sim$ 1.2 eV) for a BaO cathode: he is one of the few early workers whose experiments were sensitive enough to detect photoemission in what is now recognised

as the long-wavelength tail of the intrinsic region, but the threshold figures he quotes have little quantitative significance.

All the early determinations described used d.c. techniques, and measurements of the photoelectric current at temperatures above 700 °K were always doubtful, as the thermionic current increased rapidly above that temperature and tended to mask the photoelectric effect. In 1931 Ramadanoff (148) developed an a.c. technique which allowed the separation of thermionic and photoelectric currents. The cathode is subjected to interrupted illumination: the total anode current is now made up of a d.c. thermionic component and an alternating photoelectric component. By feeding the anode current via a transformer-coupled amplifier to an oscilloscope, only the true photoelectric component is displayed. Ramadanoff, however, confined his experiments to an investigation of the temperature variation of photoelectric emission, of much less fundamental interest than the spectral sensitivity.

In more recent years there has been considerable interest in photoelectric emission from the oxide-coated cathode and in its interpretation in terms of a solid-state model. Muto and Yamashita (130) have given a theoretical calculation of the form of the spectral

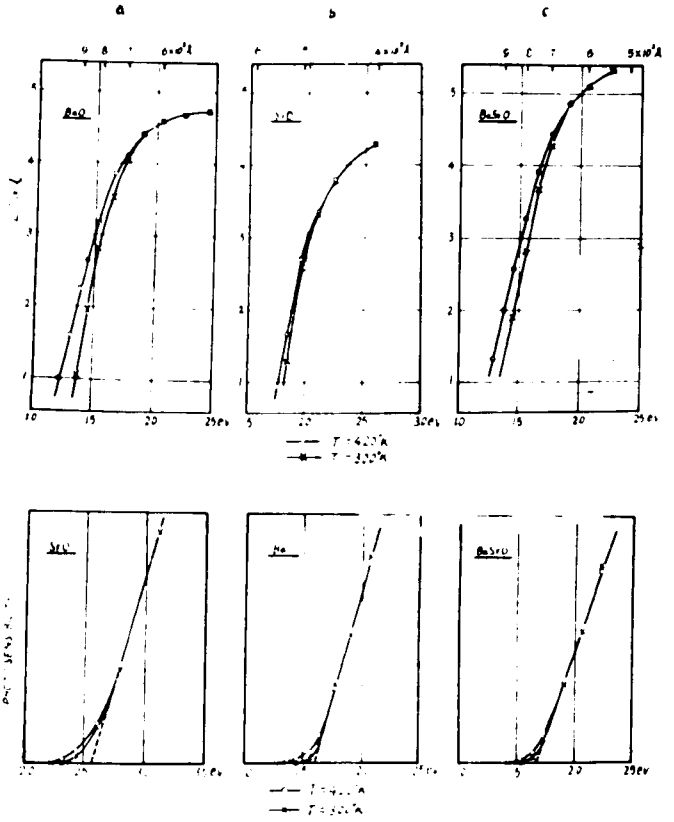

Fig. 4.1 Spectral sensitivity curves for photoelectric emission from BaO, SrO and (BaSr)O (Nisibori, Kawamura and Hirano (137))

sensitivity curve to be expected for a semiconductor with one sharp impurity level, and include the possibility of excitation from the conduction band. It is unfortunate that their paper is extremely condensed, and that an amplified version including details of the calculation and of its assumptions has not appeared. Muto and Yamashita base their calculation on the experimental results obtained by Nisibori, Kawamura and Hirano (137), some of whose spectral sensitivity curves are reproduced in Fig. 4.1. The upper curves are plots of the logarithm of the photocurrent versus photon energy for two cathode temperatures for BaO, SrO and (BaSr)O coated cathodes. It is noted that, as discussed in Sec. 3.4, the form of the curve makes it difficult to assign any sensible value for the threshold photon energy: the curves are nearly linear at low photon energies. However, the Japanese workers observe that for a certain range of photon energies the curves obtained at the different temperatures are coincident, and assume that this coincidence implies that over this range a true photoelectric effect is observed, without thermal effects which displace the characteristic at lower photon energies. They thus deduce a value for the photoelectric threshold by extrapolating the photo-emission characteristics in a linear plot of photocurrent

versus photon energy (lower figures: the vertical axis is labelled "photosensibility" where "photosensitivity" would be the more common western usage, and although no scale is shown on this axis, it is clear from the text that it is an arbitrary linear scale). It is felt that these thresholds are, in fact, quite arbitrary, and the assumption that a portion of the photoelectric spectral sensitivity curve remains unchanged by temperature is certainly not borne out by more recent work (cf. Fig. 4.2.2) (46). Nisibori, Kawamura and Hirano relate the photoelectric work function $\chi' + \Delta E'$ to the Richardson work function $\chi + \Delta E/2$ for barium oxide by taking $\chi = 0.3$ eV, a rather low value, and by assuming that thermal and optical activation energies are equal, i.e. by ignoring the Franck-Condon effect.

Mahlman (115) applied photoelectric sensitivity results to a Fowler plot (Sec. 3.4) and found that the photoelectric work function obtained by this method depended on the applied field, in agreement with the earlier observations of Huxford (95). The zero-field work function was 1.8 eV, but it is felt that this has little significance on semiconductor theory; Mahlman's results were, in fact, a rather poor fit to a curve derived for photoemission from metals.

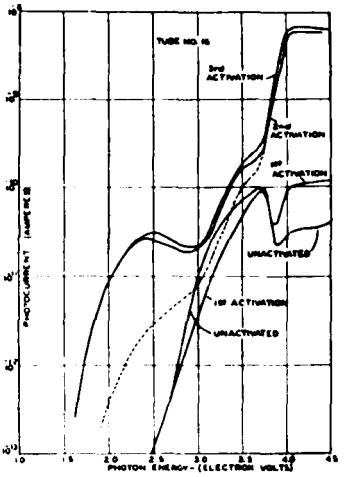

Dependence of photoelectric emission on activation.

Fig. 4.2.1

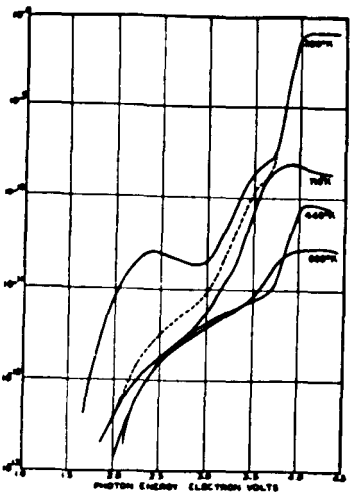

Photoemission from activated BaO—temperature variation.

Fig. 4.2.2

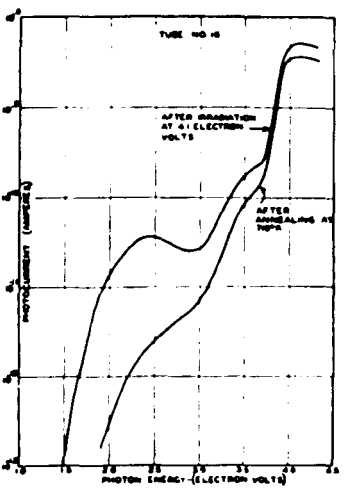

Effect of irradiation and annealing on photoemission.

Fig. 4.2.3

Fig. 4.2 Photoelectric emission in BaO (DeVore and Dewdney (46))

A comprehensive investigation of photoeffects in barium oxide coated cathodes by DeVore and Dewdney (46) included the measurement of the spectral sensitivity of photoemission at various temperatures and in various states of cathode activation (Figs. 4.2.1, 2). Common to all cathode temperatures was an increase in photocurrent in the region of 3.5 - 3.9 eV, which was assumed by the authors to represent intrinsic photoemission. Although considerable differences in the form of the spectral sensitivity curve for photon energies less than 3.5 eV were observed in different activation states, the Richardson work function changed only over a range of 1.87 - 1.97 eV and it was not possible to correlate changes in photoelectric emission with changes in thermionic activity. DeVore and Dewdney observed that previous irradiation of the cathode by ultra-violet light enhanced the photoelectric emission considerably and changed the character of the spectral sensitivity curve, a pronounced peak appearing at about 2.5 eV (Fig. 4.2.3). The enhanced emission decayed slowly at room temperature, but more rapidly at higher temperatures. This enhanced effect was first observed in 1922 (17, 68), but received no attention until recent years. McNary (114) has made a detailed study of the effect, showing that irradiation

by light of visible as well as ultra-violet wavelengths is effective in producing it, and it has also been investigated by Dickey and Taft (49), Noga and Kawamura (138) and Mee (116).

Sakamoto (158) confirmed the spectral sensitivity curve obtained by DeVore and Dewdney, but assigned the 3.9 eV structure to photoemission from surface states. Apker, Taft and Dickey (16) extended the range of observations further into the ultra-violet, measuring both the spectral sensitivity and the energy distribution of the photoelectrons by a retarding potential method in spherically symmetrical tubes. A sharp rise in the photoelectric yield was observed at photon energies of about 5.0 eV, and in conjunction with optical absorption studies (Sec. 4.3) the filled band was deduced to be at a depth of 5.0 eV below vacuum potential, which does not agree with the interpretation of DeVore and Dewdney. The results of Dueker and Hensley (52) and Philipp (144), who used a magnetic velocity analyser to determine the energy distribution of photoelectrons, confirm those of Apker, Taft and Dickey. Extending the measurements to low as well as high photon energies, Taft and Apker (174) found donor states only 0.8 eV below vacuum potential.

Carroll and Coomes (32) and Carroll (33) have applied

the accelerating-field analysis (Sec. 3.4) to photo-emission from a barium oxide cathode. The value obtained for the photoelectric work function, 2.0 eV, presumably indicates the depth of the principal impurity level below vacuum potential. The method has been applied by Mee (116) to a number of BaO cathodes: values of 1.7, 2.0 and 2.1 eV were obtained for three different cathodes.

A number of the earlier investigations have been repeated and more modern theories applied to the results. Narita (133), in a series of experiments similar to those of Case (34), evaporated BaO on to a clean metal plate, and found that for very thin films the photoemission current as a function of photon energy could be fitted accurately to a Fowler plot; for thicker films, agreement was less good. The enhancing effect of pre-irradiation by ultra-violet light was found to depend on the proportion of barium in the evaporated layer. Debiesse and Champeix (43) have also reported on the photosensitivity of evaporated films of BaO on the anode. Biguenet (26) has discussed photoemission from the anode in terms of a thin surface film of barium metal (the evaporated substance undoubtedly contains a high proportion of free barium) which suffers photo-ionisation and thus causes a modification in the work function of the cathode surface.

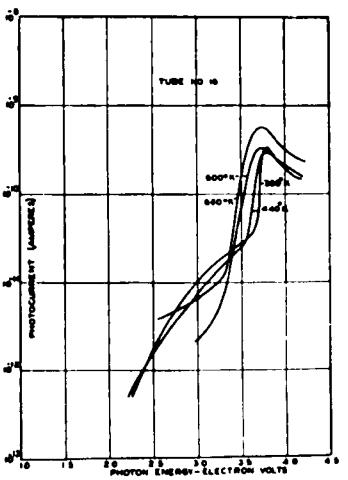

Photoconductivity in unactivated BaO.

Fig. 4.3.1

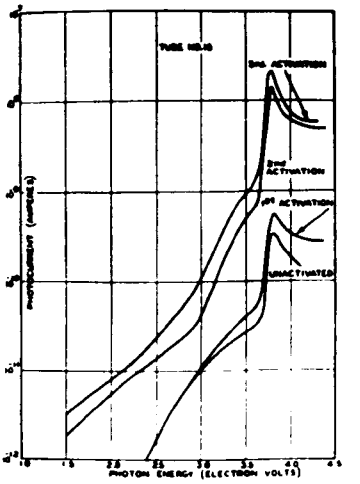

Dependence of photoconductivity on activation.

Fig. 4.3.2

Fig. 4.3 Photoconductivity in BaO

(DeVore and Dewdney (46))

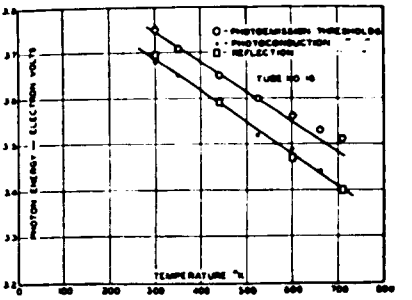

Temperature dependence of threshold energies.

Fig. 4.5

4.3. Optical absorption and photoconductivity

Rather less information has been published on the optical absorption of and photoconductivity in barium oxide coated cathodes. DeVore and Dewdney (46), using probe diodes, found a large increase in photoconductivity at about 3.7 eV (Fig. 4.3). Optical absorption could be studied by shining monochromatic radiation on to the cathode surface and comparing the relative intensities of the incident and reflected light; a pronounced decrease in reflectivity, showing an increase in absorption, was also found at 3.7 eV. A later determination by DeVore (47) investigated the effect of activation of the cathode by studying the development of the long-wavelength tail of the photoconductivity curve. DeVore deduced the presence of two photoconductivity thresholds, at 2.3 and 1.4 eV, although his method of determination (by linear extrapolation of a plot of photoconductivity current versus photon energy) is open to criticism. Ortusi (141), in a theoretical discussion of the nature of the donor centres in the oxide cathode, suggests that the 2.3 eV threshold is due to oxygen vacancies, while the 1.4 eV level may be due to colloidal barium. Sakamoto (158) confirmed the spectral sensitivity curve of DeVore and Dewdney and found that irradiation with the ultra-violet

produced an enhanced photoconductivity current at 2.4 eV, similar to the enhancement found in external photoelectric emission. Additional structure at 2.0 eV was found by Mee (116).

Following the successful production of single crystals of barium oxide (173) a number of determinations of photoconductivity and optical absorption in single crystals, as compared with the porous polycrystalline structure of the cathode, have been made. Tyler (180) and Tyler and Sproull (182) found an increase in optical absorption at about 3.8 eV, accompanied by photoconductivity; this structure was attributed to exciton formation. A further increase in absorption starts at about 4.8 eV. Dash (41) studied the effects in the visible and near infra-red, and found that absorption structure, accompanied by photoconductivity, can be induced at 0.8, 1.4, 2.0 and 2.6 eV by ultra-violet or X-ray irradiation or by additive coloration with excess barium. Kane (100) found a temperature-dependent absorption with a maximum at 2.4 eV in deep red crystals of BaO, and attributed the level to interstitial barium or to oxygen vacancies. Sproull, Bever and Libowitz (174) have observed the diffusion of colour centres in BaO crystals, and their work suggests that the 2.0 eV band observed by Dash is due to oxygen vacancies.

A number of determinations of optical absorption in films of barium oxide evaporated on to glass or quartz have been reported. Although the structure and composition of evaporated films are very different from those of the cathode or single crystals of BaO, the absorption spectra obtained show certain similarities to those previously discussed. Tyler (181) found a strong absorption threshold at 3.8 eV; Takazawa and Tomotika (178) found the threshold to be at a slightly higher photon energy, 3.9 eV, and observed a second rapid rise in absorption at about 5.0 eV, with two bands at 4.2 and 4.5 eV. In the presence of oxygen, the film becomes transparent for photon energies under 5.0 eV. Okumura (140) generally confirmed these results, finding that absorption bands begin at 4.0 eV and 5.0 eV, with peaks at 4.1 and 4.4 eV distinguishable in the first band. Zollweg (200) investigated the optical absorption of a barium oxide film at temperatures between 15 and 650 ^{o}K. Below 60 ^{o}K four peaks could be resolved between 3.8 and 4.5 eV, and the strongest ones were thought to be due to exciton absorption. Further measurements (201) extended the measurements to about 5 eV. In the region of lower photon energies, Mee (116) found peaks in the absorption spectrum at 2.0 and 2.6 eV for an evaporated film of BaO, and a peak at 2.0 eV for a

FIG. 4.4. OPTICAL ACTIVATION ENERGIES FOR BaO – COLLECTED RESULTS

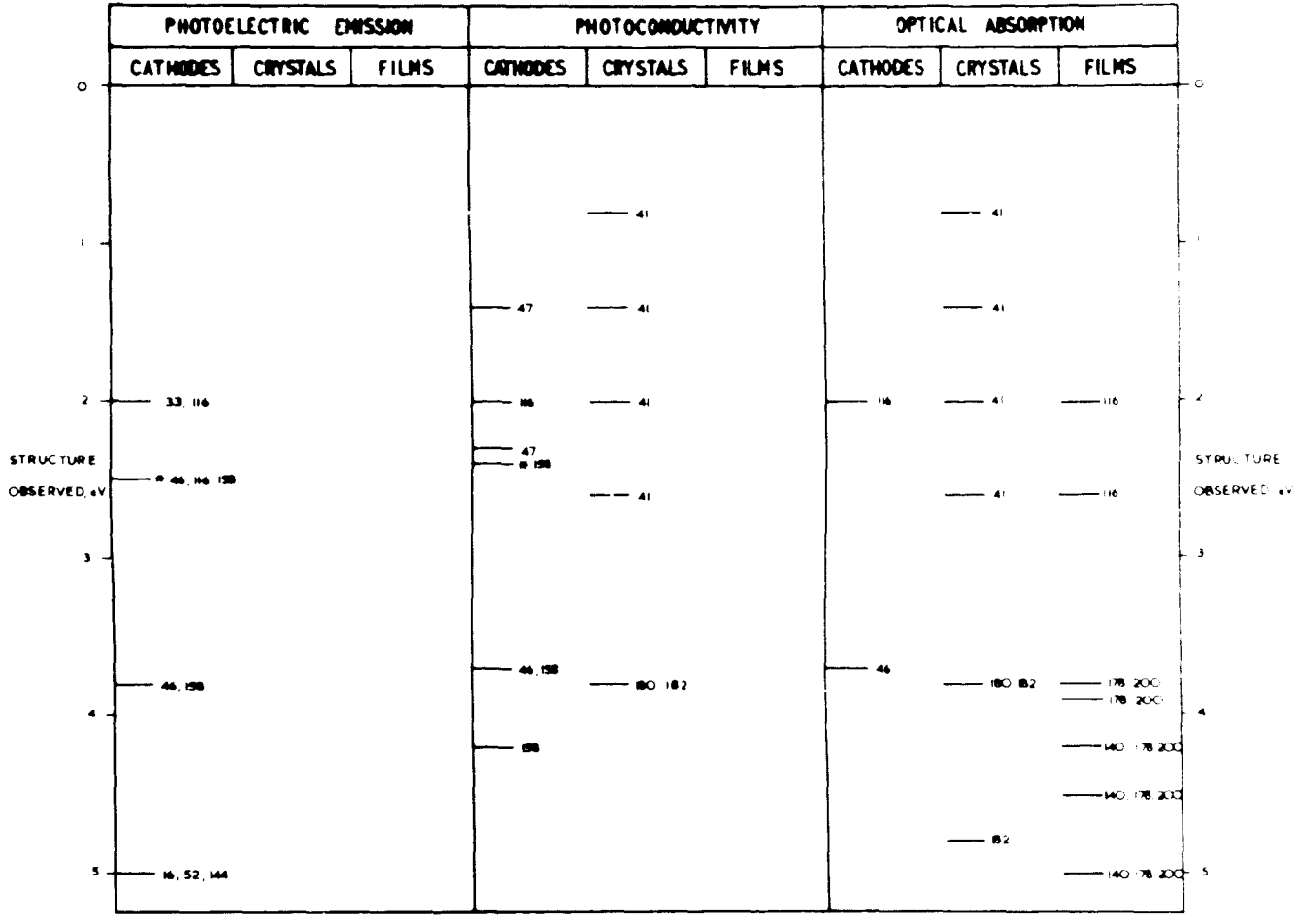

BaO cathode, measured by the reflectivity method.

4.4. Luminescence

Few measurements of the luminescence spectra of barium oxide are reported, and correlation with other optical information is not easy.

An early investigation was by Ewles (57), who found peaks at 2.1, 2.3 and 2.7 eV. Stout (175) bombarded a cathode sample, which could be maintained in vacuo at temperatures above and below room temperature, with electrons of 1.5 keV energy, and found luminescent bands in cathodes of varying states of activation at photon energies of 3.6, 3.0, 2.7, 2.3, 2.1, 1.9 and 1.8 eV. Stout suggests that the 3.6 eV band may be due to donor levels at 3.6 eV above the filled band, while the 2.7 eV band may arise from acceptor levels at 2.7 eV below the conduction band; the other bands remain unallocated. Noga and Nakamura (139) bombarded BaO samples with 250 volt electrons, and observed cathodoluminescent bands at 2.7, 2.5, 2.2, 2.1 and 1.9 eV, in general agreement with some of the bands found by Stout.

4.5. Optical energy level scheme for barium oxide

Fig. 4.4 shows the collected results of the determinations reviewed in the previous sections. The

numbers represent the references, and are placed at points on the vertical energy scale corresponding to the structure found. In each of the three classes of determination - photoemission, photoconductivity and optical absorption - the results are allocated to groups depending on the nature of the barium oxide sample. Photoelectric emission results quoted refer to definite structure in the spectral sensitivity curve, and arbitrary thresholds are omitted.

Since the results are for such a wide variety of samples in quite different states of activation and impurity concentration, exact agreement between levels in any class for results from cathodes, single crystals and evaporated films would not be expected. In fact, for certain levels agreement is surprisingly good. A general correspondence between levels for photoconductivity and optical absorption is expected theoretically (Sec. 3.2) and is observed in practice.

Another point of correspondence is between photoemission and photoconduction levels. DeVore and Dewdney (46), comparing the structure at about 3.7 eV for photoemission with that for photoconductivity and reflectivity, found that the thresholds had the same temperature coefficient and differed by only about 0.05 eV over a range of temperatures from 300 to 700 ^{o}K (Fig. 4.5). The

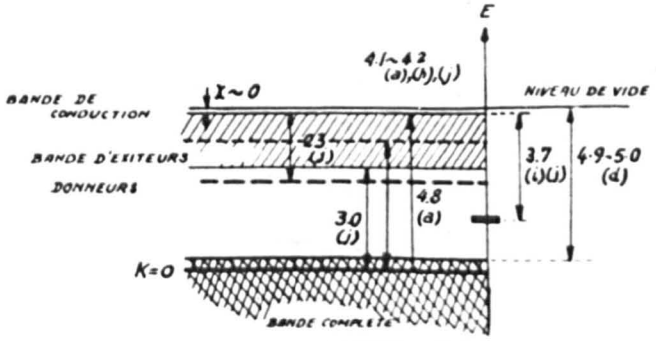

Fig. 4.6

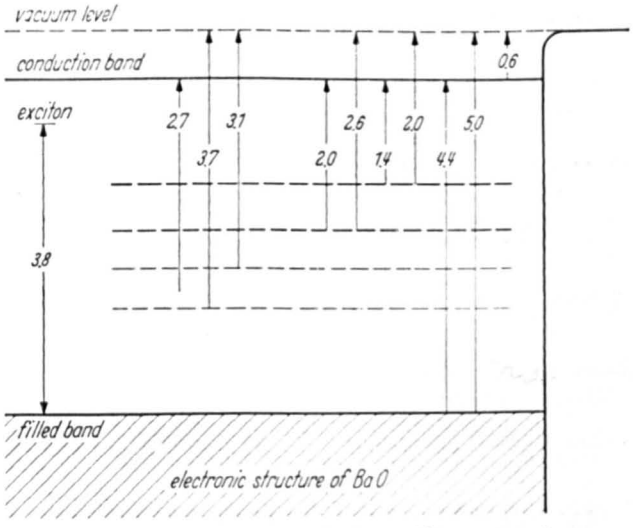

Energy level diagram for barium oxide as prepared by HENSLEY. Energies expressed in ev.

Fig. 4.7

enhanced peak at about 2.5 eV which can be induced by ultra-violet irradiation occurs in both photoemission and photoconductivity (158). This general similarity between the levels led Sakamoto (158) to suppose that the external work function χ' must be practically zero. On the basis of this assumption he put forward an energy level scheme (Fig. 4.6) showing the main energy levels found by other workers. The scheme is not entirely satisfactory, for Sakamoto assumes that the 3.7 eV peak is due to cathode surface states, suggesting that it is found only in cathodes and not in single crystals: he must, however, have overlooked the results of Tyler and Sproull (182).

Another diagram has been prepared by Hensley (79) (Fig. 4.7). He appears to have neglected the similarity between photoelectric emission and photoconductivity levels and assumes a value of 0.6 eV for χ'. The justification for this is not obvious, and it seems possible that Hensley has merely used a value commonly deduced from thermionic emission and dark conductivity studies (Sec. 2.5).

An alternative energy level scheme based on the main results is given in Fig. 4.8. It is assumed, following Sakamoto, that χ' is very small. Much of the structure

FIG. 4.8. ALTERNATIVE OPTICAL ENERGY LEVEL SCHEME FOR BaO

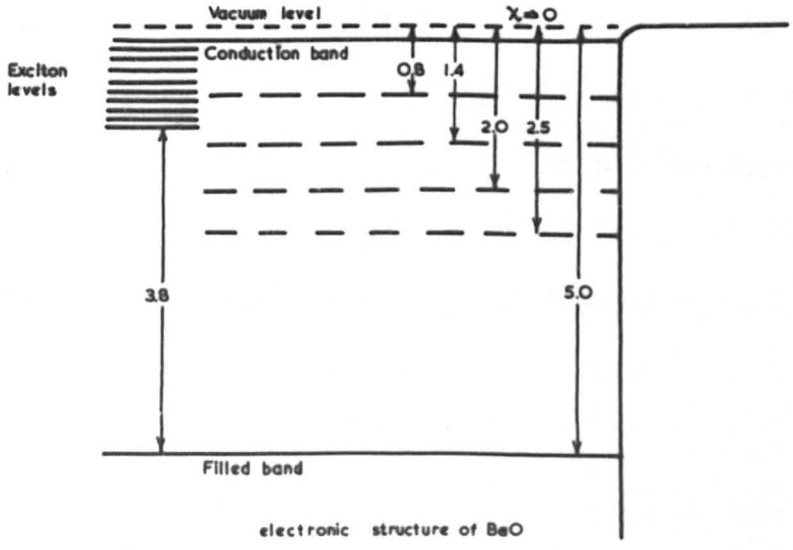

electronic structure of BaO

Energies expressed in eV

at high photon energies has been ascribed to exciton-induced absorption: thus a series of exciton levels starting at 3.8 eV above the top of the filled band is introduced, the total depth of the top of the filled band below vacuum potential being about 5.0 eV. As χ' is small, exciton-induced photoemission can take place from the same levels as exciton-induced photoconductivity. It must be pointed out that this diagram merely represents a combination of information from various sources, and it will appear from later work (Chap. 8) that photo-conductivity results must be critically re-assessed.

4.6. Correlation of optical and thermal information for barium oxide

Although the Franck-Condon principle forbids, in general, the direct equivalence of thermal and optical activation energies, a certain similarity would be expected between the two schemes, subject to a scaling factor. In the case of the energy level schemes for barium oxide, two difficulties are encountered. The first, and most obvious, relates to the external work function. On the thermal scheme it is customarily supposed to lie between 0.5 and 1.0 eV, and, indeed, must be of this order of magnitude unless the interpretation of

conductivity and emission results is incorrect. On the other hand, fairly strong experimental evidence suggests that it must be small, certainly less than 0.1 eV, in the optical case. The reasoning of Sakamoto (158) is not easy to follow, but it appears that he may offer an explanation of the fact that the external work function is very small in the optical case. He points out that if an appreciable portion of the apparent photoconductivity current is carried by photoelectrons which travel through the pores of the coating, rather than by true photoconductivity electrons which pass through the crystallites themselves, the apparent photoconductivity current will be, in reality, a photoemission current in the pores of the matrix. Thus the spectral sensitivity curves for photoconductivity and photoemission in a cathode should be very similar in structure. No experimental proof of this hypothesis was offered.

This extension of the Loosjes-Vink hypothesis of dark conductivity to photoconductive effects is investigated in greater detail, with special reference to calcium oxide coated cathodes, in the course of the present work. It should be pointed out that Sakamoto does not consider all the evidence available from single crystal measurements, and the agreement between single

crystal and cathode experiments is not emphasised by him. Although the experimental work carried out in the course of the present work is in favour of the Sakamoto hypothesis, the features of agreement between results obtained with porous cathodes and non-porous single crystals of barium oxide suggest that both a pore and a solid photoconductivity process may operate in parallel.

The second difficulty relates to the Franck-Condon scaling factor. Although a number of the early workers, particularly in the field of photoelectric emission, used their arbitrary thresholds (taken as being equal to $\chi + \Delta E$) to attempt a direct correlation with the thermionic work function ($\chi + \Delta E/2$), such agreement as was obtained can only be, at the best, fortuitous. But attempts to reconcile the optical and thermal information by means of the Mott and Gurney approximate scaling factor ϵ/ϵ_0 are not very successful. For BaO, the refractive index is about 2.0 (74), so the optical dielectric constant is about $2.0^2 = 4$. Two quite different values have been quoted for the static dielectric constant, 14 (4) and 34 (25). The value of 14 was found by extrapolation from values obtained for the other alkaline earth oxides (86), and it has been suggested (25) that these values may be unreliable: thus the extrapolated value is

likely to have little significance. The value of 34 was obtained by measurement in an experimental arrangement in which precautions were taken against the conversion of oxide to hydroxide: readings were taken over a frequency range from 60 to 6×10^7 c.p.s. In this case, too, extrapolation was used to find the static dielectric constant, and there was evidence that the value of the dielectric constant might be greater than 34 at low frequencies. Thus the two possible values of ϵ_o lead to values of ϵ/ϵ_o of about 0.29 and 0.12. If we take the maximum depth of the top of the filled band below vacuum potential as 5.0 eV, for which there is strong experimental evidence from photoelectric information, using the two Franck-Condon scaling factors the corresponding depths on the thermal scale would be 1.4 and 0.6 eV. The fact that Richardson work functions for thermionic emission from unactivated BaO cathodes are often greater than 1.4 eV shows that a direct correlation between optical and thermal information, using the Mott and Gurney approximation, is impossible: the impurity level from which thermionic emission originates cannot be fitted into the theoretical forbidden energy zone.

Reasons for this discrepancy may be examined. It is possible that the structure at 5.0 eV observed in the

optical absorption and photoemission spectra of BaO does not represent the onset of intrinsic absorption, but may be merely another exciton level, intrinsic absorption occurring at even higher photon energies. The experiments of Zollweg (201) would suggest that this is most unlikely. The uncertainty in the value of ϵ_o allows the conversion factor to take two quite different values: but for ϵ/ϵ_o to be large enough to make a sensible correlation ϵ_o would have to be rather less than 14, the less favoured value of ϵ_o quoted in the literature. The discrepancy may well lie in the use of the rather simplified model used by Mott and Gurney.

It is customary to invoke the idea of surface energy states to explain apparently paradoxical results obtained with the oxide cathode. In this case, although photoelectric emission from and optical absorption in surface levels of the oxide crystallites may well be quite different from the effects in the oxide in bulk, the fact that some degree of agreement is obtained between results from oxide samples prepared in widely differing ways - the porous oxide cathode coating, for example, yields similar photoconductivity results to single crystals of the oxide, despite the considerable difference in the surface to volume ratios of the two systems - suggests that

the main optical features discussed are probably properties of the bulk oxide rather than of the surface.

4.7. Photoeffects in calcium oxide

It has been necessary to devote some time to a discussion of the photoelectric properties of barium oxide, for calcium oxide has not received the same attention as the other alkaline earth oxides in investigations of photoelectric effects.

A determination by Berger (24) of photoemission from a number of oxides included calcium oxide, but no results were quoted as difficulty was found in obtaining reproducibility. Hopkins (87) observed a pronounced photoconductivity current when a CaO cathode was exposed to bright sunlight, with a further enhancement when irradiated with ultra-violet light. No measurement of the spectral sensitivity was attempted. A blue coloration of the cathode was also observed after use, and it was suggested that this may show the presence of colour centres analogous to F-centres in the alkali halides.

A number of determinations and theoretical discussions of the luminescence spectra of pure calcium oxide and of calcium oxide activated with various impurities have been reported (57, 58, 157). Interpretation in terms of the energy level scheme is difficult, as with barium oxide.

FIG. 5.1.1. THE VACUUM SYSTEM

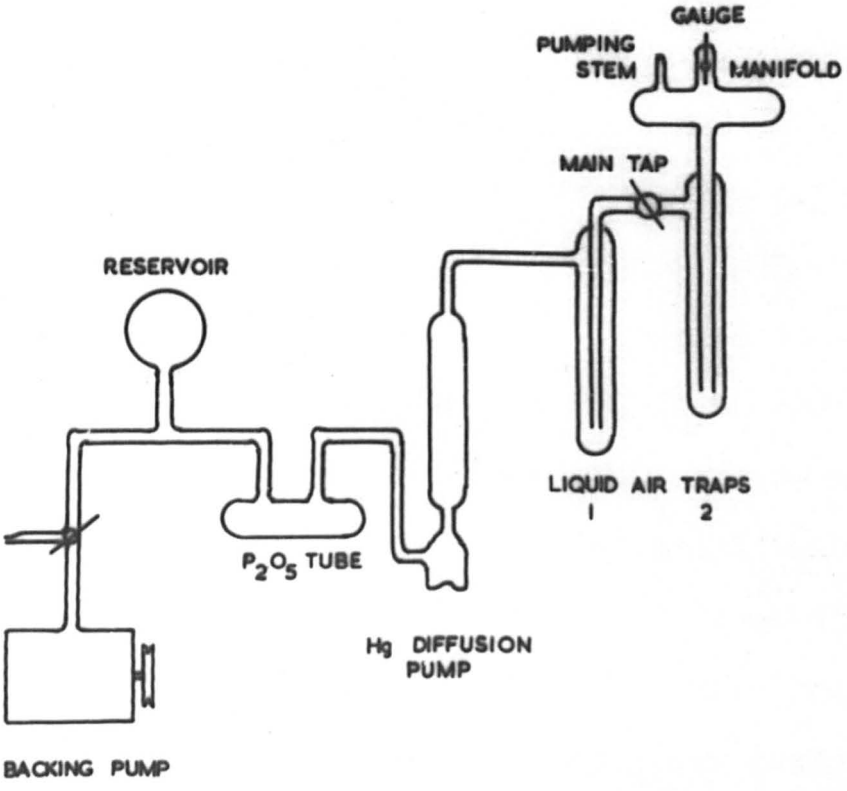

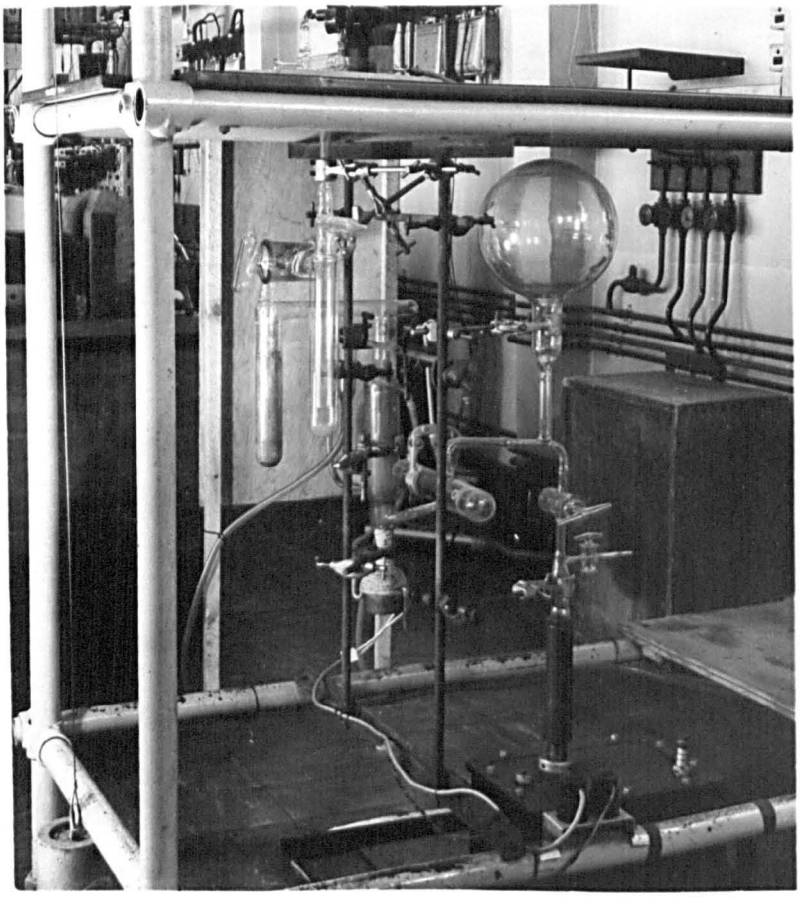

Fig. 5.1.2 The vacuum system

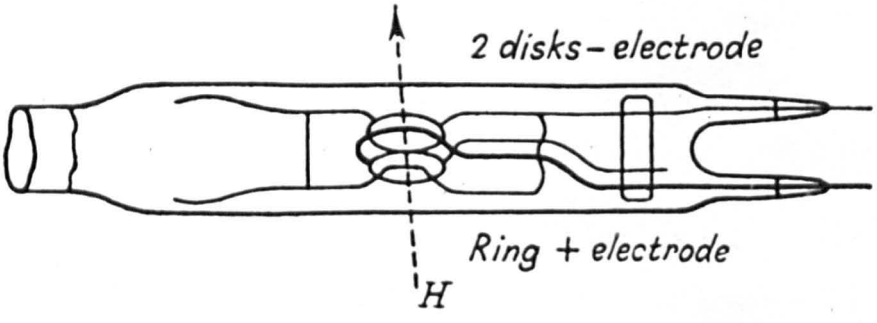

Fig. 5.2.1 Penning gauge

PART III

Chapter 5 General experimental techniques

5.1. Introduction

Although several different effects in calcium oxide coated cathodes have been studied in the present work, and different designs of experimental tube have been necessary, a number of techniques have been common to all of them. Thus most tubes are subjected to the same schedule of vacuum processing, and the techniques for studying the electrical and photoelectric properties are similar from tube to tube. The general techniques are discussed in this chapter.

5.2. The vacuum system

It has already been mentioned that poor vacuum conditions made much of the early work, both in thermionic and photoelectric studies, of doubtful value. The vacuum system employed in the present work was designed so as to remove as quickly as possible the large volume of gas evolved during the breakdown and activation processes and to attain a low ultimate pressure, less than 10^{-6} mm Hg.

The hard-glass system is illustrated in Figs. 5.1.1 and 5.1.2. The Edwards Speedivac Type 2 two-stage rotary backing pump is connected via a 3-litre reservoir and a phosphorus pentoxide drying tube to a single-stage mercury

diffusion pump, with a pumping speed of the order of 1 l sec $^{-1}$. Connected to this pump are two liquid air traps in series; between them is the 20 mm bore main tap. The central tube of the second trap passes through an asbestos table to the pumping manifold, which bears an ionisation gauge and a stem for the experimental tube. The connecting tubes are as short and as wide as possible.

The glassware is securely clamped to a tubular steel frame which carries at one end the asbestos table and, at the other, power-packs and other equipment used in the processing of the tubes. A counterpoised oven, whose temperature is controlled by a Sunvic unit, may be lowered over the tube when it is attached to the manifold.

The ionisation gauge is of the Penning (143) type (Fig. 5.2.1). It consists of two parallel circular nickel plates separated by a distance of about 1 cm forming the cathode, and a ring anode between the plates. A magnetic field of about 600 oersted is applied between the plates and perpendicular to them by a small permanent magnet. A potential difference of 2 kV is applied between the anode and cathode: a discharge results, and the electrons move in long helical paths to the anode, and may oscillate about it. There is thus a fairly high probability of ionisation of the gas in the gauge by

FIG. 5.2.2. PENNING GAUGE CALIBRATION CURVE USING AIR

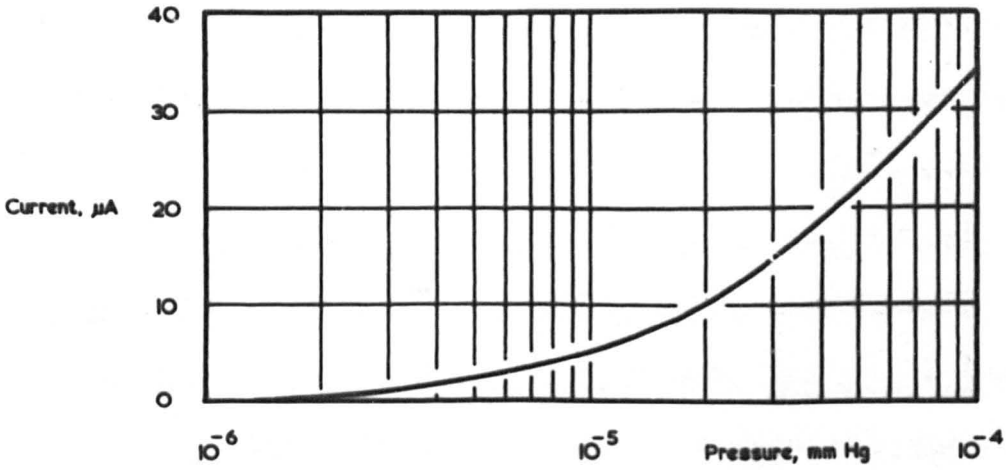

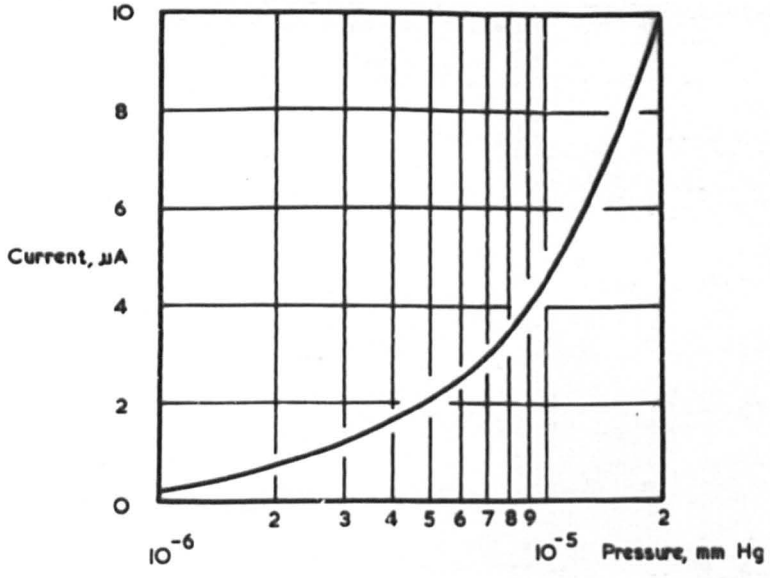

collision, a measurable ionisation current being produced even at low pressures. A calibration curve for such a gauge is given in Fig. 5.2.2. Ion currents are measured approximately with a 0 - 500 μA meter fitted on the power-pack, and more accurately with a Tinsley multi-range microammeter.

It should be noted that the gauge used in the system has not been calibrated against a Macleod or other type of standard gauge. Its use here is more to indicate orders of magnitude than to give a precise measurement of pressure.

5.3. Preparation of the experimental tubes

A large proportion of the tubes constructed for the present work were of the probe diode type, and a description of the method of construction of the standard type of tube will be given in this section. Modifications necessary to carry out particular experiments are discussed in the relevant experimental chapters.

It is important that all components of a tube should be as clean as possible at all stages of assembly. Initially, metal parts are cleaned by heating to redness in a stream of hydrogen, and the glass envelope of the tube is cleaned with chromic acid and distilled water. When the tube is attached to the vacuum system, it is

baked out at 400 °C to remove gas adsorbed on to the glass; baking is repeated after the carbonate has been broken down to oxide. The anode and other metal parts inside the tube not provided with electrical heaters are outgassed by heating to redness with an r.f. heater. Barium getters, fired immediately after sealing off the tube from the pumps, are also carefully outgassed. Before sealing off, the glass stem is heated gently with a luminous flame. Tubes are not normally sealed off until the indicated pressure is less than 10^{-6} mm Hg. Firing the getters after seal-off should reduce the pressure considerably.

5.3.1. Construction of a probe diode tube

The cathode base of a probe diode is a 68 mm long '0'-nickel tube of 2.5 mm external diameter. This tube has a 0.095 mm tungsten wire welded to it internally to form the hot junction of a thermocouple for the measurement of cathode temperatures. The tube bears 24 swg nickel supports at top and bottom, together with four thin nickel tapes which serve to hold the ceramic probe supports securely to the base. The cathode heater consists of two hairpin heaters of 0.18 mm diameter tungsten wire, insulated by twin hole ceramic tubes,

FIG. 5.3. PROBE DIODE ASSEMBLY

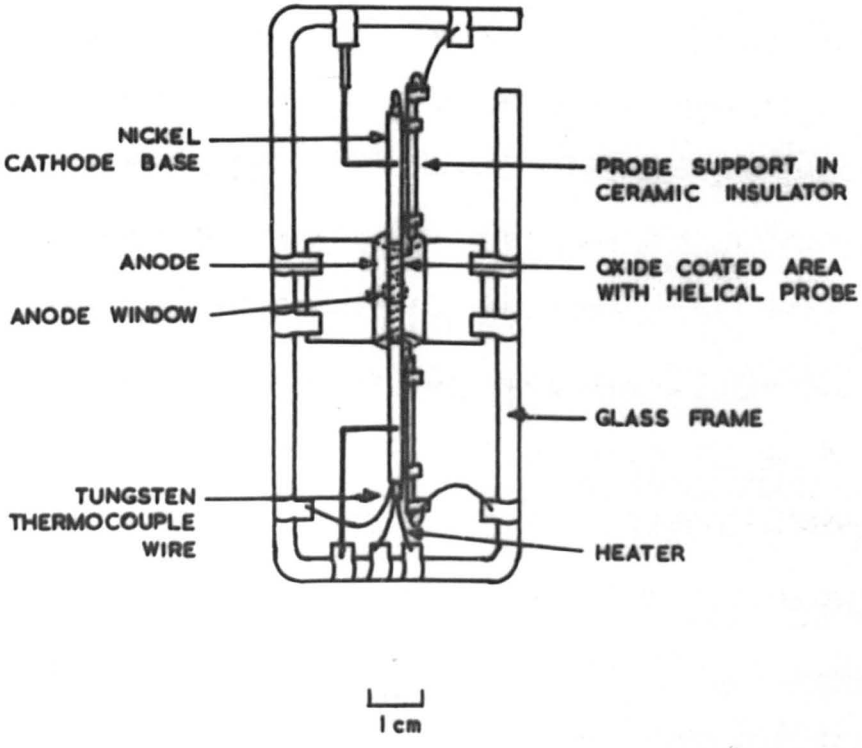

connected in parallel. The cathode base is hydrogen furnaced before the first layer of carbonate suspension is sprayed on, using a rotating jig and masks to confine the sprayed portion to the central 2 cm length of the cathode base. The thickness of the first layer can be checked by an optical projection method, and is usually about 50 μ. The probe supports are 3 cm long, 1 mm external diameter ceramic tubes: after the first spray, a 32 swg nickel wire is passed down the centre of each so as to project slightly over the coated area of the cathode, and the other end of the wire is welded to a nickel tag on the ceramic support. The probe consists of from 5 to 10 turns of 0.0005 " diameter '0'-nickel wire, wound closely over the coating and welded to the wire supports at each end. A further layer of carbonate suspension is sprayed over the probe so that before breakdown the thickness is about 100 μ.

The cathode assembly is now attached to a glass frame, shown in Fig. 5.3. Connections are made to nickel tags bent round the frame. The upper cathode support slides in a nickel tube to allow for thermal expansion effects when operating. The cylindrical anode of '0'-nickel sheet, prepared in two halves, in one of which is pierced a small circular window, is hydrogen furnaced

and attached to the glass frame.

The glass frame is attached to a commercial FK 10 seven lead pinch, using 24 swg nickel wire to make connections from the pins to the metal tags on the frame. Two barium getters are attached to the frame in positions convenient for r.f. heating. A C 9 glass envelope is drop-sealed to the pinch, and the tube is attached to the pumping stem on the vacuum system.

The pinches and envelopes were supplied by the Siemens-Edison-Swan Co., Ltd.

5.3.2. Cathode processing

After attachment of the tube to the vacuum system, it is baked out at 400 ^{o}C for at least 4 hours. Gas from the glass envelope may have been adsorbed on to the metal parts: to remove it, they are r.f. heated to redness while the glass is still hot ($\sim$ 100 ^{o}C).

In order to convert the calcium carbonate completely to oxide, the temperature of the cathode must be raised to about 1100 ^{o}K. This can be done by slowly increasing the voltage supplied to the heater, but great care and patience must be exercised. Too rapid heating of the cathode causes rapid evolution of gas in the thick cathode coating, which in the extreme case may crack or flake away from

the base. Heater supplies are obtained from a Variac transformer, connected to the primary of a 20 : 1 step-down transformer, giving 0 - 12 V a.c. The Variac is driven through reduction gearing by a d.c. electric motor, whose speed may be controlled by the input voltage. When the motor is run at 100 V to give its maximum speed, the cathode temperature can be raised from about 900 to 1100 ^{o}K in about 6 hours; at 24 V, it takes about 48 hours.

The breakdown procedure is as follows. The cathode temperature can be increased fairly rapidly to about 700 ^{o}K by turning the Variac by hand. A further increase to about 900 ^{o}K, where evolution of gas commences, should be made less rapidly, over a period of about 2 hours. The power drive is now engaged and the final increase, to about 1100 ^{o}K, is arranged to take place over a period which depends on the type of cathode, probe diodes requiring the longest. The temperature is held constant at 1100 ^{o}K until the pressure in the system decreases to between 10^{-5} and 10^{-6} mm Hg, when the temperature can be reduced, either slowly by hand or by the power drive. When the cathode has cooled, the tube is rebaked. This is followed by further r.f. heating of the anode, to remove adsorbed carbon dioxide. During this process the cathode is also raised to red heat.

The tube may now be sealed off and the getters fired, but it is often convenient to at least commence the process of activation while the tube is still being pumped. In the present work the activation process adopted is that of drawing emission current (Sec. 1.3). The cathode temperature is held constant at about 1000 ^{o}K and an anode potential of 100 V is applied. Normally the emission current suffers an initial fall and then increases until it reaches a steady value.

5.4. Measurement of cathode temperature

The cathode temperature is measured by determining the thermoelectric e.m.f. developed between the hot and cold junctions of the tungsten-nickel thermocouple provided at the cathode base. The hot junction is the internal weld between the tungsten wire and the nickel cathode base: the cold junction is formed outside the tube, and may, for certain determinations, be maintained at 0 ^{o}C by an ice - water mixture. In many cases the cold junction is merely exposed to room temperature. The e.m.f. is measured with a Croydon Precision Instrument Company thermocouple potentiometer, reading to 0.01 mV up to 21 mV and to 0.05 mV above this.

During the course of the present work doubts were

FIG. 5.6. TUNGSTEN-NICKEL THERMOCOUPLE CALIBRATION CURVE

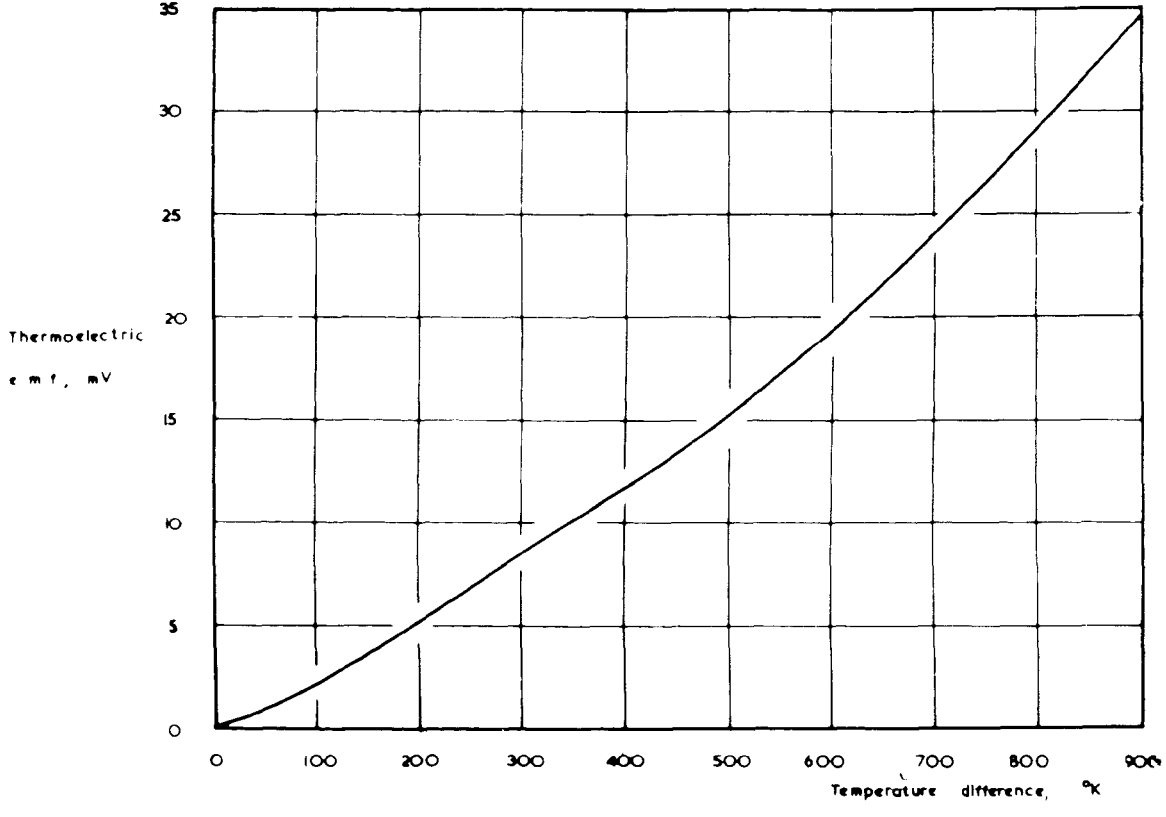

felt as to the reproducibility of temperatures measured with different W-Ni thermocouples. Twelve tubes were constructed in which the e.m.f. set up between a hot and a cold junction was measured on a tungsten-nickel and a chromel-alumel thermocouple, the e.m.f.-temperature relationship of which is known (74). There is some evidence that the e.m.f. depends on the state of the weld at the junction and whether it has been subjected to hydrogen furnacing. The calibration curve given (Fig. 5.6) is the mean of the twelve comparative determinations with the chromel-alumel couple. The thermocouple gives the temperature of the nickel cathode base, and not the calcium oxide coating; there is evidence from electrical conductivity and thermoelectric power measurements that there may be a temperature drop of the order of 10 ^{o}K across the coating at cathode temperatures of about 1000 ^{o}K (Secs. 6.3.2, 6.4).

5.5. Emission and conductivity measurements

As has been pointed out previously, even in a thermionically active state calcium oxide has a low thermionic emission and electrical conductivity compared with the other alkaline earth oxides, and at a given temperature currents are at least two orders of magnitude

FIG. 5.4.1. ELECTROMETER CIRCUIT

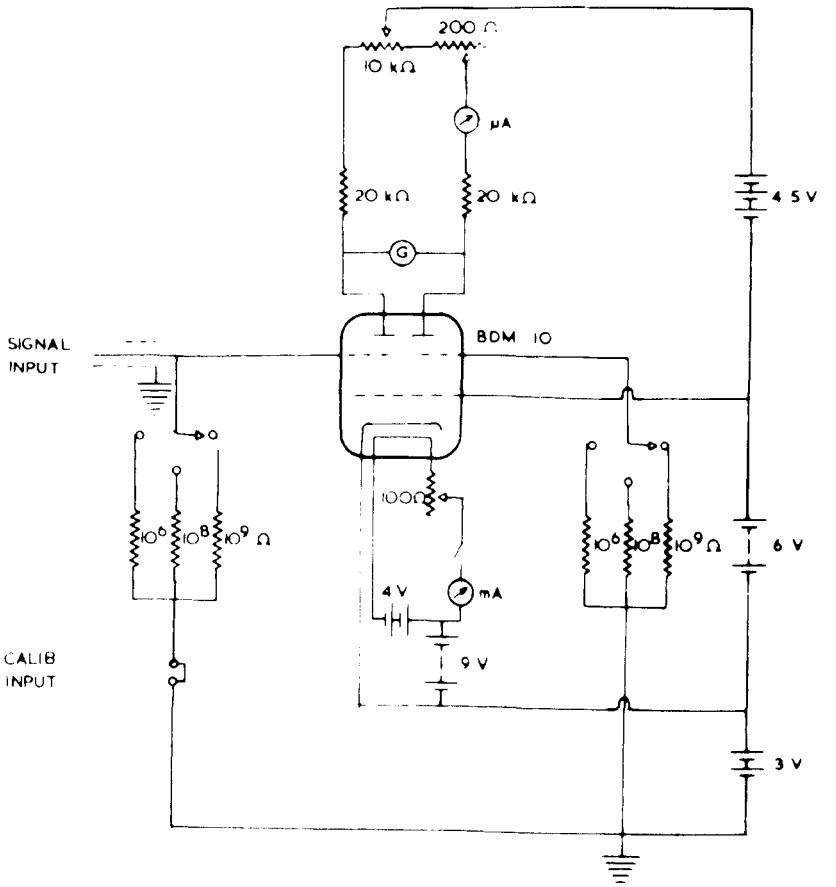

FIG. 5.4.2. ELECTROMETER CALIBRATION

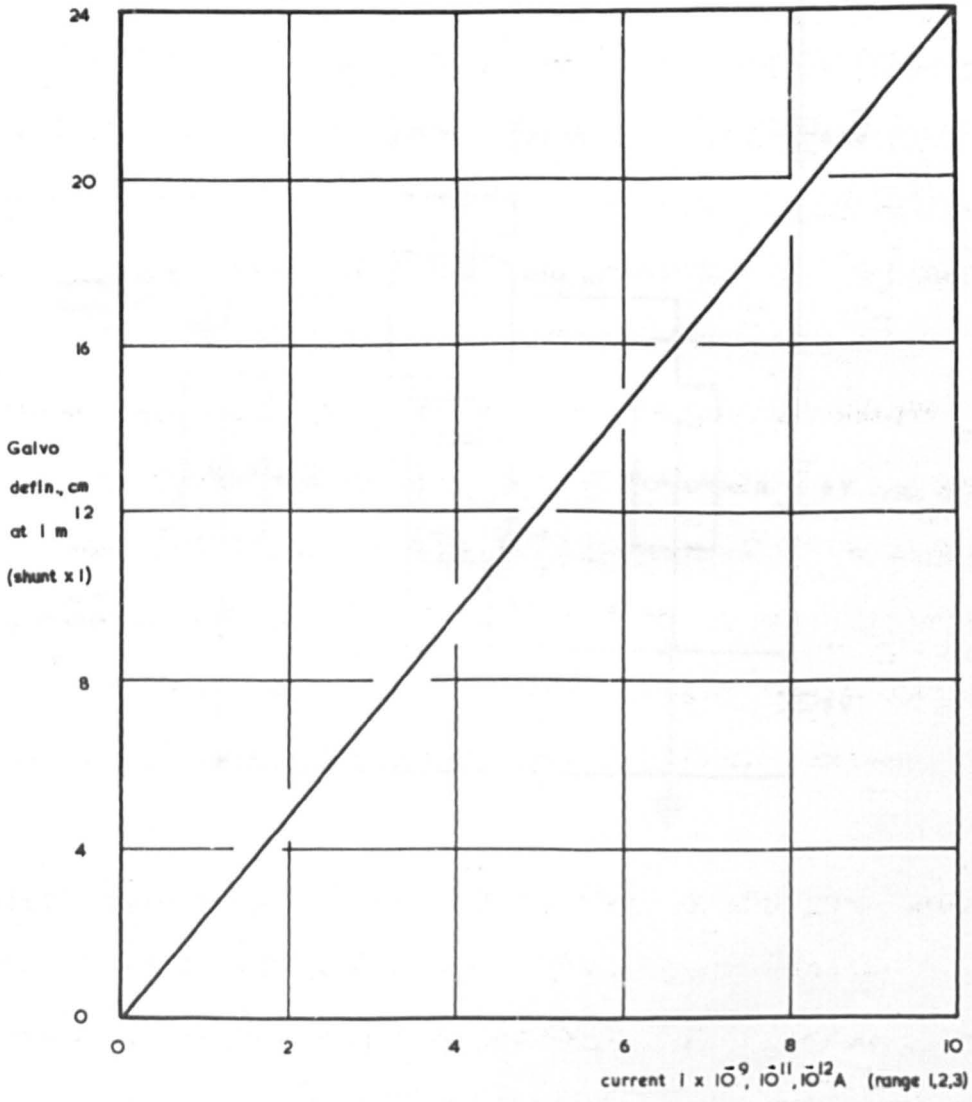

smaller than with barium oxide. The electrometer constructed by Hopkins (87) to measure currents down to 10^{-12} A has been used in the present work. The circuit (Fig. 5.4.1) was designed around a Ferranti BDM 10 double beam tetrode, using half of the valve as a reference circuit. A small current passing through one of the input resistors of 10^6, 10^8 or 10^9 ohms causes a change in the control grid voltage; this produces an out-of-balance current between the two halves of the valve, which is registered on the sensitive galvanometer G. The galvanometer used in conjunction with the electrometer is a Cambrell instrument, of current sensitivity 1.07×10^{-8} amp cm^{-1} at 1 metre, and resistance 1125 ohms, which can be used with a universal shunt. A calibration curve for the electrometer is given in Fig. 5.4.2.

For purposes of screening, the experimental tube is normally placed in a heavy steel box, the leads to which are made as rigid as possible and are carefully screened. Heater supplies are obtained from the a.c. Variac supply already described, or from batteries. Thermionic emission measurements are made by applying d.c. voltages from a potentiometer unit with coarse and fine controls and measuring the anode current; potentials are measured

FIG. 5.5. POTENTIOMETER UNIT CIRCUIT

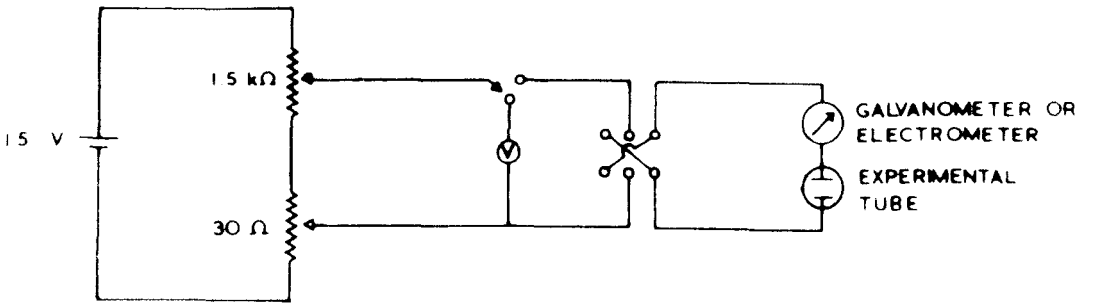

with a Crompton universal indicator, fitted with a suitable multiplier. The circuit (Fig. 5.5) is arranged so that the voltmeter is removed from the circuit before the potential is applied to the anode.

For conductivity measurements, it is normal to apply potentials up to $\pm$ 100 mV between the probe and cathode base, but occasionally a greater voltage is used. Provision is made in the screened box for reversing the polarity of the applied potential.

5.6. Light sources and photoelectric measurements

A 240 volt, 500 watt tungsten filament lamp, mounted in a metal lamp-house with an electric blower unit to prevent over-heating, is used as a source of white light. In some applications, a 250 watt high-pressure mercury arc is used.

Monochromatic illumination in the wavelength range 9000 - 4000 Å (1.4 - 3.1 eV) is obtained using a Hilger constant deviation spectrometer, Model D.186, as a monochromator in conjunction with the tungsten filament source. The narrowest possible exit slit is normally used, which passes a band of wavelengths of the order of 80 Å at 5900 Å: in order to obtain sufficient illumination of the specimen, a rather wide entrance slit must

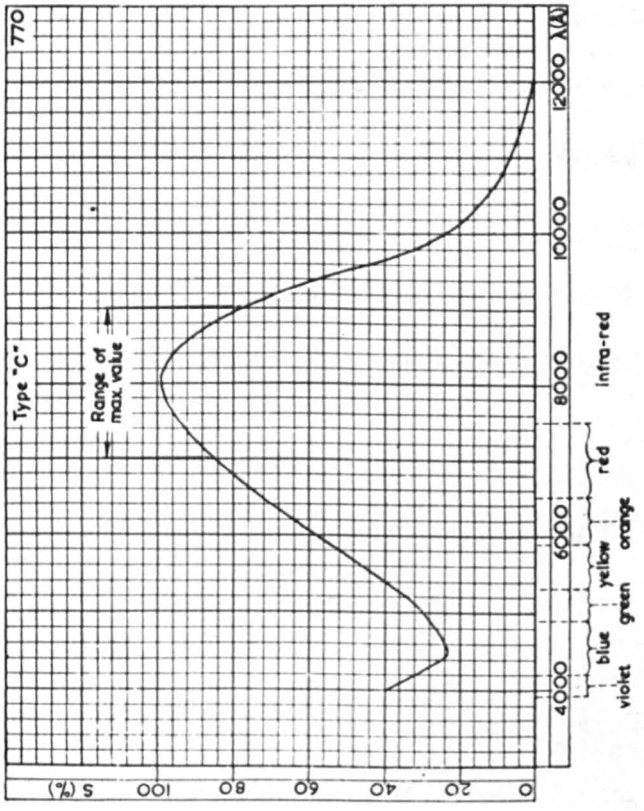

SPECTRAL RESPONSE CURVE FOR PHOTOCATHODE TYPE "C"
(Caesium on Oxidised Silver)

Fig. 5.7

be used, normally 0.35 mm. This increases the total dispersion to about ± 0.02 eV at 1.40 eV and about ± 0.03 eV at 3.10 eV. The proportion of scattered light at any wavelength has not been estimated. Wavelengths are read directly from the drum on the instrument, after the position of the prism table has been adjusted with a line of known wavelength from a mercury lamp.

In order to produce curves of spectral sensitivity per unit incident intensity, the intensity of illumination at each wavelength must be found. This may be done by allowing the light from the monochromator to fall on the cathode of a Mullard 53 CV photocell: the frequency response of this vacuum photocell, with an Ag-O-Cs cathode, is known (Fig. 5.7) (129), and has been confirmed over a range of wavelengths by comparison with a Cambridge Instrument Company radiation thermopile. The cell is operated at an anode potential of 50 V, and photocurrents are measured with the electrometer. The photocurrent obtained at any wavelength is divided by the relative sensitivity of the cell at that wavelength, obtained from Fig. 5.7, to give the relative intensity of the light incident on the cell.

Photoelectric measurements were made with the arrangement of apparatus given in Fig. 5.8. The

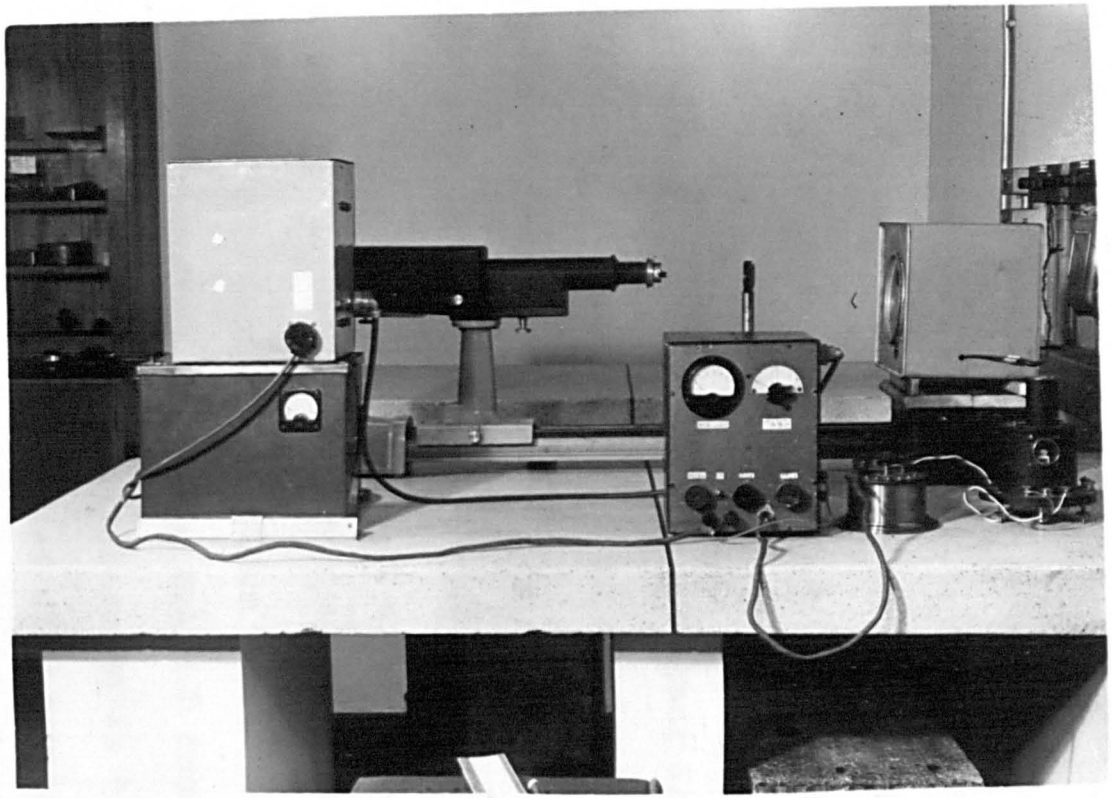

Fig. 5.8 (opposite) Optical system for photoelectric measurements

In the background of the photograph, reading from right to left, are the light source in its electrically ventilated lamp-house, the lens and monochromator. In the foreground at the left is the screened box containing the experimental tube at the exit slit of the monochromator, standing on the box containing the battery supplies for the heater of the electrometer (centre foreground). In the right foreground are the universal shunt and galvanometer; the lamp and scale for the galvanometer are not included in this photograph.

FIG. 5.8. OPTICAL SYSTEM FOR PHOTOELECTRIC MEASUREMENTS

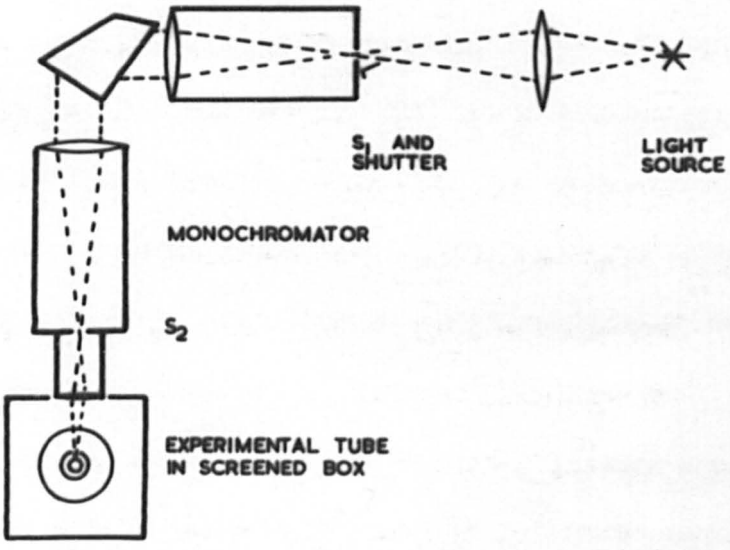

experimental tube in its screened box is placed near the exit slit of the monochromator and its position adjusted until the exit slit and anode window are in alignment and maximum illumination of the cathode is obtained. Anode or probe potentials can be applied with the potentiometer unit, currents being measured with the electrometer. In order to obtain spectral sensitivity curves the photocurrent (either external photoemission, to or from the anode, or photoconductivity, to or from the probe) is divided by the intensity of illumination at the relevant wavelength to give a value for the photocurrent per unit incident energy at that wavelength. Photocurrents are measured by observing the difference in electrometer readings when the shutter at the entrance slit is closed and when it is open. An average of the readings obtained in several exposures is taken and the spread of these readings gives a measure of the probable error in each case. The process is repeated over a range of wavelengths.

It is normal to correct the intensity of illumination values for absorption in the envelope of the experimental tube: the absorption may change from tube to tube on account of different quantities of evaporated materials on the envelopes. This may be done by taking two sets

of illumination readings with the photocell, one with a direct beam from the monochromator and another after the beam has passed through two thicknesses of the envelope of the experimental tube near the anode window. Light striking the cathode passes through only one thickness, so an approximate value for the intensity of illumination striking the cathode is obtained by taking the average of the two photocell readings and dividing this by the relative sensitivity of the cell at the relevant wavelength.

The use of the monochromator represents a considerable improvement over the techniques employed in work described in a previous thesis (116), where optical filters were used. The dispersion, although still large, has been considerably reduced. In the previous work, photocurrents were large enough to measure with the galvanometer alone: in the present case, the intensity of illumination is much less and the photocurrents, correspondingly smaller, must be measured with the electrometer.

Chapter 6 Thermionic emission and electrical conductivity in calcium oxide

6.1. Introduction

Although the main object of the present work has been to study photoelectric processes in calcium oxide coated cathodes, conventional thermionic measurements have been made on all tubes. It has been thought desirable to gather the results together into a separate chapter, where they can be discussed independently of photoelectric results; they are of interest in a comparison with the results of Hopkins (87), described in Sec. 2.6.

6.2. Experimental methods

The general experimental arrangement for the measurement of thermionic emission and electrical conductivity has been described in Sec. 5.5.

Emission characteristics are determined by applying retarding and accelerating anode potentials up to 4.8 V from the potentiometer unit. If only low anode potentials are employed, poisoning effects and instability due to high-energy electron bombardment of materials evaporated on to the anode are avoided. By extrapolating the retarding and accelerating field characteristics, the zero-field emission current i_0 and the contact potential difference between the anode and cathode, v_c, can be

obtained. Emission characteristics are obtained over a range of cathode temperatures T and a Richardson plot can be obtained by plotting $\log_{10} i_o/T^2$ versus $1/T$. The Richardson work function ϕ can be deduced from the gradient of the graph.

For applications where information on contact potential difference and its variation with temperature is not required, a quick form of Richardson plot can be made by using the emission current i_a at a given value of anode voltage instead of the zero-field value i_o: thus the determination consists merely of one emission current reading at each temperature. The Richardson work function as determined by this analysis differs very little from that obtained in the more detailed method, provided that measurements are made in the saturation region (39).

Conductivity measurements are made by applying a series of small potential differences between the probe and cathode base and determining the corresponding conductivity currents. As will be seen in Sec. 6.3.2, the current - voltage characteristics thus obtained are not always linear, and the apparent conductivity is obtained from the slope of the characteristic near the origin. The specific conductivity σ_s of the cathode

material is related to the apparent conductivity σ by the equation

$$\sigma_s = \sigma \frac{\cosh^{-1} t/a}{2\pi l} \qquad 6.1.$$

where a is the radius and l the length of the probe wire, and t is the thickness of oxide between probe and base; the relation holds if $t \gg a$. In this type of probe tube, t is greater than a by a factor of about 10. However, no advantage is to be gained by calculating the value of the specific conductivity: as $\sigma_s \propto \sigma$, the gradient of the conductivity plot of $\log_e \sigma$ versus 1/T is unchanged whether $\log_e \sigma_s$ or $\log_e \sigma$ is plotted.

It is also possible, if the conductivity current - voltage characteristics are nearly linear, to determine the conductivity from two values of the applied potential instead of from a number of values. Thus, the difference between electrometer readings when ± 10 mV is applied between the probe and cathode base usually gives a value for the conductivity very close to that obtained from the gradient of the characteristic at the origin, and this procedure very much reduces the number of current readings which require to be taken.

The fact that a temperature gradient exists across the coating at temperatures above room temperature is

apparent from the conductivity characteristics, which do not pass through the origin at high temperatures (cf. Fig. 6.3.4). The thermoelectric e.m.f. due to the difference in temperature between the probe and cathode base is given by the negative intercept on the voltage axis. When the electrometer is used to determine the conductivity characteristics, it is normal to balance off this thermoelectric e.m.f. by means of the coarse and fine controls on the electrometer.

6.3. Results

Eleven calcium oxide probe diodes of the type described in Sec. 5.3.1 and six probe diodes employing a smaller cathode area (Sec. 8.2.2) have been constructed. Not all have yielded measurements of both emission and conductivity: it is not uncommon for the fine probe wire to become discontinuous during processing, and in a number of cases the cathode heater has burnt out during activation. A number of other types of tube have been designed which yield emission or conductivity results, and these will also be considered.

The method of nomenclature adopted for tubes constructed during the course of the work is as follows: the cathode material is designated first, followed by a

combination of letters showing the type of tube and a number giving its order in the series. A superscript number gives the activation state of the cathode. Thus CaO PC 5^2 represents the second activation state of the fifth CaO probe diode in the present programme. Tubes CaO PC 1 - 4 were coated with a calcium carbonate suspension supplied by G.E.C., Ltd. and used by Hopkins (87); the remainder were coated with a suspension from B.D.H., Ltd., with the following specification:

630 g calcium carbonate (AnalaR)

760 ml necoloidine soln 5 % in butyl acetate

500 ml butyl acetate

420 ml amyl acetate (AnalaR)

140 ml ethyl oxalate.

The various types of experimental tube used are listed in Appendix II.

It is unnecessary to review results from all the tubes in detail: the more important points are discussed, specimen curves given, and activation energies and work functions tabulated.

6.3.1. Typical thermionic emission results - CaO PC 5^2

Thermionic emission characteristics covering the range of cathode temperatures T from 660 to 940 ^{o}K are

FIG. 6.1.1 THERMIONIC EMISSION CHARACTERISTICS — CaO PC 5[2]

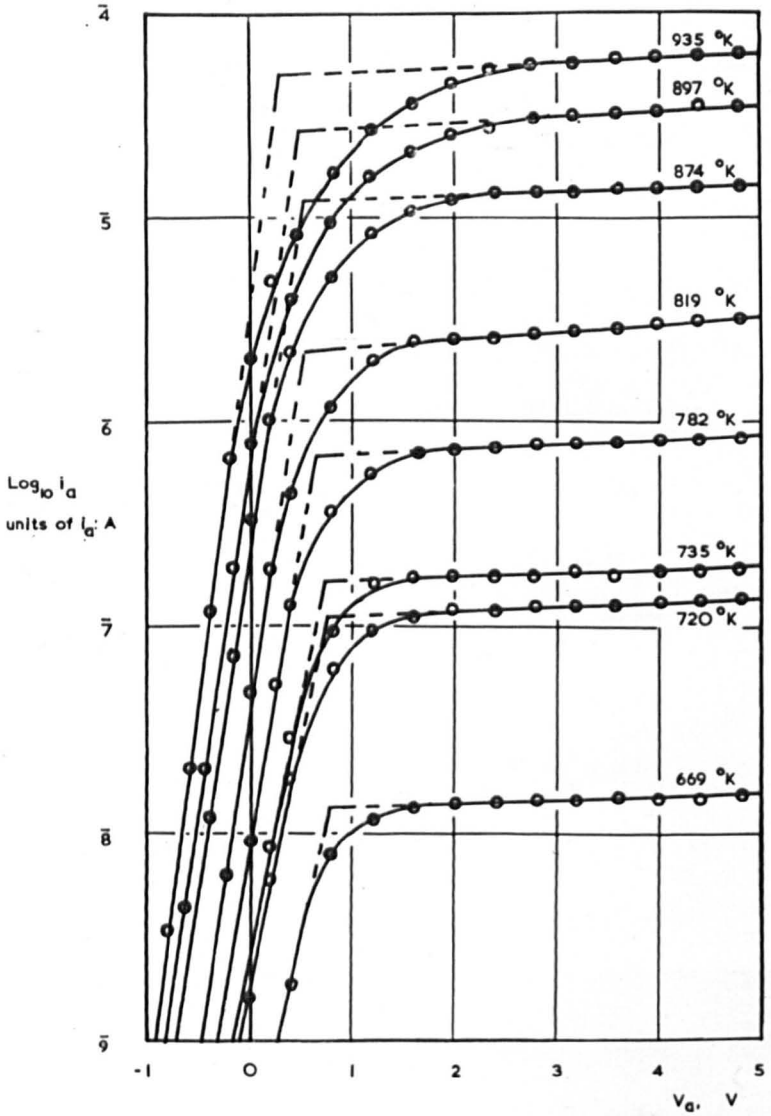

FIG. 6.1.2. TEMPERATURE VARIATION OF C.P.D. – CaO PC 5[2]

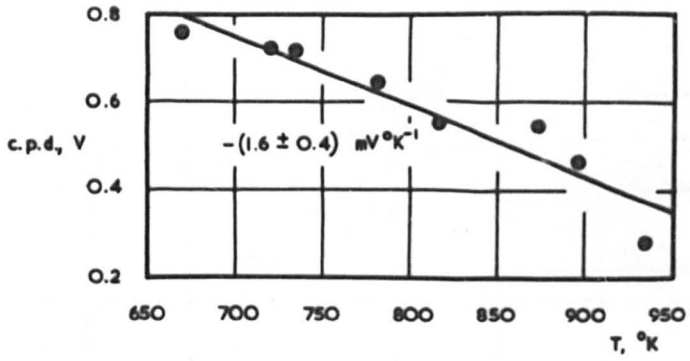

FIG. 6.1.3. RICHARDSON PLOT FOR THERMIONIC EMISSION – CaO PC 5[2]

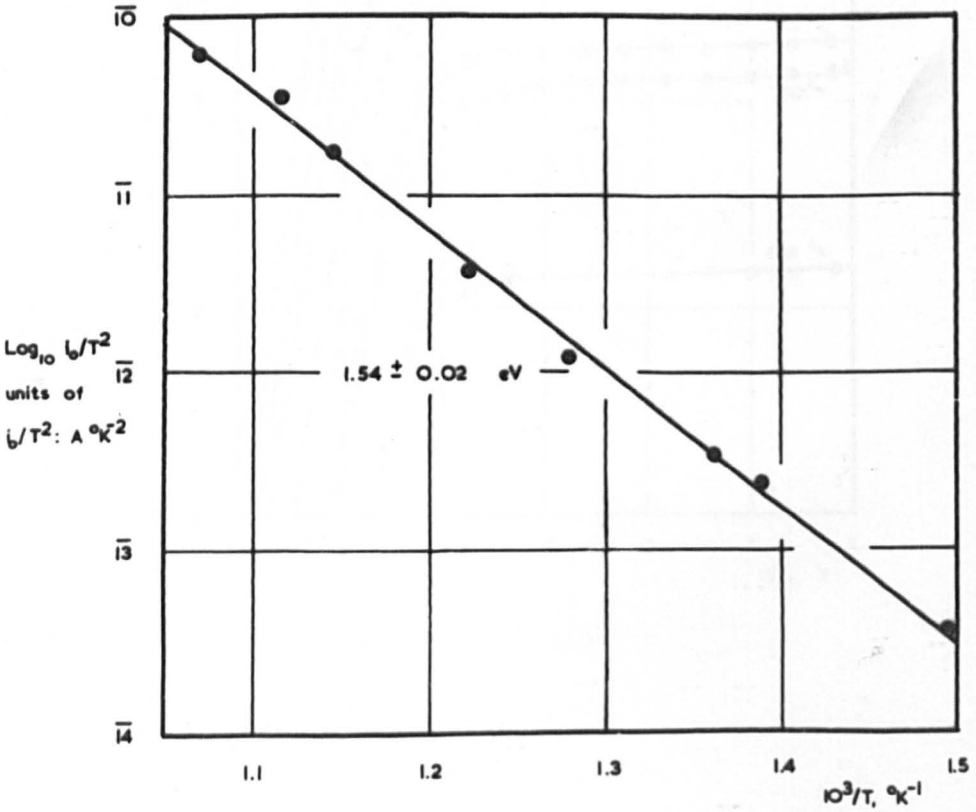

FIG. 6.2. MODIFIED RICHARDSON PLOT FOR THERMIONIC EMISSION — CaO PC 10^{1}

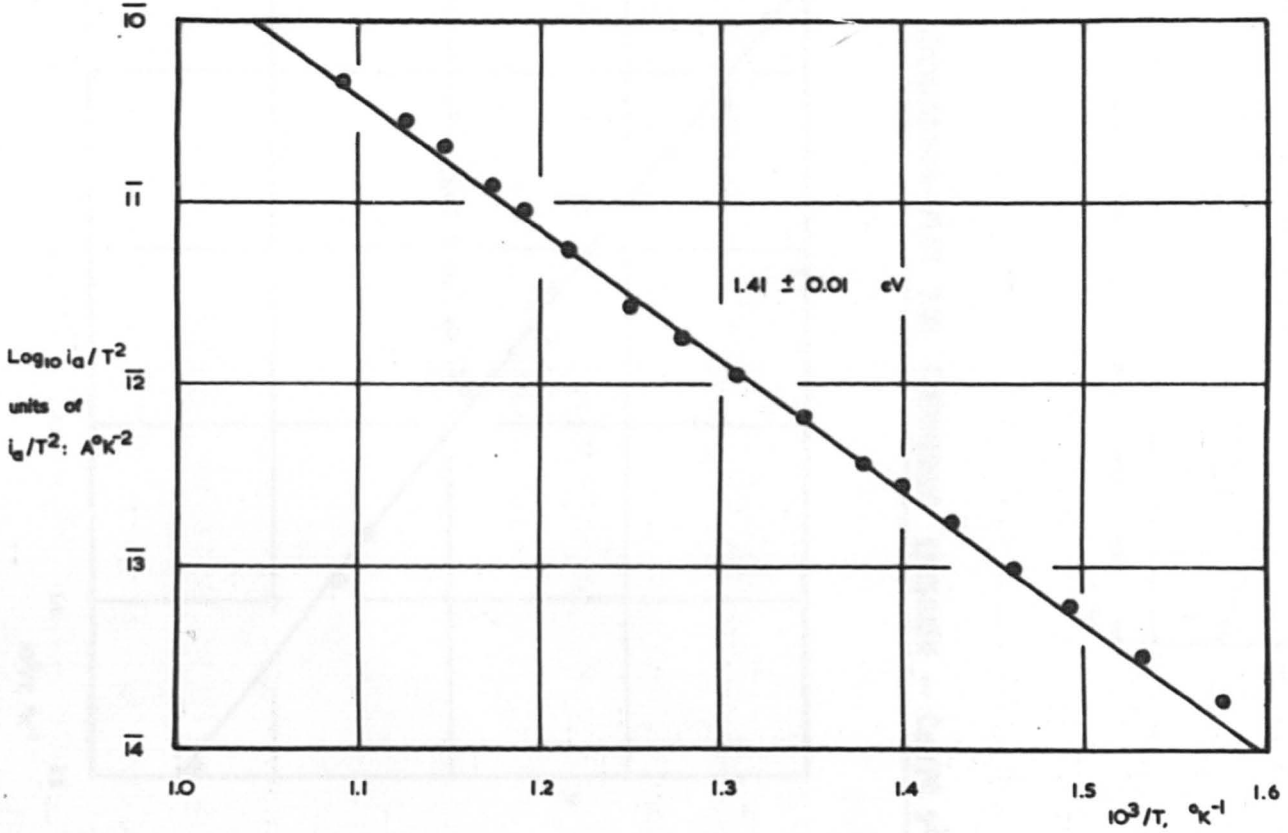

given in Fig. 6.1.1. The maximum anode voltage applied was 4.8 V. The characteristics show good saturation in the accelerating field region, and can be extrapolated to find by intersection with the retarding field characteristic the zero-field current and the c.p.d. for each temperature.

It is observed that there is an apparent change of c.p.d. with temperature, the c.p.d. becoming smaller as temperatures increase. This variation is displayed in Fig. 6.1.2, and is seen to be approximately linear.

The zero-field emission current i_0 is used to prepare a Richardson plot of $\log_{10} i_0/T^2$ versus $10^3/T$ (Fig. 6.1.3). The graph is approximately linear (but see Sec. 6.3.5) with a slope corresponding to a Richardson work function of 1.54 ± 0.02 eV, the error being calculated by a least-squares analysis of the experimental points.

CaO PC 10^1

Richardson plots prepared by using the saturated instead of the zero-field emission currents (Sec. 6.2) reduce the labour of determining thermionic work functions. Such a curve for a constant voltage of 4.8 V applied to the anode of CaO PC 10^1 yields an approximately linear plot (Fig. 6.2) with a gradient corresponding to a

FIG. 6.3.I. CURRENT–VOLTAGE CHARACTERISTICS FOR DARK CONDUCTIVITY – CaO PC 6[2]

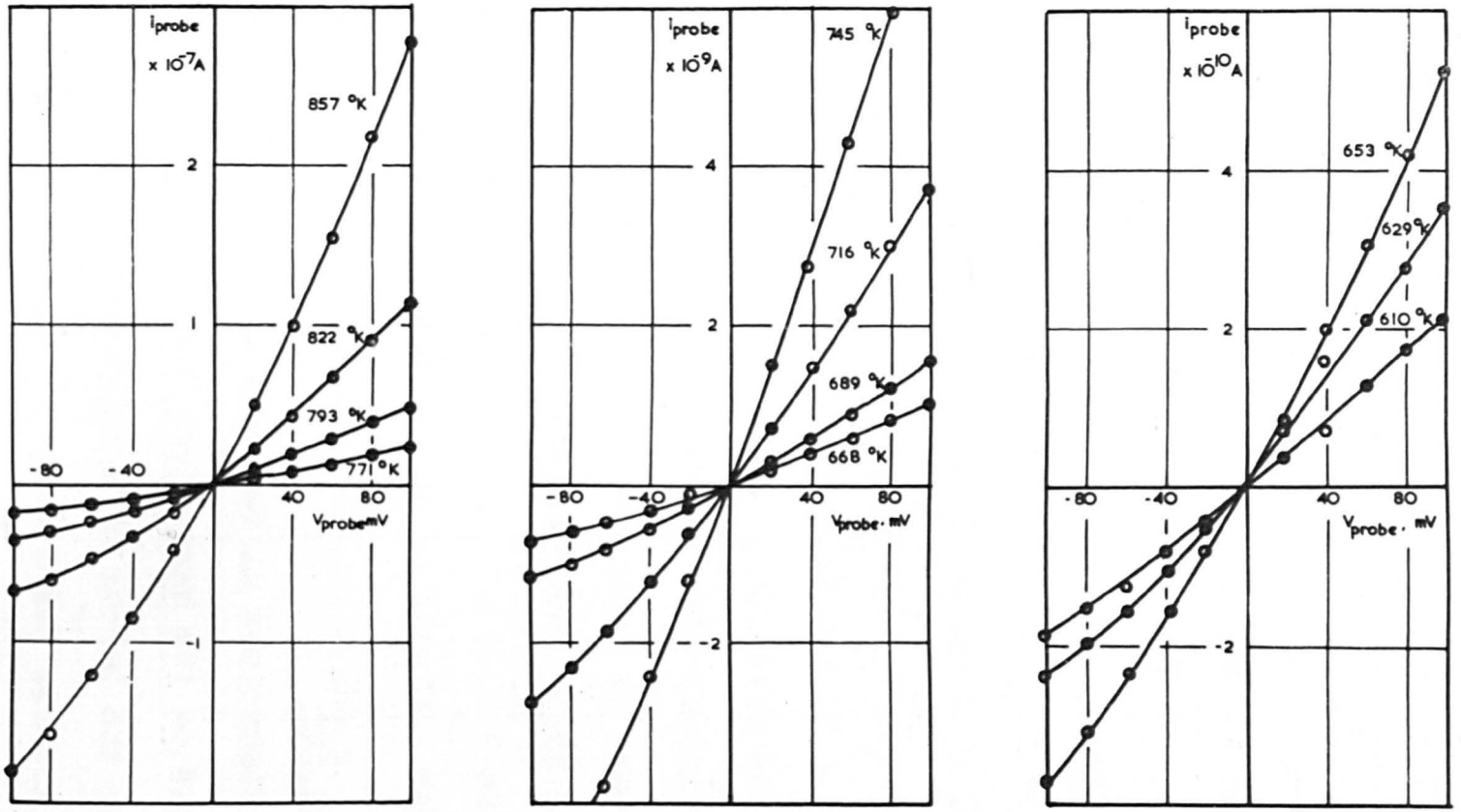

FIG. 6.3.2 GRAPH OF Log σ VERSUS 1/T FOR CaO PC 6[2]

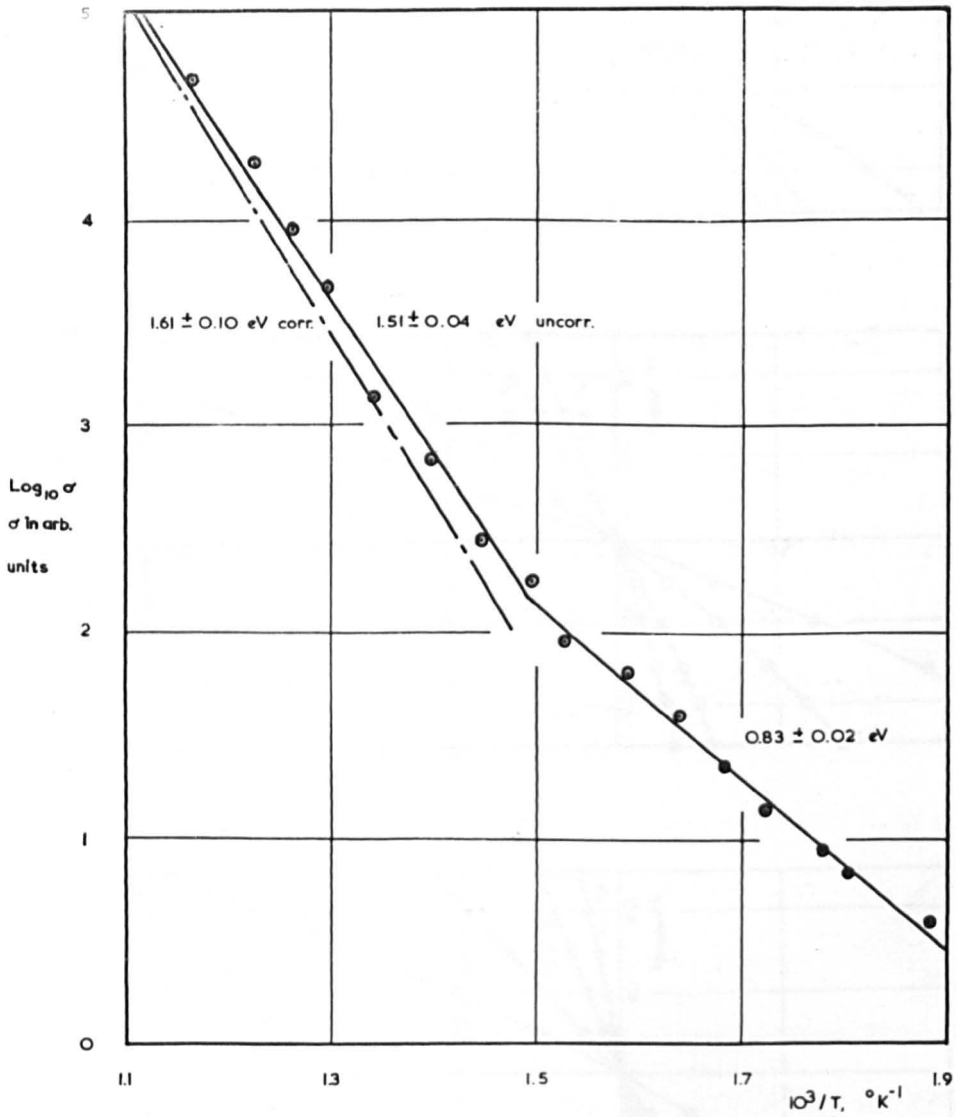

thermionic work function of 1.41 ± 0.01 eV.

6.3.2. Typical electrical conductivity results - CaO PC 6[2]

Current - voltage characteristics for potentials of up to ± 100 mV applied between the probe and cathode base are given in Fig. 6.3.1 for cathode temperatures between 590 and 860 °K. The electrometer was used to detect the current: characteristics have been shifted so as to pass through the origin, the thermoelectric e.m.f. being balanced off.

At low temperatures the characteristics are nearly linear: at higher temperatures they are curved. The apparent conductivity σ of the coating is given by the gradient of the characteristic at the origin, and the logarithm of the apparent conductivity is plotted against reciprocal temperature to give the characteristic conductivity plot of Fig. 6.3.2, showing two approximately linear regions intersecting at about 670 °K. As shown in Sec. 2.4, the high-temperature region must be corrected for the parallel low-temperature mechanism by the following analysis: the low-temperature line is extrapolated towards higher temperatures, and the conductivity determined from this extrapolated line at

FIG. 6.3.3. CORRECTED CURRENT–VOLTAGE CHARACTERISTICS FOR DARK CONDUCTIVITY – CaO PC 6^2

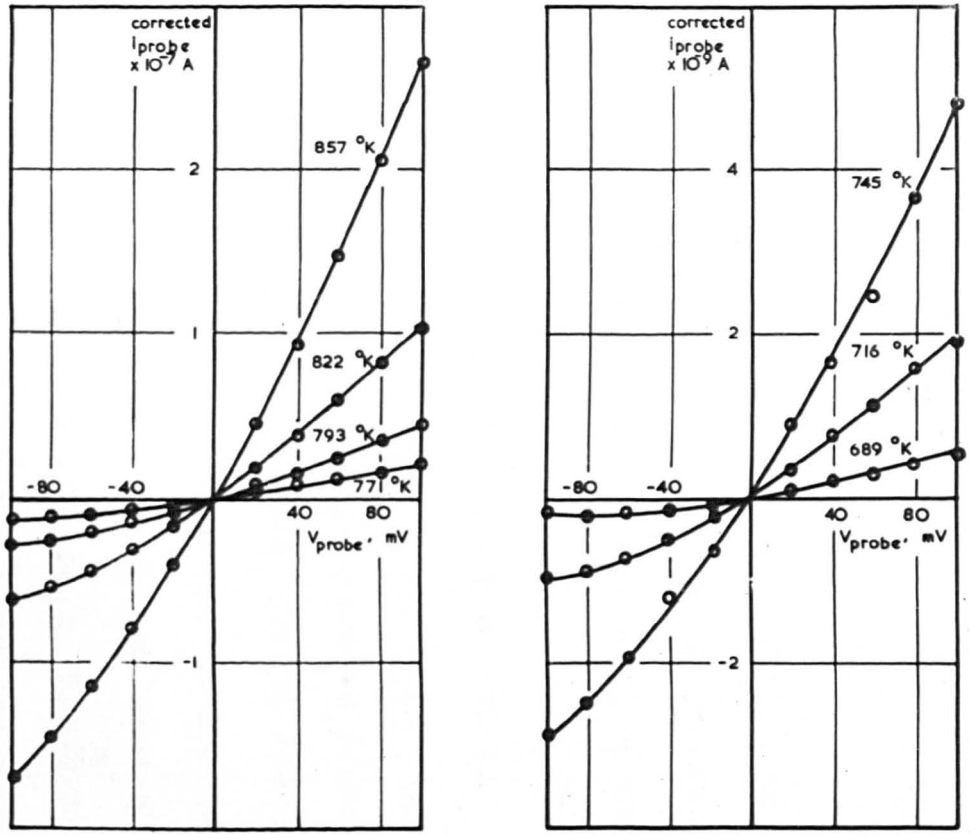

FIG. 6.3.4. DARK CONDUCTIVITY CURRENT–VOLTAGE CHARACTERISTICS, SHOWING THERMOELECTRIC E.M.F. BETWEEN PROBE AND CATHODE

BASE – CaO PC 6[4]

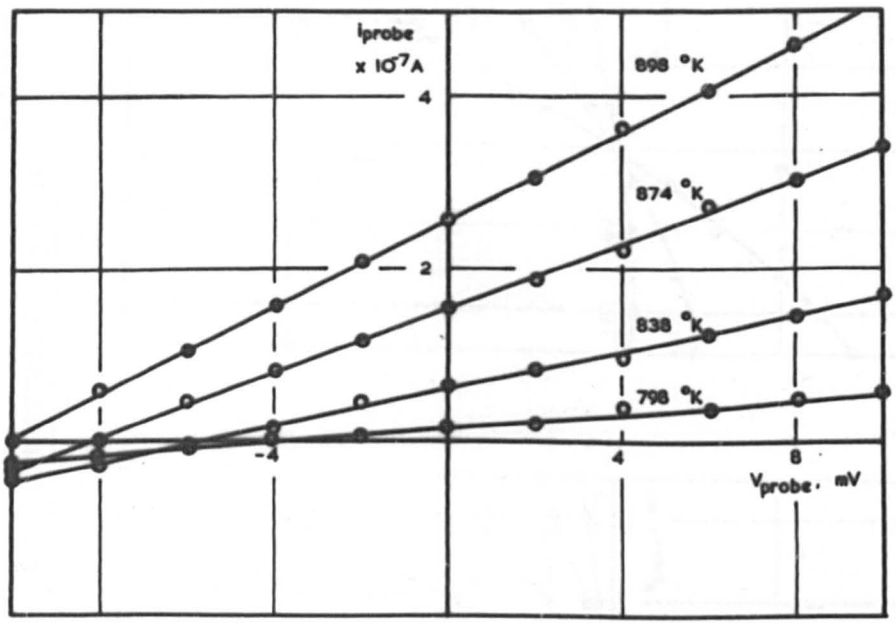

a number of values of 1/T. These values are subtracted from the corresponding values of the apparent high-temperature conductivity, to give the corrected high-temperature conductivity. The logarithm of the corrected conductivity, plotted against reciprocal temperature, always yields a line of steeper gradient than the uncorrected portion of the plot. In the present case, following the interpretation of Loosjes and Vink, the activation energy $\Delta E/2$ of the low-temperature region is 0.83 ± 0.02 eV; the upper portion yields an apparent gradient corresponding to 1.51 ± 0.04 eV, and the corrected value of $\chi + \Delta E/2$ is 1.61 ± 0.10 eV.

To find the true form of the current - voltage characteristic in the high-temperature range, the linear component due to the low-temperature mechanism must be subtracted from it (111). This can again be done by extrapolating the low-temperature line to find the value of the low-temperature component (assumed to be linear) at the temperatures at which the characteristics were obtained. Corrected characteristics are shown in Fig. 6.3.3: the correction makes most difference at temperatures near the break between high- and low-temperature regions.

Fig. 6.3.4 shows characteristics obtained with CaO PC 6^4 for temperatures between 800 and 900 °K using the

Table 6.1 (continued)

(1)	(2)	(3)	(4)	(5)	(6)
CaO PC 6^4			1.21 ± .01	1.29 ± .06	0.82 ± .03
PC 7^1	1.74 ± .02	0.4	1.57 ± .02	1.77 ± .20	0.57 ± .04
PC 8^1	1.77 ± .04	I.1			
PC 9^1	1.52 ± .01	0.5	1.68 ± .02		
PC 9^2	2.16 ± .06	2.7	2.26 ± .02	2.35 ± .07	1.35 ± .02
PC 9^3	2.52 ± .02	4.4	2.39 ± .02		
PC 9^4	2.40 ± .04	4.1			
PC 10^1	1.41 ± .01	I.3	1.65 ± .02	1.85 ± .05	1.19 ± .01
M 5^1	2.00 ± .01	I.7	1.58 ± .04	1.71 ± .12	0.59 ± .02
M 5^2	1.65 ± .01	I.1	1.50 ± .04	1.73 ± .10	0.68 ± .01
Averages	1.8 ± .4		1.5 ± .4	1.6 ± .3	0.7 ± .3
Hopkins (87)	1.7		1.1	1.3	0.8

All energies are expressed in eV.

Table 6.1

Tube and activation state (1)	Richardson plot ϕ, eV (2)	Richardson plot $\log_{10} A^*$ (3)	Conductivity plot gradients High temp. uncorrected (4)	Conductivity plot gradients High temp. corrected (5)	Conductivity plot gradients Low temp. (6)
CaO PC 1^1	2.11 ± .07	4.8			
PC 1^2	2.37 ± .07	5.4			
PC 1^3	2.01 ± .03	3.2			
PC 5^1	1.96 ± .03	1.2	0.95 ± .01		
PC 5^2	1.54 ± .02	$\bar{1}$.0	1.44 ± .01	1.52 ± .06	0.71 ± .02
PC 5^3	1.71 ± .02	$\bar{2}$.4	1.68 ± .02	1.73 ± .11	0.63 ± .03
PC 5^4	1.79 ± .03	$\bar{2}$.9	1.65 ± .03	1.69 ± .11	0.51 ± .02
PC 5^5	1.01 ± .03	$\bar{5}$.2	0.93 ± .01	1.05 ± .09	0.39 ± .01
PC 5^6	1.04 ± .01	$\bar{5}$.2	1.00 ± .01	1.07 ± .06	0.49 ± .02
PC 5^7			1.39 ± .02	1.44 ± .06	0.78 ± .02
PC 6^1	1.58 ± .02	$\bar{3}$.7			
PC 6^2	1.39 ± .01	$\bar{3}$.8	1.51 ± .04	1.61 ± .10	0.83 ± .02
PC 6^3	1.49 ± .03	$\bar{2}$.3	1.35 ± .02	1.39 ± .09	0.56 ± .02

(continued)

galvanometer alone to measure the conductivity current. The negative intercepts on the voltage axis represent the thermoelectric e.m.f. due to the difference in temperature between the probe and cathode base.

6.3.3. Summary of work functions and activation energies from probe diodes

Table 6.1 (opposite) shows the thermal activation energies and work functions for the calcium oxide probe diodes constructed in the course of the present work. A comparison with the results of Hopkins (87) (see Table 6.1) for the fully activated states of five cathodes shows that the results obtained in the present work are in reasonable agreement, taking into account the fact that Hopkins' values would be expected to be lower as they deal with the most active states. In Table 6.1, it is doubtful whether an average for the activation energies over all states of activation can have much significance; on the other hand, the selection of any activation state in a given tube as being the fully activated state must also be dubious.

The value of $\log_{10} A^*$ quoted in the table represents the intercept of each Richardson plot on the $\log_{10} i_o/T^2$ axis, with a constant factor to account for the emitting

FIG. 6.4. RELATION BETWEEN Log A^* AND ϕ

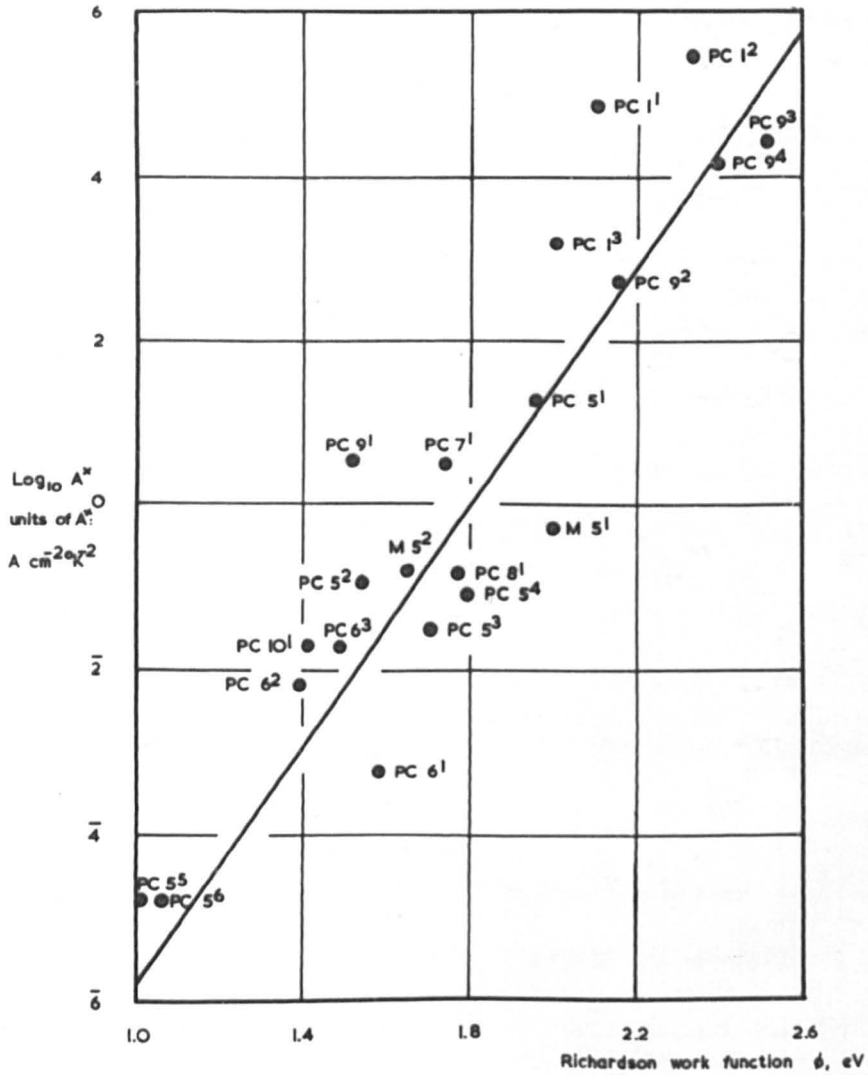

area of the cathode: values of A^* are in units of A cm^{-2} $^oK^{-2}$. A considerable spread of values is observed, extending over ten orders of magnitude in A^*; and there is some evidence to suggest that there is a linear relation between $\log_{10} A^*$ and ϕ. A graph of $\log_{10} A^*$ versus ϕ is given in Fig. 6.4, and although the scatter of the points is very large, there at least appears to be a tendency for high values of log A^* to be associated with high work functions. The slope of the least-squares line is about 7.

It is observed that rather low Richardson work functions have been obtained in the present work: for instance, in its most active state CaO PC 5 yielded a value of 1.0 eV. Values as low as this were not reported by Hopkins; the possibility that the difference was due to the different cathode suspensions used (Sec. 6.3) could not be dismissed. To compare the suspensions a double diode, CaO D 1, consisting of a box cathode coated on opposite sides with the G.E.C. and B.D.H. suspensions, and with two similar planar anodes, was constructed. Each cathode, being on a common base, was thus subjected to exactly the same breakdown and activation schedules, and emission measurements could be compared at the same cathode temperature. In two activation states the

FIG. 6.5. COMPARISON OF THERMIONIC PROPERTIES OF OXIDES PREPARED FROM G.E.C. AND B.D.H. CALCIUM CARBONATE SUSPENSIONS

CaO D I

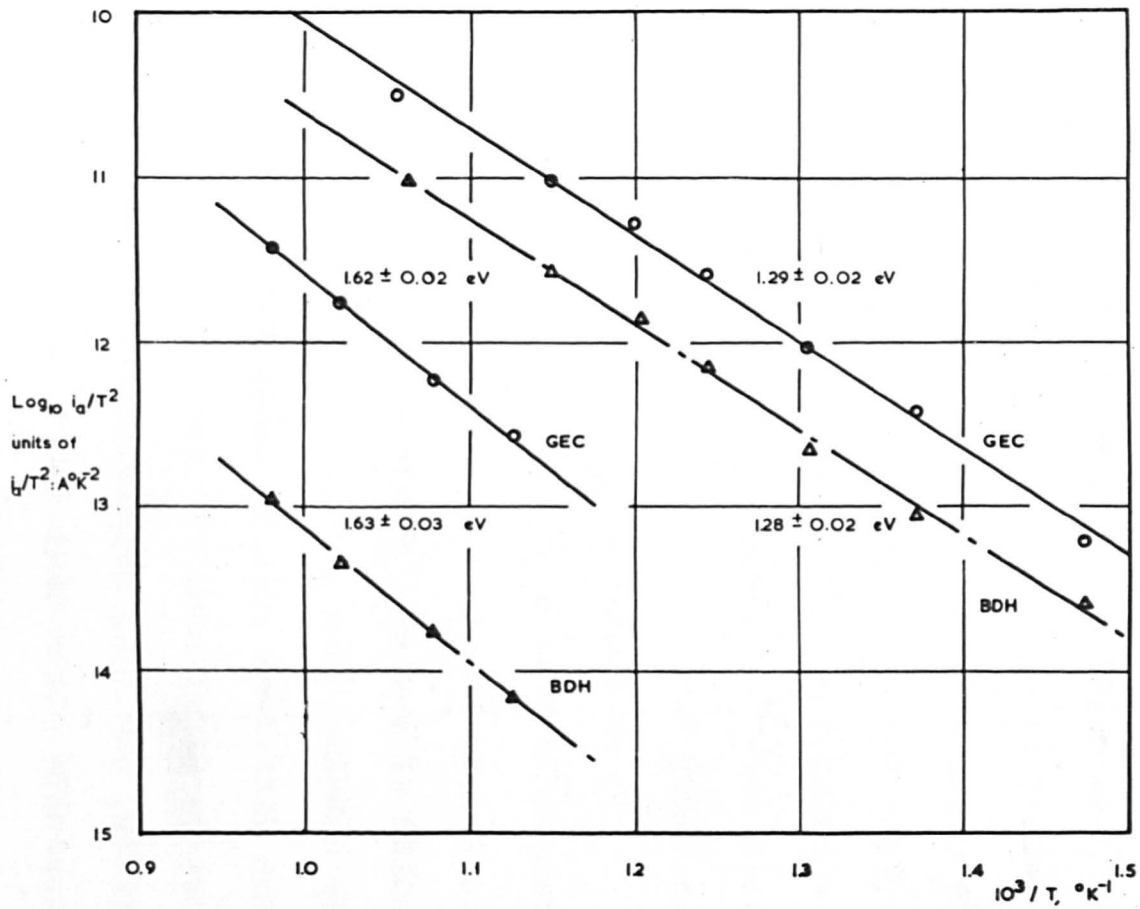

Richardson work functions obtained were the same, within experimental error (Fig. 6.5 and Table 6.2) and the two suspensions are apparently the same thermionically. The difference in the absolute magnitudes of the emission currents is probably due to a difference in the effective emitting area of the cathodes.

Table 6.2

Comparison of G.E.C. and B.D.H. $CaCO_3$ suspensions

Activation state (CaO D 1)	Richardson work function ϕ , eV	
	G.E.C.	B.D.H.
1	1.62 ± .02	1.63 ± .03
2	1.29 ± .02	1.28 ± .02

6.3.4. Contact potential difference measurements; anode work functions

The contact potential difference (c.p.d.) between the anode and cathode can be found from the point of intersection between the retarding and accelerating field characteristics, and since (4)

$$\text{c.p.d.} = \phi_a - \phi_c \qquad 6.2.$$

where ϕ_a and ϕ_c are the anode and cathode work functions respectively, the anode work function can be determined, as ϕ_c is known from the Richardson plot. This indirect

Table 6.3 (continued)

(1)	(2)	(3)	(4)	(5)
CaO PC 9^2	2.16 ± .06	0 ± .1	2.2 ± .2	8 V
PC 9^3	2.52 ± .02	0 ± .1	2.5 ± .1	100 V

Table 6.3

c.p.d.'s and anode work functions

Tube and activation state (1)	ϕ_c, eV (2)	mean c.p.d., V (3)	ϕ_a, eV (4)	Activation treatment - current at (5)
CaO PC 5^1	1.96 ± .03	+ 0.2 ± .1	2.2 ± .1	100 V
PC 5^2	1.54 ± .02	+ 0.6 ± .1	2.2 ± .1	100 V
PC 5^3	1.71 ± .02	+ 1.1 ± .1	2.8 ± .1	4 V
PC 5^4	1.79 ± .03	+ 1.5 ± .2	3.3 ± .2	8 V
PC 5^5	1.01 ± .03	+ 0.2 ± .1	1.3 ± .1	8 V
PC 5^6	1.04 ± .01	+ 0.3 ± .1	1.3 ± .1	4 V
PC 6^1	1.58 ± .02	+ 1.9 ± .2	3.5 ± .2	100 V
PC 6^2	1.39 ± .01	+ 0.4 ± .2	1.8 ± .2	100 V
PC 6^3	1.49 ± .03	+ 0.1 ± .1	1.6 ± .2	100 V
PC 7^1	1.74 ± .02	+ 0.5 ± .4	2.2 ± .4	100 V
PC 8^1	1.77 ± .04	- 0.3 ± .1	1.5 ± .1	100 V
PC 9^1	1.52 ± .01	- 0.2 ± .2	1.3 ± .2	100 V

(continued)

method of studying the anode properties is open to criticism, but Hopkins (89) has compared this method with one in which the c.p.d. between the anode and a clean gold film, of known work function, is determined. Although results differed by as much as 15 %, the method at least gives a reasonable estimate of the anode work function.

In a number of activation states of the tubes employed in the present work, thermionic emission characteristics have been obtained and c.p.d. measurements made. Table 6.3 (opposite) gives a summary of the anode work functions obtained in this way: it must be noted that the values of the c.p.d.'s quoted are averages over the ranges of temperatures at which emission characteristics are determined.

There is insufficient experimental evidence to substantiate the observation of Hopkins (89) that activation with low anode potentials (4 V) causes an increase in the anode work function.

6.3.5. Temperature coefficient of the cathode work function

Closer examination of the emission characteristics (Fig. 6.1.1) shows a definite relation between the c.p.d.

FIG. 6.6. TEMPERATURE VARIATION OF ANODE-CATHODE C.P.D. FOR CaO DIODES

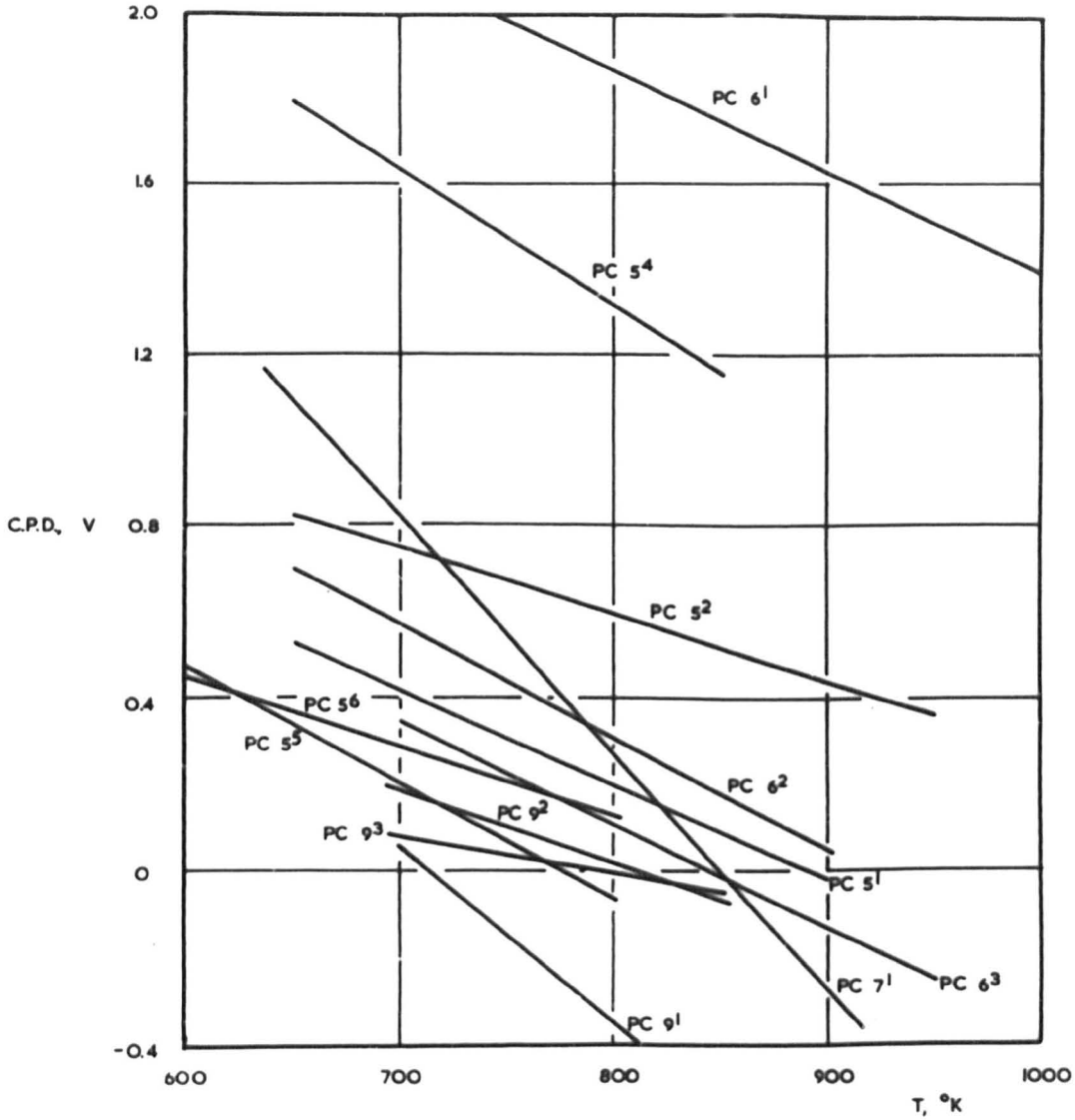

CATHODE	TEMP. COEFF. mV °K⁻¹	CATHODE	TEMP. COEFF. mV °K⁻¹	CATHODE	TEMP. COEFF. mV °K⁻¹	CATHODE	TEMP. COEFF. mV °K⁻¹
PC 5¹	- 2.2 ± 0.5	PC 5⁵	- 2.6 ± 0.5	PC 6²	- 2.6 ± 0.1	PC 9¹	- 4.0 ± 0.1
PC 5²	- 1.6 ± 0.5	PC 5⁶	- 1.7 ± 0.3	PC 6³	- 2.0 ± 0.2	PC 9²	- 1.7 ± 0.1
PC 5⁴	- 3.2 ± 0.2	PC 6¹	- 2.3 ± 0.1	PC 7¹	- 5.6 ± 0.1	PC 9³	- 1.0 ± 0.2

and temperature: as the temperature increases, the c.p.d. decreases (Fig. 6.1.2). This variation with temperature is displayed for a number of diodes in Fig. 6.6, and apparently follows an approximately linear relation. The average value for the temperature coefficient of the c.p.d. is -2.5×10^{-3} V $^{o}K^{-1}$ over the temperature range from 650 to 950 ^{o}K, but values as low as -1.0×10^{-3} V $^{o}K^{-1}$ and as high as -5.6×10^{-3} V $^{o}K^{-1}$ have been recorded. The average value is in approximate agreement with a result quoted by Hopkins (87), who found the temperature coefficient of the c.p.d. for one diode in the temperature range 600 - 1000 ^{o}K to be -1.1×10^{-3} V $^{o}K^{-1}$.

If it is assumed that the anode work function remains constant, the change in the c.p.d. with temperature suggests that the cathode work function must also be temperature-dependent. Although the Richardson plots have hitherto been treated as linear, the lines should in fact display a curvature if the work function varies with temperature. In the various activation states of CaO PC 5, not only has a linear regression line been fitted to the results, but also an equation of the second degree, and a Richardson work function can be defined at any temperature by the gradient of the tangent

FIG. 6.7.1. THERMIONIC EMISSION CHARACTERISTICS — CaO PC 5[4]

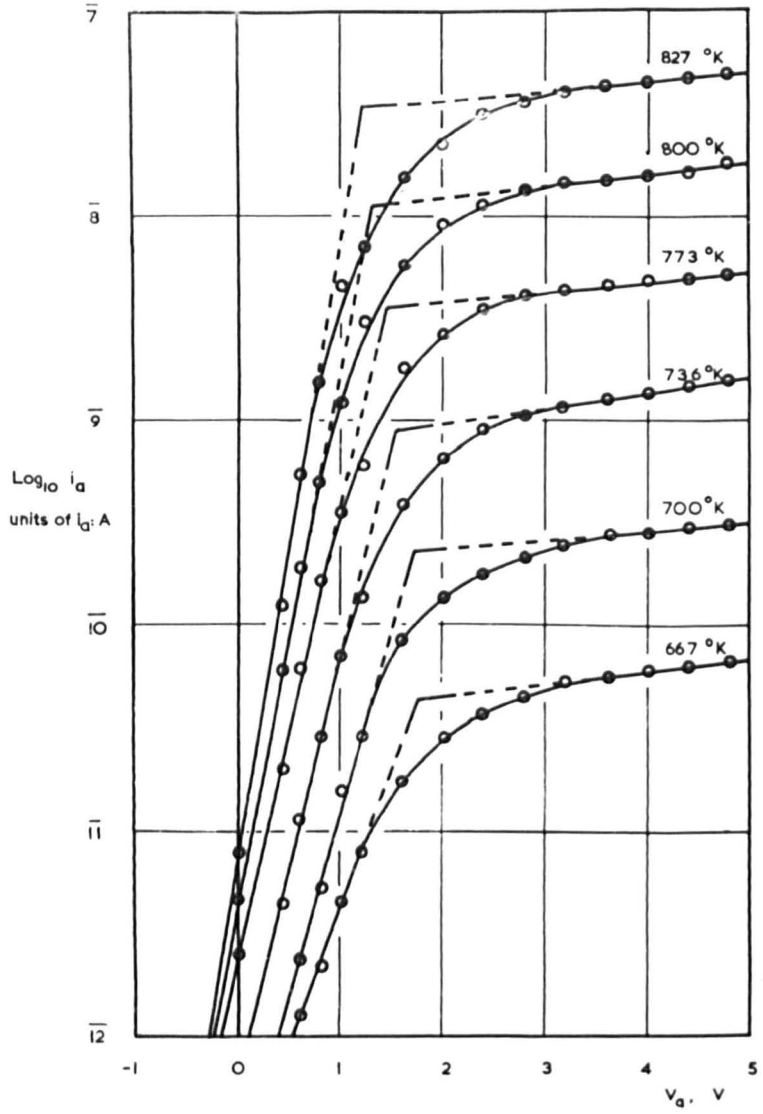

FIG. 6.7.4 FIRST AND SECOND ORDER RICHARDSON PLOTS FOR THERMIONIC EMISSION

CaO PC 5^4

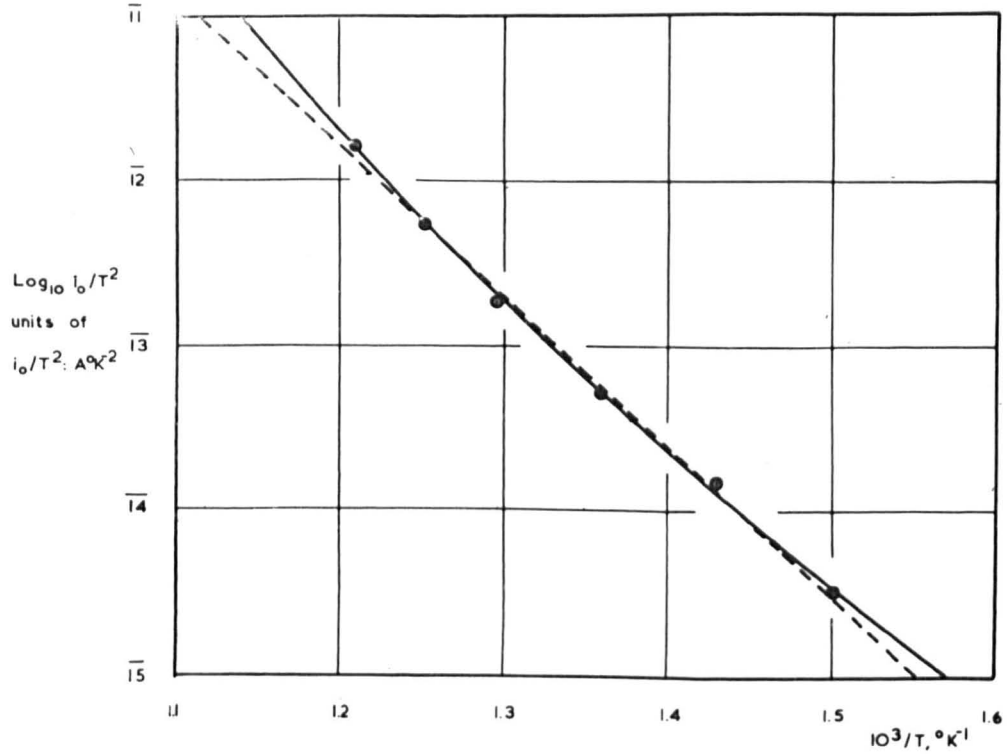

FIG. 6.7.5. TEMPERATURE VARIATION OF THE CATHODE WORK FUNCTION — CaO PC 5^4

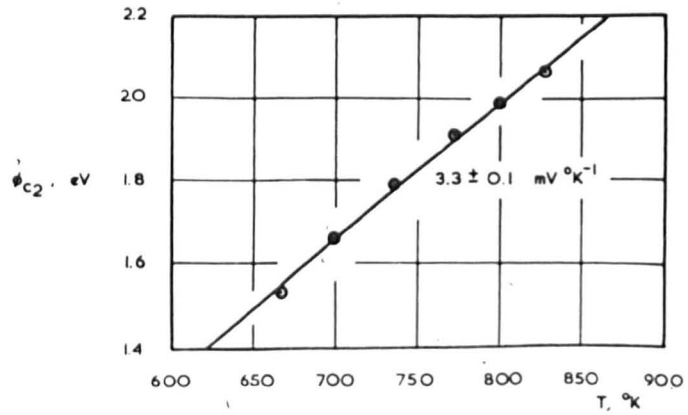

to this curve. Figs. 6.7.1, 2 and 3 show the emission characteristics for CaO PC 5^4, the first order Richardson line calculated from the results, and the temperature variation of the c.p.d., respectively. Fig. 6.7.4 compares the second and first order Richardson lines, and Table 6.4 (below) gives the cathode work functions calculated from the gradient of the second order curve at the experimental points. ϕ_{c_1} and ϕ_{c_2} are the cathode work functions obtained by the first and second order analyses, respectively.

Table 6.4

First and second order Richardson line analysis: CaO PC 5^4

T, ^oK	$10^3/T$, $^oK^{-1}$	ϕ_{c_2}, eV	ϕ_{c_1}, eV	c.p.d, V	ϕ_a, eV
827	1.209	2.06	1.79	1.21	3.27
800	1.250	1.98		1.30	3.28
773	1.294	1.90		1.42	3.32
736	1.359	1.79		1.52	3.31
700	1.429	1.66		1.68	3.34
667	1.499	1.53		1.70	3.23

It should be noted that the calculation gives an approximately constant value for the anode work function ϕ_a, and this suggests that the temperature variation of the c.p.d. may be completely accounted for by a corres-

ponding temperature variation in the cathode work function, the anode work function remaining constant.

Although the calculation gives a linear variation of ϕ_{c_2} with 1/T, the variation of ϕ_{c_2} with T is practically linear over the comparatively small range of temperatures employed (Fig. 6.7.5). The temperature coefficient of the cathode work function in the temperature range from 650 to 850 ^{o}K is thus 3.3 ± .1 mV $^{o}K^{-1}$, the numerical value of the temperature coefficient of the c.p.d.

This analysis has been repeated for all activation states of CaO PC 5, and in each case the anode work function is found to be sensibly constant. Over all the diode determinations, the average temperature coefficient of the cathode work function is 2.5×10^{-3} V $^{o}K^{-1}$ over the temperature range 650 - 950 ^{o}K.

Below 650 ^{o}K Hopkins (67), using a Kelvin c.p.d. method, found that a CaO cathode showed a negative temperature coefficient of the cathode work function. In the present case, emission measurements could not be made at sufficiently low temperatures to verify this observation.

6.3.6. External work function

The external work function χ can be determined by

FIG. 6.8. EXTERNAL WORK FUNCTION — GRAPH OF Log $i_\theta/\sigma T$ VERSUS 1/T — CaO PC 5^2

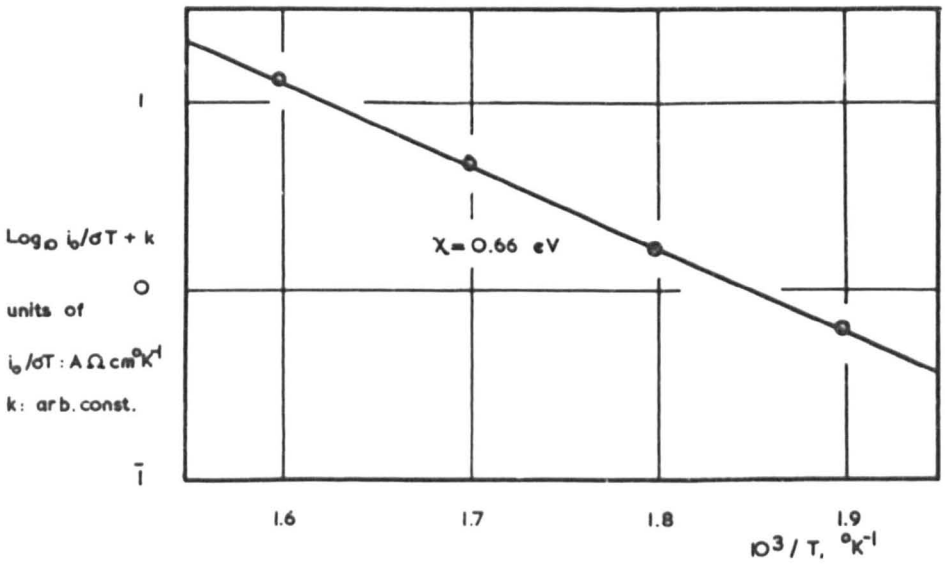

Table 6.5

External work function χ

Tube and activation state	χ, eV: (1)	(2)	(3)
CaO PC 5^2	0.83	0.81	0.66
PC 5^3	1.08	1.10	0.85
PC 5^4	1.28	1.18	1.00
PC 5^5	0.62	0.66	0.55
PC 5^6	0.51	0.58	0.45
PC 6^2	0.56	0.78	0.49
PC 6^3	0.93	0.83	0.99
PC 7^1	1.17	1.20	0.91
PC 9^2	0.81	1.00	0.65
PC 10^1	0.22	0.66	0.21
M 5^1	1.41	1.12	1.09
M 5^2	0.97	0.91	0.72
Averages	0.9 ± .3	0.9 ± .2	0.7 ± .3

The above values of χ have been obtained in three ways:

(1) From the Richardson and low-temperature conductivity plots;

(2) From the corrected high- and low-temperature conductivity plots;

(3) From eqn. 2.19.

a number of different methods: by direct subtraction of the activation energy $\Delta E/2$ obtained from the slope of the low-temperature portion of the conductivity plot from the Richardson work function, or from the value of $\chi + \Delta E/2$ obtained from the corrected high-temperature gradient of the conductivity plot. It can also be obtained from a Richardson-type plot of $\log j_o/\sigma T$ versus $1/T$ (Sec. 2.5, eqn. 2.19), provided the conductivity σ is measured in the low-temperature region. As emission measurements can only seldom be obtained at such low temperatures with CaO diodes, values for χ have been calculated using a linear extrapolation of the Richardson line to find the thermionic emission. Fig. 6.8 shows a plot of $\log_{10} i_o/\sigma T$ versus $10^3/T$ for CaO PC 5^2, the gradient yielding a value of 0.66 eV for χ. Table 6.5 (opposite) gives the values of χ calculated in these three ways.

None of these methods can be said to give a 'true' external work function. That obtained using the Richardson work function suffers from the doubts already expressed as to the validity of the Richardson analysis; that from the two slopes of the conductivity plot probably refers to surfaces which are not the same as those studied in thermionic emission; and the calculation based on semi-

conductor theory has in most cases relied on an extrapolation of the emission measurements to lower temperatures.

Because of the wide spread of results, there is no significant difference between the average values of found by the three methods, although in any particular activation state the three values may vary considerably. An overall average for χ is 0.8 ± .3 eV. There is no evidence to suggest that for any particular cathode χ remains constant during activation: although this result was suggested by Hopkins (87) the deduction must be treated with reserve as, in using eqn. 2.19, he used values from the high- instead of from the low-temperature conductivity region.

6.4. Thermoelectric power and electrical conductivity

A number of tubes, originally designed to observe photoconductive effects, have been employed in the measurement of thermoelectric power in calcium oxide. They consist, in general, of two calcium oxide coated cathodes in contact, the temperature of each cathode being measured by a tungsten-nickel thermocouple, and the heaters being connected independently so that a temperature gradient can be maintained across the oxide

sample. The type of cathode varies from tube to tube: small button cathodes, of area 1.5 mm^2, fitted with commercial heaters and pressed into contact with springy tungsten rods or strips, larger button cathodes of area 40 mm^2, and box cathodes crossed so as to have a common area of about 8 mm^2 have been employed. As tubes to study photoconductivity they were unsuccessful, mainly due to difficulties in the illumination of a sample of CaO only 100 μ thick, but preliminary results of some interest have been obtained when the tubes were used for determinations of thermoelectric power and electrical conductivity.

The carbonate is broken down to oxide in the usual way, and the sample is activated by applying a potential of 4 V between the cathodes with frequent reversals of polarity. A pronounced polarisation effect is noted in the early stages of activation.

The electrical conductivity of the sample is measured by applying potentials of $\pm$ 100 mV between the cathodes and observing the conductivity current, the heaters having been previously adjusted so that the temperatures of the cathodes, as indicated by the thermocouples, are approximately the same. The thermoelectric power of the oxide at any temperature is determined by setting the

FIG. 6.9.1. THERMOELECTRIC E.M.F. VERSUS TEMPERATURE DIFFERENCE CHARACTERISTICS

CaO TC 2[1]

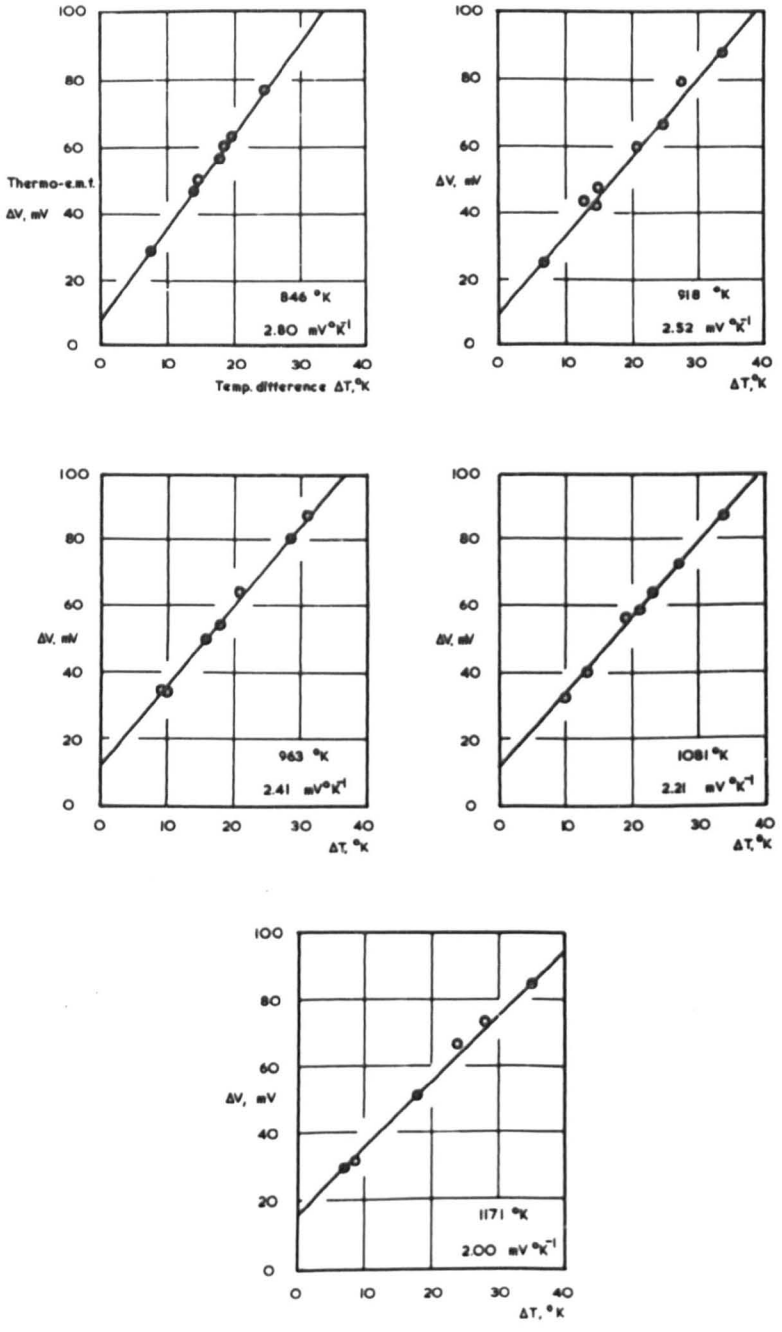

FIG. 6.9.2. THERMOELECTRIC POWER AND ELECTRICAL CONDUCTIVITY AS FUNCTIONS OF TEMPERATURE — GRAPHS OF $\Delta V/\Delta T$ AND Log σ VERSUS $1/T$ — CaO TC 2[1]

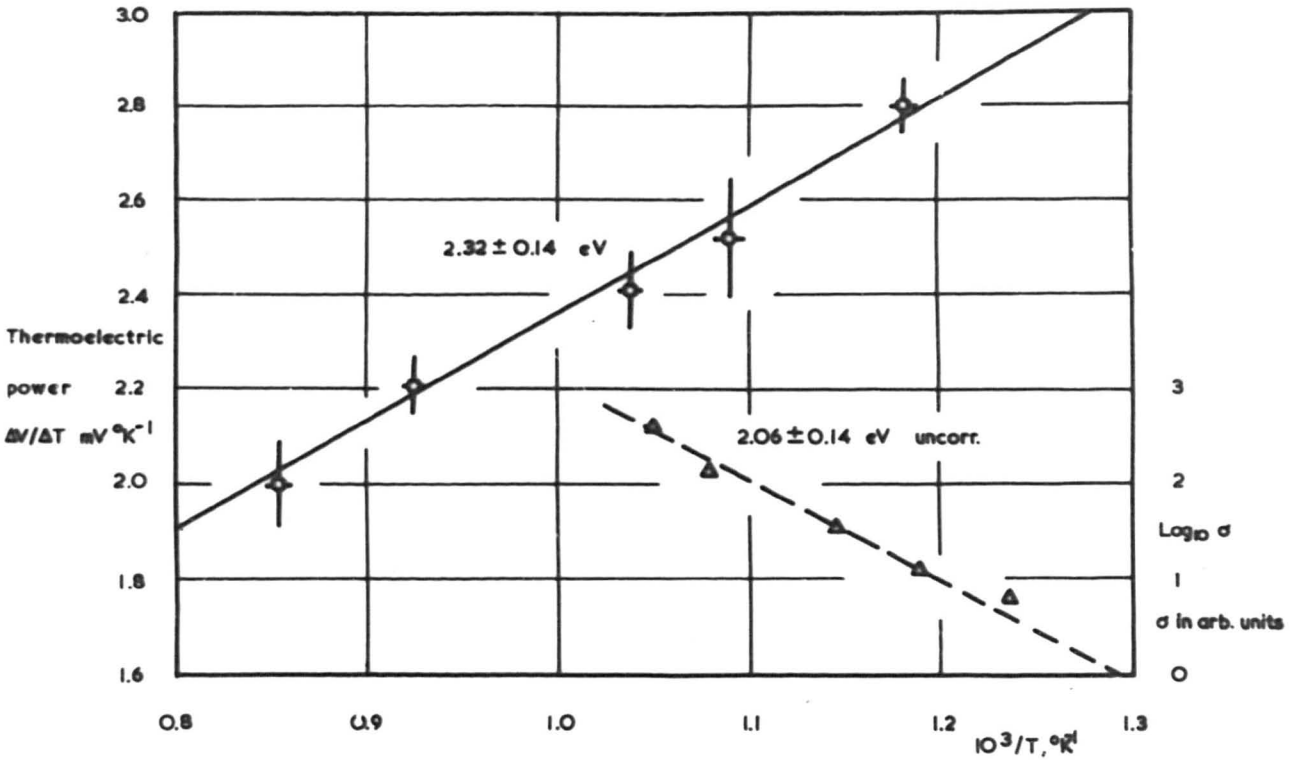

cathodes at temperatures which differ by amounts up to 40 °K, maintaining a constant average temperature and measuring the thermoelectric e.m.f. between the cathodes using a Muirhead Type D 72 A potentiometer with the Cambrell galvanometer as a current indicator. Measurements of the thermoelectric e.m.f. ΔV and temperature difference ΔT are repeated over a range of values and graphs of ΔV versus ΔT have gradients which correspond to the thermoelectric power $\Delta V/\Delta T$ of the sample at the relevant average temperature. Fig. 6.9.1 shows a number of thermoelectric e.m.f. characteristics obtained from CaO TC 2^1. All are linear, but do not pass through the origin. This may be due to differences between the e.m.f. - temperature characteristics of the two tungsten-nickel thermocouples; that this is possible at high temperatures has been mentioned in Sec. 5.4. Thus values of the thermoelectric power obtained from these results may well be in error. In Fig. 6.9.2 the thermoelectric power $\Delta V/\Delta T$ is plotted against $10^3/T$, and a subsequent determination of the electrical conductivity of the specimen is also displayed in the figure. According to the theoretical work of Hensley (78) (Sec. 2.4), the gradients of a graph of the thermoelectric power versus reciprocal temperature for a porous semi-

FIG. 6.9.3. ELECTRICAL CONDUCTIVITY IN CaO SANDWICH DIODES:

GRAPH OF Log σ VERSUS 1/T

CaO TC 4[1]

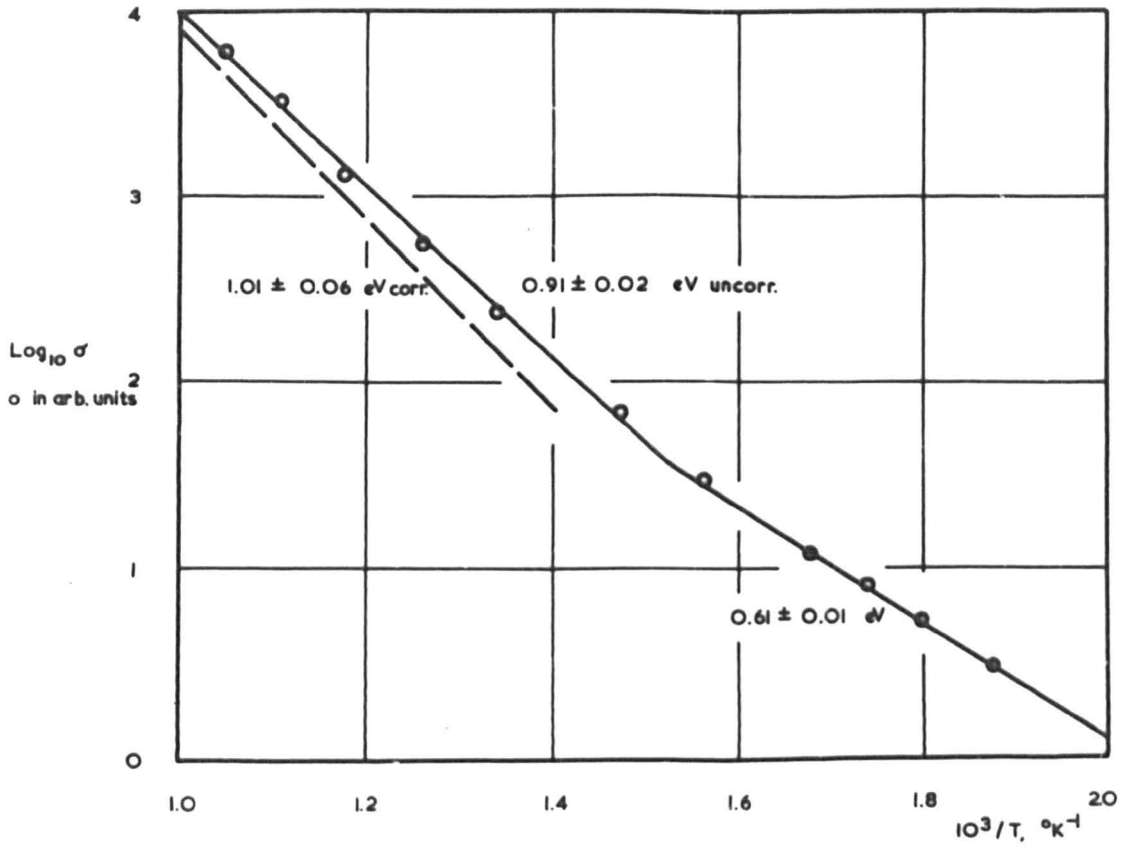

conductor should give the activation energies $\chi + \Delta E/2$ and $\Delta E/2$ of the semiconductor, in the same way as they may be obtained from a graph of log σ versus 1/T. The electrical conductivity of CaO is so small, however, that measurements could not, in this case, be extended below 840 ^{o}K: the smaller the conductivity, the more sensitive the indicator required for the potentiometer. In the small temperature range covered both thermoelectric power and conductivity plots are linear, and their gradients (2.32 ± 0.14 eV and 2.06 ± 0.14 eV, uncorrected) are in fair agreement; but as the low-temperature conductivity region could not be reached, it was not possible to correct the conductivity gradient for the parallel low-temperature mechanism. The effect of the correction is to increase the apparent activation energy, normally by the order of 0.1 eV; this might improve the agreement, but can merely be conjecture.

If conductivity plots obtained from this type of tube are extended to lower temperatures - see, for example, Fig. 6.9.3 for CaO TC 4[1] - the characteristic two-component pattern is produced. Activation energies obtained from this series of diodes are summarised below in Table 6.6.

Values obtained are in general agreement with those

Table 6.6

Activation energies in CaO "sandwich" diodes

Tube and activation state	Conductivity plot gradients		
	High temp. uncorr., eV	High temp. corr. $= \chi + \Delta E/2$, eV	Low temp. $= \Delta E/2$, eV
CaO TC 1^1	2.04 ± .02		
TC 1^2	1.96 ± .04		
TC 2^1	2.06 ± .14		
TC 2^2	1.84 ± .02		
TC 3^1	0.93 ± .03	1.27 ± .10	0.72 ± .02
TC 4^1	0.91 ± .02	1.01 ± .08	0.61 ± .02
TC 5^1	1.75 ± .08		

observed in probe diodes (Table 6.1). Low-temperature activation energies can only be quoted in two cases, due to difficulty in gaining reproducibility of conduction currents at low temperatures: this is thought to be due to mechanical forces caused by thermal expansion of the sprung cathode arrangement, which cause considerable changes in the contact area of the crystallite. This would be expected to affect the low-temperature conductivity to a greater extent than the high-temperature mechanism.

6.5. Discussion of results

There is general agreement between the average values

of the Richardson work function ϕ and the activation energy $\Delta E/2$ obtained in the present work and those given by Hopkins (87), although on occasion low Richardson work functions, of the order of 1.0 eV, have been obtained. It has been established that these are not due to a difference in the thermionic properties of the cathode spray employed compared with that used by Hopkins.

The question of the interpretation of Richardson plots is a vexed one. The gradient has been taken by a number of authors (4, 9) to represent the work function determined by an extrapolation to absolute zero, assuming the work function to be a linear function of temperature over the entire range. In the present work the deduction of 'work functions' by taking the gradient of the second order Richardson curve at a number of temperatures may not be theoretically sound, as here the work functions are a linear function of reciprocal temperature; but the fact that the temperature coefficient of the c.p.d., which, assuming the anode work function to be constant, must numerically give the temperature coefficient of the cathode work function, is found to agree with the approximate temperature coefficient obtained from the second order curve argues in favour of the method.

The measurements on thermoelectric power, although

hampered by the low electrical conductivity of the oxide, have been more successful than those reported by Glascock and Mensley (70), and suggest a field for further investigation.

Chapter 7 Photoelectric emission and photoconductivity in calcium oxide: preliminary results and discussion

7.1. Introduction

Preliminary measurements reported in a previous thesis (116) suggested that, for comparable illumination, activated BaO and CaO cathodes yield photoelectric emission and photoconductivity currents of about the same order of magnitude. BaO, however, is thermionically much more active: thermionic emission currents from BaO and CaO cathodes at the same temperature might be in the ratio of about 100 : 1. With respect to measurements of its photoelectric properties, the very low thermionic emission and electrical conductivity of CaO are not disadvantageous; dark emission and conductivity currents, which in BaO must be allowed for even at room temperature (116), are of little consequence in CaO up to about 600 ^{o}K, and below this temperature photoelectric measurements can be made relatively easily.

A number of designs of tube have been employed in the course of the present study of the photoelectric properties of calcium oxide. Although the geometry of the probe diode is excellent for photoelectric emission measurements when a small anode window is provided, it

is not so suitable for measurements of photoconductivity between the probe and cathode base. The electrodes and sample are bound to be unevenly illuminated, the probe always receiving a greater intensity of illumination than the base. In spite of this, the relative ease of construction of the probe diode has made it the most valuable type of tube used in the present work. Before the oxide sample in a sandwich-type diode (described in Sec. 6.4) can be made thick enough to be adequately illuminated, the dark conductivity will become too small to measure except at high temperatures, and comparison with the dark electrical properties is impossible. Tubes in which evaporated films of the oxide are deposited between electrodes on a non-conducting surface have also been constructed; as their electrical and photoelectric properties are rather different from those of the bulk oxide cathode, they are discussed separately in Chap. 9.

7.2. External photoelectric emission

7.2.1. Current - voltage characteristics

The normal procedure has been to determine the current - voltage characteristic for external photo-emission for white-light illumination by the tungsten filament lamp for each activation state of each cathode.

FIG. 7.1. PHOTOELECTRIC EMISSION FROM CaO : WHITE-LIGHT CURRENT – VOLTAGE CHARACTERISTIC – CaO PC 5[5]

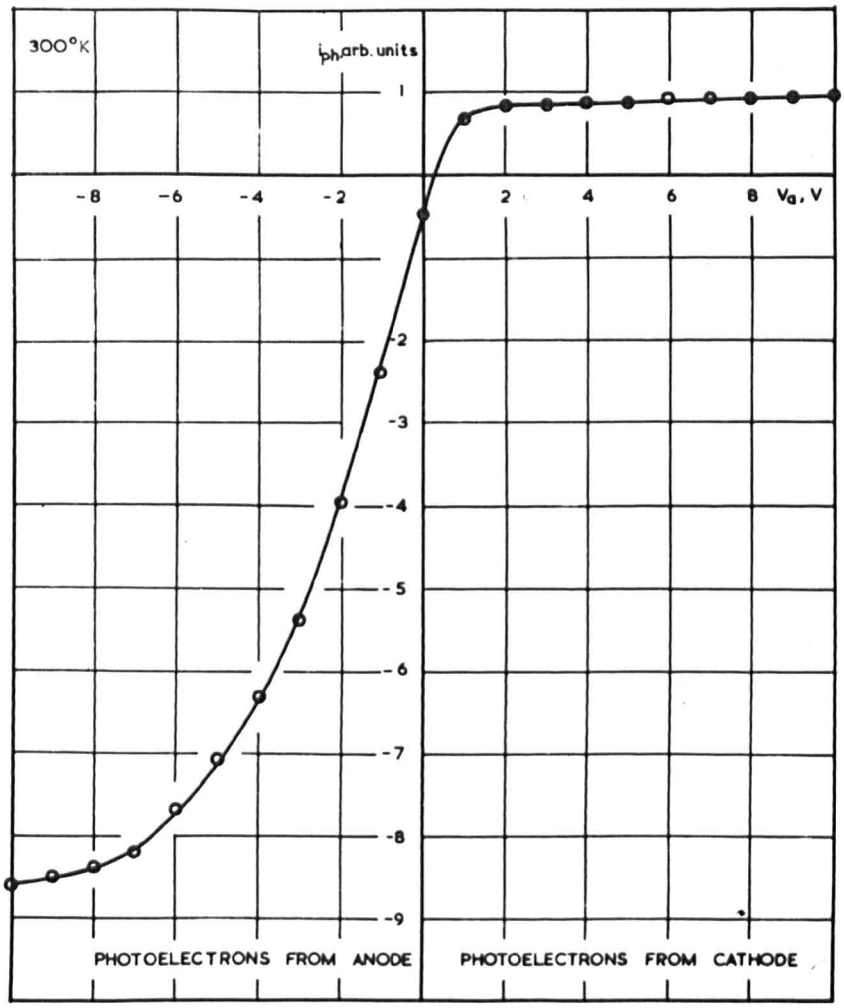

The magnitude of the currents gives a rough guide as to the photosensitivity of the cathode. A typical curve is given in Fig. 7.1 for CsO PC 5^5 at room temperature. It is observed that both cathode and anode are photosensitive. In this case the anode is very much more photosensitive than the cathode, as not only is the photocurrent from the anode greater than that from the cathode by a factor of about 10, but the illumination of the anode is much less; it can only receive light by reflection from the cathode surface. Photocurrents saturate in each direction.

Fig. 7.1 illustrates another general phenomenon: a photocurrent may be observed for zero applied potential. Electrons are drawn from the cathode (or anode) under the influence of the c.p.d. between the electrodes.

7.2.2. Spectral sensitivity of photoemission

In many cases the magnitude of the white-light photoemission from the cathode is not sufficient to allow the determination of the spectral sensitivity of the effect with the electrometer available. In cases where the saturated white-light emission is sufficiently large ($\sim 10^{-7}$ A with the 500 watt source) the sensitivity is determined using the method described in Sec. 5.6,

FIG. 7.2.1. INTENSITY OF ILLUMINATION AS A FUNCTION OF WAVELENGTH

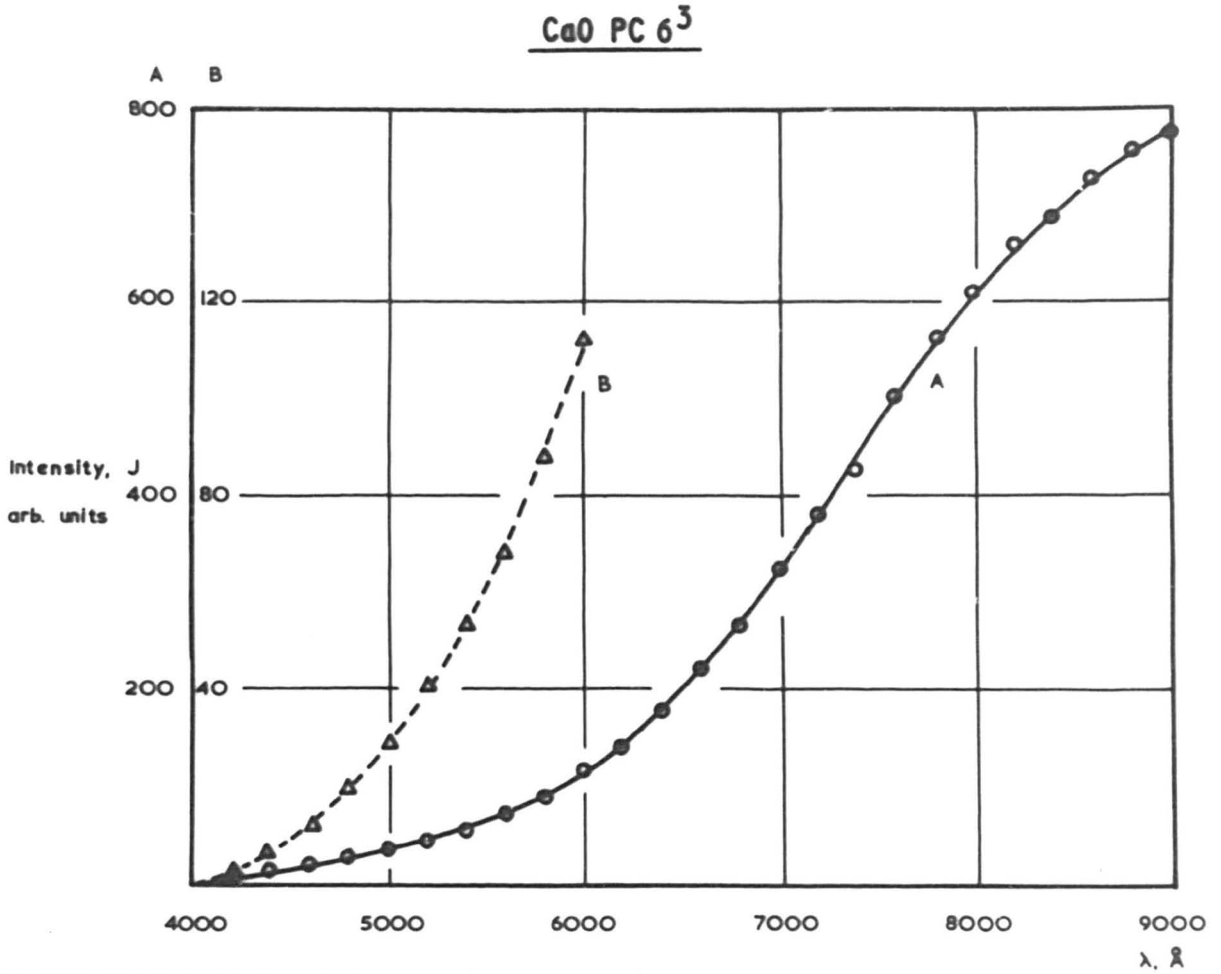

FIG. 7.2. SPECTRAL SENSITIVITY OF PHOTOELECTRIC EMISSION FROM CaO — CaO PC 6[3]

FIG. 7.2.2.

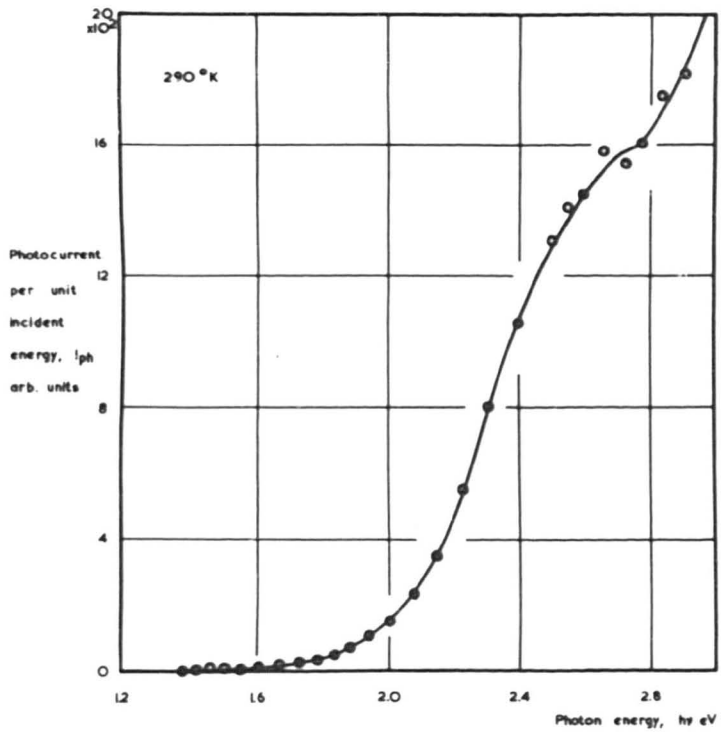

FIG. 7.2.3.

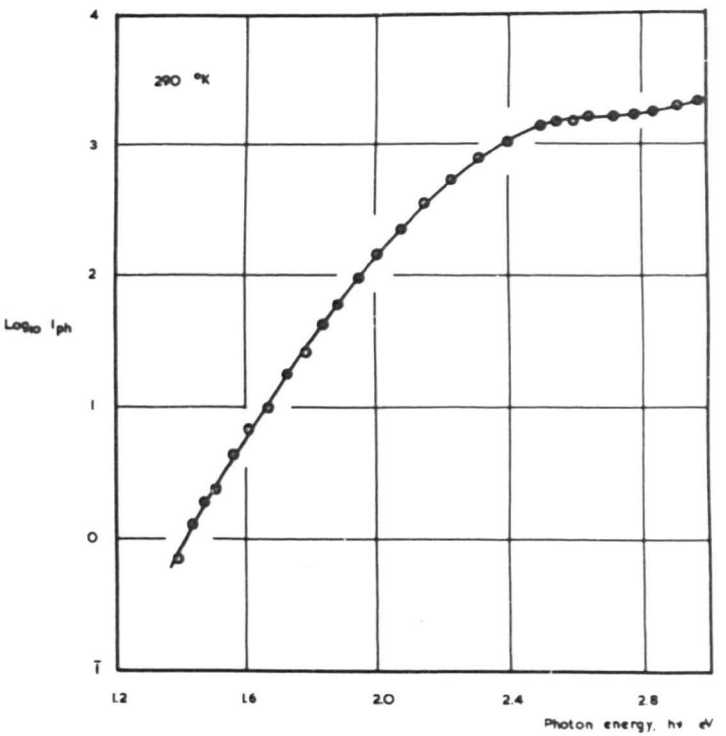

the absorption of the envelope of the tube being allowed for. A typical calibration curve for the relative intensity of illumination reaching the cathode surface as a function of wavelength is given in Fig. 7.2.1 for CaO PC 6^3. The intensity, by the nature of the tungsten filament source, is strongest in the red and near infra-red, and is rather weak in the blue and violet regions of the spectrum. Experiment shows, however, that the photosensitivity of calcium oxide is least in the red and increases towards the violet, so that the photo-currents obtained by illuminating a cathode with the combination of tungsten filament lamp and monochromator do not change by more than two orders of magnitude over a considerable wavelength range. The actual photo-current at any wavelength for an anode potential sufficient to cause saturation is divided by the relative intensity of illumination at that wavelength to give the photocurrent per unit incident intensity; repeated over the whole wavelength range, a spectral sensitivity curve may be traced. The curve for CaO PC 6^3 is given in linear and logarithmic forms in Figs. 7.2.2 and 7.2.3. The photocurrent per unit incident energy at a given wavelength is given in arbitrary units in all cases, but for the typical case of CaO PC 6^3 the photocurrent

FIG. 7.3. SPECTRAL SENSITIVITY OF PHOTOELECTRIC EMISSION FROM CaO — CaO PC 5^{2-5}

FIG. 7.3.1.

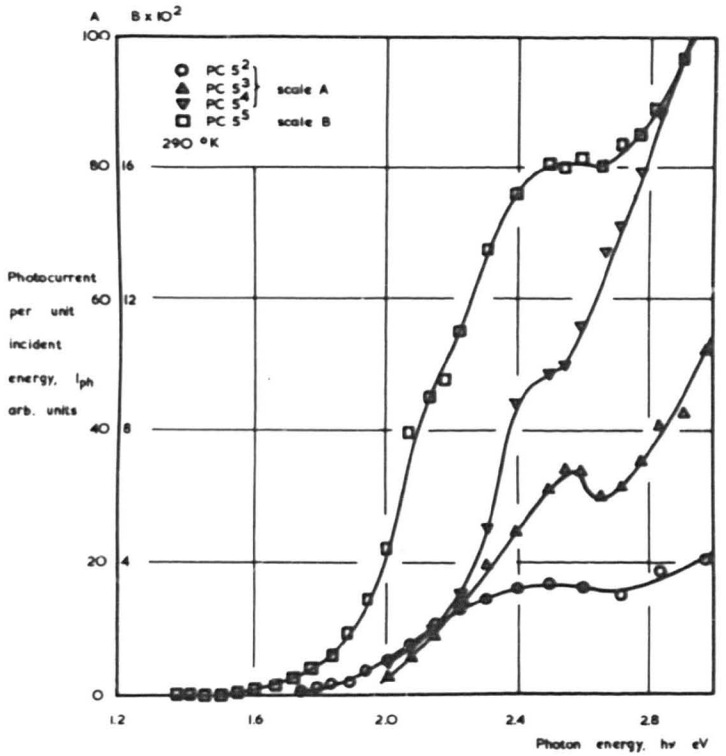

FIG. 7.3.2.

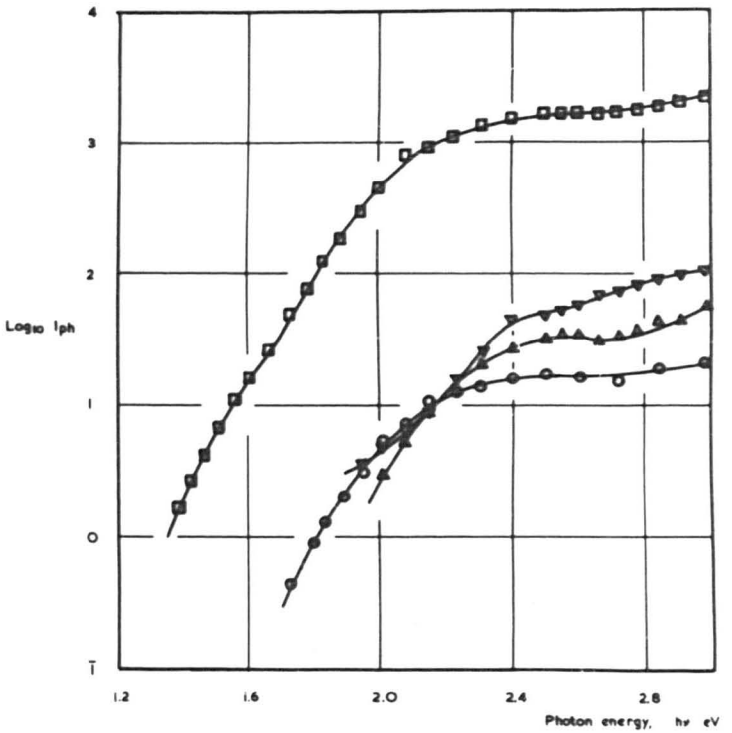

FIG. 7.4. SPECTRAL SENSITIVITY OF PHOTOELECTRIC EMISSION FROM CaO

FIG. 7.4.1. CaO PC 8^2, CaO X 1

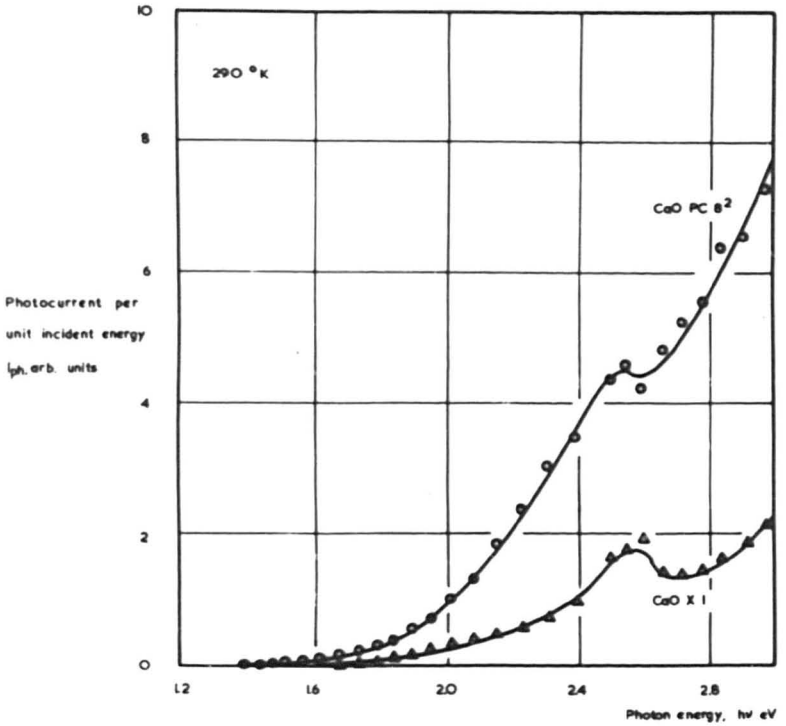

FIG. 7.4.2. CaO PC 9^4, CaO PC 10^1

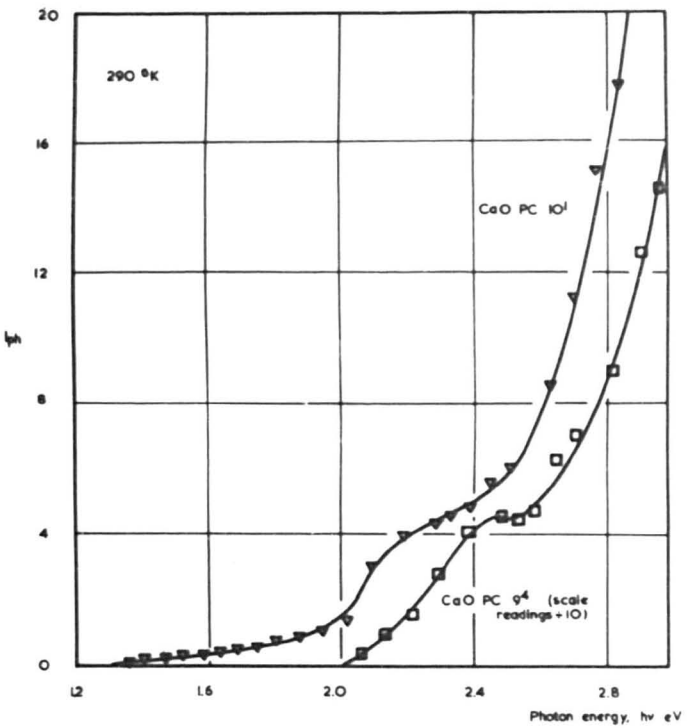

FIG. 7.4.3. SPECTRAL SENSITIVITY OF PHOTOELECTRIC EMISSION FROM CaO – CaO PC 8^2, CaO PC 9^4, CaO PC 10^1, CaO X I

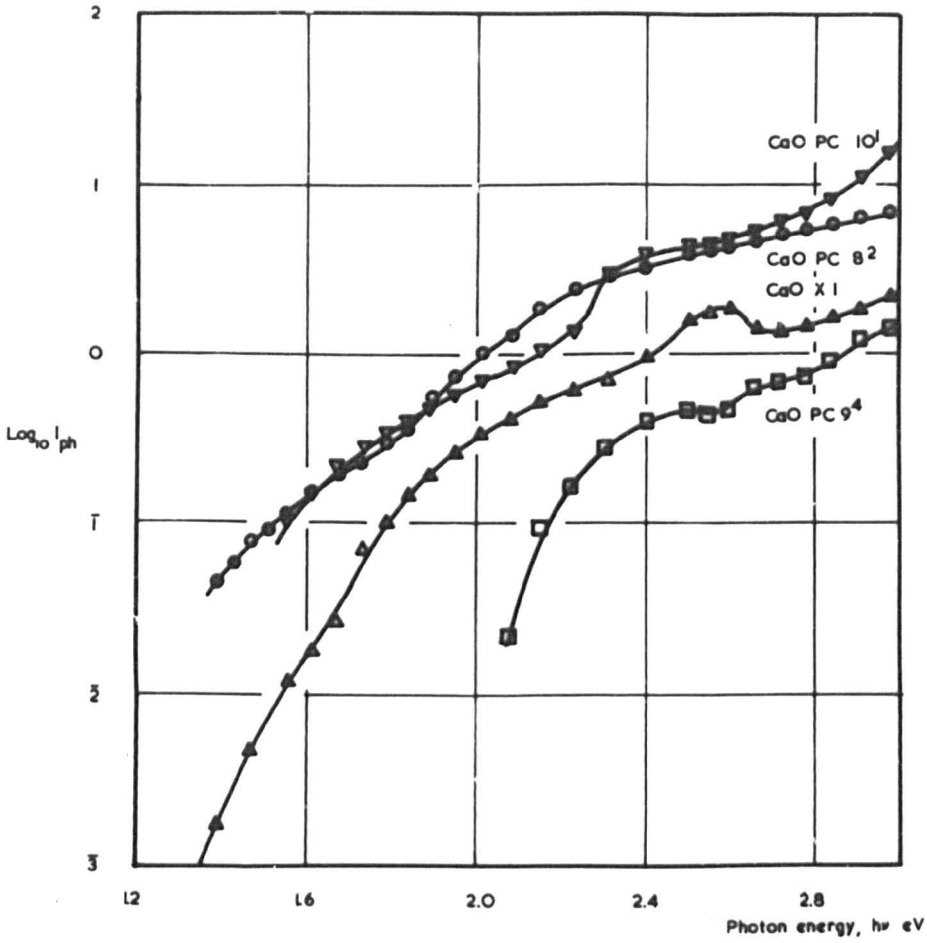

for light of an incident wavelength of 5600 Å (2.23 eV) and incident power about 10^{-6} watts was about 10^{-11} A.

Similar curves are given in Figs. 7.3.1 and 7.3.2 for the spectral sensitivity of photoemission from the cathode in activation states 2 - 5 inclusive of CaO PC 5, and in Figs. 7.4.1, 2 and 3 for a number of activation states of different cathodes. The structure of the curves will be discussed in detail in Sec. 7.5, but it can be noted at this stage that the characteristics approach the photon energy axis approximately exponentially, as shown by the nearly linear portions of the logarithmic curves at lower photon energies, and that some structure is apparent at about 2.6 eV in all cathodes. The structure is more obvious in the curves drawn against linear scales, and may take the form of a definite peak (e.g. CaO PC 5^2, CaO X 1), but is more often merely a point of inflexion.

7.2.3. Complete photoelectric emission

The method of complete photoelectric emission (Sec. 3.4) has been used to obtain the photoelectric work function of a number of cathodes. The considerable doubt attached to the theory of the method (81) suggests that the values obtained cannot be treated as more than

FIG. 7.5. PHOTOELECTRIC WORK FUNCTION BY COMPLETE PHOTOEMISSION – CaO PC 1

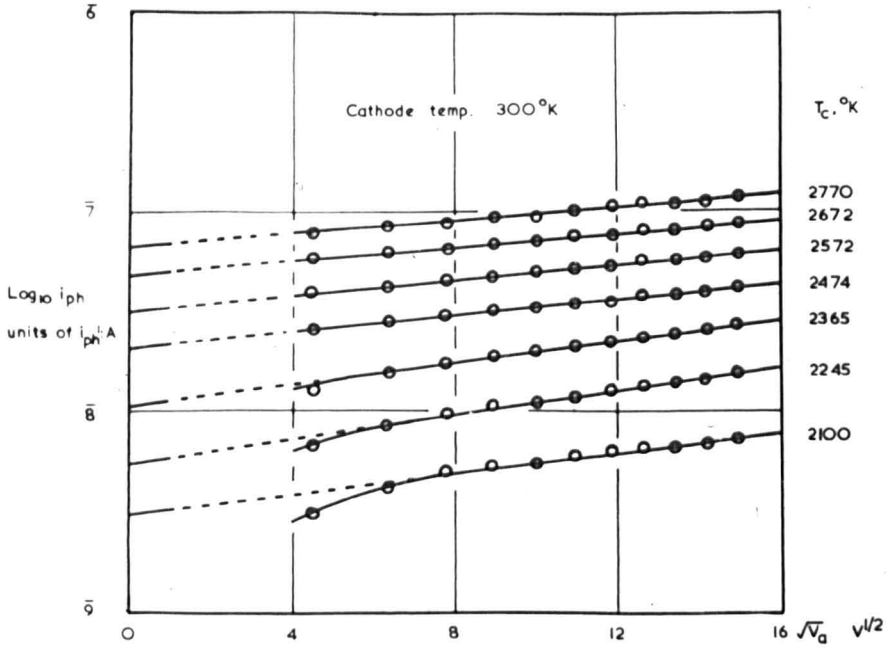

FIG. 7.5.1. 'SCHOTTKY' PLOTS

FIG. 7.5.2. 'RICHARDSON' PLOT

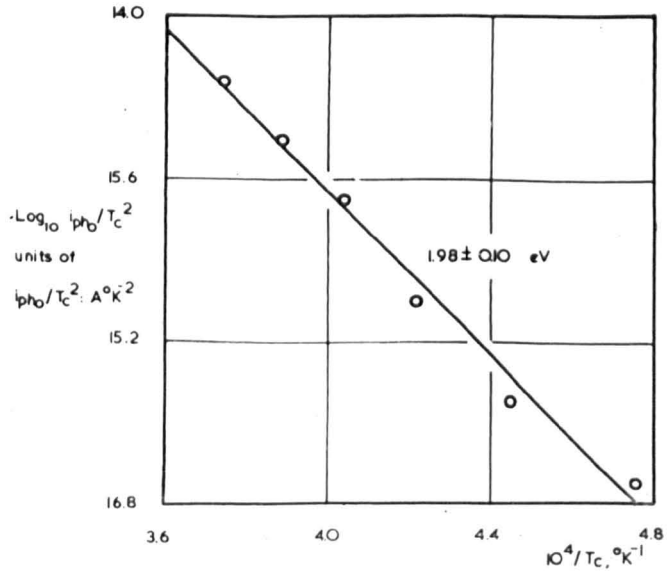

an arbitrary measure of the photosensitivity.

The method employed has been described more fully in a previous thesis (116) and is given here in an outline form. It is assumed that the spectral distribution of wavelengths from a tungsten filament lamp at temperature T is equivalent to that from a black-body at a corresponding colour temperature T_c. The temperature T of the filament of the 500 watt lamp is deduced from its resistance, and the appropriate values of T_c are obtained from tables (13). At various temperatures of the source filament, the input voltage of which is controlled by means of a Variac transformer, the photocurrent i_{ph} is determined as a function of anode voltage V_a. "Schottky" plots of $\log_{10} i_{ph}$ versus $V_a^{\frac{1}{2}}$ for various values of the filament colour temperature are linear and their intercepts on the vertical axis give the zero-field emission, i_o. A "Richardson" plot of $\log_{10} i_o/T_c^2$ versus $1/T_c$ has a gradient from which the photoelectric work function may be deduced.

Figs. 7.5.1 and 2 show the "Schottky" and "Richardson" plots for complete photoemission from CaO PC 1^1 at 300 °K. The arbitrary photoelectric work function obtained from the gradient of the latter curve is 1.98 ± 0.10 eV; a determination at a cathode temperature

FIG. 7.6. TEMPERATURE VARIATION OF PHOTOELECTRIC EMISSION – CaO PC 5[2]

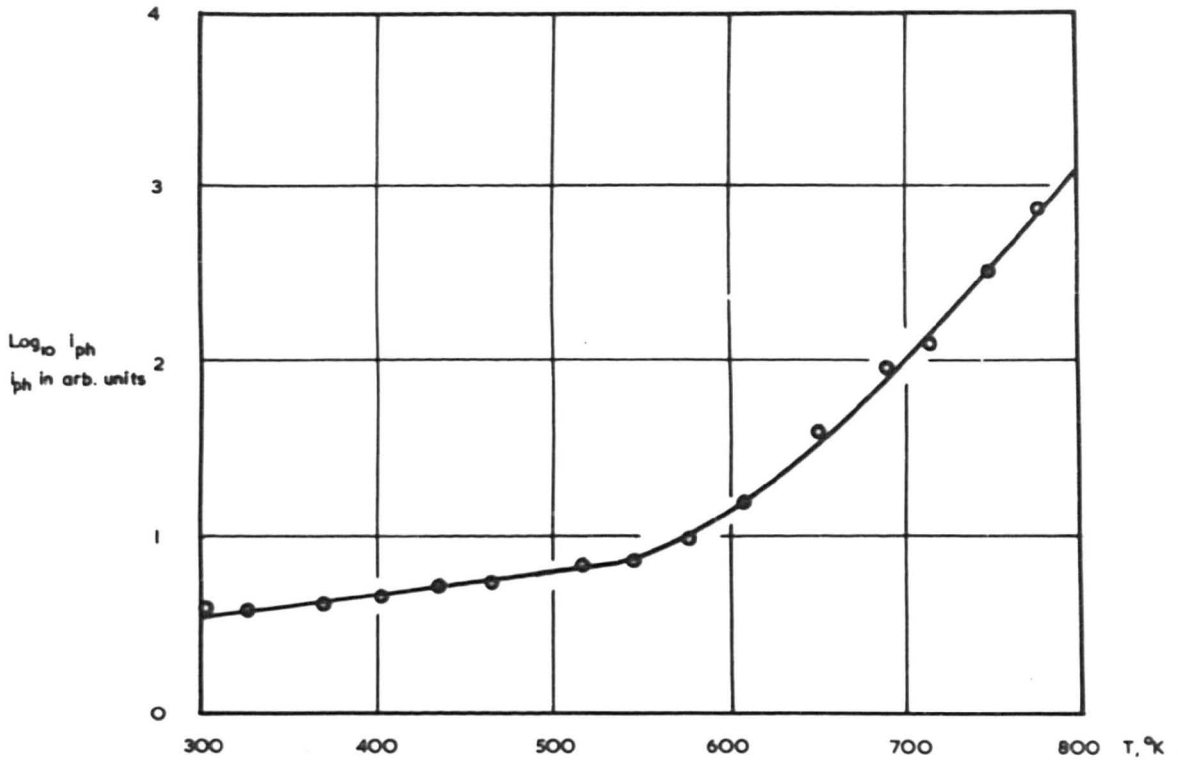

of 425 ^{o}K gave a value of 1.83 ± 0.03 eV. This reduction in the photoelectric work function with increasing cathode temperature has also been noted with barium oxide cathodes (116); in the present case the experimental error is so large that the reduction may not be significant.

The method is slow and involves considerable computation; thus, it is not employed regularly as a measure of photosensitivity in all cathode states.

7.2.4. Temperature variation of external photoelectric emission

The temperature variation of photoelectric emission due to white-light illumination can be determined by observing the saturated photocurrent as the cathode temperature is increased, making allowance for thermionic emission.

Results obtained for CaO PC 5[3] are shown in Fig. 7.6: a slow increase of photoemission with temperature is observed up to about 600 ^{o}K, where a more rapid rise is noted. Above about 800 ^{o}K photocurrents are small compared with thermionic emission, and accurate results cannot be obtained.

FIG. 7.7. MAGNETIC VELOCITY ANALYSIS TUBE – SCHEMATIC ARRANGEMENT

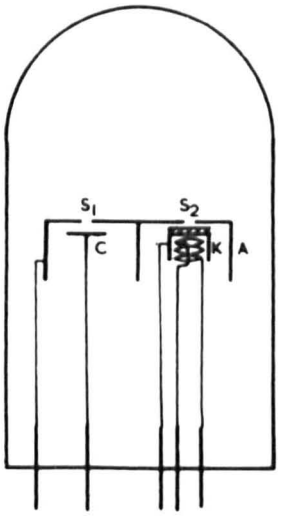

FIG. 7.9. RETARDING POTENTIAL TUBE – SCHEMATIC ARRANGEMENT

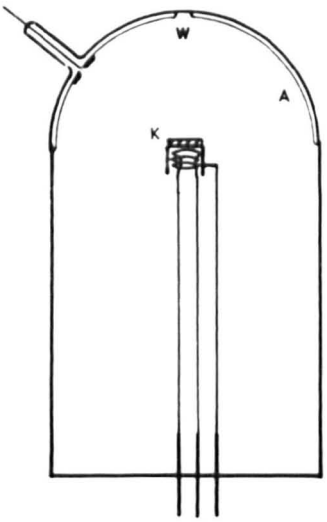

1 cm

7.2.5. Energy distribution of photoelectrons

Attempts have been made to measure the energy distribution of photoelectrons emitted from CaO cathodes in two ways. The first used the method of magnetic velocity analysis, the second a retarding potential method; but in each case the photocurrents under monochromatic illumination were too small to measure with sufficient accuracy to obtain the energy distribution, and this section must represent an account of the preliminary development of the two methods.

The magnetic velocity analysis tube (CaO X 2) follows the design employed by Philipp (144) in his work on barium oxide and is shown diagrammatically in Fig. 7.7. The tantalum box anode A bears in its upper face two 1 mm wide slits, S_1 and S_2, separated by 2.5 cm. Behind S_2 is mounted the button cathode K, coated with the usual calcium carbonate suspension and provided with a commercial heater. A collector C is mounted behind S_1: a partition in the box prevents the direct transition of electrons from K to C. The normal evacuation and breakdown procedure is carried out.

The tube is placed so that the plane containing the slits is vertical between two horizontal Helmholtz coils, each of 500 turns and mean diameter 35.4 cm, separated

by a vertical distance of 15 cm. The coils are connected in series with a 24 V battery through a rheostat, reversing switch and an ammeter; the direction of current flow is normally such that the magnetic field produced by the coils reinforces the vertical component of the earth's field. If the current I in the coils is measured in amps, the total vertical magnetic field at the point midway between the coils is given by

$$H_T = \pm 27.72\ I + V_e \text{ oersted} \qquad 7.1.$$

where the sign of the first term depends on the direction of current flow and V_e is the vertical component of the earth's magnetic field. The magnetic elements at the position of the Helmholtz coils were obtained by a subsidiary experiment using a deflection and vibration magnetometer and a dip circle: the vertical component V_e was found to be 0.257 oersted, and was undoubtedly influenced by the propinquity of a quantity of magnetic materials and of a mass-spectrometer magnet, which, however, was running at the same current throughout the determinations.

The principle of the method is as follows. The cathode is irradiated with monochromatic illumination and the anode and collector potentials are fixed at a

suitable value (e.g. 6 V each, independently connected). Photoelectrons are attracted towards the box anode and some pass through the slit. Under the influence of the magnetic field H_T, perpendicular to their direction of motion (the tube is placed so that the slits lie in the same E - W line), they move in semicircular paths of radius r given by

$$V = \tfrac{1}{2}(e/m)r^2H_T^2 \qquad 7.2.$$

where V is the energy of the electron. The experimental arrangement fixes the radius r at 1.25 cm, assuming that all electrons pass through the slits normally, and electrons of any energy V may be selected and collected at the collector by applying the corresponding value of H_T so that the electrons move in the semicircular path defined by the line joining the two slits as diameter. Expressing V in volts and H_T in terms of the current I in the coils, from eqn. 7.1

$$V = 0.137 \ (27.72\ I + 0.257)^2 \qquad 7.3.$$

The collector current, i_C, is a measure of the number of electrons of energy V corresponding to the field produced by the magnet current I.

A typical curve showing the energy distribution of thermionic electrons from the cathode at 1200 ^{o}K

FIG. 7.8. ENERGY DISTRIBUTION OF THERMIONIC ELECTRONS — CaO X 2

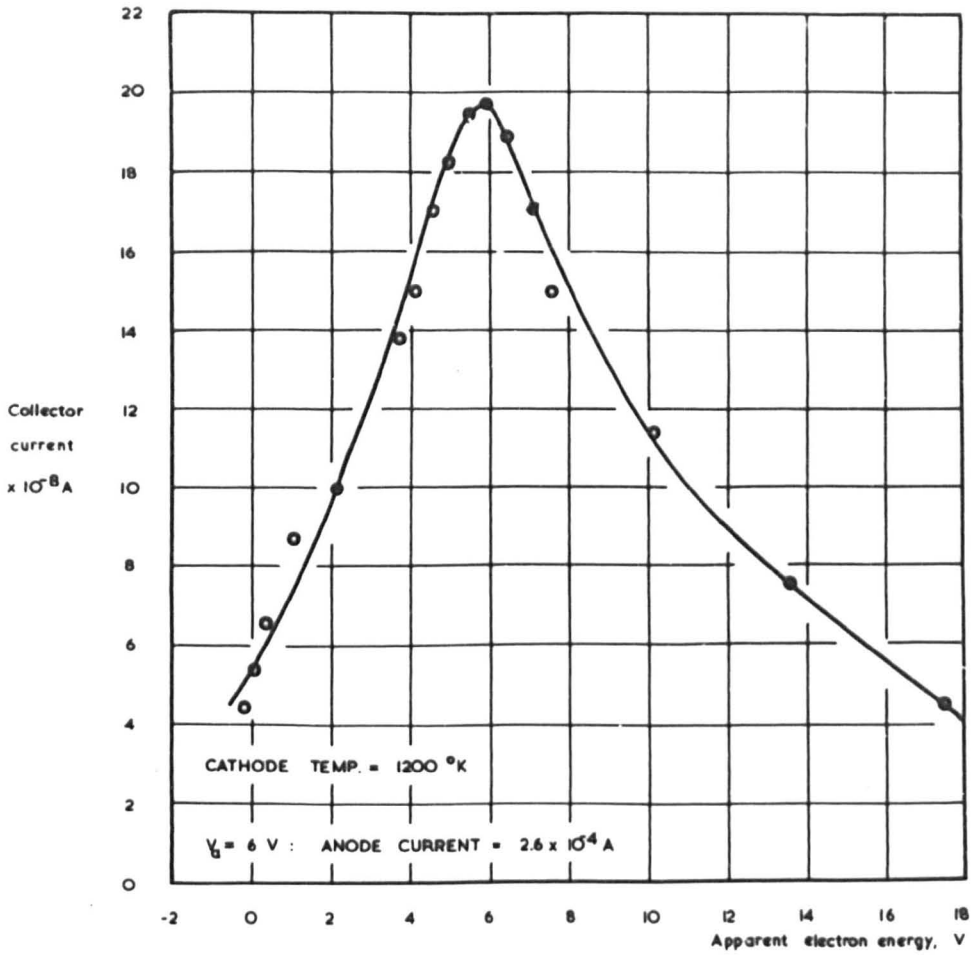

and at an anode potential of 6 V is shown in Fig. 7.8. The peak current, 2.2×10^{-7} A, is rather less than 0.1 % of the anode current, 0.26 mA, and occurs at approximately 6 eV. According to theory (144) the peak should appear at an energy of $(V_a + kT)$, neglecting any c.p.d. between collector and cathode: at a cathode temperature of 1200 °K and an anode voltage of 6 V the value of $(V_a + kT)$ is about 6.1 eV. The spread of energies is apparently very considerable, and includes some electrons which appear to have negative energies. It is suggested that this may in part be due to the fact that the design of tube does not ensure that the electrons pass through the slit normally, and thus the radius of curvature of the electron path may take values both greater and less than 1.25 cm, tending to extend the high- and low-energy tails of the distribution. The insertion of an additional slit to define the semi-circular path would probably reduce the fraction of the total anode current reaching the collector even further. Electrons with "negative energies" were also observed by Philipp (144) and were ascribed by him to the finite resolution of the velocity analyser.

Even after continued activation, photoelectric currents from the cathode are small: the white-light

photoemission to the anode is of the order of 10^{-7} A (the same order of magnitude as is found with probe diodes), and thus the currents reaching the collector would be expected to be of the order of 10^{-12} to 10^{-11} A. It is not, in fact, possible to use the electrometer to measure these small currents; the tube cannot be screened and the electrometer currents are very unstable. If monochromatic illumination was employed, the intensity of the radiation would be reduced and the photocurrents would be expected to be less by a factor of about 10^2, if optical filters were used, or 10^4 if the monochromator was used to provide the illumination. Thus, with the present design of tube and the methods available for the measurement of small currents, the energy distribution of photoelectrons cannot be obtained.

The second method attempted employs the principle of finding the energy of the photoelectrons by applying a retarding potential to the anode just sufficient to prevent electrons from the cathode from reaching it. The distribution of energies is obtained by differentiating the retarding potential characteristic. Only the normal component of the electron velocity is affected by the retarding field, and to ensure that the photoelectrons strike the anode normally, it is necessary to carry out

the investigations in tubes of spherical symmetry, with a small cathode at the centre of a large spherical anode. It is also advisable to choose a system where photo-electrons are not likely to be emitted from the anode, to avoid carrying out a correction for a component of the retarding field current due to electrons travelling from the anode to the cathode. The spurious results which can arise from a neglect of these factors have been discussed by Hughes and DuBridge (5). Although retarding potential characteristics are easily obtained from the probe diode type of tube, they would not yield the true energy distribution.

Accordingly two retarding-potential tubes (CaO R series) have been constructed embodying a different diode geometry. Instead of employing spherical symmetry, an arrangement of some practical difficulty, a hemi-spherical anode formed by the inner surface of the end of the standard envelope, coated with a conducting layer, is used, with a small button cathode 7.5 mm in diameter at the centre of the sphere of which the hemisphere forms part. The cathode is provided with a heater and is coated with the usual carbonate suspension. The hemi-spherical arrangement (Fig. 7.9) ensures that electrons striking the anode do so normally. The conducting

FIG. 7.10. CURRENT-VOLTAGE CHARACTERISTICS FOR PHOTOCONDUCTIVITY IN CaO CATHODES

FIGS. 7.10.1,2. WHITE-LIGHT ILLUMINATION – CaO PC 5^2

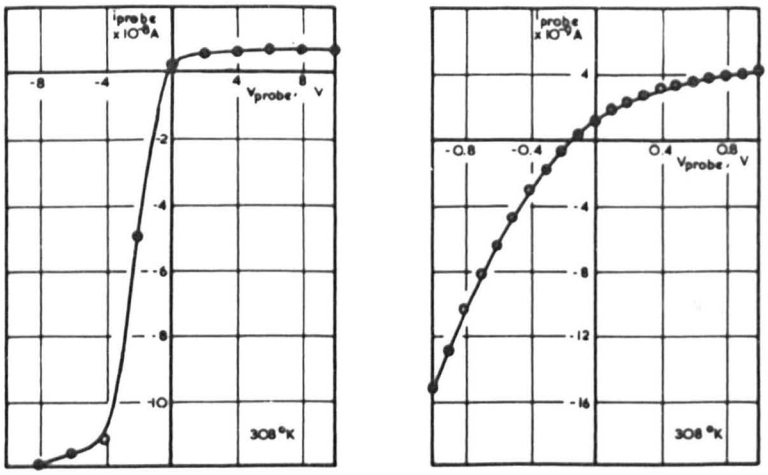

FIG. 7.10.3. MONOCHROMATIC ILLUMINATION – CaO PC 6^4

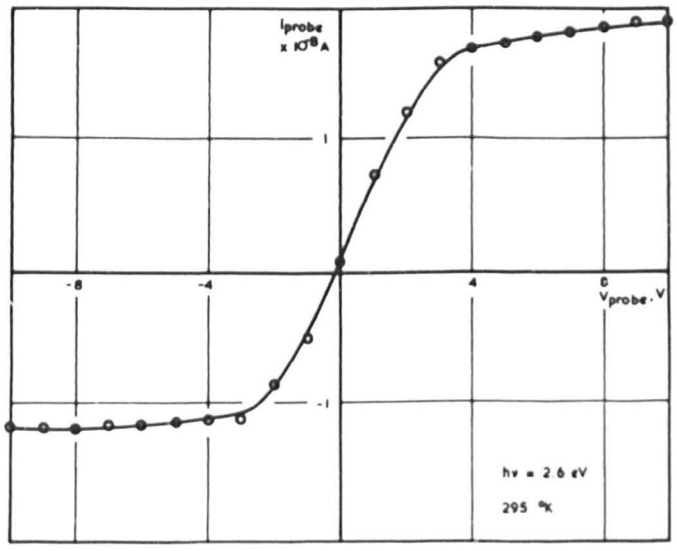

of the characteristic accurately; either due to the instability of the electrometer over the periods of time involved, or to temporal changes in photocurrents (116), the electrometer readings fluctuate too much for any weight to be placed on the results. Particular care is needed in the determination of the characteristics, as the energies are to be obtained by differentiation and a slight error in the form of the curve would involve a large error in the energy distribution.

7.3. Photoconductivity

7.3.1. Current - voltage characteristics

Current - voltage characteristics for photoconductivity induced by white-light illumination are determined by illuminating the cathode with light from the 500 watt tungsten filament lamp, applying potentials of up to ± 10 V between the probe and cathode base, and determining the corresponding photocurrents with the galvanometer or electrometer. Dark conductivity currents need not be allowed for at temperatures up to about 500 ^{o}K.

Typical characteristics are shown in Figs. 7.10.1 and 2 for CaO PC 5^{2}. Probe potentials of up to ± 10 V, very much greater than in dark conductivity measurements, are employed to display the marked saturation effect in

FIG. 7.11. SPECTRAL SENSITIVITY OF SATURATED POSITIVE AND NEGATIVE PHOTOCONDUCTIVITY CURRENTS IN CaO CATHODES – CaO PC 9[4]

FIG. 7.11.1.

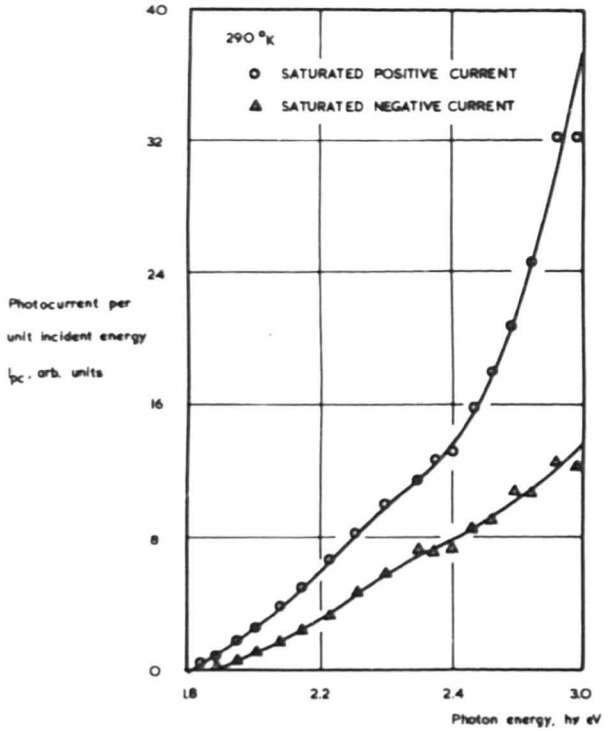

FIG. 7.11.2.

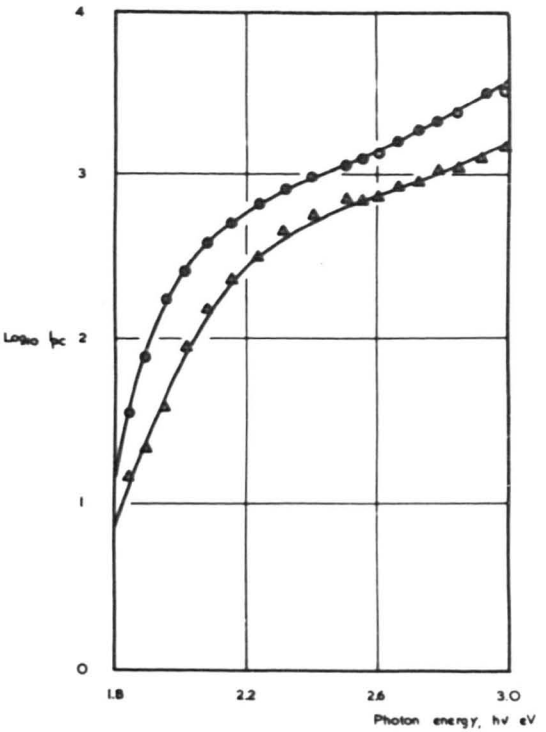

each direction (Fig. 7.10.1): later work will suggest that it is the saturated photoconductivity currents which are of importance in defining the photoconductivity of the cathode rather than, for instance, the slope of the characteristic near the origin (Fig. 7.10.2).

Similar characteristics are obtained when monochromatic illumination is provided. Fig. 7.10.3 shows the curve for CaO PC 6^4, illuminated with light of wavelength 4850 Å (2.6 eV), using a Kodak Wratten Filter No. 75 with the tungsten filament lamp.

7.3.2. Spectral sensitivity of photoconductivity

The spectral sensitivity of photoconductivity currents is determined in exactly the same way as for external photoelectric emission. In some cases (e.g. Fig. 7.10.1) the photoconductivity current is very much greater in one direction than in the other, and it may only be possible to determine the spectral sensitivity of the current in one direction. Figs. 7.11.1 and 2 show the spectral sensitivity curves for saturated positive and negative photoconductivity currents in CaO PC 9^4. The logarithmic plot shows that the negative current differs from the positive by an approximately constant multiplying factor throughout the photon energy

FIG. 7.12. SPECTRAL SENSITIVITY OF PHOTOCONDUCTIVITY IN CaO — CaO PC 5^{2-5}

FIG. 7.12.1.

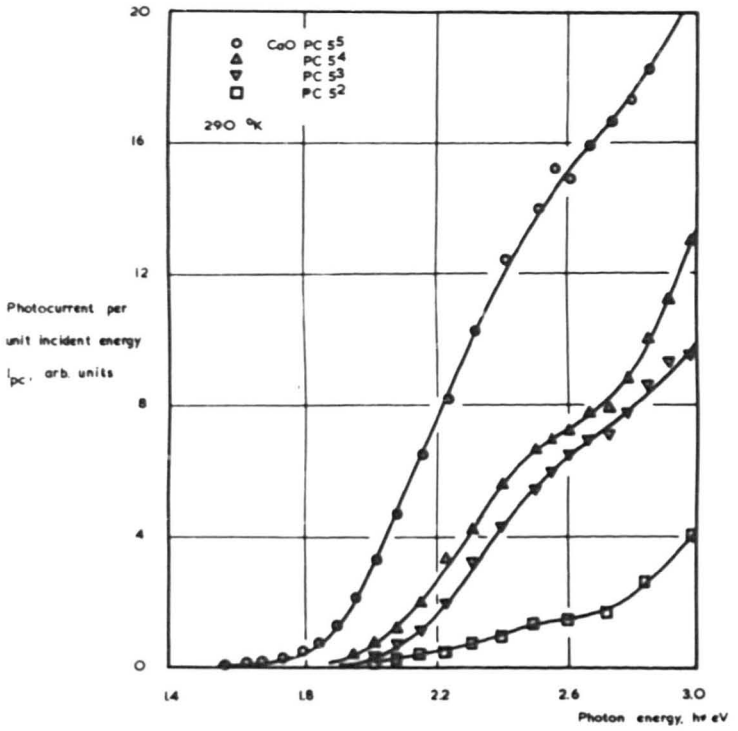

FIG. 7.12.2.

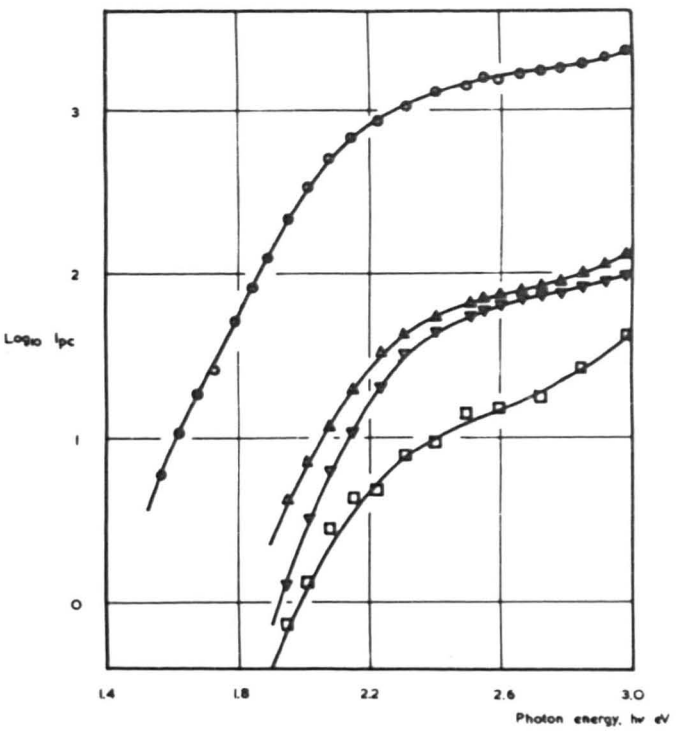

range, and there is no reason to suppose that there should be any serious discrepancy between the characteristics in cases where only one could be determined.

Further curves are given in Figs. 7.12.1 and 2 for four activation states of CaO PC 5. In all cases the saturation photoconductivity currents, for 10 V applied between probe and cathode base, are measured.

It should be noted that practically all the plots on linear scales show some structure at about 2.6 eV.

7.3.3. Photoconductivity - intensity relationship

The relation between the magnitude of the photoconductivity currents and the intensity of illumination has been investigated by moving the tungsten filament lamp so that it stands at different distances from the tube under investigation in the screened box and measuring the photoconductivity currents as a function of distance and hence of intensity of illumination. The intensity calibration is carried out using the 53 CV photocell in place of the tube, using a neutral filter to reduce the intensity falling on the photocathode. This procedure is to be preferred to an inverse-square calculation, which fails at small distances as the tungsten filament can no longer be regarded as a point

FIG. 7.13. PHOTOCURRENT—ILLUMINATION RELATIONSHIP FOR PHOTOCONDUCTIVITY CURRENTS

CdO PC 5[2]

FIG. 7.13.1.

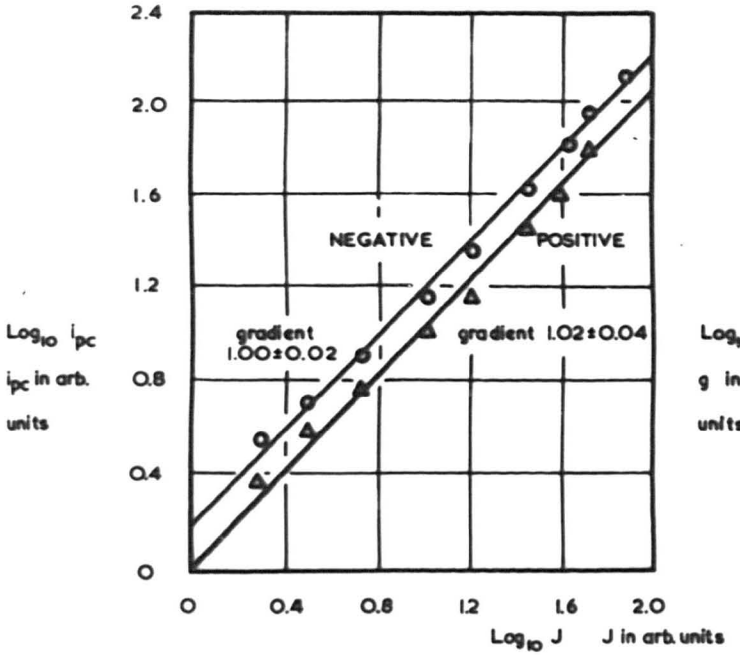

FIG. 7.13.2.

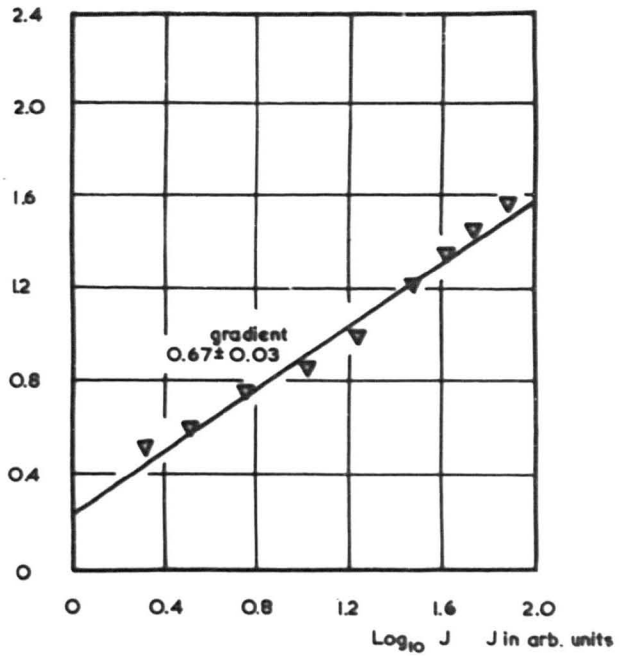

source.

Fig. 7.13.1 (for CaO PC 5^2) shows the logarithm of the saturated positive and negative photoconductivity currents plotted against the logarithm of the intensity of illumination, which was varied over nearly two orders of magnitude. In each case a line of gradient unity, within experimental error, is obtained: thus the saturated photocurrents are directly proportional to the exciting light intensity. In Fig. 7.13.2 the photoconductivity is measured by the gradient g of the current - voltage characteristic near the origin (cf. Fig. 7.10.2), and the logarithm of the gradient is plotted against the logarithm of the light intensity. In this case, a line of gradient 0.67 ± 0.03 is obtained, and when the experiment is repeated at higher temperatures, the gradient is found to take a number of non-reproducible values all less than unity. The non-reproducibility may, in part, be attributed to the difficulty of obtaining the characteristic and its gradient at elevated temperatures, but it may also be taken as an indication that the method of defining the photoconductivity by the gradient is not of fundamental significance. On the other hand, the direct proportionality between saturated photoconductivity currents and intensity is apparently

FIG. 7.14.1. TEMPERATURE VARIATION OF PHOTOCONDUCTIVITY CURRENTS - CaO PC 5[3]

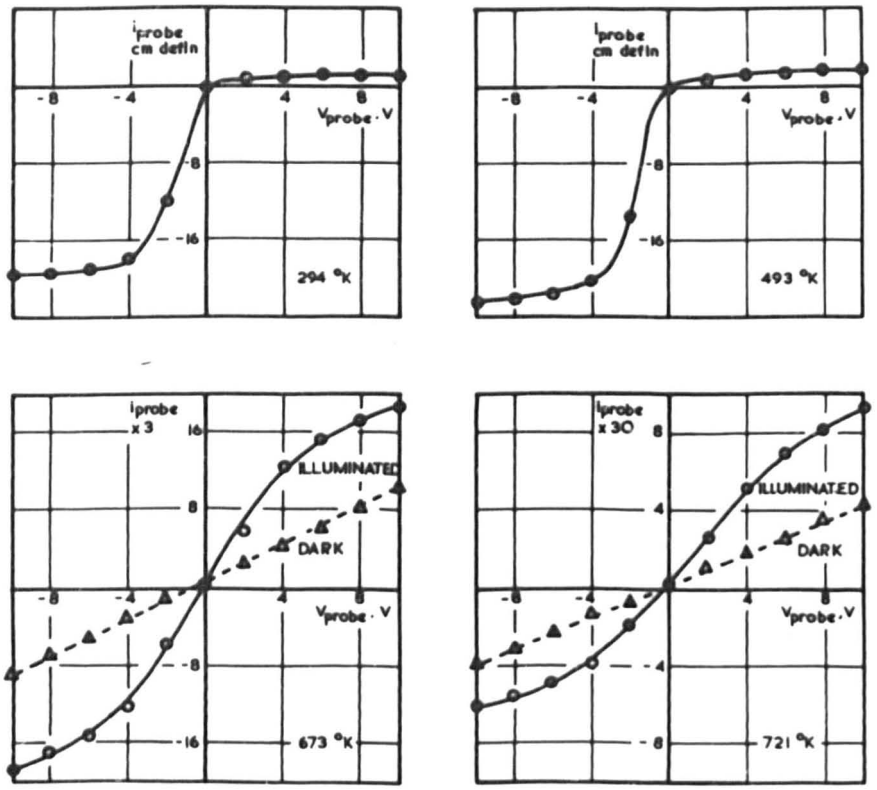

FIG. 7.14.2. TEMPERATURE VARIATION OF PHOTOCONDUCTIVITY CURRENTS – CaO PC 5[3]

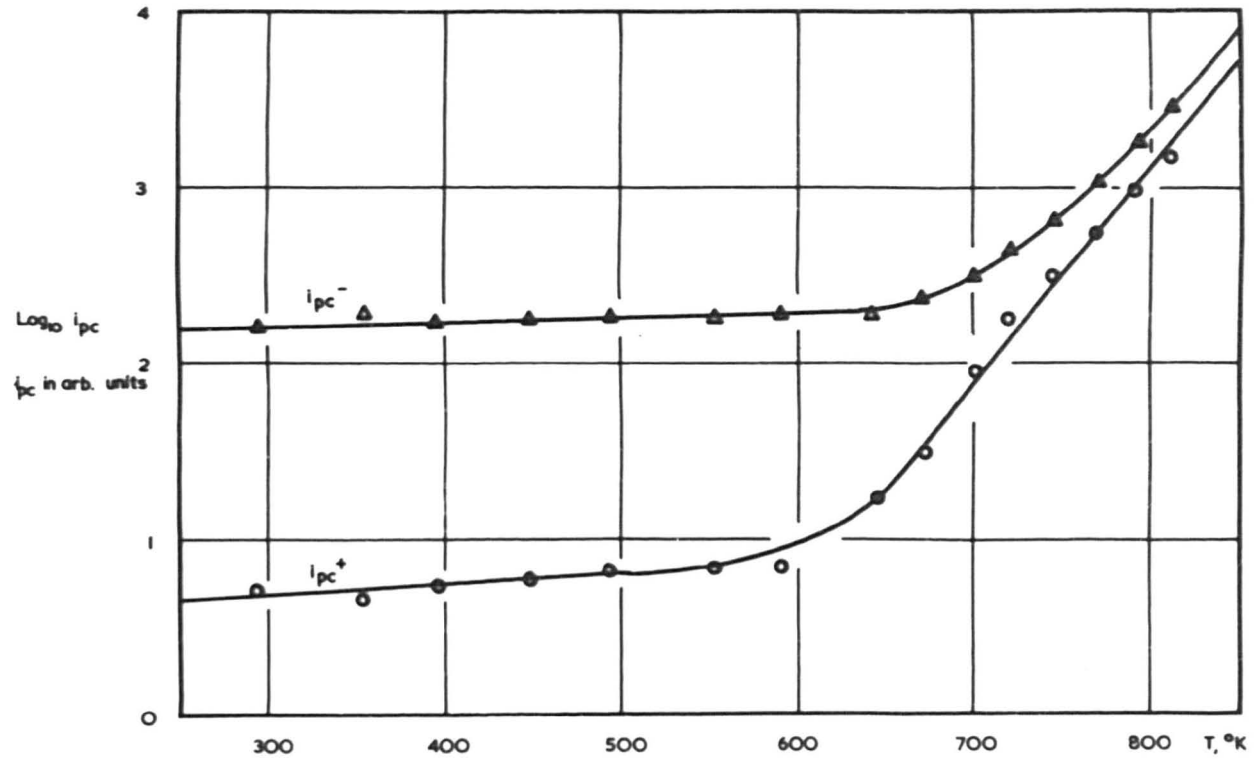

general for all cathodes.

7.3.4. Temperature variation of photoconductivity

Photoconductivity and dark conductivity current - voltage characteristics can be determined over a range of temperatures from 300 to 800 ^{o}K. Below 500 ^{o}K, dark conductivity is negligible, even for potentials of 10 V applied to the probe; above 500 ^{o}K, the approximately linear dark conductivity characteristic must be subtracted from the illuminated characteristic to obtain the current due to illumination alone. Above 800 ^{o}K, the dark conductivity current becomes very large compared with that due to illumination alone.

Typical characteristics for CsO PC S[3] are given in Fig. 7.14.1, and the temperature variations of the saturated positive and negative photoconductivity currents are given in Fig. 7.14.2. In the former figure the currents due to the thermoelectric e.m.f. and to the apparent photovoltaic effect (Sec. 7.4) have been balanced out. The two temperature variations are of a similar in nature, with only slight increases in photo-conductivity for large changes in temperature at low temperatures, and at higher temperatures showing a more rapid rise. The temperature at which the rapid rise

commences is about 600 °K for the positive photocurrent (i.e. photoelectrons from the cathode base to the probe) and about 660 °K for the negative photocurrent (i.e. photoelectrons from the probe to the cathode base). This suggests that there may be a rather large temperature drop across the cathode coating, assuming that the processes of positive and negative photoconductivity are the same.

7.4. Apparent photovoltaic effect

The photoconductivity current - voltage characteristics of Fig. 7.11.2 show that a photocurrent may flow on illumination for zero applied potential between the probe and cathode base. This effect is quite general, having been observed in all cathodes in which photoconductivity currents could be measured, and the analogous effect in barium oxide cathodes has been described in a previous thesis (116). There it was pointed out that conditions in cathodes with the probe diode geometry are favourable for the observation of a photovoltaic effect; the electrodes and sample are unevenly illuminated, and it seems possible that the zero-field current observed may be due to a photovoltaic e.m.f. set up between the brightly illuminated probe and

FIG. 7.15. TEMPERATURE VARIATION OF CURRENT DUE TO APPARENT PHOTOVOLTAIC E.M.F.

FIG. 7.15.1. CaO PC 5^3

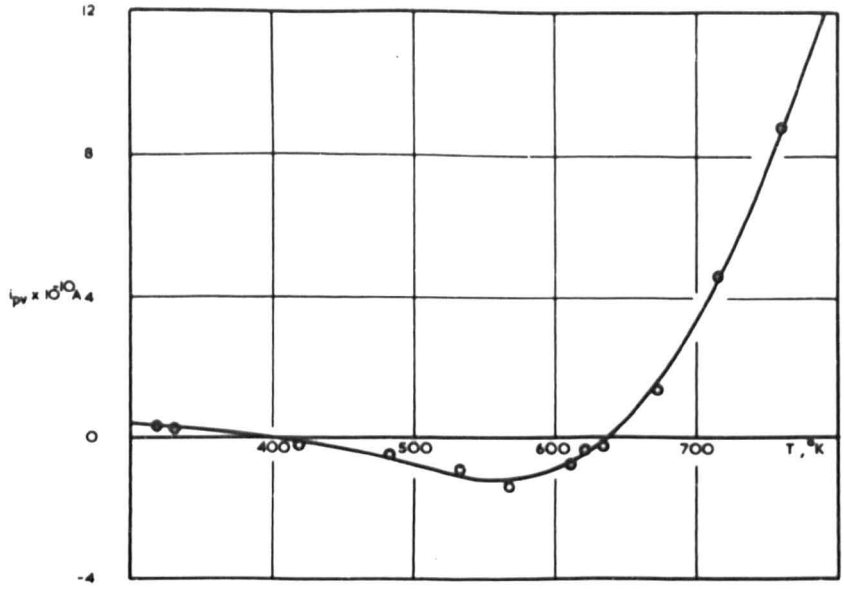

FIG. 7.15.2. CaO PC 5^6

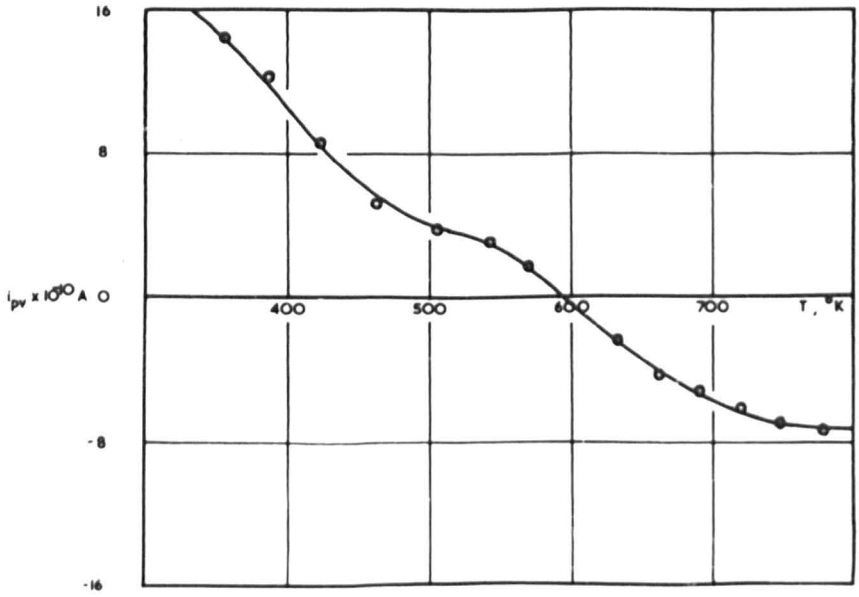

the less brightly illuminated (due to absorption in the cathode matrix) cathode base. It might also be possible to explain the current by invoking the Dember photo-diffusion effect (Sec. 3.3.3), but as the effect is observed in regions of not very strong optical absorption, the conditions are not strictly those under which the Dember effect would be expected to appear.

The temperature variation of the zero-field current has been determined for a number of cathodes, allowing for any zero-field dark current due to the thermoelectric e.m.f. across the cathode coating. Figs. 7.15.1 and 2 show the temperature variation for CaO PC 5^2 and 5^5. It is important to note that there is little similarity between the curves for different activation states of the same cathode apart from the fact that over a certain temperature range the current has changed direction. The significance of these observations is discussed in Sec. 7.6.

7.5. Cathode coloration

After measurements had been completed on the activated cathodes the tubes were stored in a dark drawer. On examination after a period of weeks, the cathodes were found to have developed a marked bluish

FIG. 7.16. CaO CATHODE COLORATION — OPTICAL ABSORPTION OF BLUE AND WHITE CATHODES

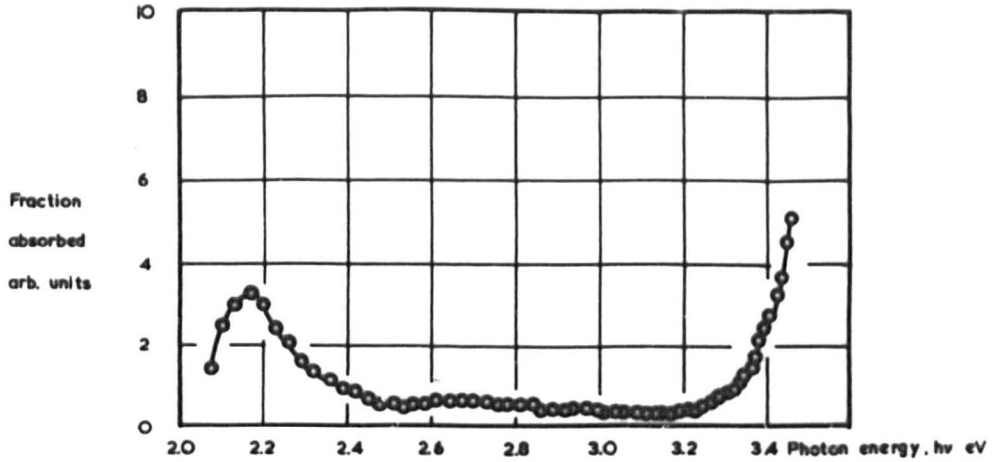

FIG. 7.16.1. BLUE CATHODE (CaO PC 1)

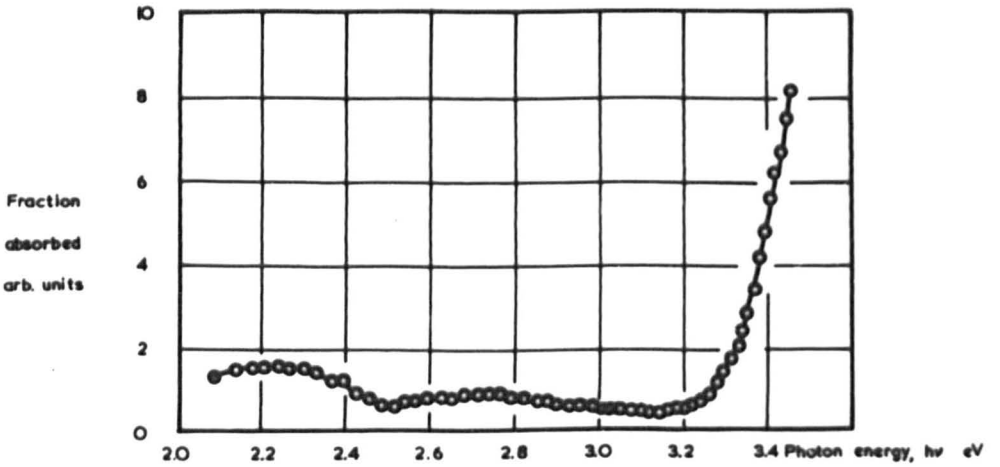

FIG. 7.16.2. WHITE CATHODE — COLORATION REMOVED BY WARMING

coloration. This was noted only in cathodes which had undergone the full processing and activation procedure; cathodes whose heaters had failed during breakdown, stored under the same conditions, remained white. The coloration is completely removed by heating the cathode, but returns when the cathode is again left in the cold for a period of some days. If the tube is opened to atmospheric pressure, the coloration disappears immediately and permanently. A similar effect was observed by Hopkins (87) (Sec. 4.7).

Figs. 7.16.1 and 2 show curves of the optical absorption of such a cathode (CaO PC 1) before and after removal of the blue coloration by warming. The curves were obtained by the photographic method described in a previous thesis (116). Light from the tungsten filament lamp is focused on the cathode, which is placed in a vertical position in front of the slit of the spectrometer (now fitted with the Hilger D.72 camera) so that light reflected by the cathode is focused by a second lens on to the slit. A photographic record of the spectrum of reflected light is compared with the spectrum of light which has passed directly through the envelope without reflection by means of a simple photoelectric micro-photometer. To calibrate the spectra for wavelength, a

mercury lamp is also focused on the slit by means of a lens and a small prism to give the lines of the mercury spectrum alongside each continuous spectrum. The microphotometer readings can be used to give the fraction of light reflected by the cathode sample at each wavelength. The method is slow, as a number of trial exposures must be made to obtain a suitable density on the photographic plate, and has only been used in the present work in the study of the optical absorption of this particular cathode. The method has been modified to improve the speed of determinations: a description of the new technique is given in Sec. 9.3.6.

The main feature of interest in the curves is the pronounced peak at about 2.15 eV observed in the optical absorption spectrum for the 'blue' cathode. This peak is absent in the curve for the white cathode; the curve shows very little resolvable structure in the whole of the visible region. Both curves show an increase in absorption at higher photon energies, starting at about 3.2 eV. The absorption peak at 2.15 eV means that the blue cathode absorbs strongly in the red and yellow regions of the spectrum, and thus when illuminated by white light the reflected light will be relatively stronger in the green and blue regions of the spectrum, and hence

the cathode appears to be blue.

It is worth remarking that a similar general coloration has not been observed for BaO cathodes, although on occasion a green or greenish-blue tinge is found. All activated CaO cathodes appear to go blue on standing; only a very few BaO cathodes show a colour effect and this is by no means as reproducible.

7.6. Summary of results; preliminary discussion

It is clear from the form of both the external photoelectric emission and photoconductivity spectral sensitivity curves that significant photoelectric work functions cannot be defined by determining the cut-off photon energy, i.e. the photon energy at which the characteristic meets the axis: the curves are approximately exponential at low photon energies. The logarithmic curve does not resemble the theoretical Fowler curve (Secs. 3.4, 9.2) to a sufficient degree for a reasonable fit to be obtained, even assuming that the fitting of semiconductor data to an equation derived for photoemission from a metal is valid. The technique used by Nisibori, Kawamura and Hirano (137) of extrapolating the linear portion of the photoemission plots on linear scales and ignoring the exponential tail

Table 7.1

Arbitrary thresholds for photoemission

Tube and activation state	ϕ'_{arb}, eV	Richardson ϕ, eV	$\chi+\Delta E$, eV from Richardson and cond. plots
CaO PC 5^2	1.73	1.54	2.25
PC 5^3	2.01	1.71	2.34
PC 5^4	1.95	1.79	2.30
PC 5^5	< 1.39	1.01	1.40

Table 7.2

Arbitrary thresholds for photoconductivity

Tube and activation state	ϕ'_{arbpc}, eV	$\Delta E/2$, eV
CaO PC 5^2	1.95	0.71
PC 5^3	1.84	0.63
PC 5^4	1.79	0.51
PC 5^5	1.51	0.39

could, indeed, be applied, as most of the spectral sensitivity curves do show an approximately linear region, but it is not felt that this treatment yields results of any theoretical significance (Sec. 3.4). It is possible to define a completely arbitrary photoelectric threshold, ϕ'_{arb}, which is probably merely a measure of the state of activation of the cathode, by traversing the wavelength range towards decreasing photon energies until the photocurrent has fallen to an arbitrary small value (about 10^{-12} A). The photon energy at which this 'least measurable photocurrent' occurs defines the arbitrary threshold, but it must be pointed out that it is entirely arbitrary and depends on the conditions of illumination and measurement of current employed. If a more intense source had been used, the arbitrary threshold would have been at a lower photon energy. Table 7.1 (opposite) shows how the arbitrary threshold varies for the different activation states of CaO PC 5, and how it compares with the Richardson work function for thermionic emission. A similar arbitrary threshold can be defined for photoconductivity: in Table 7.2 (opposite) it is compared with values of $\Delta E/2$ from the low-temperature slope of the dark conductivity plot.

It would appear from Tables 7.1 and 2 that there is

FIG. 7.17. RELATION BETWEEN PHOTOELECTRIC EMISSION AND PHOTOCONDUCTIVITY – CaO PC 5[5]

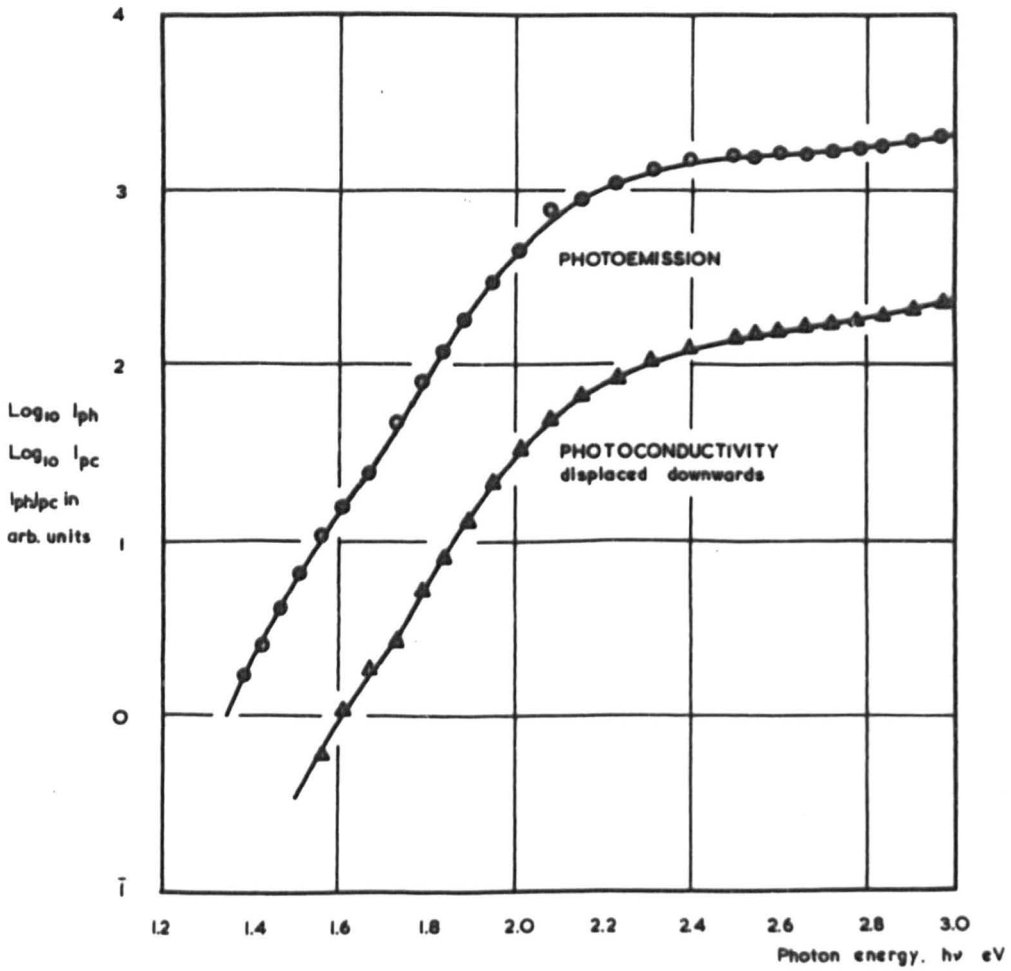

a very rough correlation between the thermionic work function ϕ and activation energy $\Delta E/2$ and the arbitrary thresholds of photoemission and photoconductivity: high thermal activation energies are associated with high arbitrary thresholds. The use of arbitrary thresholds can only be as a guide to the state of activation of the cathode; no deduction of energy levels can be made.

At this stage attention can be drawn to the general similarity between the spectral sensitivity curves for photoelectric emission and photoconductivity. The linear plots of both effects show some structure at about 2.6 eV, and the logarithmic curves are of similar shape and can be approximately superimposed merely by a vertical translation; any horizontal translation required is not more than 0.1 eV (cf. Fig. 7.17 for the curves for CaO PC 5[5]). This similarity is general in all activation states, and leads to the deduction made by Sakamoto (158) in the case of barium oxide cathodes (Sec.4.5) that the optical external work function χ' must be small, of the order of 0.1 eV. This result is unexpected, in view of the fact that the thermal external work function is about 0.8 eV (Sec. 6.3.6).

General similarity is also observed between the temperature variations of external photoemission and

photoconductivity, and also between the current - voltage characteristics for photoemission and photoconductivity: both show marked saturation in both directions. Photoconductivity current - intensity experiments suggest that the saturated photoconductivity current is of primary importance in defining the photoconductivity of the cathode sample.

A further unexpected result is obtained in the temperature variation of the current ascribed to a photovoltaic e.m.f. According to theory (Sec. 3.3.2) the photovoltage should be directly proportional to the absolute temperature, and thus the current set up by the voltage should vary in a way which depends on the absolute temperature and on the electrical conductivity under dark and illuminated conditions. The temperature variations of dark and illuminated conductivity are known, and do not suggest that the photovoltaic current should change its direction as temperature is increased, as is observed by experiment. Thus, although the conditions under which the current is set up suggest that it may be due to a photovoltaic e.m.f., the temperature variation of the current is not compatible with this assumption.

Chapter 8 Hypothesis of pore photoconductivity

8.1. The problem and hypothesis

The preliminary discussion of the photoelectric results (Sec. 7.6) showed that an explanation of the similarity between photoelectric emission and photoconductivity spectral sensitivity curves could be obtained by supposing that the optical external work function was not greater than 0.1 eV. This assumption, which is hardly acceptable by comparison with the thermal energy level scheme, does nothing to explain the further similarities between the current - voltage characteristics and the photocurrent - temperature variation for photoemission and photoconductivity, nor can it explain the origin of the zero-field photoconductivity current.

Sakamoto (158) merely indicated a possible solution of the problem in the case of the photoeffects in barium oxide by supposing that a proportion of the photoconductivity current was carried through the pores of the cathode matrix, instead of by a true photoconductive process. No further discussion or experimental test was offered. In this chapter some implications of the hypothesis are discussed, together with the results of a number of experiments specifically designed to test it.

If it is assumed that the greater proportion of the

photoconductivity current is carried in the pores of the cathode by a purely photoemissive process - one which will be called 'pore photoconductivity' in contradistinction to true photoconductivity - the similarity between the spectral sensitivity curves of photoemission and photoconductivity is immediately explained. The external work function is apparently zero because the processes are effectively the same: photoconductivity is merely photoelectric emission through the cathode pores to an anode, the probe, embedded in the matrix. There may, in fact, be slight differences in the sensitivity curves for the same activation state - differences which may be large enough to appear in the linear plots but which are hardly apparent in the logarithmic plots - because the external photoemission is bound to be affected by the outermost layers of the cathode outside the probe, which have no effect on photoelectric measurements between the cathode base and the probe. The situation is analogous to one experimentally observed in dark conductivity: the corrected high-temperature gradient of the conductivity plot is seldom exactly equal to that of the Richardson plot for the same cathode, and the explanation usually advanced is that the emitting surfaces are different.

The equivalence between the photoelectric processes

also explains the marked similarity between the form of the current - voltage characteristics, with their pronounced saturation. If the hypothesis of pore photoconductivity is correct, the relation between the saturated photoconductivity currents and light intensity should be one of direct proportionality, one of the fundamental properties of photoelectric emission, and this is found experimentally. It does not, however, exclude the possibility that the process is one of true photoconductivity. The gradient of the characteristic at the origin has no such fundamental significance, and the variation of the gradient of the log g versus log J curve found with temperature (Sec. 7.3.3) could be explained by supposing the form of the characteristic near the origin to be temperature-dependent. That this may be so is suggested by the temperature variation of the zero-field photoconductivity current ('photovoltaic current'), which on the pore photoconductivity hypothesis is merely equivalent to the zero-field current frequently observed in external photoemission (cf. Fig. 7.1). In the external case, the characteristic may not pass through the origin because of two inter-related factors: the c.p.d. existing between the cathode and the anode and the possibility of photoemission from the anode to the

cathode. On the pore photoconductivity model the photovoltaic current merely represents the same zero-field photoemissive current, and its magnitude and direction will depend on the same factors. The actual temperature variation is difficult to predict, as the temperature variation of c.p.d. between the probe and cathode base is unknown, but the slope of the current - voltage characteristic is so steep in the region between the two saturated conditions that only a slight change in c.p.d. would be required to make a large difference in the zero-field current and, possibly, change the direction of the current.

It might at first appear that the pore photoconductivity process should follow the same sort of temperature dependence as does dark conductivity, and the fact that photoconductivity is apparently a pore phenomenon at room temperatures but that dark conductivity does not become one below temperatures of about 600 ^{o}K may seem curious. However, the analogy between dark and photon-induced conductivity must not be taken too far, and there is no reason to suppose that the two processes should follow the same temperature dependence; when it is realised that external photoemission gives readily measurable currents at room temperature, but that measurable thermionic

emission currents are not obtained below about 600 °K, the apparent discrepancy disappears.

8.2. Experimental investigation of the hypothesis

Methods used to test the hypothesis include techniques similar to those employed in establishing the pore nature of dark conductivity (cf. Sec. 2.4).

8.2.1. Recovery of external photoelectric emission and photoconductivity after oxygen poisoning

Experiments in which the recovery of thermionic emission and electrical conductivity for BaO and SrO cathodes after oxygen poisoning was studied have been reported (83, 166; Sec. 2.4). Above about 700 °K, it was found that emission and conductivity recovered in the same way; below this temperature, the temporal changes were quite different. It was thus deduced that the process of conductivity above 700 °K was essentially one of thermionic emission in the pores of the cathode.

Three of the calcium oxide probe diodes from which results have already been quoted were specifically designed to study the effect of oxygen poisoning on photocurrents, and contained in addition to the normal electrode arrangement a 0.12 mm diameter alumina-insulated tungsten filament, coated with a paste of barium peroxide in

FIG. 8.I. RECOVERY OF PHOTOEMISSION AND PHOTOCONDUCTIVITY AFTER OXYGEN POISONING

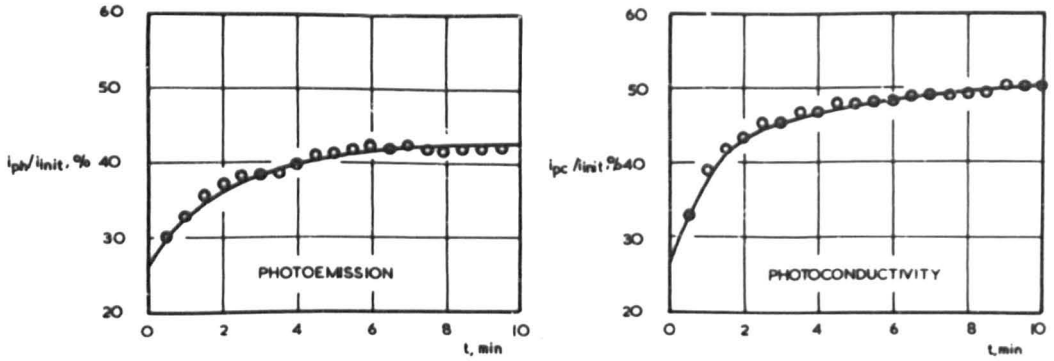

FIG. 8.I.I. CeO PC 7[1]

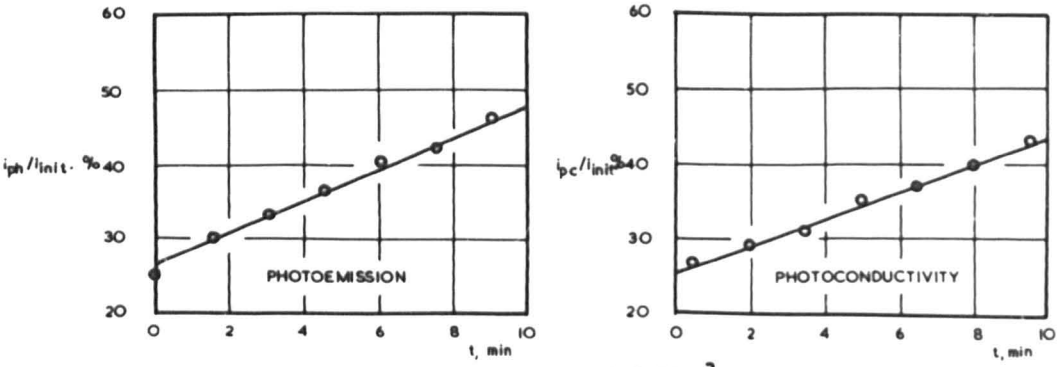

FIG. 8.I.2. CeO PC 9[2]

FIG. 8.1. RECOVERY OF PHOTOEMISSION AND PHOTOCONDUCTIVITY AFTER OXYGEN POISONING

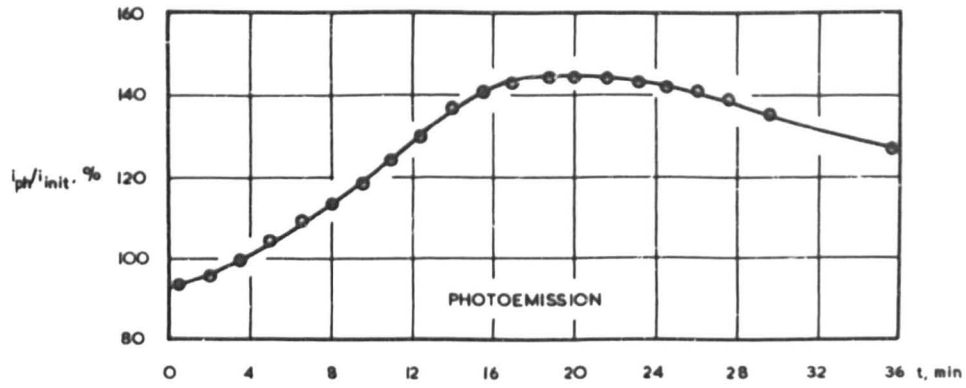

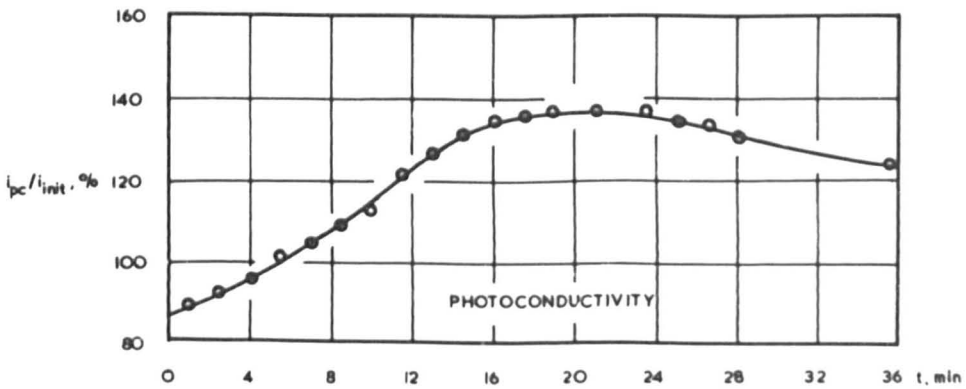

FIG. 8.1.3. CaO PC 9^3

collodion and ethyl acetate. The filament is outgassed during the processing of the tube by passing a current through it; this treatment removes the oxides of carbon from the breakdown of the organic binders. When a poisoning experiment is carried out, the outgassed filament is heated to red heat and the peroxide breaks down to barium oxide and oxygen. The filament is mounted adjacent to the anode window.

Measurements are made by illuminating the cathode with white light from the tungsten filament lamp and monitoring the photocurrent (either photoelectric emission or photoconductivity for fixed anode or probe potentials) as a function of time after the poisoning filament has been heated to redness for a few seconds to release a burst of oxygen. Results obtained from CaO PC 7[1] are shown in Fig. 8.1.1, and from CaO PC 9[2] and 9[3] in Figs. 8.1.2 and 3. The time scale is measured from the time the poisoning filament current (derived from the Variac transformer unit) is switched off, and the vertical scale represents the value of the photocurrent at any given time expressed as a percentage of the initial unpoisoned photocurrent. It is noted that in all cases the recovery of photoconductivity follows very much the same sort of curve as the recovery of

photoemission, although the actual percentage changes that the photocurrents experience may not be exactly the same. It is observed that the form of the recovery curve differs from one determination to the next, and may possibly depend on the pressure of oxygen, as the poisoning filament was heated for a different arbitrary length of time in each case. In one case (CaO PC 9^{8}) the effect of the oxygen attack is apparently to increase the photosensitivity of the cathode, the final photocurrents being greater than the unpoisoned values.

This type of behaviour is not generally observed in the case of oxygen attacks on thermionic emission and dark conductivity, where the recovery curves are all of a characteristic form and an activating effect has not been reported. The effects of oxygen on the photosensitivity of CaO cathodes have not been studied to a sufficient extent in the present work for any definite explanation to be offered, but it seems possible that photoemission, being a phenomenon which is extremely sensitive to the state of the calcium oxide surface, may be very dependent on the degree of coverage of the crystallite surfaces and on the surface diffusion processes involved.

8.2.2. Magnetoresistive effects in dark and illuminated conductivity

The work of Forman (64) and Metson (122) on the magnetoresistive effect in barium oxide cathodes in the dark has been discussed in Sec. 2.4: large magnetoresistive effects were obtained at temperatures in the pore conductivity region, but no measurable effect was found at lower temperatures.

Similar experiments have been carried out in the course of the present work. The probe diode geometry, with its cylindrical symmetry, is less suited to a study of the effect than the planar arrangement used by the earlier workers. The experiment relies on the deflection of electrons into curved paths by a combination of magnetic and electric fields; only in one orientation of the cathode, where its axis lies in the direction of the magnetic field, will the magnetic field be normal to the plane of the radial electric field between the probe and cathode base, and measurements are always carried out with the cathode in this position.

Magnetic fields have been derived from a Newport Type A Clarendon design electromagnet. The smallest pole-piece separation employed was 6.5 cm, for which a calibration curve of magnetic field versus magnet current

FIG. 8.2. ELECTROMAGNET : RELATION BETWEEN MAGNET CURRENT AND MAGNETIC FIELD

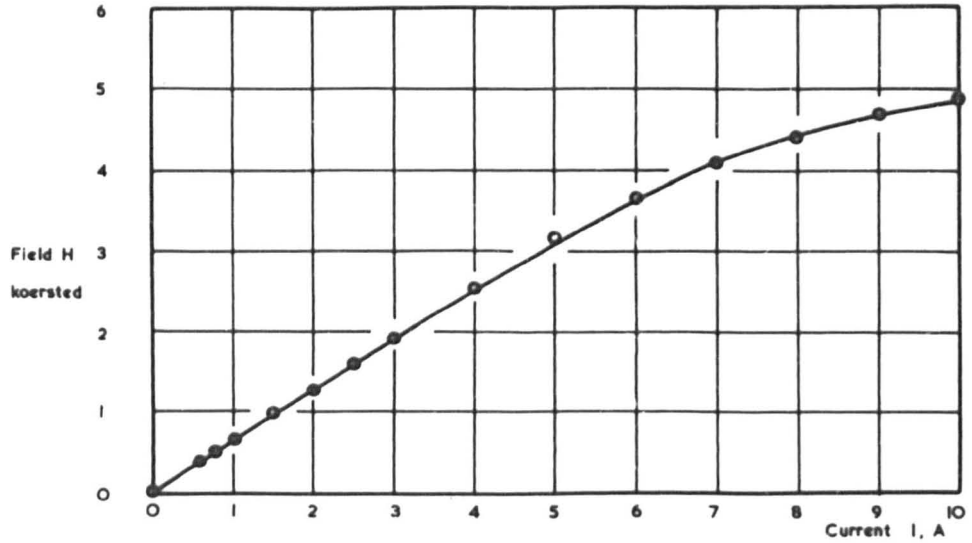

FIG. 8.2.1. 6.5 cm GAP

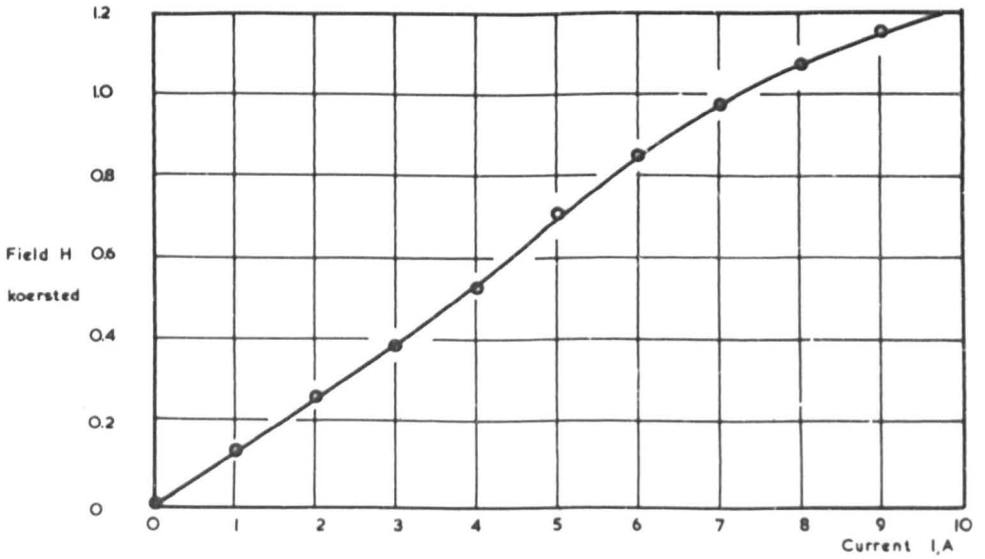

FIG. 8.2.2. 21 cm GAP

is given in Fig. 8.2.1; at this separation fields were reasonably uniform over the whole area of the pole-pieces, a rough determination of the direction of the lines of force having been made with a plotting compass. The magnetic field calibration was obtained using a search coil and fluxmeter. Tubes of the CaO M series are probe diodes with a shorter cathode base (30 mm) and cathode coated length (15 mm) than the PC series. The diode in its glass frame is mounted horizontally in the envelope, instead of vertically, so that the cathode can be orientated parallel to the direction of the magnetic field without using rather large pole separations. Experiments have, in fact, been carried out using tubes of the PC series, in which case a pole-piece separation of 21 cm is required, the pole-pieces being withdrawn a short distance into the energising coils. The magnet calibration curve for the 21 cm gap is given in Fig. 8.2.2: the large separation means that much smaller field strengths are obtained for the same current, and the field is less uniform.

Measurements of the magnetoresistive effect in the dark are made as follows. The tube is placed between the pole-pieces of the electromagnet so that the axis of the cathode base lies along the direction of the lines of force

FIG. 8.3. MAGNETORESISTIVE EFFECT IN DARK CONDUCTIVITY

CdO M 5^2

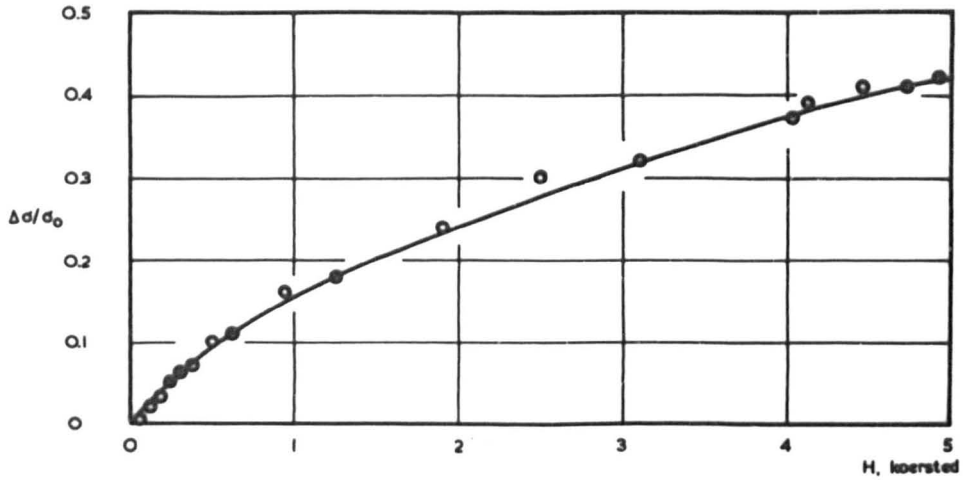

FIG. 8.3.1. GRAPH OF $\Delta\sigma/\sigma_0$ VERSUS H (FORMAN)

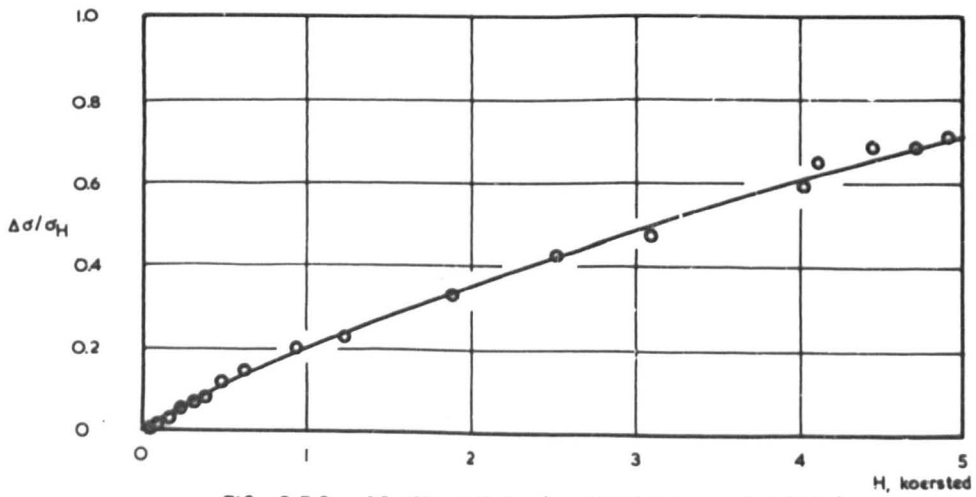

FIG. 8.3.2. GRAPH OF $\Delta\sigma/\sigma_H$ VERSUS H (METSON)

The temperature of the cathode base is adjusted to the desired value and a potential of 100 mV, derived from the potentiometer unit, is applied between the probe and the cathode base. An approximate value for the conductivity in zero magnetic field, σ_0 , is obtained by reversing the polarity of the potential and observing the difference in the galvanometer or electrometer reading of the conductivity current. D.c. voltages from a 100 V rectifier supply or from 24 V batteries are applied to the electromagnet through a rheostat, the current being adjusted to the value required to give the desired field. The conductivity in the magnetic field H, σ_H , is obtained by the same procedure, and when the energising current is removed the zero-field conductivity is redetermined. The procedure is repeated for a series of values of H and a graph of the fractional change in conductivity $\Delta\sigma/\sigma_0$, where $\Delta\sigma = \sigma_0 - \sigma_H$, is plotted against H. Because the tube cannot be screened in this series of experiments, considerable care had to be taken with the arrangement of apparatus. The electrometer and galvanometer were placed some 3 metres away from the electromagnet, and all connections were made with coaxial cable, held as rigidly in position as possible.

Such a curve is shown in Fig. 8.3.1 for CaO M 5^2 at 950 ^{o}K, and is in agreement with the type of curve

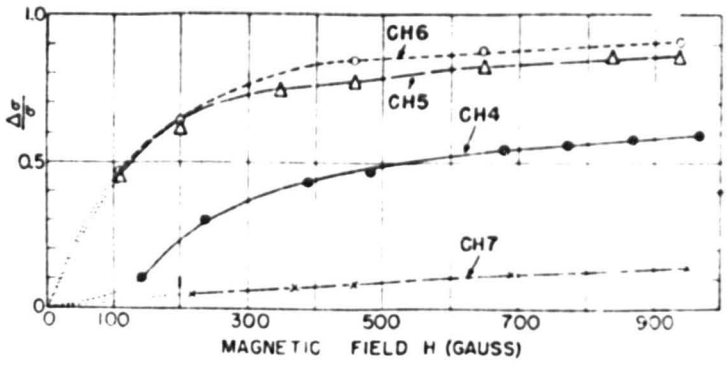

Fig. 8.3.3 Forman (64)

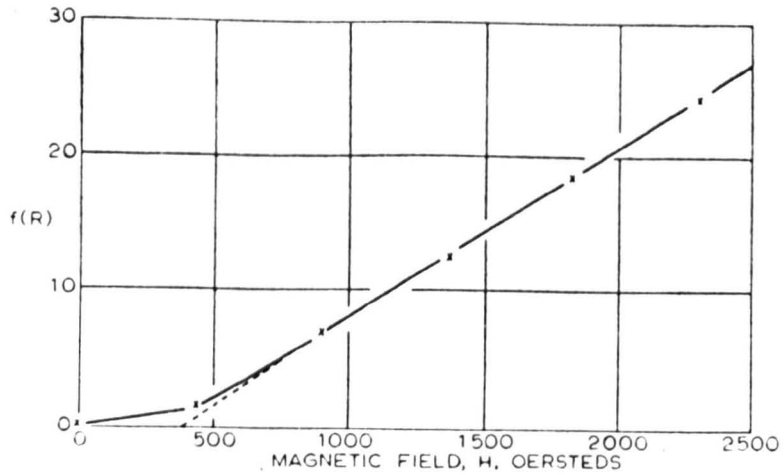

f(*R*) as a function of magnetic field.

Fig. 8.3.4 Metson (122)

Fig. 8.3 Magnetoresistive effect in dark conductivity

FIG. 8.4. TEMPERATURE VARIATION OF THE DARK MAGNETORESISTIVE EFFECT

FIG. 8.4.1 CaO PC 5[7]

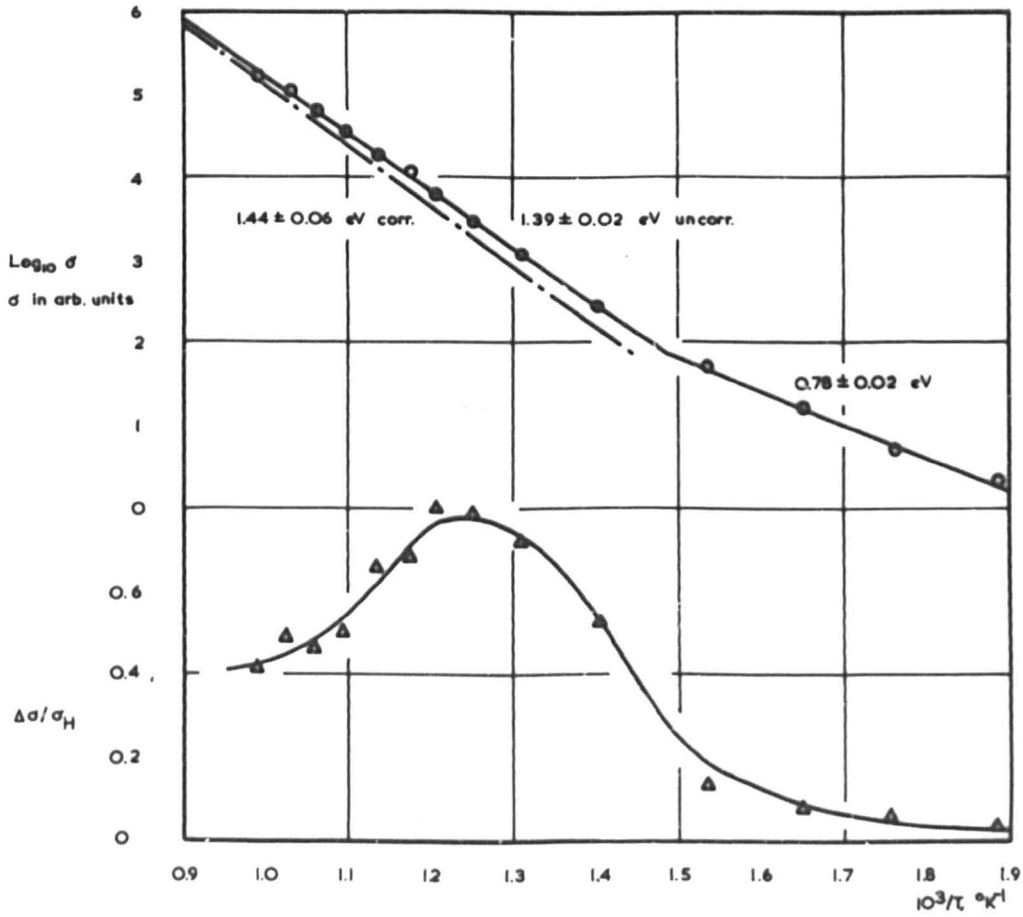

obtained by Forman (64) (Fig. 8.3.3). In the experiments described by Metson $f(R) = \Delta\sigma/\sigma_H$ was plotted against H, and a linear relation was obtained for values of H greater than 0.5 koersted (Fig. 8.3.4). In the present case, a graph of $\Delta\sigma/\sigma_H$ versus H (Fig. 8.3.2) yields a line slightly curved in the opposite sense. At 650 ^{o}K, no change in the conductivity on application of a magnetic field was detectable: the break point in the conductivity plot was at 780 ^{o}K in this activation state. Spurious results reported by Metson with nickel cathode bases below 633 ^{o}K (the Curie point for nickel) were not observed in the present case, possibly because the probe wire is kept rigid against the action of magnetic forces by the matrix sprayed around it.

The variation of the magnetoresistive effect with temperature may be conveniently studied by determining the ratio $\Delta\sigma/\sigma_H$ for a fixed value of H (normally 1 koersted) at a number of temperatures. A curve obtained for CaO PC 5[7] is given in Fig. 8.4.1, with the conventional conductivity plot. It is noted that $\Delta\sigma/\sigma_H$ is markedly temperature-dependent, showing a pronounced peak at a temperature about 100 ^{o}K above the conductivity line break point. Below the break point it falls to very low values and at temperatures more than about 100 ^{o}K below it is

FIG. 8.4. TEMPERATURE VARIATION OF THE DARK MAGNETORESISTIVE EFFECT

FIG. 8.4.2. CdO M 5^3

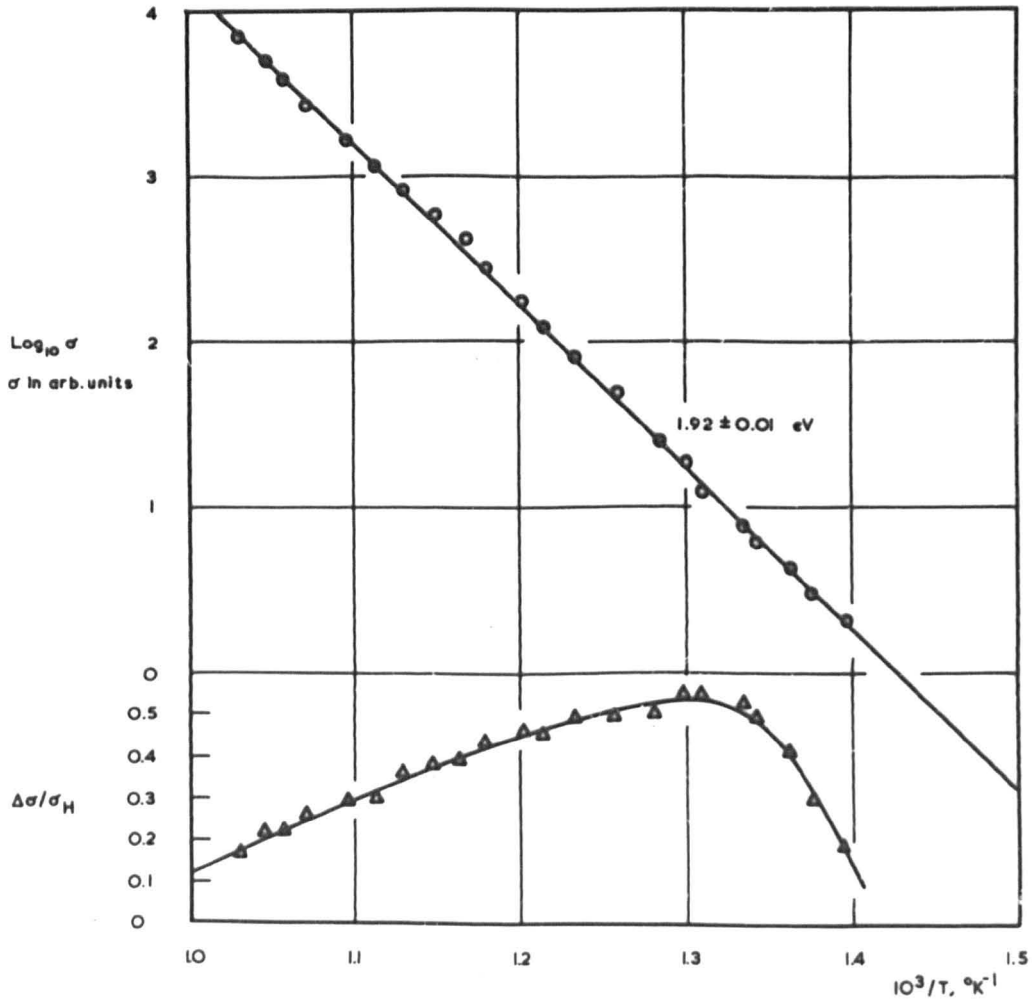

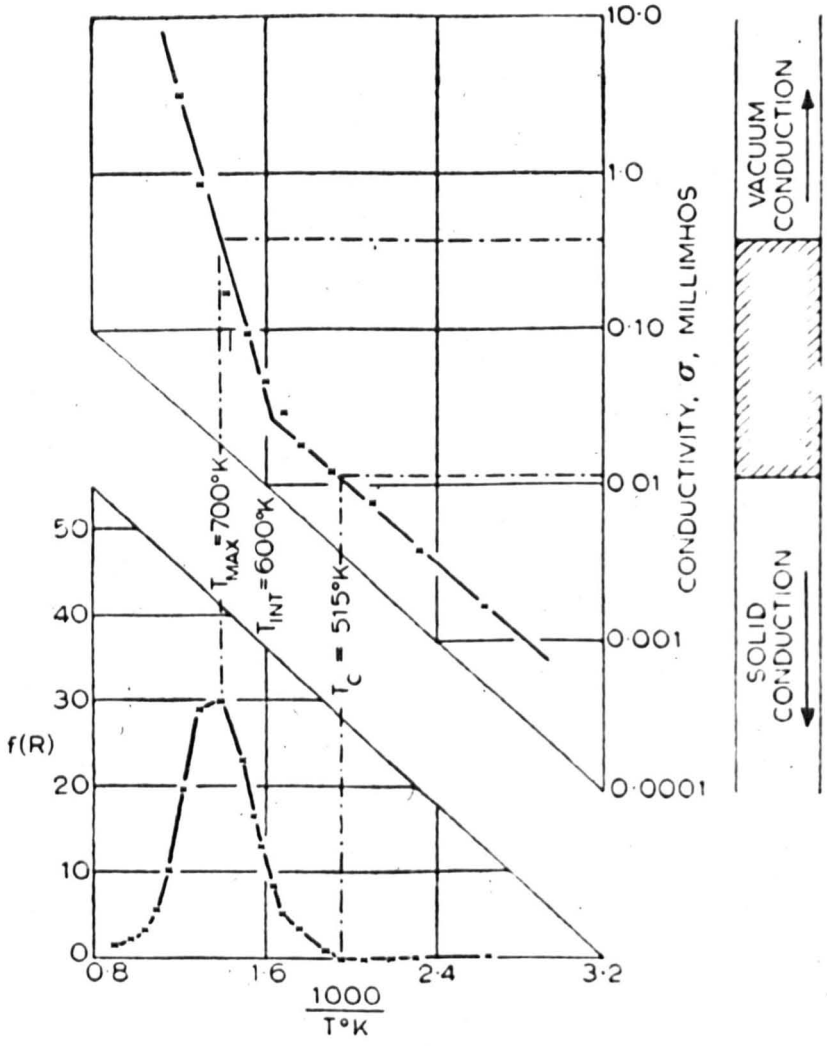

Correlation of f(*R*) with conductivity state.

Fig. 8.4.3 Temperature variation of the dark magnetoresistive effect in BaO (after Metson (122))

FIG. 8.4.4. DARK MAGNETORESISTIVE EFFECT AND CURRENT DENSITY

CeO PC 6^3

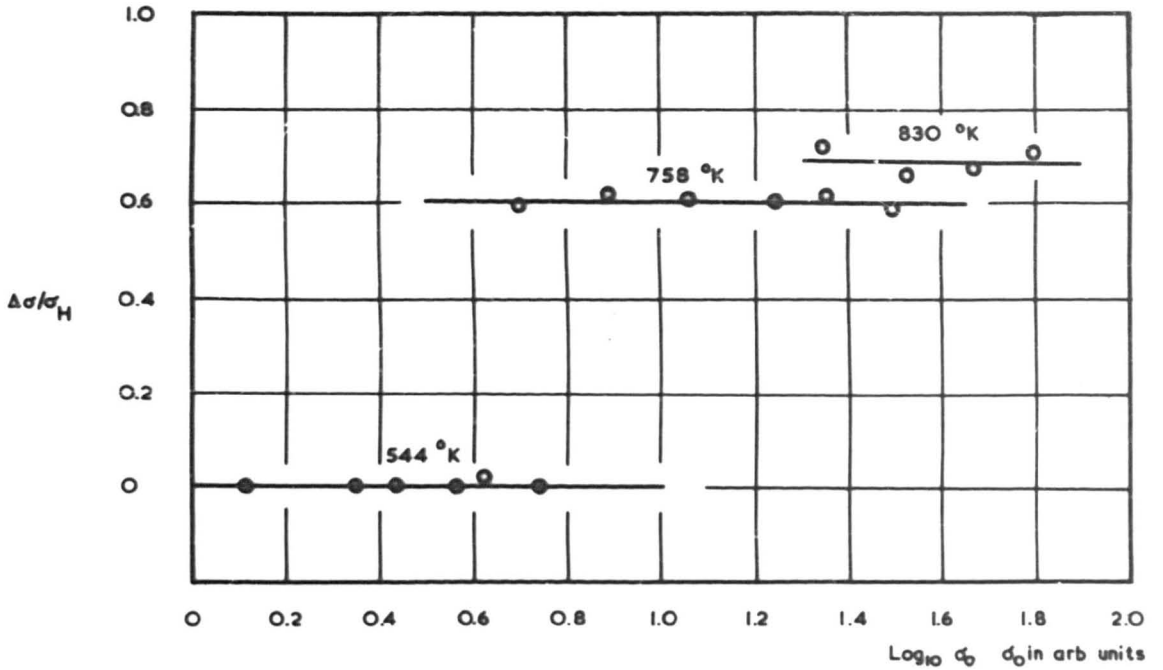

sensibly zero. Fig. 8.4.2 shows a similar curve for CaO M 5^3, where a large number of points were obtained in the high-temperature conductivity region. As the galvanometer alone was used to measure conductivity currents, measurements could not be extended to the low-temperature region. The form of the temperature variation is similar to that observed by Metson for barium oxide samples sandwiched between planar cathodes (Fig. 8.4.3).

Since the conductivity has been determined by applying a fixed potential to the probe, conductivity currents have varied over several orders of magnitude over the range of temperatures studied. The possibility exists that the form of the $\Delta\sigma/\sigma_H$ versus 1/T curve is due to the fact that $\Delta\sigma/\sigma_H$ is a function of the conductivity current. This has been investigated by varying the applied potentials at a number of temperatures and determining $\Delta\sigma/\sigma_H$ as a function of current. Fig. 8.4.4 (for CaO PC 6^3) shows that the value of $\Delta\sigma/\sigma_H$ is independent of the conductivity current and also confirms that at temperatures below the Loosjes-Vink break the value of $\Delta\sigma/\sigma_H$ is sensibly zero.

Experiments on the effect of the magnetic field on the photoconductivity current may be carried out in a similar way. The cathode, set up between the pole-pieces

FIG. 8.5. MAGNETORESISTIVE EFFECT IN PHOTOCONDUCTIVITY

FIG. 8.5.1. CaO M 5^2 (POSITIVE CURRENT)

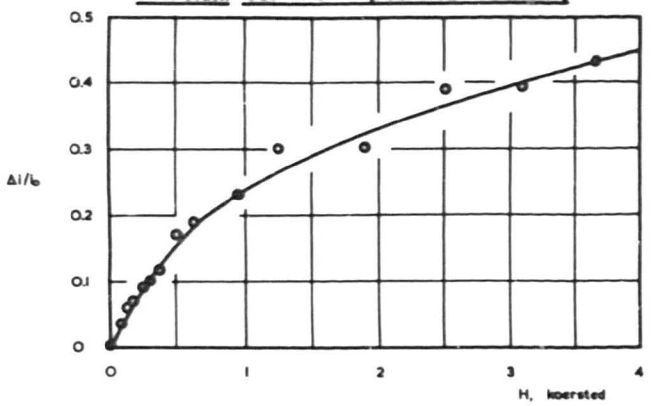

FIG. 8.5.2. CaO M 7

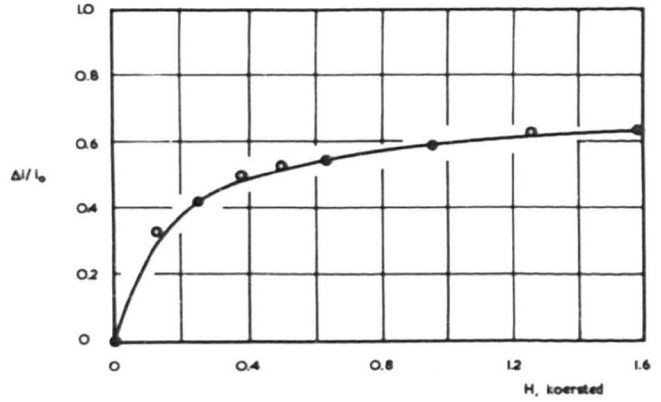

FIG. 8.5.3. CaO PC 5^7 (POSITIVE CURRENT)

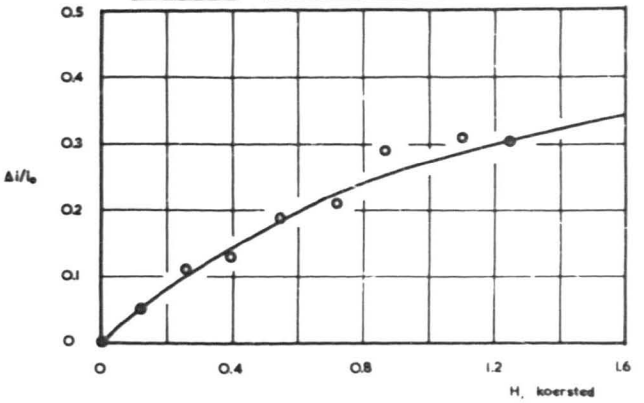

FIG. 8.5.4. CaO PC 5^7 (NEGATIVE CURRENT)

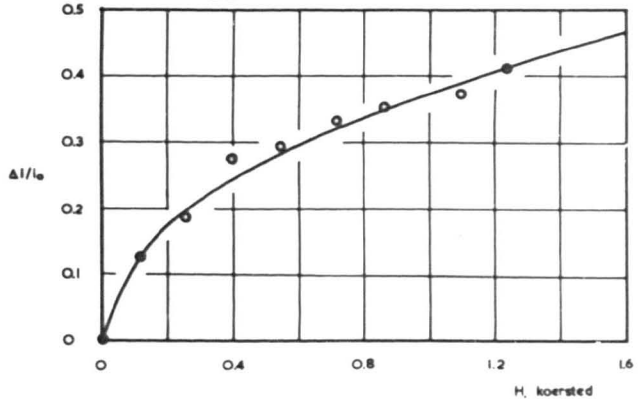

of the magnet, is illuminated with light from a high-pressure mercury arc, and the saturated positive and negative photoconductivity currents are determined in the absence and presence of magnetic fields of different magnitudes. If i_{pc_0} and i_{pc_H} are the values of the currents without and with the magnetic field H, and $\Delta i = i_{pc_0} - i_{pc_H}$, $\Delta i/i_{pc_0}$ can be plotted versus H. Fig. 8.5.1 shows the curve obtained for the saturated positive photoconductivity current in CaO M 5^2 at 290 °K, and it is observed that its form is very similar to that observed with the dark magnetoresistive effect in the pore conduction region (Cf. Fig. 8.5.1). The scatter of points is greater because the photoconductivity current at 290 °K is less than the dark conductivity current at 950 °K by a factor of more than 10^3: currents were measured with the electrometer, which was somewhat unstable because the tube could not be screened. Similar curves are given in Figs. 8.5.3 and 4 for positive and negative photoconductivity currents in CaO PC 5^7. The 21 cm gap was used, and magnetic fields were correspondingly smaller. Curves are similar in form, but the magnitude of the fraction $\Delta i/i_{pc_0}$ at any particular value of H differs for the positive and negative photocurrents; this difference is thought to be due to the geometry of

the system. Measurements are normally made at room temperature, as the introduction of heater supplies increases the instability of the electrometer and makes current measurement even more difficult.

A different sample geometry was employed in CaO M 7. The cathode base was a fused magnesia tube, 5.5 mm in diameter, with a 2 mm bore. A flat was filed at the centre of the tube to accommodate two nickel tags, separated by a gap of about 1 mm: the flat was sprayed with calcium carbonate suspension so as to cover the nickel electrodes and the gap between them evenly. The ceramic tube could be heated in the usual way by an insulated tungsten hairpin heater. The breakdown procedure was as usual, but activation on the ceramic base was extremely slow. Although thermionic emission currents to a semi-cylindrical anode were very small, a measurable photo-conductivity current was obtained between the nickel electrodes when illuminated with the tungsten filament lamp. The effect of the magnetic field (acting normally to the direction of the electric field between the electrodes) on photoconductivity is shown in Fig. 8.5.2: the geometry approximates to that employed by Forman, and the curve saturates in exactly the same way that he found the magnetoresistive effect in dark conductivity in the

high-temperature region to saturate (Fig. 8.3.3).

8.3. Discussion of results

Both poisoning and magnetoresistive measurements on photoconductivity currents show a marked similarity to the effects in dark conductivity in the pore conductivity region. Thus, previous work has shown that both electrical conductivity and thermionic emission recover in the same way after oxygen attacks at temperatures in the pore conduction region; the present work shows that both photoconductivity and photoelectric emission recover in the same way. The fact that different types of recovery curve are observed, possibly depending on the oxygen pressure, makes the similarity between photoemission and photoconductivity more marked, and the conclusion is that photoconductivity is a photoemissive phenomenon at room temperature.

The geometry of the probe diode makes a quantitative calculation of the magnetoresistive effect extremely difficult, and it is felt that at this stage a qualitative explanation of the effect is all that is required. This has been given for the simple case of planar symmetry by Forman (64) and by Metson (122), and depends on the setting up of a transverse drift velocity of the

conductivity electrons and a reduction in the electron mean free path. In the case of the temperature variation of the dark magnetoresistive effect, the results obtained in the present work are very similar to those of Metson with barium oxide, and this agreement helps to confirm the Loosjes-Vink theory of conduction in CaO cathodes. Again, the fact that the same sort of magnetoresistive effect is observed for photoconductivity as for dark conductivity in a region where the electrons are travelling freely in the pores suggests that the photoconductive process is also one of free electron flight through the pores.

The possibility exists that what has been considered to be a photoconductivity current between the cathode base and the probe embedded in the cathode matrix may be a photoemissive current to the probe supports (the exposed portions of fine nickel wire projecting from ceramic insulators above the cathode surface, to which the probe itself is connected). That this is very unlikely is shown by the following information:

1. The existence of a negative photoconductivity current, which, on the hypothesis of photoemission to the probe supports, would have to originate in the photoemission of electrons from the probe supports to the

FIG. 8.6. SCHEMATIC ARRANGEMENT OF ELECTRODES OF CaO M 6

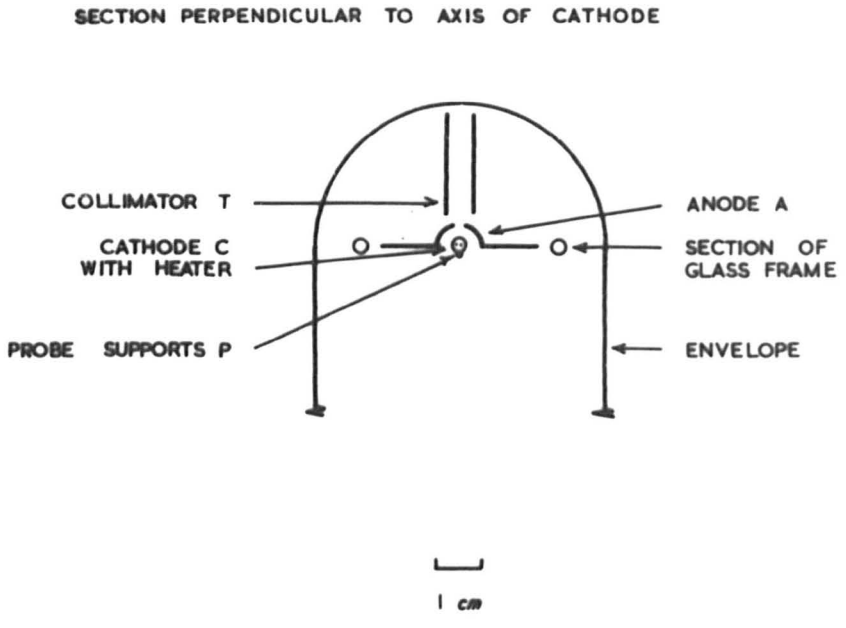

cathode surface. Tube CaO M 6 was specially constructed with this point in mind with the electrode structure shown in Fig. 8.6. The probe supports P are on the side of the cathode remote from the incident light, which passes down the collimator tube T to strike the front half of the cathode C. A semicylindrical anode A is provided, again at the front half of the cathode; thus illumination of the probe supports by reflection from the cathode and anode can only be slight. Both positive and negative photoconductivity currents are still observed, however.

2. Photoconductivity currents are also observed in CaO M 7, a design of tube (Sec. 8.2.2) which dispensed with the probe and probe supports. The leads to the embedded nickel electrodes are again on the side of the cathode base remote from the illumination.

3. Tubes in which the probe has become discontinuous at the probe supports (e.g. CaO PC 1) do not yield measurable "photoconductivity" currents when potentials are applied to the probe supports under conditions of normal illumination through the anode window, the experimental arrangement usually adopted. Small photocurrents to the probe supports may, however, be observed if the area immediately below the support is illuminated

intensely.

Thus, under normal illumination conditions through the anode window, it seems that any component of the photoconductivity current which travels by direct photo-emission to the probe supports must be negligible compared with that passing to the probe itself.

It might also be suggested that the magnetoresistive effect observed in illuminated conductivity is related to a true solid-state photoelectro-magnetic effect, as described in Sec. 3.3.4. The extreme similarity between the dark and illuminated magnetoresistive effects, however, and the fact that similar magnetic fields produce effects of a similar order of magnitude, argue against one effect being due to the free flight of electrons through the porous cathode, and the other to a true solid-state process.

Throughout the work on the pore photoconductivity hypothesis the argument has been by analogy. We have said that the current - voltage characteristics for photo-conductivity are similar to those for photoemission; that the spectral sensitivity curves are similar; that both recover from oxygen poisoning in the same way; and that photoconductivity currents are affected by a magnetic field in the same way as are dark conductivity currents in a temperature region where the electrons are known to

travel through the pores, and from all these points of similarity a connection between the processes has been deduced. To rely on any one of these arguments by analogy or similarity would be dangerous, but in several very different types of experiment the similarity appears to be too close to be fortuitous. It is thus concluded that at room temperature a large fraction of the apparent photoconductivity current in calcium oxide cathodes is, in fact, due to photoemission across the pores of the cathode matrix.

8.4. Pore photoconductivity in barium oxide cathodes

There is no reason to suppose that the pore photoconductivity meachanism observed in calcium oxide coated cathodes should not also apply to the other alkaline earth oxides: the possibility of the existence of such a process was, of course, suggested by Sakamoto (158) from the evidence of the spectral sensitivity curves for the effects in barium oxide.

A confirmatory experiment has been attempted in the present work. BaO M 1 was constructed so as to be exactly similar in diode geometry to the CaO M series, but the cathode was sprayed with a barium carbonate suspension. In an investigation of the effect of the

FIG. 8.7.1. TEMPERATURE VARIATION OF THE DARK MAGNETO-RESISTIVE EFFECT IN BaO

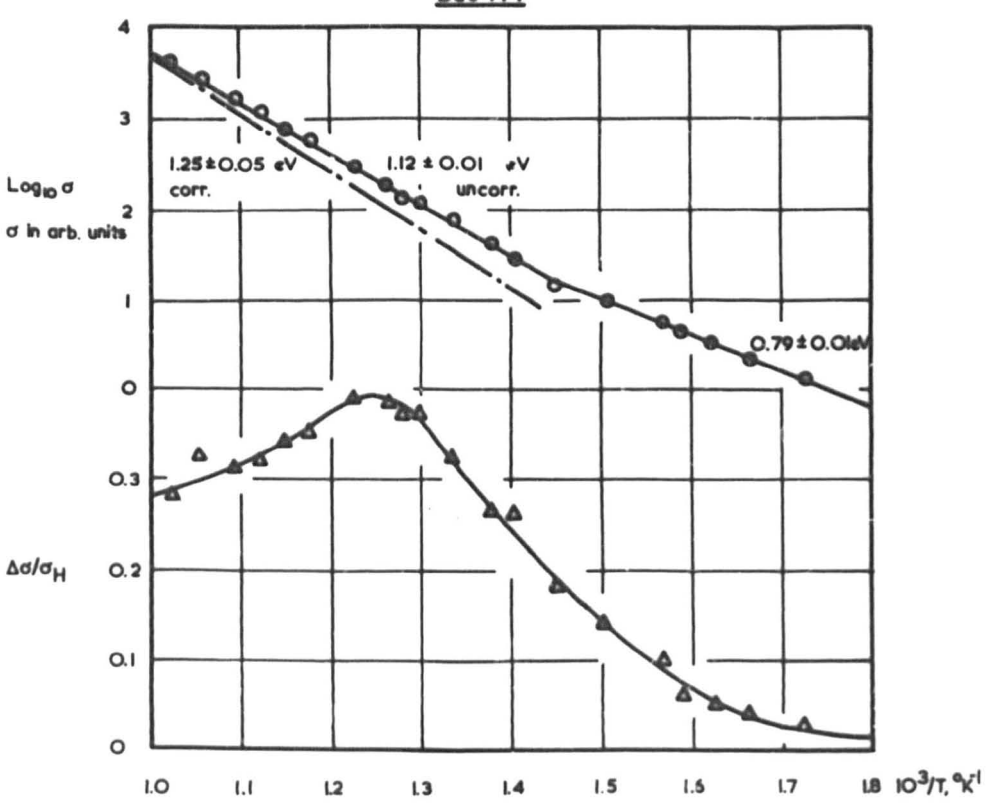

FIG. 8.7.2. MAGNETORESISTIVE EFFECT IN PHOTOCONDUCTIVITY

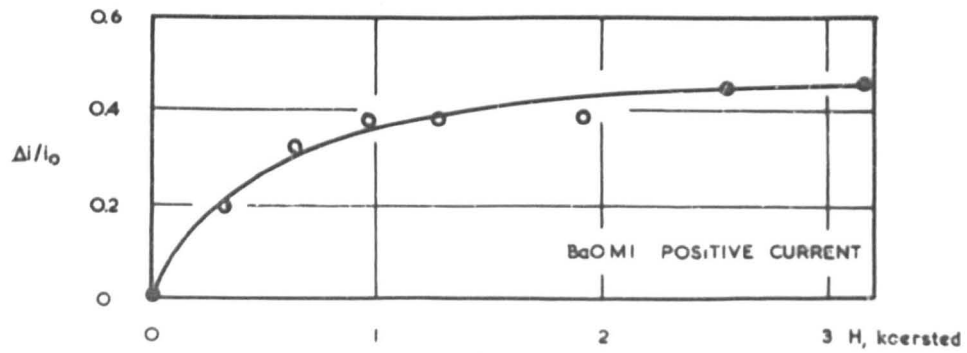

magnetic field on dark conductivity, $\Delta\sigma/\sigma_H$ depended on temperature in just the same way as was found with calcium oxide (Fig. 8.7.1). A similar reduction in the illuminated conductivity was observed on application of the magnetic field (Fig. 8.7.2).

Barium oxide cathodes thus behave in an exactly similar manner to calcium oxide samples, although dark conductivity and magnetoresistive measurements are considerably easier as the currents are larger.

Chapter 9 Anode surface effects; optical absorption and photoconductivity in evaporated films of calcium oxide

9.1. Introduction

The earliest studies on photoelectric emission from barium oxide cathodes (Sec. 4.2) established that the anode of the experimental diode was frequently more photosensitive than the cathode. The photoemission was attributed to a thin layer of the alkaline earth oxide evaporated on to the anode. The present work has established the existence of a similar effect in calcium oxide diodes (cf. Sec. 7.2.1). In this chapter a preliminary investigation of the effect is reported, together with experiments on photoeffects in films of calcium oxide evaporated on to glass.

9.2. Photoelectric emission from the anode

Photoemission from the anode has been a marked feature in all of the tubes which have yielded information on cathode photoemission. Fig. 7.1 showed that the photocurrent from the anode is normally considerably greater than that from the cathode. Taking into account the lower level of illumination at the anode, the anode photosensitivity must often be greater than that of the

FIG. 9.I. SPECTRAL SENSITIVITY OF PHOTOELECTRIC EMISSION FROM THE ANODE

CaO PC 5^2, CaO PC 7^1

FIG. 9.I.1.

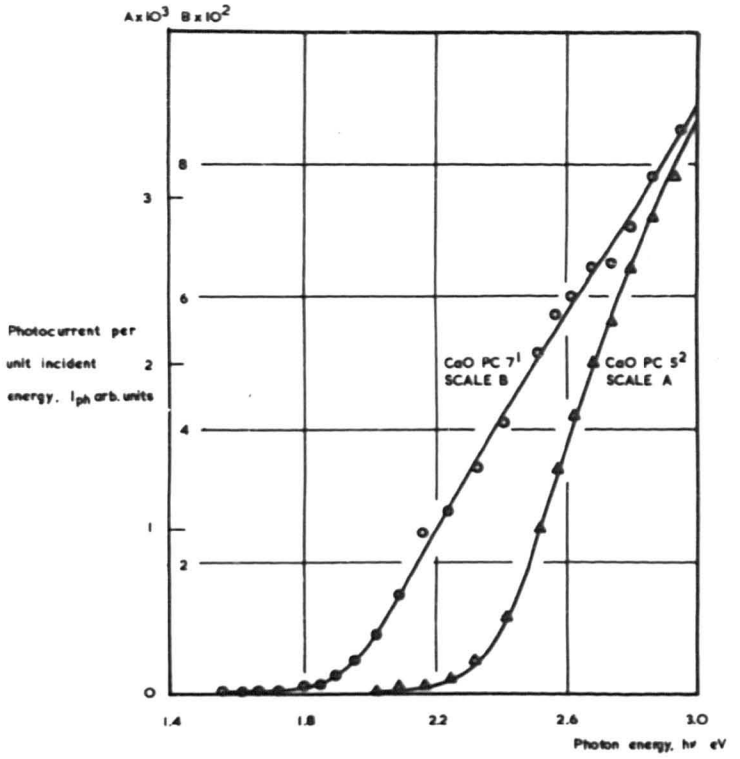

FIG. 9.I.2.

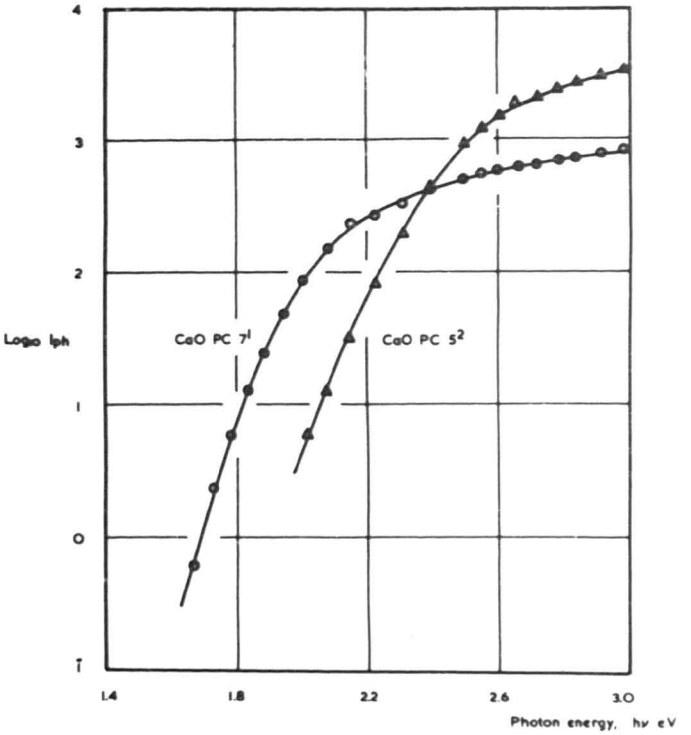

cathode by a factor of 10^2 or more. The photoemission has been ascribed to a layer of calcium-rich calcium oxide evaporated from the cathode during processing, activation and operation of the diode. As the photoelectric work function of pure nickel is about 5 eV (31) white-light illumination would not be expected to give any measurable photocurrent from the clean anode, although Hopkins (90) has suggested that clean "O"-nickel may, in fact, show photoemission when illuminated in the visible region. In the present work, however, photoemission has only been observed from the anodes of tubes where there was the possibility of evaporation from the cathode.

Typical curves for the spectral sensitivity of photoelectric emission from the anode are given in Fig. 9.1 for CaO PC 5^2 and PC 7^1. These should be compared with the curves for photoemission from the cathode (Figs. 7.2, 3 and 4); the logarithmic curves show a general similarity, but the linear plots do not show the structure at about 2.6 eV characteristically found in the cathode photoemission curves.

Following the suggestion of Narita (133) an attempt has been made to fit the anode photoemission results to Fowler plots. A graph of the Fowler function $F(h\nu/kT)$ versus $h\nu/kT$ (5) is given as the left-hand continuous

FIG. 9.2. FOWLER PLOTS FOR PHOTOELECTRIC EMISSION FROM THE ANODE

FIG. 9.2.1. CaO PC 5[2]

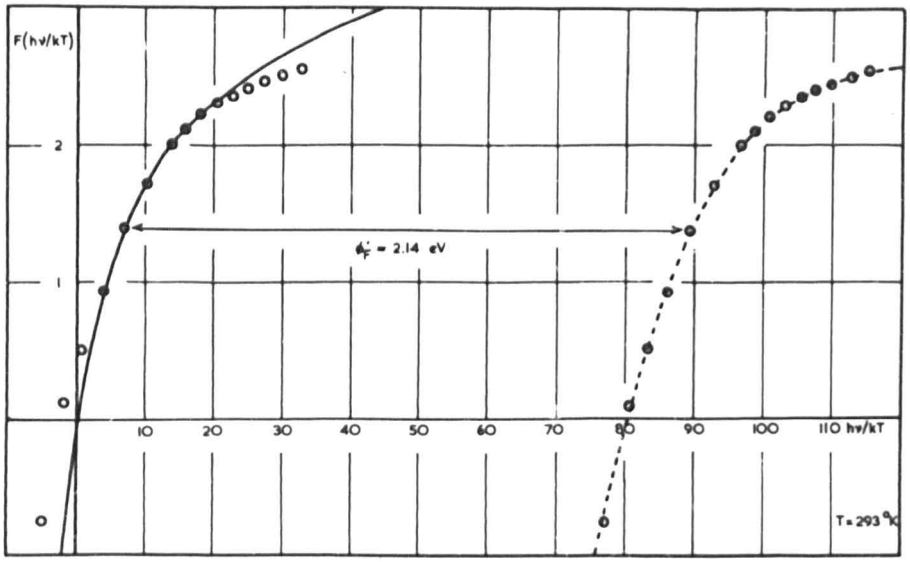

FIG. 9.2.2. CaO PC 5[5]

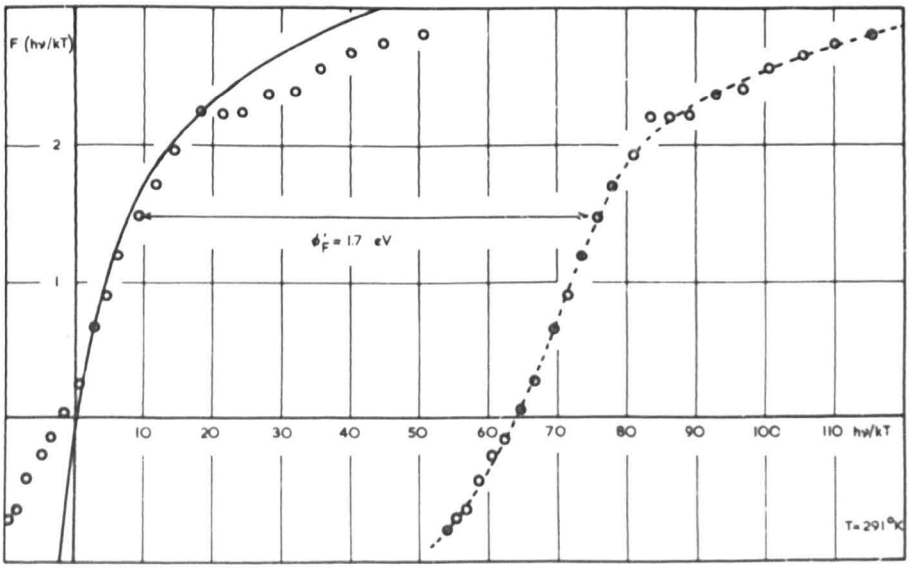

curve in Fig. 9.2.1: the right-hand dashed curve is a plot of $\log_{10} i_{ph}/T^2$ versus $h\nu/kT$ where i_{ph} is the photoelectric emission current from the anode of CaO PC 5[2], T is the anode temperature and ν is the frequency of the exciting illumination. The curves show some similarity in form: if the Fowler theory of photoemission from metals is to apply to thin evaporated films of calcium oxide, the curves should be brought into coincidence by vertical and horizontal translations of the right-hand curve. The photoelectric work function ν_0 can be obtained from the magnitude of the horizontal shift, $h\nu_0/kT$. The open points about the continuous Fowler curve show the effect of attempting the horizontal translation; the vertical translation, of no fundamental significance, has already been made in the preparation of this curve. Complete agreement cannot be obtained, but the discrepancies in this case are no greater than those observed by Marita for evaporated barium oxide. In the case of CaO PC 5[2], the horizontal shift corresponds to a Fowler photoelectric work function of 2.14 ± 0.07 eV, the experimental error quoted being obtained from the mean deviation of the points about the theoretical curve. Fig. 9.2.2 shows a case where agreement between the experimental points and the theoretical curve is much

less good (CaO PC 5^5). A summary of the Fowler work functions ϕ'_F obtained, compared with arbitrary photoelectric work functions for anode photoemission defined in the same way as in Sec. 7.5, and anode work functions obtained from thermionic and c.p.d. information, is given in Table 9.1.

Table 9.1

Anode photoemission: Fowler work functions and arbitrary thresholds

Tube and activation state	Fowler w.f., ϕ'_F, eV	Arbitrary threshold, ϕ'_{arb}, eV	Anode w.f., ϕ_a, eV
CaO PC 5^2	2.1 ± .1	2.01	2.2 ± .1
PC 5^3	1.9 ± .1	1.95	2.8 ± .1
PC 5^4	2.0 ± .1	1.74	3.3 ± .2
PC 5^5	1.7 ± .2	1.39	1.3 ± .1
PC 6^3	1.6 ± .2	1.39	1.6 ± .2
PC 7^1	1.7 ± .1	1.56	2.2 ± .4
PC 8^2	1.4 ± .1	1.39	
PC 10^4	1.5 ± .1	1.47	

It is observed that in all except a few cases the Fowler photoelectric work function agrees reasonably well with the arbitrary threshold. This can hardly be held out as evidence in favour of giving theoretical significance to the arbitrary threshold, for the theoretical

foundation of the Fowler treatment for photoemission from thin evaporated films of a semiconductor has not been established; it can merely be taken as confirmation that the methods used to express the photosensitivity of the surfaces are reasonably consistent.

There is some evidence in favour of Narita's observation that thin evaporated films appear to obey the Fowler relation rather better than thick films. Thus, in CaO PC 5, photoemission from the anode in state 2 gives a reasonable fit with theory; after a considerable period of activation and operation, which might be expected to increase the thickness of the evaporated material on the anode, the photoemission in state 5 is only a poor fit. In the present work, however, it was not possible to study a possible correlation with thickness of deposit in detail.

There appears to be little correlation between the photosensitivity of the anode and the anode work function as determined from thermionic emission and c.p.d. measurements.

9.3. Photoeffects in thin evaporated films of calcium oxide on glass

9.3.1. Experimental tubes

The information obtainable from photoelectric studies

FIG. 9.3 EVAPORATED FILM CONDUCTIVITY TUBE

SCHEMATIC ARRANGEMENT

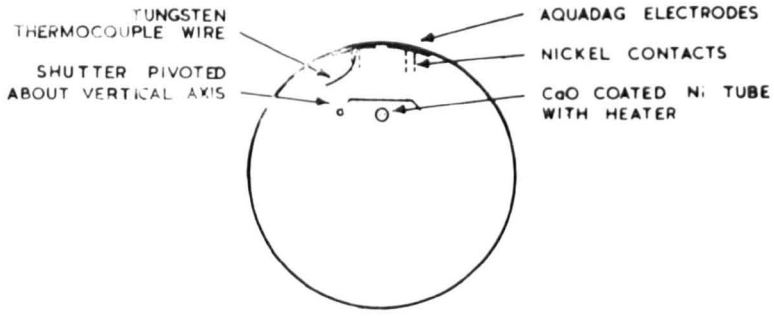

1. PLAN VIEW

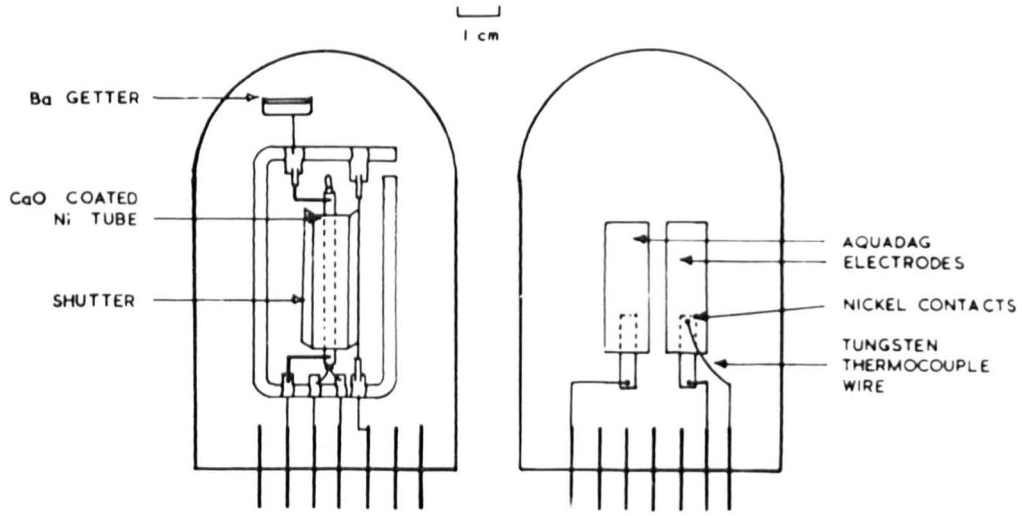

2. CATHODE & SHUTTER 3. CONDUCTIVITY ELECTRODES

of the anode of the probe diode is limited. Photoconductivity studies are not possible, and although the optical absorption of the evaporated film could be determined by studying changes in the reflectivity of the nickel anode, the geometry of the diode makes this extremely difficult.

Accordingly, a series of tubes (the CaO F series) was constructed in which the evaporated film could be deposited on to a glass substrate. For simplicity, the inner surface of the envelope of the tube was employed as the substrate: the cylindrical nickel cathode, coated over its entire length with carbonate suspension, was placed near the envelope, and shielded by a rotating nickel shutter so that evaporation could be controlled. Two Aquadag electrodes, separated by about 3 mm, were painted on to the envelope and contact was made to them by nickel strip springs, to one of which a tungsten-nickel thermocouple was attached. The schematic arrangement of the tube is shown in Fig. 9.3.

The cathode is subjected to the same breakdown schedule as usual, the shutter being closed to prevent any evaporation between the Aquadag electrodes during this process. It is found that the tungsten heaters of this type of tube are particularly prone to burn out.

This is attributed to the fact that calcium carbonate, covering the whole of the nickel cathode base, is likely to contaminate the exposed portions of the tungsten. This contamination has been shown to cause failure of the tungsten in a subsidiary experiment in which two tungsten filaments were mounted in the same envelope. One was covered with calcium carbonate suspension, the other was clean, as a control: on heating the filaments to white heat, the one covered with the carbonate suspension very quickly burnt out. This may well be due to the formation of tungsten carbonyl through reaction of the tungsten with carbon monoxide from the suspension binder. After breakdown, the tube is sealed off and the getters, placed in a position remote from the Aquadag electrodes, are fired.

9.3.2. Measurements

Measurements of the dark and illuminated conductivities and of any photoemission from the electrode region are made before any evaporation is carried out. Dark conductivities are measured by applying potentials between the Aquadag electrodes and measuring the corresponding conductivity currents; the illuminated conductivity is obtained by illuminating the area between the electrodes with light from the tungsten filament lamp and measuring

the conductivity as before. Photoemission currents from the electrode area are measured to the nickel shutter, which is used as an anode. In all cases, provided that the glass envelope and Aquadag electrodes have been thoroughly outgassed by the baking procedure, conductivity currents and photoelectric emission measured from the electrode area before films are evaporated are extremely small and can be neglected in comparison with the corresponding currents in the evaporated films.

Calcium oxide may be evaporated from the cathode on to the glass substrate by heating the cathode to about 1100 ^{o}K and opening the nickel shutter with an external magnet for an arbitrary period. It is normally found that evaporations of the order of 10 minutes at 1100 ^{o}K deposit sufficient material between the electrodes to make a marked change in the electrical and photoelectric properties of the sample; the effect of continued evaporations is usually investigated. Evaporation by stages is continued until the film just becomes visible as a dark brown deposit.

In addition to measurements of dark and illuminated conductivity and of photoemission from the film, it is possible to measure the variation of dark conductivity with temperature. Although no heater for the evaporated

FIG. 9.4. CALIBRATION CURVE FOR TUNGSTEN–NICKEL THERMOCOUPLES

200 – 400 °K

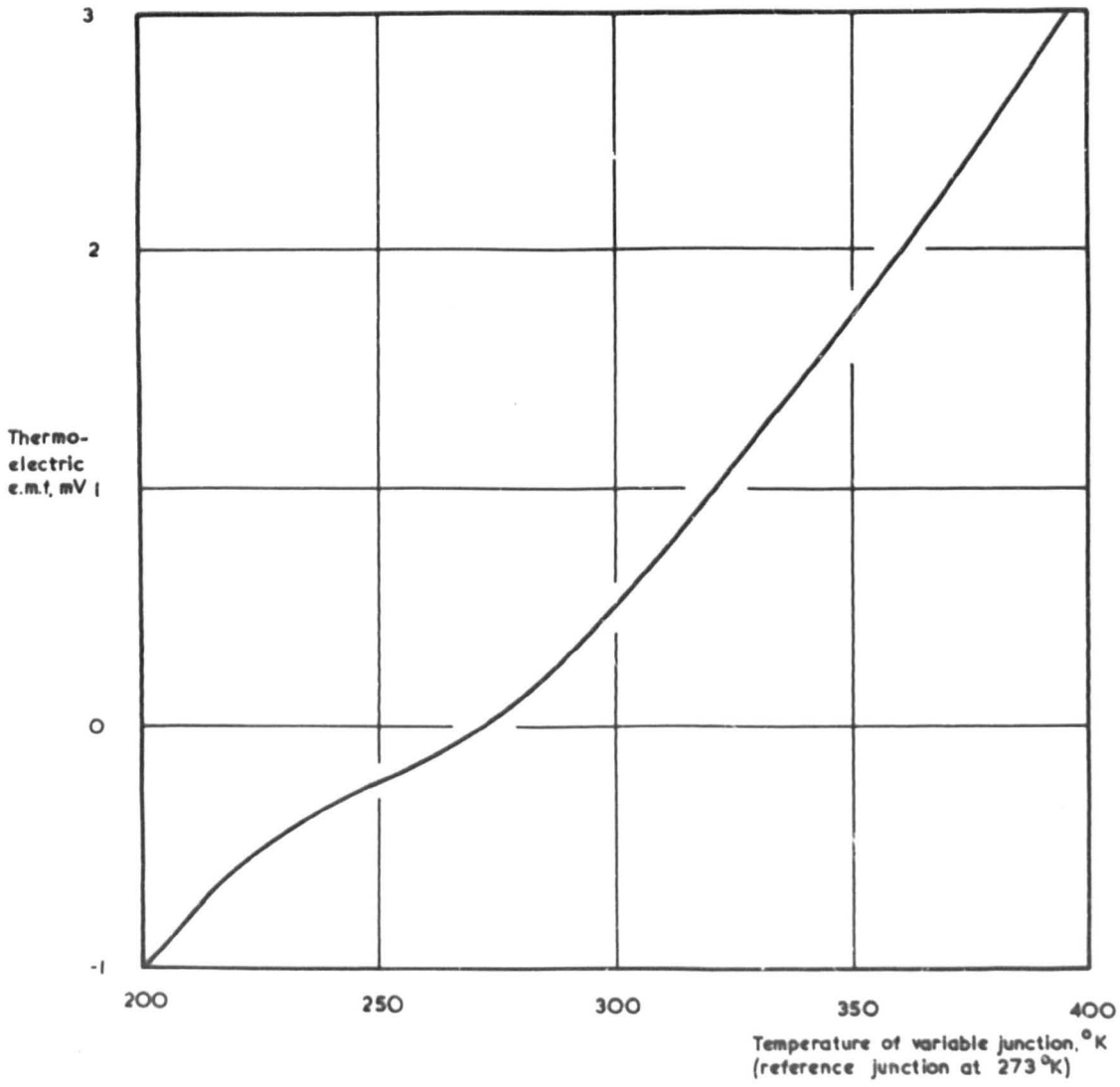

sample is provided in the tube, its temperature may be varied by immersing the tube in a liquid bath whose temperature can be controlled; the temperature of the sample is measured by the tungsten-nickel thermocouple at the nickel contact to the Aquadag electrode. A temperature range of from 200 to 400 °K may be provided by using two liquid baths: one of methyl alcohol (m.p. 178 °K), cooled in liquid air to about 200 °K, contained in a wide-mouthed Dewar flask and allowed to warm up gradually to room temperature, and one of paraffin, warmed to about 400 °K and allowed to cool to room temperature. The tube is immersed in the liquid, which is thoroughly stirred; the rate of change of temperature is quite slow enough for conductivity measurements to be made at a definite temperature. The temperature calibration of the tungsten-nickel thermocouple is extended downwards by comparing the e.m.f. produced with that from a chromel-alumel couple whose junction is at the same temperature; a calibration curve is given in Fig. 9.4.

In both dark and illuminated conductivity measurements potentials of $\pm$ 100 mV are applied between the electrodes from the potentiometer unit. Currents are normally large enough to be measured with the galvanometer alone. Both methyl alcohol and paraffin have a very low

FIG. 9.5. ELECTRICAL CONDUCTIVITY OF EVAPORATED FILMS OF CaO : CURRENT - VOLTAGE CHARACTERISTICS - CaO F 3[1-5]

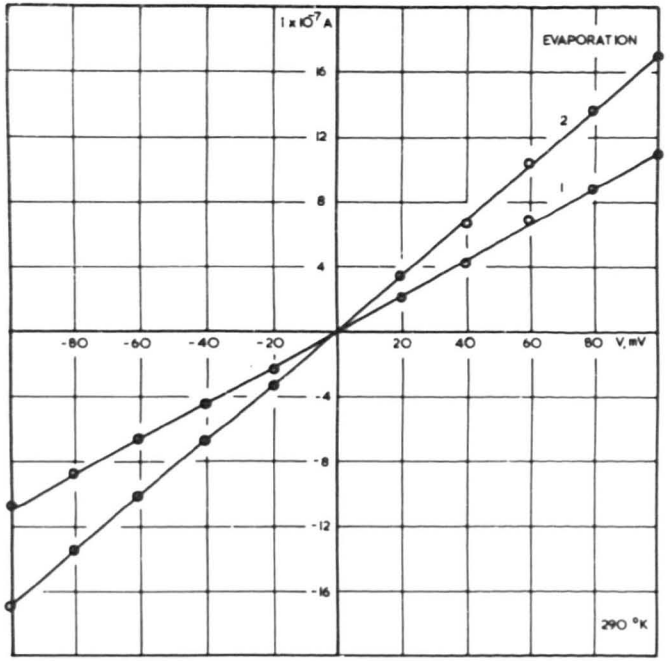

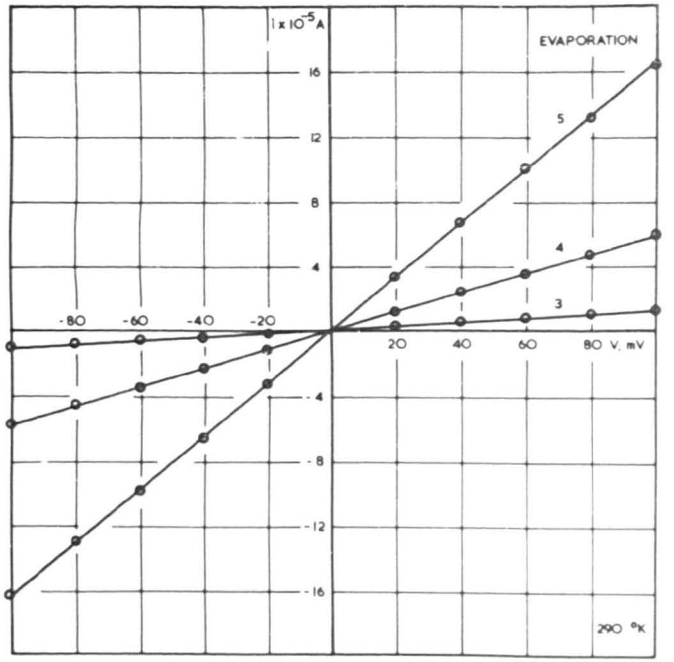

electrical conductivity, and the dark conductivity currents obtained are sufficiently large to be sure that the conductivity between the Aquadag electrodes, and not that between the pins in the pinch in the liquid bath, is being measured.

The photosensitivity of the film is determined by the method of complete photoelectric emission, potentials of up to 240 V being applied to the anode. Photocurrents are measured with the galvanometer when the film is irradiated with light from the tungsten filament lamp, run at various input voltages.

9.3.3. Dark conductivity; variation of conductivity with temperature

Fig. 9.5 shows the room-temperature current - voltage characteristics for CaO F 3 and the variation of conductivity with an increasing amount of evaporated material. Characteristics are linear in every case, and the linearity extends at least up to potentials of 10 V applied between the electrodes. The slope of these plots define the conductivity σ of the film. In each case, as expected, the evaporation of a further quantity of material increases the conductivity of the film. The evaporation periods were arbitrary, and no attempt to obtain a

FIG. 9.6.1. ELECTRICAL CONDUCTIVITY OF EVAPORATED FILMS OF CaO.

GRAPHS OF Log σ VERSUS 1/T

CaO F 3

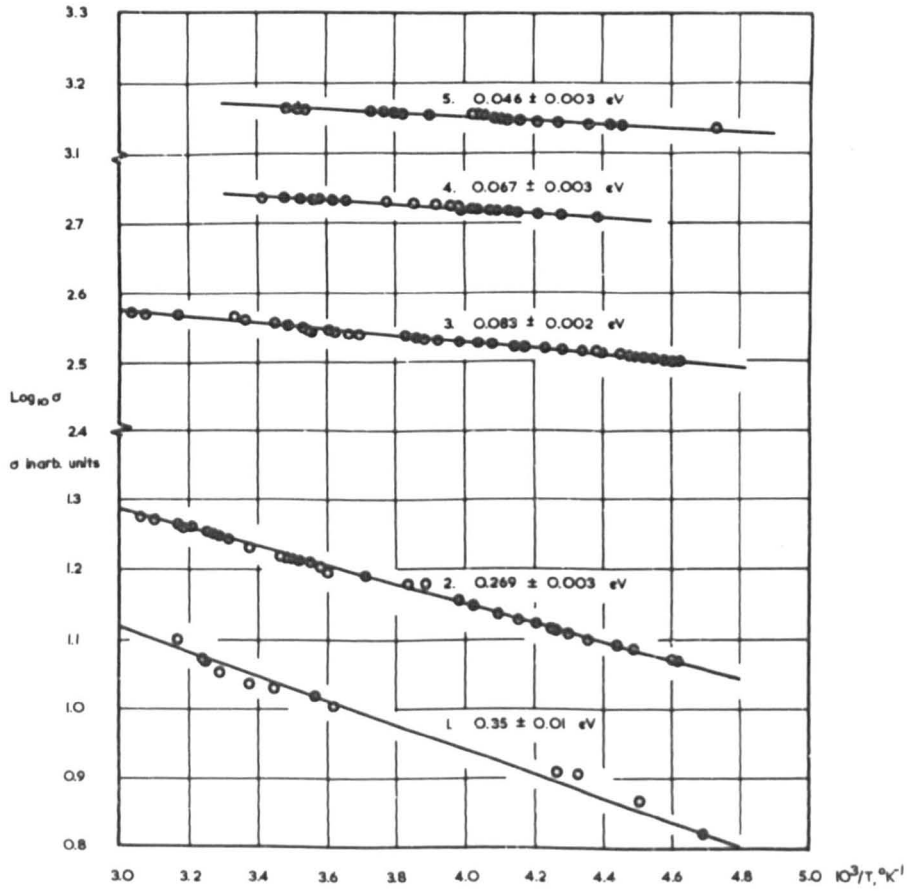

FIG. 9.6.2. RELATION BETWEEN THE GRADIENT OF THE CONDUCTIVITY PLOT AND THE RESISTANCE OF EVAPORATED FILMS OF CaO – CaO F 3

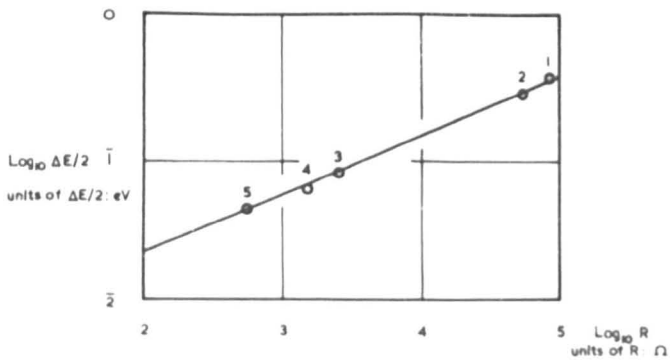

correlation between the time of evaporation and resistance was made.

Fig. 9.6.1 shows plots of $\log_{10} \sigma$ versus $1/T$ for the five evaporations of CaO F 3. It is observed that the plots are linear for a considerable range of reciprocal temperature: the gradient of the graphs has been used to define activation energies for the conductivity process, and these are quoted by each line. It is dubious if these activation energies have any significance on the simple semiconductor theory quoted in Secs. 2.2 and 2.4, since it was assumed there that the separation of the impurity levels from the conduction band, ΔE, was large compared with kT. At room temperature, kT = 0.025 eV; in the present case the activation energies $\Delta E/2$ are apparently of the same order of magnitude, at least for the last three evaporations. There is apparently some correlation between the apparent activation energy and the room-temperature resistance of the evaporated film, as the linear plot of log R versus log $\Delta E/2$ shows (Fig. 9.6.2); thus not only does further evaporation decrease the resistance of the film, but it also decreases the apparent activation energy for conductivity in the film. Although the film probably contains a large proportion of free calcium, the behaviour of the conductivity of the film as

FIG. 9.7.1. TIME VARIATION OF ILLUMINATED CONDUCTIVITY — CaO F 2[3]

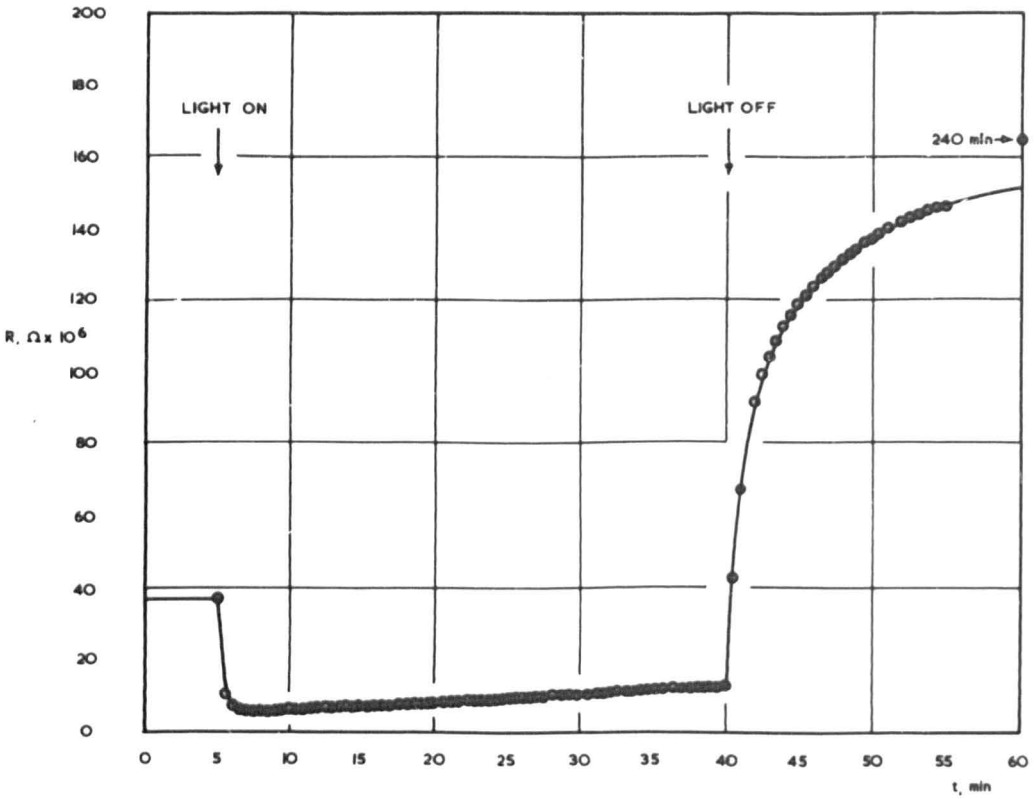

FIG. 9.7.2. TIME VARIATION OF ILLUMINATED CONDUCTIVITY - CuO F 3[3]

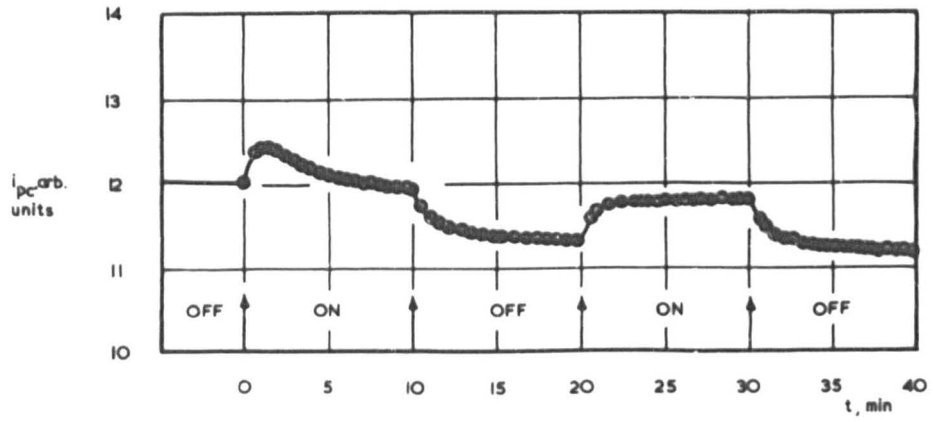

FIG. 9.7.4. EFFECT OF ILLUMINATION ON DARK CONDUCTIVITY - CuO F 3[2]

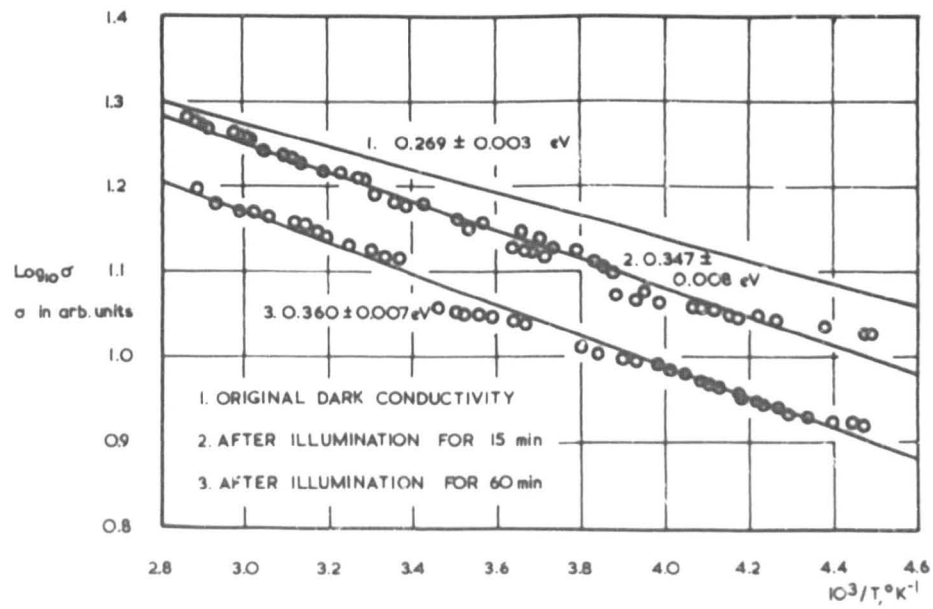

a function of temperature is characteristic of a semi-conductor rather than of a metal; pure calcium has a positive temperature coefficient of resistance, whereas the resistance of the film decreases with increasing temperature.

9.3.4. Photoconductivity

It is found that photoconductivity currents, particularly those resulting from intense illumination of the evaporated film, are unstable and change with time in a characteristic fashion, as shown in Fig. 9.7.1 for CaO F 2^3. The initial dark resistance of the sample is 36 x 10^6 ohms: on intense illumination with the 500 watt tungsten filament source the resistance quickly drops to 5 x 10^6 ohms, but continued illumination serves to increase the illuminated resistance to about 12 x 10^6 ohms. On removing the illumination, the resistance of the sample increases rapidly; the final equilibrium value of the dark resistance was 163 x 10^6 ohms, an increase by a factor of more than 4 over the original dark resistance.

This type of behaviour has been observed in all evaporation states of the tubes constructed in this series. Fig. 9.7.2 shows the relation between the photoconductivity current and time for CaO F 3^3: in this case an initial

FIG. 9.7.3. TIME VARIATION OF ILLUMINATED CONDUCTIVITY

CaO F 3^2

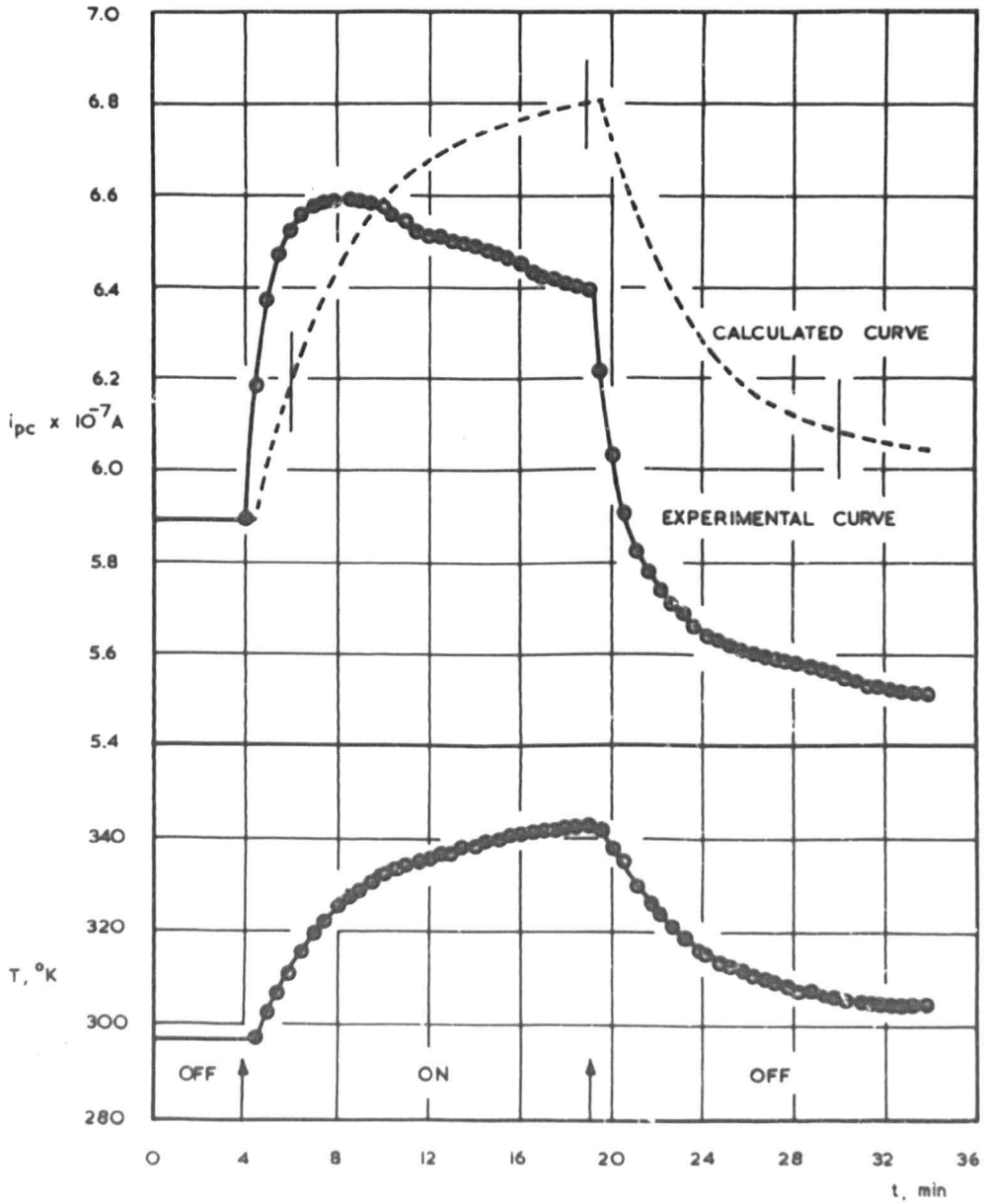

period of illumination of less than 10 minutes is required to increase the illuminated resistance to above its initial value in the dark.

In addition to any photon-induced effects, the illumination will certainly have the effect of warming the film, and the increase in temperature should cause an increase in the dark conductivity of the film. Fig. 9.7.3 shows the results of an experiment (with CaO F 3^2) in which conductivity and temperature were simultaneously monitored. The continuous upper curve is the total conductivity current for 100 mV applied between the electrodes: it shows the usual increase and decrease on illumination, and when the illumination is cut off, it falls to a value less than the original dark conductivity current. The lower continuous curve shows the variation in the temperature of the film with time, as measured with the tungsten-nickel thermocouple. Assuming that the effect of the illumination is only to warm the film, the expected dark conductivity can be calculated from these temperatures and from the information of Fig. 9.6.1. This is represented by the dashed upper curve, the error bars resulting from the experimental error in the determination of the conductivity plot. Normally, the illuminated conductivity would be expected to be greater than the

FIG. 9.8. DARK AND ILLUMINATED CONDUCTIVITY IN EVAPORATED FILMS OF CaO : CURRENT-VOLTAGE CHARACTERISTICS FOR WEAK ILLUMINATION

CaO F 2^4

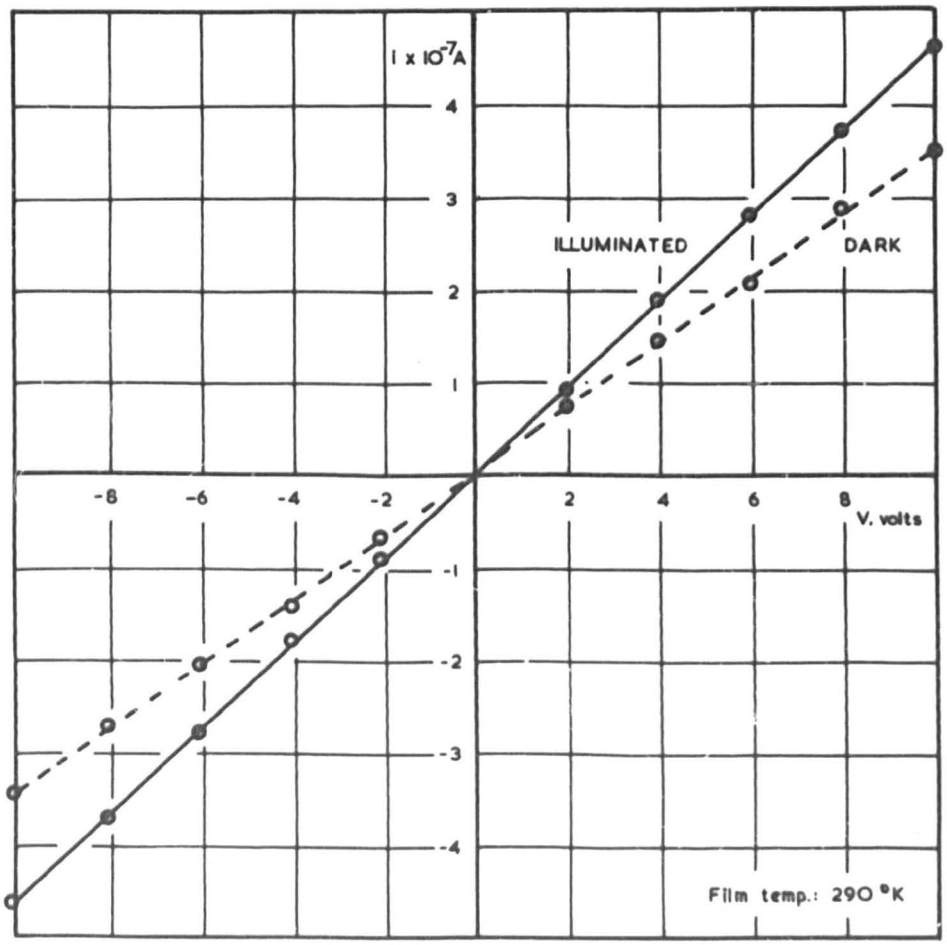

dark conductivity. The interesting result revealed by this experiment shows that this is only so for the first few minutes of illumination, and after this the illuminated conductivity is less than the calculated dark conductivity. This behaviour suggests that the effect of intense irradiation is to modify the properties of the evaporated film, and this hypothesis has been investigated by redetermining the relation between conductivity and temperature after periods of intense illumination. Fig. 9.7.4 shows conductivity plots for CaO F 3^2 after periods of intense illumination of 15 and 60 minutes' duration. The gradient of the plots increases with increasing irradiation and the magnitude of the conductivity current at room temperature decreases. It is thus apparent that intense illumination has an important effect on the electrical properties of the film.

Less intense illumination leads to greater stability in photoconductivity currents. Fig. 9.8 shows a current - voltage characteristic for dark and illuminated conductivity in CaO F 2^4, illuminated by the 500 watt tungsten filament source used in conjunction with a 5 mm thickness of Chance ON 19 glass, which removes the infra-red component of the light. Stable currents are obtained, and it is apparent that illuminated and dark conductivity both

FIG. 9.9. TIME VARIATION OF PHOTOELECTRIC EMISSION

CaO F 2^5

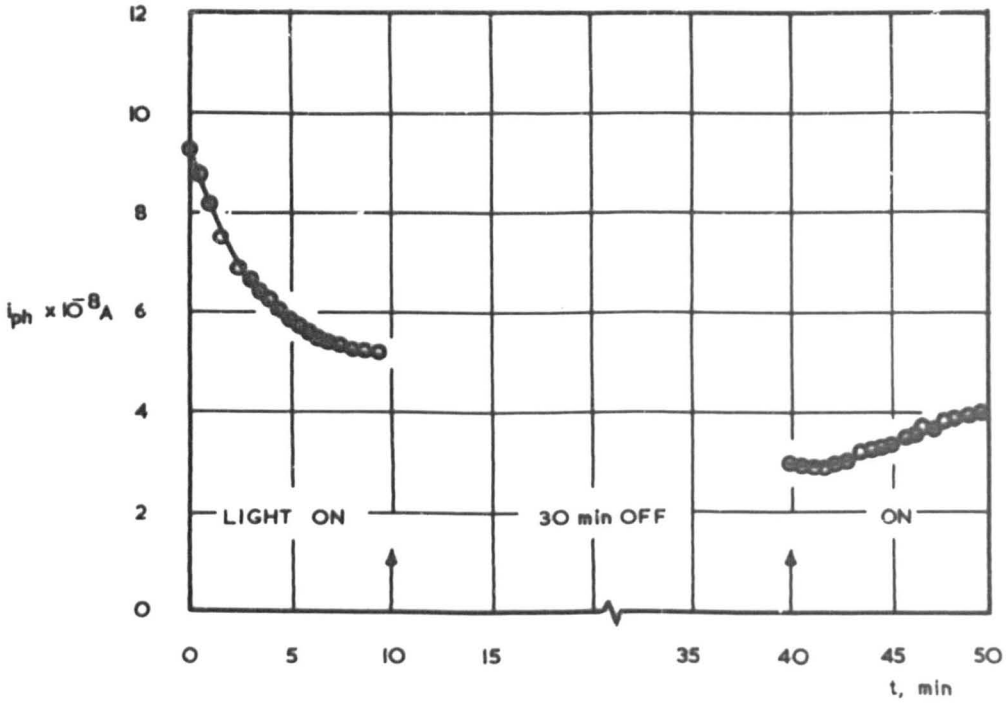

follow an ohmic relationship. This result is in striking contrast to the behaviour of the porous calcium oxide coated cathode.

Measurements of the spectral sensitivity of photoconductivity were not found to be practicable. The rather weak illumination obtained from the monochromator provides only a very small increase in the already considerable dark conductivity, and it is not possible to balance off this large dark conductivity with the electrometer and measure only the photoconductivity.

9.3.5. Photoelectric emission

To a lesser extent, photoelectric emission from the evaporated film is unstable under intense illumination. Fig. 9.9 shows the variation of photoelectric emission with time for CaO F 2^5: the initial period of illumination causes a reduction in the photocurrent by a factor of 3. After a period of 30 minutes in the dark, the photocurrent apparently recovers slightly on further illumination.

This instability makes the determination of photoelectric work functions by the method of complete photoelectric emission, undertaken as a measure of the photosensitivity, unreliable at the most intense illuminations. Accordingly, to avoid the time spent in tracing "Schottky"

FIG. 9.10. PHOTOELECTRIC WORK FUNCTION OF EVAPORATED FILMS BY COMPLETE PHOTOEMISSION – CaO F 2[1]

'RICHARDSON' PLOT

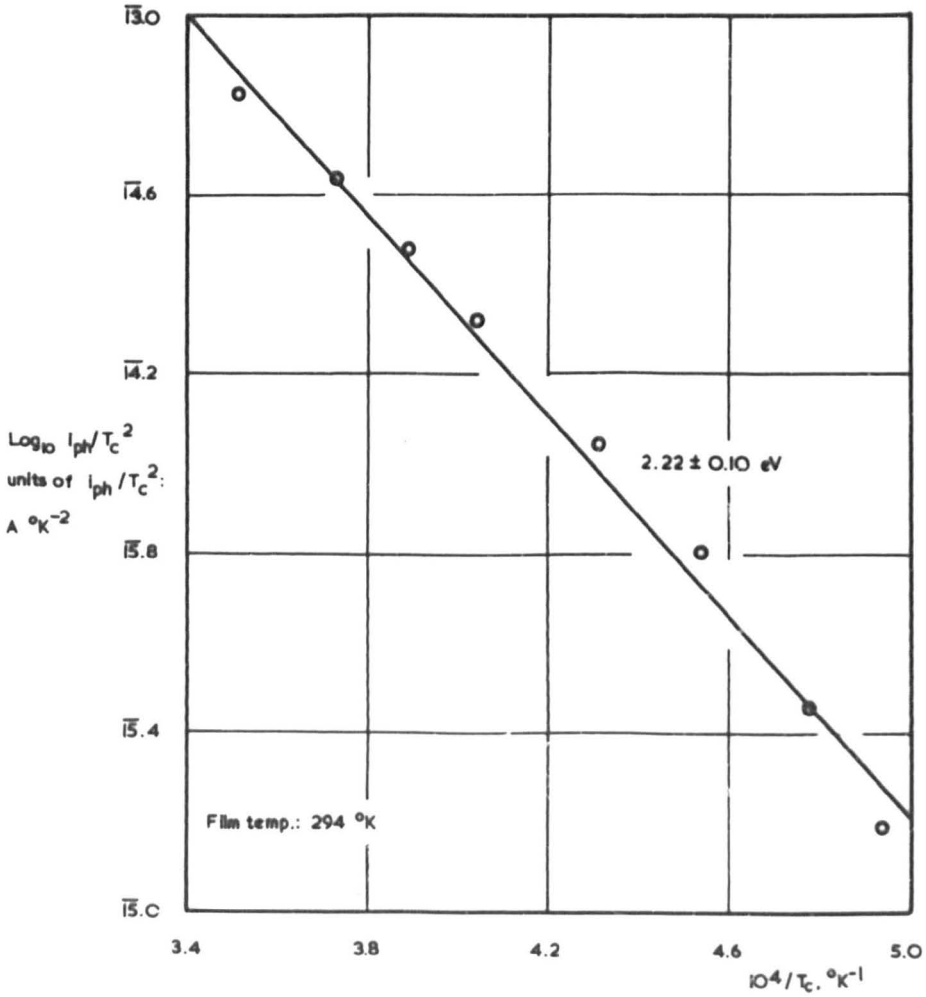

plots for each value of the tungsten filament temperature, the photoemission current for V_a = 240 V is taken instead of the zero-field photocurrent in the "Richardson" plot of $\log_{10} i_{ph}/T^2$ versus $1/T$ - a procedure similar to that carried out in certain thermionic emission determinations (Sec. 6.2). The "Richardson" plot for the first evaporation in CaO F 2 is given in Fig. 9.10. The photoelectric work functions deduced from the gradients of such plots generally decrease with an increasing quantity of material evaporated. Table 9.2 (below) gives the work functions for five evaporations in CaO F 2.

Table 9.2

Photoelectric work functions of evaporated films of calcium oxide by complete photoemission - CaO F 2

Evaporation	ϕ_{bk}, eV
1	2.2 ± .1
2	2.1 ± .1
3	2.0 ± .1
4	1.4 ± .2
5	1.7 ± .2

As the apparent photoelectric work function decreases, the instability of the photocurrent becomes greater and the error in the slope increases. The values obtained

probably have very little absolute significance. Measurements of the spectral sensitivity of photoemission were not attempted.

9.3.6. Optical absorption in evaporated films of calcium oxide

In a previous thesis (116) the optical absorption of evaporated films of barium oxide was studied by a photographic technique. Films were prepared by evaporation from a conventional cylindrical cathode situated along the axis of a 12 mm diameter glass tube: the tube was placed in front of the entrance slit of the spectrometer, and a photographic record of the spectrum of light from the tungsten filament lamp which had passed through the tube with its evaporated film was obtained. This spectrum was compared with one taken using a clean glass tube in place of the absorption tube in the same way as has been described for a reflectivity study in the present work (Sec. 7.5), where the disadvantages of the method were pointed out.

The method has been modified in the present work. The principle of comparing the intensities of spectra obtained for light which has passed through an evaporated film of calcium oxide with light which has not is retained,

FIG. 9.11.1 OPTICAL ABSORPTION TUBE — SCHEMATIC ARRANGEMENT

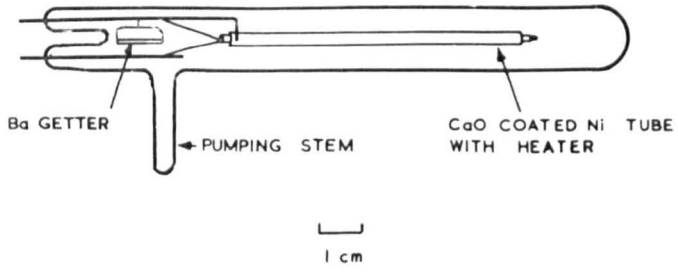

FIG. 9.11.2. OPTICAL SYSTEM FOR ABSORPTION MEASUREMENTS

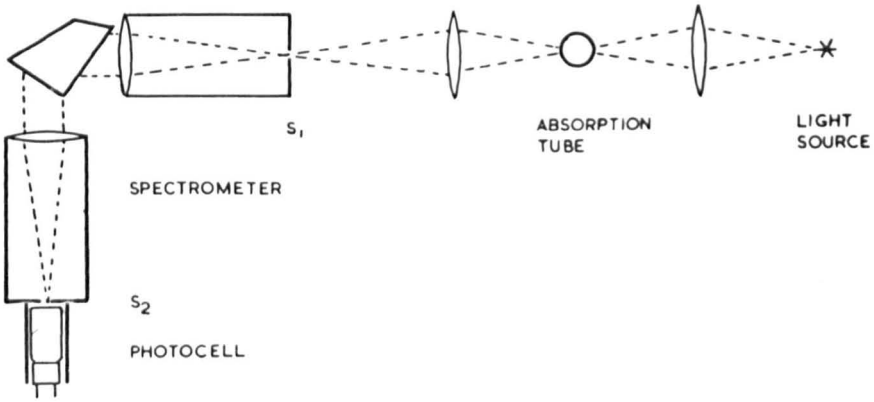

but the comparison is carried out directly by comparing the photocurrents produced in the 53 CV photocell placed at the exit slit of the spectrometer; the cell, mounted in a cork, takes the place of the eyepiece.

An absorption tube is shown diagrammatically in Fig. 9.11.1. Similar in construction to those used for barium oxide studies, it consists of the normal cathode base provided with a heater and coated along its entire length with calcium carbonate suspension, and sealed into a 12 mm diameter Pyrex tube. The tube is attached to the pumping system by the stem, and the normal breakdown procedure is applied. After baking out, the tube is sealed off and the getter, which is shielded to prevent deposition in the part of the tube near the cathode, is fired. Layers of calcium oxide are evaporated on to the glass tube by raising the temperature of the cathode to about 1100 ^{o}K until a visible darkening of the glass appears.

Absorption readings are taken as follows. The absorption tube is placed in a vertical position in front of the entrance slit of the spectrometer, as shown in Fig. 9.11.2. Light from the tungsten filament lamp is focused on the absorption tube; a black paper mask with a slit 2 mm wide cut in it and wrapped round the tube defines

FIG. 9.12. OPTICAL ABSORPTION OF EVAPORATED FILMS OF CaO

FIG. 9.12.1. CaO PC 10

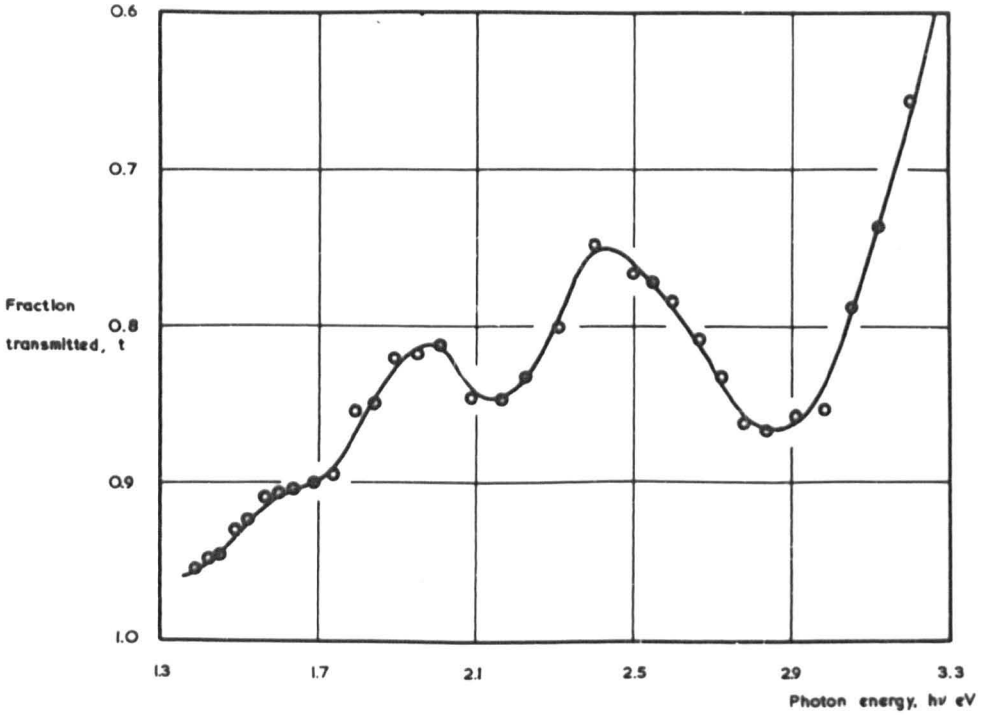

FIG. 9.12.2. CaO F 7

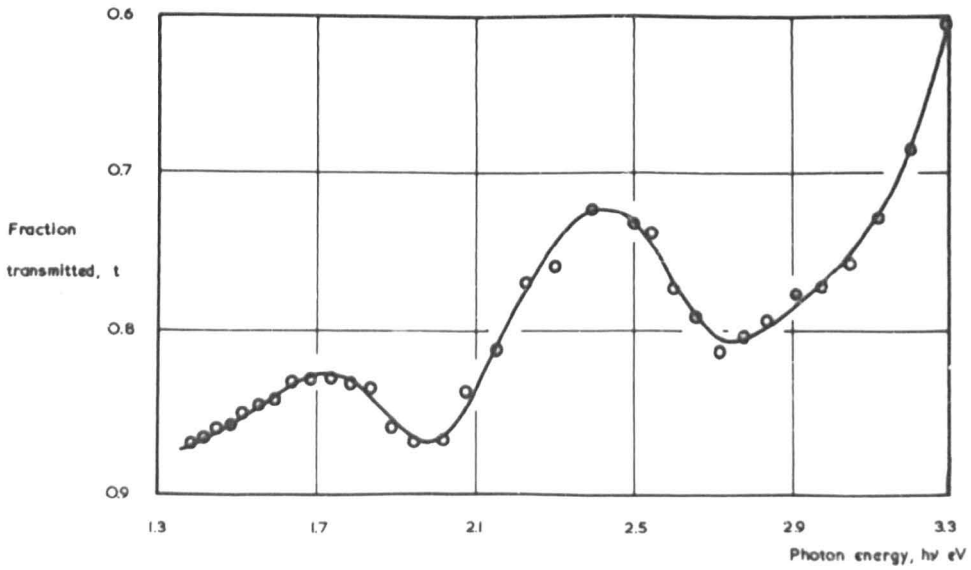

the area of illumination; a second lens focuses the light which passes through the absorption tube on to the slit of the spectrometer. Using the narrowest possible exit slit, readings of the current produced in the photocell are obtained with the electrometer for the range of wavelengths between 9000 Å and 3800 Å at intervals of 50 Å at the violet end and 250 Å at the red end of the spectrum. The experiment is then repeated using a piece of clean 12 mm diameter Pyrex tube in place of the absorption tube. If θ_a and θ_c are the deflections obtained at any given wavelength with the absorption and control tubes respectively, then t, the fraction of light transmitted by the film at that wavelength, is given by

$$t = \theta_a/\theta_c \qquad 9.1.$$

Since $$a + t = 1 \qquad 9.2.$$

where a is the fraction absorbed by the film, the variation of optical absorption with photon energy can be studied by drawing a graph of 1 - t versus $h\nu$, where ν is the frequency of the incident radiation.

The results obtained for CaO F 7 are displayed in Fig. 9.12.2. It must be pointed out that the scale of the fraction transmitted axis is much enlarged; the variations in optical absorption between 1.3 and 2.7 eV,

FIG. 9.12. OPTICAL ABSORPTION OF EVAPORATED FILMS OF CaO

FIG. 9.12.3. CaO PC 5, CaO PC II

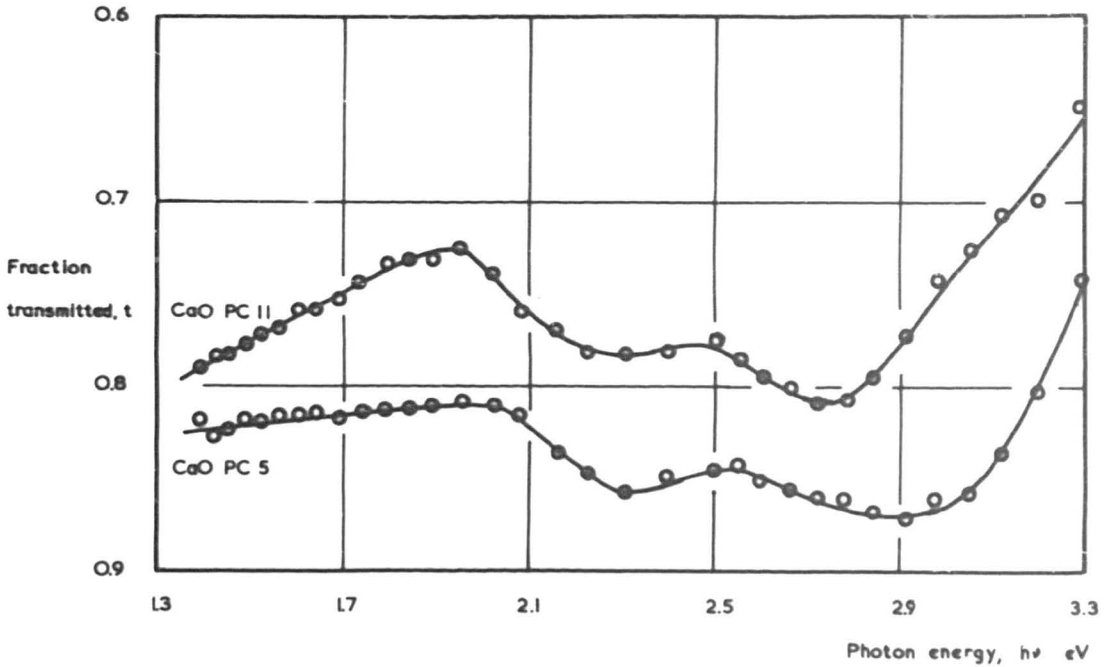

with peaks at about 1.7 and 2.5 eV, are small compared with those that would be expected in the range of intrinsic absorption. It is, however, possible that the increase in optical absorption (i.e. the decrease in the fraction transmitted) at photon energies greater than 3.0 eV may represent the onset of intrinsic absorption in the film.

Evaporated films on the envelopes of probe diodes have also been studied by this method, although there is a possibility that the film may contain a proportion of evaporated nickel from the exposed portions of the cathode base; in the tubes designed for absorption studies the whole length of the nickel cathode base is covered with carbonate suspension. Curves for three probe diode envelopes are given in Figs. 9.12.1 and 3. All three curves are rather similar, with barely resolvable structure at about 1.7 eV, peaks at about 2.0 and 2.5 eV, and a general rise beyond 3.1 eV, although the relative heights of the peaks differ from envelope to envelope.

9.4. Discussion of results

It must be emphasised that the work presented in this chapter is of a preliminary nature only and that any interpretation of results can only be tentative. It is for this reason that the results will be discussed separately and

not combined with the information obtained by experiments on cathodes.

The electrical properties of the films are evidently somewhat different from those of cathodes. For the films, conductivity current - voltage characteristics are accurately linear up to potentials of at least 10 V applied between the electrodes. The variation of electrical conductivity with temperature yields linear plots of log σ versus $1/x$, with gradients which are too low to interpret on the simple theory at present advanced. Although the composition of material evaporated from oxide cathodes on to glass has not been investigated, work on evaporation of the alkaline earth oxides on to metallic anodes (12, 192) suggests that the evaporated substance will contain a high proportion of the free alkaline earth metal. Thus, in the present case, the film under investigation probably consists of a layer of calcium oxide with a high proportion of free calcium, in a state of aggregation which may be difficult to define. It is possible that the gradients of the conductivity plots may be related to the activation energies for the diffusion of calcium ions over the surface of the film, and it is to be expected that the more calcium present between the electrodes, the lower the activation energy

will be. However, no experimental test of this suggestion can as yet be offered.

An important effect of illumination on the film is to cause an apparently permanent change in its electrical properties: the resistance of the film is increased, and the activation energy, as deduced from the gradient of the conductivity plot, is also increased. Three explanations may be put forward. The first depends upon a modification of the semiconducting properties of the film by the infra-red component of the white light illumination. Illumination by photons of low energy liberates positive holes, trapped at recombination sites in the lattice of the crystallites making up the film: these holes recombine with trapped electrons, leaving a number of empty traps which are now available to reduce the number of charge carriers. The experimental fact that photoconductivity currents induced by white-light illumination without the infra-red component are stable is a point in favour of this explanation, but is, of course, far from being proof.

A second explanation recognizes that the conductivity process in the film is almost certainly a surface effect and that a small change in the surface conditions induced by illumination may have a marked effect on the electrical conductivity. The use of illumination to disturb the

surface equilibrium conditions is a standard technique in surface physics (127), and rather similar effects to those observed in the present work have been reported by Kobayishi and Kawaji (103) for evaporated films of zinc sulphide. The experimental tube containing the evaporated film was connected to a pressure gauge, and a plot of pressure in the tube versus time shows a reduction when illumination is applied to the specimen, followed by an increase in pressure if illumination is continued. When the illumination is cut off the pressure rises again, but not to the original dark value. Similar changes can be followed in the work function of the film. The changes were attributed to the photo-enhanced adsorption of oxygen on to the film. Melnick (117) found a similar effect in films of zinc oxide: light causes a reversible desorption of oxygen from the film, with a re-adsorption which is linear with the logarithm of the time when the light is extinguished. Levinstein (109) reported an increase in the resistance of PbTe films due to strong illumination.

In the present case a film of calcium-rich calcium oxide would be expected to be particularly susceptible to attack by oxygen. Oxidation of a proportion of the metallic constituent due to a photon-induced adsorption

would reduce the electrical conductivity, and the reduction of the proportion of Ca to CaO in the film would tend to increase the activation energy of the conduction process.

A third explanation is possible. Infra-red illumination of thin evaporated metallic films may cause a kind of 'annealing', producing irreversible structure changes in the state of aggregation of the crystallites of the film. The changes depend to a certain extent on the state of the substrate, for example its temperature during evaporation and surface condition. It is possible that this type of process may also apply to evaporated films of calcium oxide.

The hypothesis of changes in the surface equilibrium, in particular leading to the adsorption or desorption of oxygen under the influence of illumination, is susceptible to experimental investigation. Accordingly, a tube (CaO F 6) was constructed which employed the usual electrode structure, but the envelope bore a side-arm connected to an inverted ionisation gauge of the Bayard-Alpert type (14). The gauge consists of a tungsten filament cathode, a cylindrical molybdenum grid and a fine etched tungsten collector mounted along the axis of the grid. The gauge was constructed using the standard FK 10 pinch and envelope. Although the gauge can be used as a pump in

FIG. 213. CHANGE OF PRESSURE ON ILLUMINATION OF AN EVAPORATED CaO FILM - CaO F 6

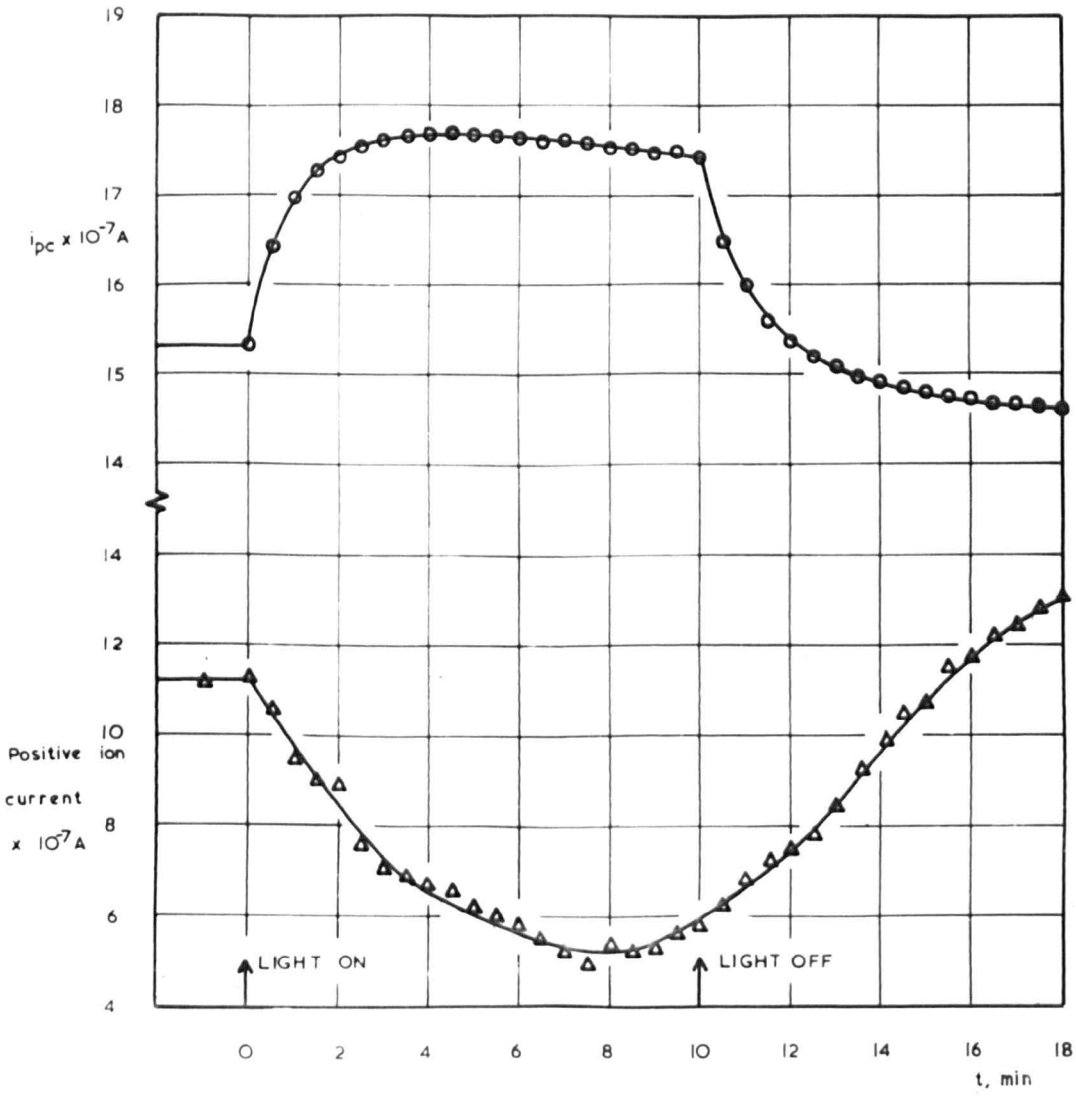

ultra-high vacuum applications, its use here is merely as a pressure indicator. The tungsten cathode filament is heated from the a.c. Variac supply, the grid being maintained at + 100 V with respect to the cathode; the collector is maintained at - 50 V with respect to the cathode. The positive ion current reaching the collector for a fixed electron current to the grid may be taken as a measure of the pressure in the gauge.

The carbonate is broken down to oxide in the usual way and after outgassing and sealing off the tube and gauge a film of calcium oxide is evaporated between the Aquadag electrodes. The pressure gauge attached to the tube allows the pressure to be monitored as the illuminated conductivity current is studied as a function of time. Preliminary results are shown in Fig. 9.13. The upper curve represents the time variation of the photoconductivity current with 10 V applied between the Aquadag electrodes, and follows the familiar behaviour (cf. Fig. 9.7). The lower curve shows the variation of the positive ion current with time. The pressure in the system before illumination was about 10^{-5} mm Hg. On illumination, a definite decrease in positive ion current, and hence in the pressure in the system, is observed. As illumination is continued, the pressure shows a tendency to rise again,

and when illumination is removed, the rise in pressure is more rapid. The changes in positive ion current are considerably greater than those due to random fluctuations in the pressure in the system and the general slow decrease in ion current due to the pumping action of the gauge. The changes cannot be due to photoeffects in the gauge itself, as the illumination is directed only on to the film and the gauge is screened from external illumination (the collector and grid of the gauge are subjected to a steady illumination from the cathode of the gauge).

The results are rather similar to those obtained with other semiconductors which have been discussed previously. It seems reasonable to infer that the reduction in the pressure in the tube on illumination of the calcium oxide film is due to the photo-enhanced adsorption of residual gas on to the film, and that the increase in pressure when the illumination is cut off is due to the desorption of this gas. It is tempting to suggest that this residual gas is oxygen which affects the electrical properties of the film in such a way as to increase the resistance of the film and to increase the activation energy of the conduction process, but this cannot be regarded as proved. A closer examination of the conditions under which the curves of Fig. 9.13 were

obtained reveals further difficulties. The pressure of residual gas in the system was about 10^{-5} mm Hg: if the partial pressure of oxygen was of this order of magnitude, there would be no question of there being any free calcium in the film, as it would all have been oxidised prior to any illumination effect. It is possible that the residual gas in the system might be a mixture of carbon dioxide and carbon monoxide from an imperfectly broken-down cathode, released during the evaporation process. These gases would not be taken up by the barium getter in the same way that oxygen would be, and it is probable that they would not have a poisoning effect on the film. The pressure changes observed on illumination may thus be due to the adsorption and desorption of any or all of the residual gases in the tube, and as the gauge cannot discriminate between gases the changes in the electrical properties of the film cannot be correlated to the effects of any particular gas.

The photoelectric emission results quoted for the films evaporated on to glass are of little quantitative significance: work functions quoted are the arbitrary ones defined by the complete photoemission method, and serve merely to show an increase in photosensitivity with increasing evaporation. The Fowler photoelectric work

functions obtained for photoemission from the anode are again probably only arbitrary, although for the thinner films agreement with the form of the theoretical Fowler curve is good. Arbitrary photoelectric thresholds, defined by a consideration of the least measurable photocurrent, are clearly correlated with the Fowler work functions. A number of different values have been quoted for the photoelectric work function of bulk calcium - 2.4 (164), 2.7 (97) and 3.2 eV (110) - but it seems likely that the work functions of films of calcium oxide evaporated on to nickel (the Fowler work functions vary between 1.4 and 2.1 eV) do not tend to the value for the bulk metal, in spite of the fact that the film probably contains a high proportion of the free metal.

A comparison of the optical absorption curves for thin films of calcium oxide evaporated on to glass in two types of tube, one in which only calcium oxide can be evaporated and the other in which there is the possibility of the evaporation of nickel from exposed portions of the cathode base, suggests that the structure at about 1.7 and 2.5 eV, common to both types of tube, may be a feature of the calcium oxide film. The 2.0 eV peak is observed only in the latter class of tube and may possibly be due to nickel impurities in the film.

In spite of the considerable difference between the electrical properties of the films and the cathodes, it is tempting to suggest that the 2.5 eV structure may be related to structure observed at 2.5 - 2.6 eV in photoelectric emission and photoconductivity in cathodes. This tentative suggestion must be tempered with the observation that the 1.7 eV absorption structure is not generally apparent in photoelectric studies on cathodes. By analogy with determinations on barium oxide, however, some general resemblance between structure in the spectral sensitivity curves for cathodes and for evaporated films might be expected.

Chapter 10 Discussion of results; suggestions for further work

10.1. Scope of the present work

In the present work an attempt has been made to investigate the photoelectric and photoconductive properties of calcium oxide coated cathodes and to relate these properties, if possible, to the thermionic and electrical properties. A secondary aim has been to collect as much information as possible on the thermal activation energies for the purpose of comparison with previously published results.

It must be pointed out that the oxide cathode is an extremely complicated system, and to specify the state of a cathode the values of many variables must be defined. Thus the preparation of a number of cathodes to have exactly similar properties is difficult unless the most rigorous control is exercised in all stages of the preparation and activation of a tube. This difficulty is reflected in the considerable spread of results obtained in this and other investigations (83, 87, 116) of the thermal activation energies of oxide cathodes.

10.2. Thermal activation energies

Thermionic work functions ϕ, obtained from Richard-

son plots of emission as a function of temperature, have been summarised in Table 6.1. It has been pointed out that the average Richardson work function, 1.8 eV, is in reasonable agreement with the value of 1.7 eV quoted by Hopkins (87).

The values of A* obtained from the intercept of the Richardson line on the log i_o/T^2 axis show a considerable variation, ranging from approximately 10^{-5} to 10^5. Values of A* greater than A, the theoretical constant (A = 120 amp cm^{-2} $^oK^{-2}$), cannot be explained merely by supposing that $A^* = A(1 - \rho)$, where ρ is the reflection coefficient for electrons at the cathode surface, as in this case ρ would require to be negative. Some adjustment to the values of A* could certainly be made to account for the fact that the emitting area of the porous cathode is considerably greater than the geometrical area of the cylindrical cathode customarily employed, and an increase in the emitting area would decrease the value of A*. Dewsberry (48) has found a similar variation in values of A* obtained from Richardson plots of emission from barium oxide cathodes, and in one case a value of A* as high as 10^9 was obtained. The slopes of the log A* versus ϕ curves given by Dewsberry are about 5 and 6; the slope of the line in Fig. 6.4 was about 7, in reasonable

agreement.

Conductivity plots of log σ versus 1/T show the characteristic form of two linear portions meeting at a sharp break. The average values of the gradients of the low-temperature and corrected high-temperature portions, 0.7 and 1.6 eV respectively, are in reasonable agreement with those obtained by Hopkins (0.8 and 1.3 eV respectively). The fact that a strong magnetoresistive effect is observed at high temperatures and that no effect is observed in the low-temperature region (Sec. 8.2.2) suggests that the conduction mechanism is different in the two regions and lends weight to the adoption of the Loosjes-Vink interpretation of the form of the conductivity plot. There seems to be no doubt that conduction in the high-temperature region is through the electron gas in the pores of the cathode, and that at low temperatures it is by a semiconducting process, more probably a surface than a volume effect, by analogy with current theories of conductivity in barium oxide cathodes. On the Loosjes-Vink interpretation, the slope of the low-temperature conductivity plot represents $\Delta E/2$, the depth of the Fermi level below the conduction band (the impurity level is at a depth of ΔE below the conduction band). On the basis of the present work, the average value of ΔE is

FIG. 10.1. PROPOSED ENERGY LEVEL SCHEME FOR CaO FROM THERMIONIC EMISSION AND ELECTRICAL CONDUCTIVITY DETERMINATIONS

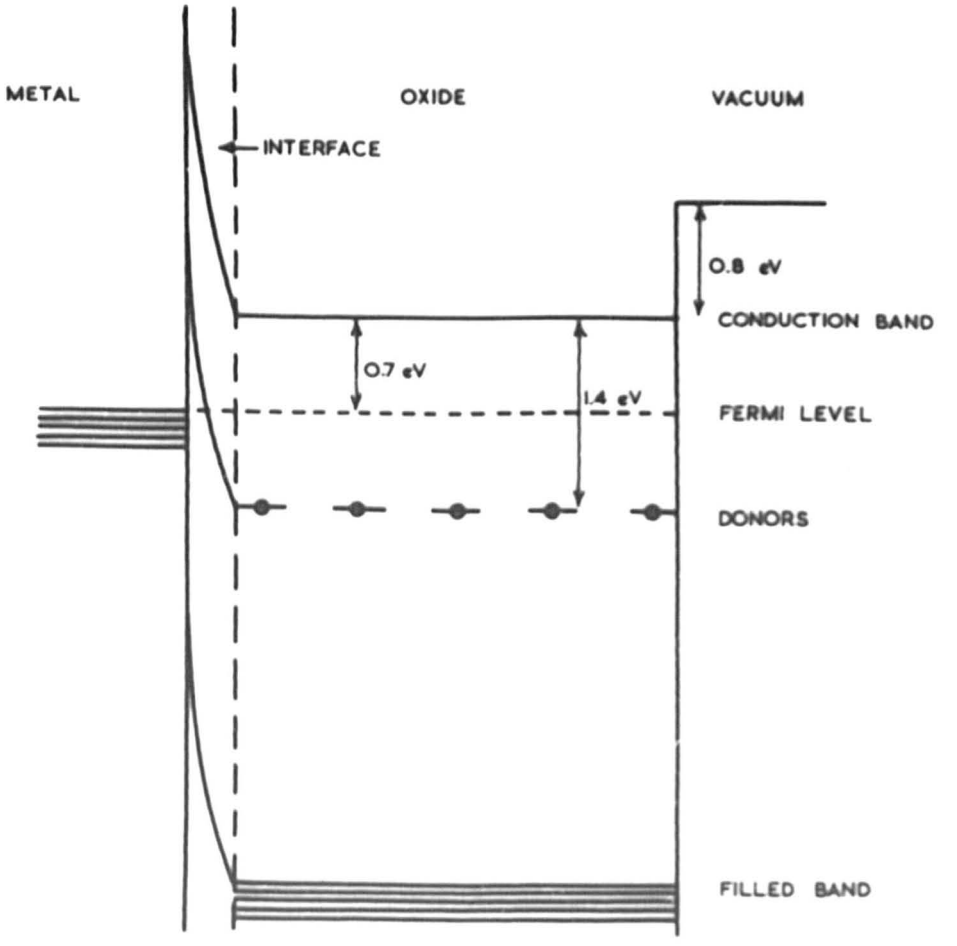

about 1.4 eV. In Sec. 6.3.6 the average value of the external work function χ was shown to be about 0.8 eV, using three different methods of calculation, and is again in agreement with the result quoted by Hopkins (0.7 eV; but this value was obtained by a method unlikely to yield the true external work function). The top of the filled band is placed, rather tentatively, at a depth of 4.0 eV below the conduction band, following the calculations of Wright (194) for a number of semiconductors and insulators. Wright carried out the calculation at a time (1948) when there was very little accurate knowledge of optical and thermal activation energies in the alkaline earth oxides and made recourse to a number of approximations and assumptions which might well be modified in the light of more recent work. The energy level scheme deduced from the thermionic emission and electrical conductivity measurements is displayed in Fig. 10.1 and differs little from that of Hopkins (Fig. 2.10).

10.3. Optical activation energies

10.3.1. Experimental results

In the range of photon energies studied (1.4 to 3.1 eV) a certain amount of structure is detectable in the

spectral sensitivity curves of photoemission and photoconductivity. Representation of the results by plots against logarithmic rather than linear axes is probably more realistic, as this procedure displays the form of the curve at lower photon energies, where in fact most of the change in photosensitivity takes place. A study of the logarithmic curves (e.g. Figs. 7.2.3, 7.3.2, 7.4.2, 7.11.2 and 7.12.2) shows that the photocurrent per unit incident intensity usually increases by up to two orders of magnitude between 1.4 and 2.2 eV; between 2.2 and 2.9 eV the logarithmic curves show only a slight increase with increasing photon energy and above 2.9 eV there are indications of a slightly more rapid rise. The linear curves (e.g. Figs. 7.2.2, 7.3.1, 7.4.1, 7.11.1 and 7.12.1) are of interest in the region above 2.2 eV, where the logarithmic curves show comparatively little change. They display structure at about 2.6 eV, which may take the form of a definite peak or a point of inflexion in the spectral sensitivity curve.

In Chapter 8 attention has been drawn to the close similarity of photoelectric emission and photoconductivity effects, both in their spectral sensitivities and temperature variations. Two interpretations were discussed there: the possibility that the photoelectric

external work function χ' should be zero, or nearly so, which would not be expected from a comparison with the thermal activation energies, and the possibility that the photoconductivity current may really be due to photoelectric emission in the pores of the cathode. The latter hypothesis was investigated by a number of means, all of which yielded results in support of it. On the strength of this agreement the discussion will proceed on the assumption that results obtained from photoconductivity and photoelectric emission spectral sensitivity curves are effectively indistinguishable, both arising from the process of photoemission.

The general increase in photosensitivity with increasing photon energy cannot be associated with photoemission from any particular impurity level, the transition from the rapid to the less rapid rise being too gradual even to use Moss's $\lambda_{\frac{1}{2}}$ method of defining photoelectric thresholds (Sec. 3.4). The structure at 2.6 eV may, however, be due to the presence of an impurity level at this depth below vacuum potential. This is the only optical activation energy which can be deduced as a result of the present experimental work, as the adoption of the hypothesis of pore photoconductivity of necessity precludes a deduction of the activation energies relative

to the conduction band from photoconductivity results.

Without any other photoelectric information available, it might be suggested that the rapid rise in photosensitivity at low photon energies over two orders of magnitude might represent the onset of intrinsic photoemission. However, a similar rise is obtained in the same range of photon energies in the spectral sensitivity curves for barium oxide (cf. Figs. 4.2.2, 4.3) and intrinsic photoemission is probably not observed with barium oxide until the values of the incident photon energy reach about 5 eV. The deciding factor lies in the spectral sensitivity curve for optical absorption, which will show a rapid increase to very strong absorption at photon energies corresponding to intrinsic transitions. The single determination of optical absorption in the cathode by the reflectivity method (Sec. 7.5) did not show such an increase at low photon energies, and a common-sense argument shows that the optical absorption cannot change very rapidly in the visible region (about 1.5 to 3.0 eV) as the cathode is normally uncoloured, neglecting for the moment the blue cathodes referred to in Sec. 7.5. Thus there can be no question of the optical absorption undergoing a change from impurity to intrinsic absorption over the visible region, although there may well be some less marked

structure in the optical absorption curve corresponding to absorption by impurity levels in this region. Such structure has, in fact, been observed with films of calcium oxide evaporated on to glass (Sec. 9.3.6). Peaks which represented only a comparatively small change in the optical absorption, and hence could not be due to intrinsic absorption, were observed at about 1.7 and 2.5 eV. A tentative correlation between the 2.5 eV structure and the structure observed at about 2.6 eV in photoelectric emission and photoconductivity curves has already been put forward, but it is felt that this should not be pursued too far until the relation between the two very different systems of porous cathode matrix and evaporated film can be investigated further.

The blue cathode coloration commonly observed in activated calcium oxide cathodes is of considerable interest in a discussion of the photoelectric properties of the cathodes. Hopkins (87) has suggested that the coloration may be due to the formation of F-centres such as those invoked by Pohl (146) to explain the properties of additively coloured alkali halide crystals. The colour centres in alkali halides are associated with a stoichiometric excess of the alkali metal, and may be described in terms of an alkali atom adjacent to a vacant

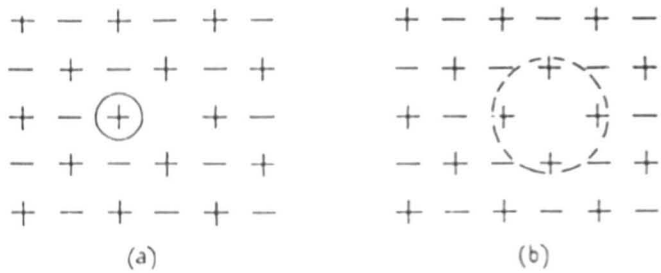

Two ways of describing an F-centre. (*a*) An alkali atom at the point adjacent to that from which a negative ion is missing. (*b*) An electron shared between the six neighbours of a vacant lattice point.

Fig. 10.2.1

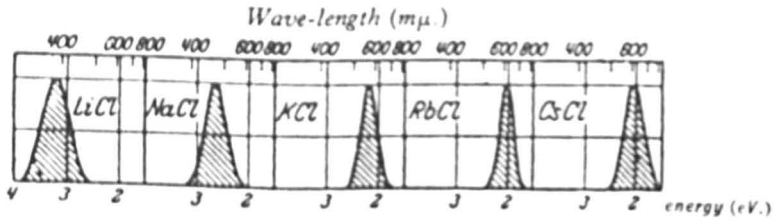

Absorption bands of the colour centres at 20° C.

Fig. 10.2.2

negative lattice site, or alternatively as an electron shared between the six metal ions surrounding a vacant negative ion site (Fig. 10.2.1). Although the activated calcium oxide cathode also contains a stoichiometric excess of the electropositive constituent and the absorption spectrum of the coloured calcium oxide cathode shows a peak very similar to those observed in coloured alkali halide crystals (Fig. 10.2.2) there is no definite evidence to suggest that the blue coloration is actually due to the presence of F-centres. An argument against the F-centre hypothesis is that while the stoichiometric excess of calcium in the cathode is produced during the activation process the blue coloration does not appear for a period of days or even weeks after prolonged use. If the coloration was related to the excess of metal in the cathode, it might be expected to appear as soon as the cathode cooled down after activation. No difference between the thermionic and electrical properties of coloured and white cathodes is, of course, detectable, as the cathode must be heated to make the measurements and heating causes dispersal of the coloration. Photoelectric measurements have been made on the blue cathodes at room temperature, but no detectable difference in the shape of photoelectric emission or photoconductivity characteristics

can be observed between blue and white cathodes.

An alternative explanation of the blue coloration to the F-centre hypothesis can be found in terms of a surface layer of some substance, condensing slowly on the cool cathode. Carbon from the organic binder of the suspension is frequently blamed for a greyish coloration occasionally observed during the early stages of operation of both barium oxide and calcium oxide cathodes, but the blue coloration is unlikely to arise from the binder, as after activation and operation the binder compounds should all have been burnt off, and as the blue coloration is due to a material which oxidizes spontaneously on exposure to air to form a white compound. It may be possible that calcium-rich calcium oxide, evaporated on to the anode when the cathode is hot, returns to the cold cathode by some unspecified process. This is, however, unlikely, as Hopkins (89) has shown that the electropositive constituent of the evaporated material reaching the anode (i.e. free calcium) is much more tightly bound to the anode than is the electronegative oxygen. Metson (123) has suggested that the coloration might be due to sodium, obtained by evaporation from impurities in the ceramic insulators, but no convincing proof has yet been put forward. If merely due to sodium evaporation, the effect

is presumably a function of time and of temperature of operation, and would not depend in the first instance on the cathode material. Although calcium oxide cathodes certainly require considerably longer activation periods than barium oxide cathodes, the effect would be expected to appear regularly in well-activated barium oxide cathodes, but the same blue coloration is not observed.

10.3.2. Theoretical predictions and comparison with experimental results

No attempt has so far been made to correlate thermal and optical activation energies. The possible effects of the Franck-Condon principle will now be considered.

In Sec. 3.1 the Mott and Gurney approximate calculation of the effect was discussed, and it was stated that the ratio of the thermal to the optical activation energies is given, approximately, by the ratio of the optical dielectric constant to the static dielectric constant. The refractive index of calcium oxide is about 1.84 (74), so the optical dielectric constant ϵ is about $1.84^2 = 3.4$. The value quoted by Højendahl (86) for the static dielectric constant ϵ_0 is 11.8 and has been criticised (25) on the grounds that inadequate precautions were taken to dry the liquids used, the immersion method being employed. There

is thus the possibility of the value quoted being the dielectric constant of the hydroxide rather than of the oxide. Neglecting this criticism, for the time being, the ratio of ϵ/ϵ_0 is roughly 0.3.

Now the presence of an impurity level at a depth of about 2.2 eV below vacuum potential in the thermal activation energy scheme has been established by measurements of thermionic emission and electrical conductivity. There is no evidence from conductivity information for levels at much lower energies (i.e. nearer the conduction band): the lowest value for $\Delta E/2$ given in Table 6.1 was 0.4 eV, which, using the average value of χ, would place the impurity level at a depth of 1.6 eV below vacuum potential, and this seems to be about the lower limit. Using the Mott and Gurney approximation, the level on the optical scheme corresponding to the average thermal level would be nearly 9 eV below vacuum potential. There is no experimental evidence to show that there should not be an optical level at this depth, but the present work suggests that there is a much lower level; and this scale seems unreasonably large for the optical scheme. Working back from the optical result of an impurity level at 2.6 eV below vacuum potential, the corresponding thermal level would be at about 0.8 eV below vacuum, the position

assigned to the conduction band rather than to the impurity level.

It would thus appear that a correlation between thermal and optical energy level schemes using this conversion factor yields unrealistic results. There is, of course, no a priori reason to suppose that the optical level found in the present work should be associated with the thermal level and it is for this reason that a conversion factor cannot be deduced from the ratio 2.2/2.6, say. It should also be pointed out that the 2.6 eV photoelectric structure remains practically unchanged in position over a considerable range of thermionic activation energies. For example, in the various activation states of CaO PC 5, the Richardson work function takes values between 2.0 and 1.0 eV, while the position, although not the detailed form, of the 2.6 eV structure remains sensibly constant.

It is also worth pointing out that in a period when the study of the oxide cathode was of a less critical nature the rather approximate agreement of arbitrary photoelectric work functions with values of $\chi + \Delta E$ deduced from thermionic emission and conductivity measurements would be greeted with some satisfaction. But it must be emphasised that although the Mott and Gurney

approximation obviously does not give a satisfactory scaling factor to account for the Franck-Condon effect, there is no evidence at all which would suggest that the effect should be entirely neglected, or that work functions deduced in the arbitrary methods described can have any significance on semiconductor theory.

The conclusion arrived at is one which has also been found in a study of photoelectric effects in barium oxide cathodes (Sec. 4.6): in the present state of knowledge, no correlation between thermal and optical energy levels can be made. Although this statement may appear to be somewhat disappointing, it would have been optimistic to hope that the present work could produce a complete solution of optical and thermal activation energies for calcium oxide, about which very little is known, when the energies of a large number of workers have for a number of years failed to uncover the solution for barium oxide, about which rather more is known. The present work has succeeded in showing that the process of photoconductivity through the cathode matrix induced by photons whose energies lie in the visible region is really one of photoemission within the pores, and the photoelectric activation energy lying within this range has been obtained. The secondary aim of the work, to confirm the previously published thermal

activation energies for calcium oxide, has also been satisfactorily completed.

10.4. Suggestions for further work

Before discussing a number of interesting secondary effects worthy of further investigation the continuation of the main work will be considered. It is obvious that a great deal of useful information could be obtained if the determinations could be extended to higher photon energies so as to detect the onset of intrinsic photo-electric emission and photoconductivity. Barium oxide shows intrinsic photoemission at about 5.0 eV (2500 Å); calcium oxide might be expected to show it at even higher photon energies, from the calculations of Wright (193). Thus a quartz optical system and ultra-violet light source will be required in place of the glass monochromator and tungsten filament lamp. In the intrinsic region, the photosensitivity will be high and although the intensity of illumination may be small the photocurrents should be measurable with the present electrical instruments.

Further fundamental information on the energy level scheme could be obtained from a determination of the energy distribution of photoelectrons over a range of values of incident photon energy. Unfortunately the two

methods attempted in the present work (Sec. 7.2.6) proved unsuccessful, but this was entirely due to difficulties in the measurement of small photocurrents. Although it is probably less accurate than the magnetic method, the retarding-potential technique involves the measurement of rather larger currents and may possibly prove more fruitful. The currents to be measured are of the order of 10^{-12} A, but it will be possible to screen the tube, a precaution which cannot be taken in the magnetic method.

The fact that true photoconductivity has not been observed in calcium oxide cathodes in the case of illumination by visible radiation makes it tempting to seek a system under which it might be observed. There is little reason to suppose that an increase in photon energy to regions of intrinsic absorption should cause a change in the character of the photoconductive process in the cathode matrix, unlike the changes in the dark conductivity mechanism observed in the high- and low-temperature ranges. Work which would undoubtedly be of considerable interest both in electrical and photoelectric studies of the oxide would be the investigation of the properties of single crystals of calcium oxide. Techniques for the preparation of single crystals of barium oxide have been described (173), but the procedure is one of considerable practical

difficulty, and the preparation of calcium oxide crystals of reasonable dimensions (say 5 x 1 x 1 mm) would be a major undertaking. Once such crystals could be made available, a considerable amount of information on the dark and illuminated conductivities and on optical absorption under conditions of controlled impurity content could be obtained.

The preliminary results on photoeffects in evaporated films of calcium oxide (Chap. 9) suggest that a programme of investigations under more controlled conditions of the electrical and photoelectric properties of these films, and of films of barium oxide, might be of considerable value. The recent interest in the practical aspects of the direct conversion of heat to electricity by thermionic emission (76, 126, 190) has led to the development of a number of new types of diode. In its simplest form, such a diode consists of a hot thermionic emitter as cathode, with a cold collector or anode, insulated from each other and mounted in a vacuum envelope. Provided that the c.p.d. between the collector and cathode is of the correct polarity, electrons will flow from the cathode to the collector without the necessity of applying any external potential difference to the electrodes; the heat supplied to the cathode has been converted to electricity. Nearly

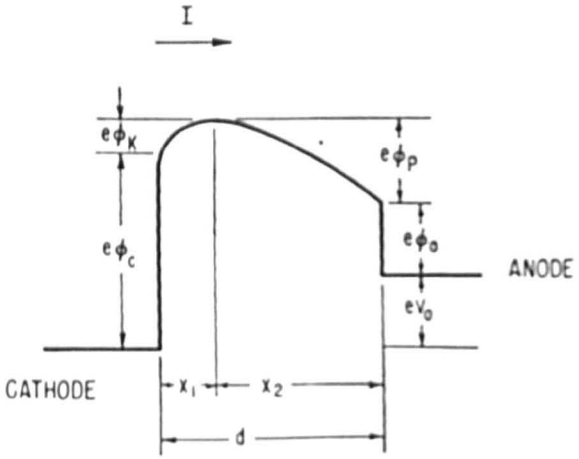

$$V_0 = (\phi_c - \phi_a) + (\phi_K - \phi_p)$$

. Electron energy diagram for a vacuum thermionic energy converter. ϕ_c and ϕ_a are the work functions of the cathode and anode. ϕ_i and ϕ_p are the potential differences that appear in the vacuum as a result of the presence of space charge. V_0 is the voltage that appears across the external load. d is the separation of cathode and anode. X_1 and X_2 are the distances from the peak of the potential barrier to the cathode and anode. e is the electronic charge. I is the electron current density flowing to the anode.

Fig. 10.3

all the tubes constructed in the present work show a measurable thermionic current to the anode at zero applied potential (e.g. Fig. 6.1.1) and are thus operating as direct converters (albeit of low efficiency) of the heat supplied to the cathode to electricity. Fig. 10.3 (187) shows the potential diagram for such a diode: electron energies have been measured upwards in this diagram. If sufficient thermal energy is imparted to the electrons in the cathode, they can surmount the potential barrier $e\phi_c$ caused by the work function ϕ_c of the cathode. The peak in the relation between energy and distance between the cathode and anode is due to the influence of space-charge. Once the space-charge barrier has been overcome the electrons fall down the anode work function barrier, $e\phi_a$. There will normally be a difference in energy of eV_0 between the final and initial energy states of the electron: if the polarity of V_0 is as shown in the diagram, this energy is available to do external work. It is obvious that the value of eV_0, apart from space-charge modifications, will depend on the difference between cathode and anode work functions, $\phi_c - \phi_a$. One method which has been applied using conventional oxide cathode materials is to coat both cathode and anode with the mixed oxide (BaSr)O (186). Since the oxide has a positive temperature

coefficient of work function (cf. Sec. 6.3.5 for results on calcium oxide) the hot cathode has a higher work function than the cooler anode, and the requirement that $\phi_c > \phi_a$ is automatically satisfied. The evaporation of active material from the cathode on to the anode during operation actually tends to depress the anode work function still further. However, although a low anode work function is essential for the operation of the converter, it also introduces secondary effects which may tend to reduce the efficiency of the process. Thus, unless the cathode work function is also extremely low, the cathode must be operated at reasonably high temperatures, at least at red heat, and a certain amount of illumination of the anode by the hot cathode cannot be avoided in most experimental arrangements. Photoemission from the low work function anode takes place, and the photoelectrons will make a contribution to the space-charge effect and tend to cause an increase in the height of the space-charge barrier. A study of the photoelectric properties of the alkaline earth oxides in the form of evaporated films on various anode materials may thus assist in the development of an important class of energy transducers, and it is hoped to continue this work.

Further interesting preliminary results are those on

the thermoelectric power of calcium oxide. The low-temperature region might be expected to be of particular interest in this work. Hensley (78) has proved theoretically that the gradient of the thermoelectric power versus reciprocal temperature curve at low temperatures (below the break in the conductivity plot) should be equal to the activation energy for the low-temperature conductivity process; however, results obtained by Young (199) with barium oxide and the mixed oxide (BaSr)O do not support this hypothesis and suggest the possibility of an alternative conduction mechanism. An investigation of this temperature range with a third oxide might be of some value. The difficulties encountered in the present work were due, first of all, to the difficulty of detecting the very small out-of-balance potentiometer currents and, secondly, to the problem of allowing for thermal expansion of the diode structure without modifying the state of the cathode matrix. A method employed by Lovett (112) might well prove more suitable than the sandwich diode used in the present work in reducing the mechanical forces on the cathode material. Miss Lovett used a normal cylindrical sprayed cathode, with a probe which consisted of a thermo-junction, so that the hot junction of a thermocouple was, in effect, embedded in the cathode. The temperature of

the base was measured by a second thermocouple. A temperature gradient was set up between the base and a subsidiary heater tape embedded in the coating. Measurements were made of the difference in temperature between the probe and cathode base and of the thermoelectric e.m.f. produced as a consequence of this temperature gradient.

FIG. A1.1.1. GRAPH OF Log σ VERSUS 1/T – BeO PC 1

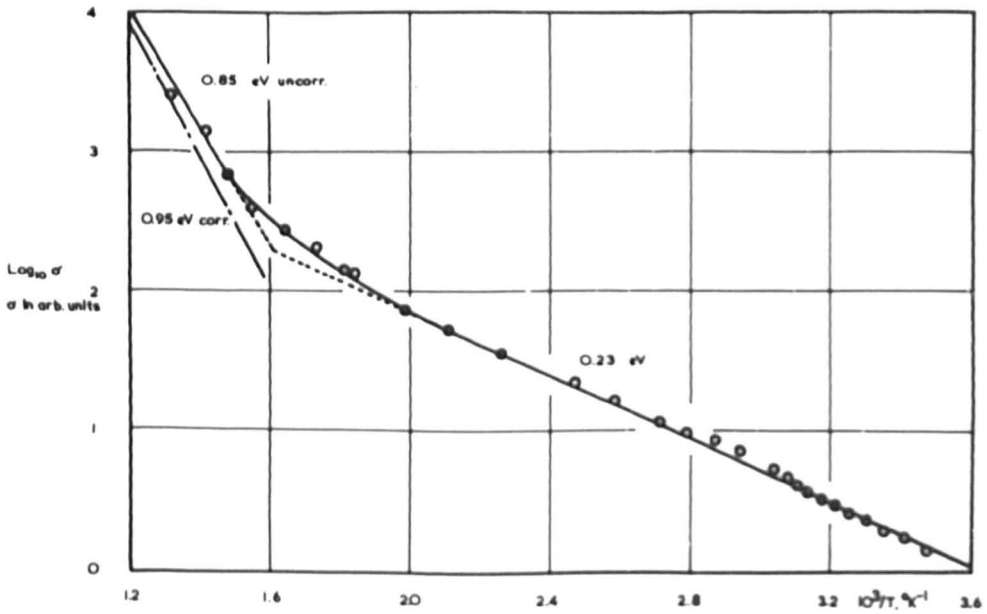

FIG. A1.1.2. EFFECT OF ULTRA-VIOLET ILLUMINATION ON THE TEMPERATURE VARIATION OF DARK CONDUCTIVITY – BeO PC 1

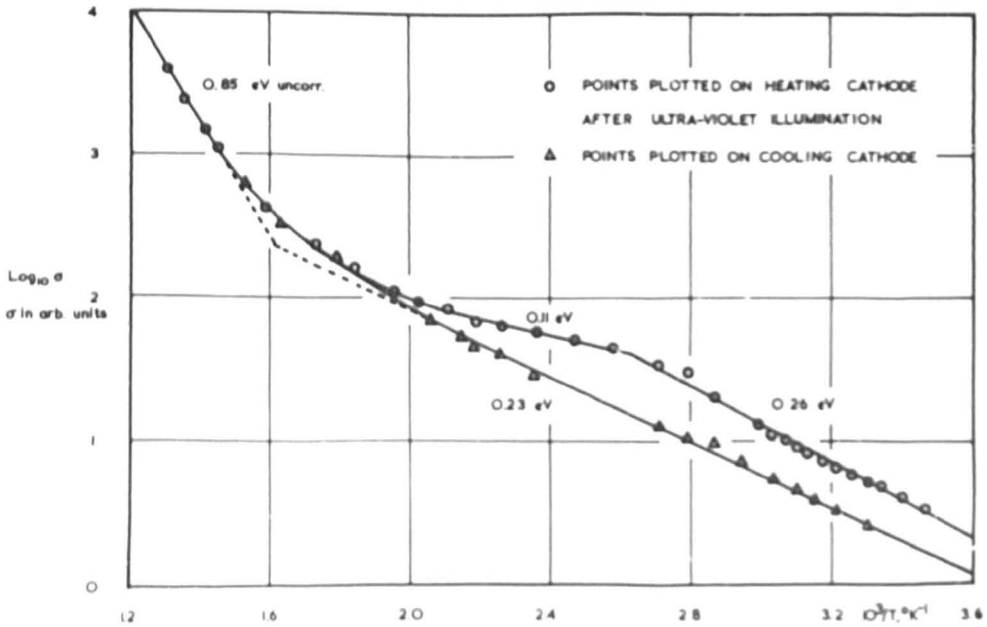

Appendix 1 The effect of ultra-violet illumination on the dark conductivity of barium oxide cathodes

A1.1. Introduction

In a previous thesis (116) it was observed that curves of log σ versus 1/T for barium oxide cathodes obtained after ultra-violet irradiation of the cathode differed very considerably from those obtained before irradiation, showing two linear portions in the former low-temperature region, one of steeper gradient between about 290 and 400 ^{o}K and one of more shallow gradient between 400 ^{o}K and the normal break temperature of about 600 ^{o}K. Further investigations of this effect have been carried out, but because they deal with barium oxide rather than with calcium oxide cathodes, they are discussed in this appendix to the main body of the work.

A1.2. Apparent modification of low-temperature conductivity by ultra-violet illumination

Tubes used during this section of the work were normal probe diodes coated with barium carbonate suspension. Fig. A1.1.1 shows the normal dark conductivity plot of log σ versus 1/T for BaO PC 1, with the characteristic form of two linear portions. The conductivity of activated barium oxide cathodes is so much greater than that of

calcium oxide cathodes that the determinations can be taken right down to room temperature ($10^3/T = 3.45\ ^{\circ}K^{-1}$) without any difficulty in measuring the current. In the case illustrated conductivities were determined by applying ± 20 mV between probe and cathode base, and currents were large enough to measure with the galvanometer alone. The activation energy $\Delta E/2$ of the low-temperature portion is 0.23 eV: the uncorrected gradient of the high-temperature region is apparently about 0.58 eV, but this is by no means certain as readings were not extended to sufficiently high temperatures. The actual magnitude of the high-temperature gradient is, in any case, immaterial in this particular investigation.

The cathode was irradiated with the total output of a high-pressure mercury arc, containing a high proportion of ultra-violet light, for 1 hour, and the conductivity was redetermined, starting at room temperature and heating the cathode. The log σ versus $1/T$ curve is given in Fig. A1.1.2: the upper line represents the points obtained on heating the cathode. The initial room temperature conductivity is nearly twice what it was before irradiation, and as the temperature is increased the gradient of the conductivity plot is found to be somewhat greater, 0.26 eV as compared with 0.23 eV. At a temperature of about

400 °K the plot shows what is apparently another linear region, of gradient corresponding to an activation energy of 0.11 eV, and at about 600 °K the conductivity is now very much the same value as before irradiation. Above 600 °K the temperature variation is almost exactly what it was before irradiation. On cooling the cathode, conductivity measurements are continued, giving the lower line, which is in exact agreement with the plot obtained before irradiation. The curves confirm the form of those discussed in the earlier investigation.

Subsequent determinations show that although the same general form of curve is obtained the gradients of the new low-temperature regions are not reproducible, depending on a number of factors such as the length of ultra-violet irradiation, the period between the end of irradiation and the beginning of conductivity measurements, and the rate of heating of the cathode.

The variation of the dark conductivity at room temperature with time after the end of ultra-violet illumination has been investigated by maintaining a constant positive potential of 20 mV between the probe and cathode base and measuring the conductivity current as a function of time over a period of 28 days. The results for BaO PC 1 after ultra-violet illumination for 90 minutes are displayed

FIG. AI.2. TIME VARIATION OF ROOM TEMPERATURE DARK CONDUCTIVITY AFTER ULTRA-VIOLET ILLUMINATION — BaO PC I

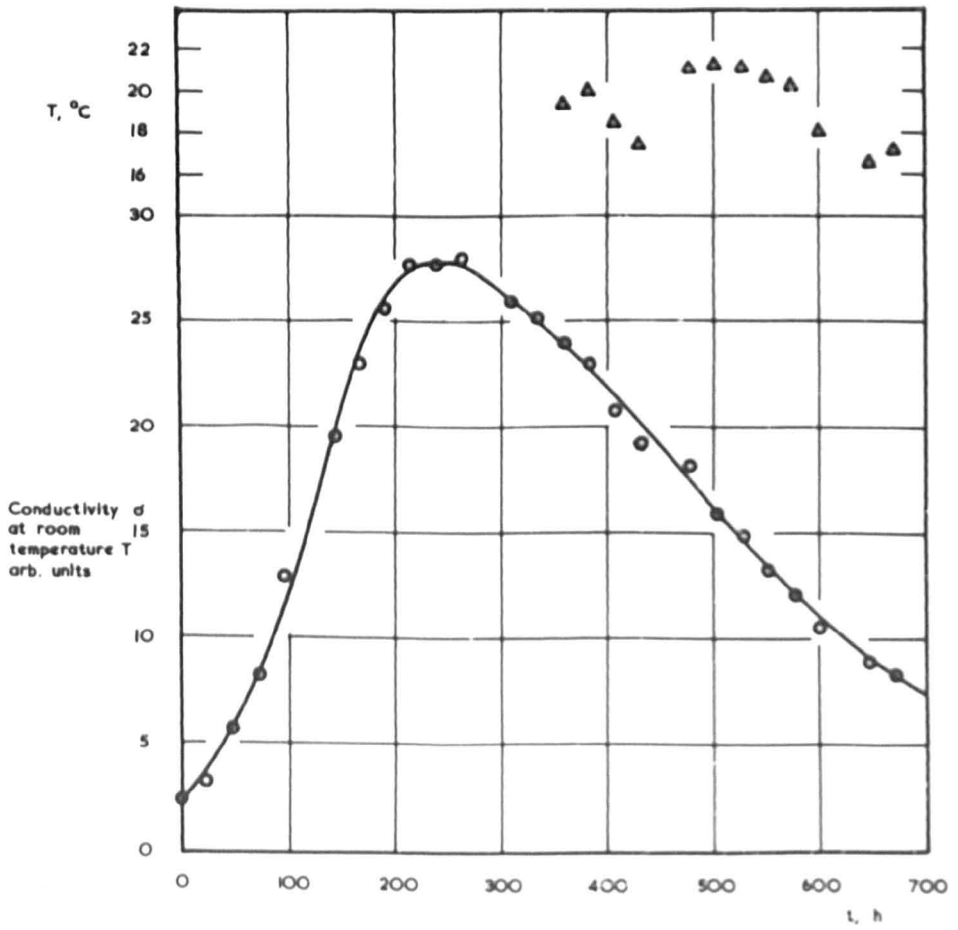

in Fig. A1.2. The conductivity σ is seen to increase by a factor of about 13 over a period of 10 days. That the effect is not merely due to the activating effect of passing current through the coating is shown by the fact that the current passes through a maximum and falls, in the course of a further 18 days, to a value about 4 times greater than the initial value. The upper points show the variation of room temperature T during the later stages of the determination. Although T varies through about 3 ^{o}C and fluctuations in T are reflected in the conductivity curve, the variations in T are quite insufficient to account for the total change in conductivity.

It has been suggested that the enhancing effect of the ultra-violet irradiation on dark conductivity, unreported in the oxide cathode literature, is very similar to thermoluminescent effects in phosphors (116; 30). Excitation of the semiconducting cathode material by photons whose energies lie in the ultra-violet region may cause the excitation of electrons from the filled band and a number of these electrons may be trapped at vacant levels in the forbidden zone. Warming the cathode in the dark in the course of conductivity determinations causes the thermal release of these trapped electrons, which pass through the conduction band causing an enhanced conductivity

FIG. AL3. HYPOTHESIS OF THERMAL RELEASE OF TRAPPED ELECTRONS

FIG. AL 3.1. GRAPH OF Log σ VERSUS 1/T AFTER ULTRA-VIOLET ILLUMINATION

BaO PC 1

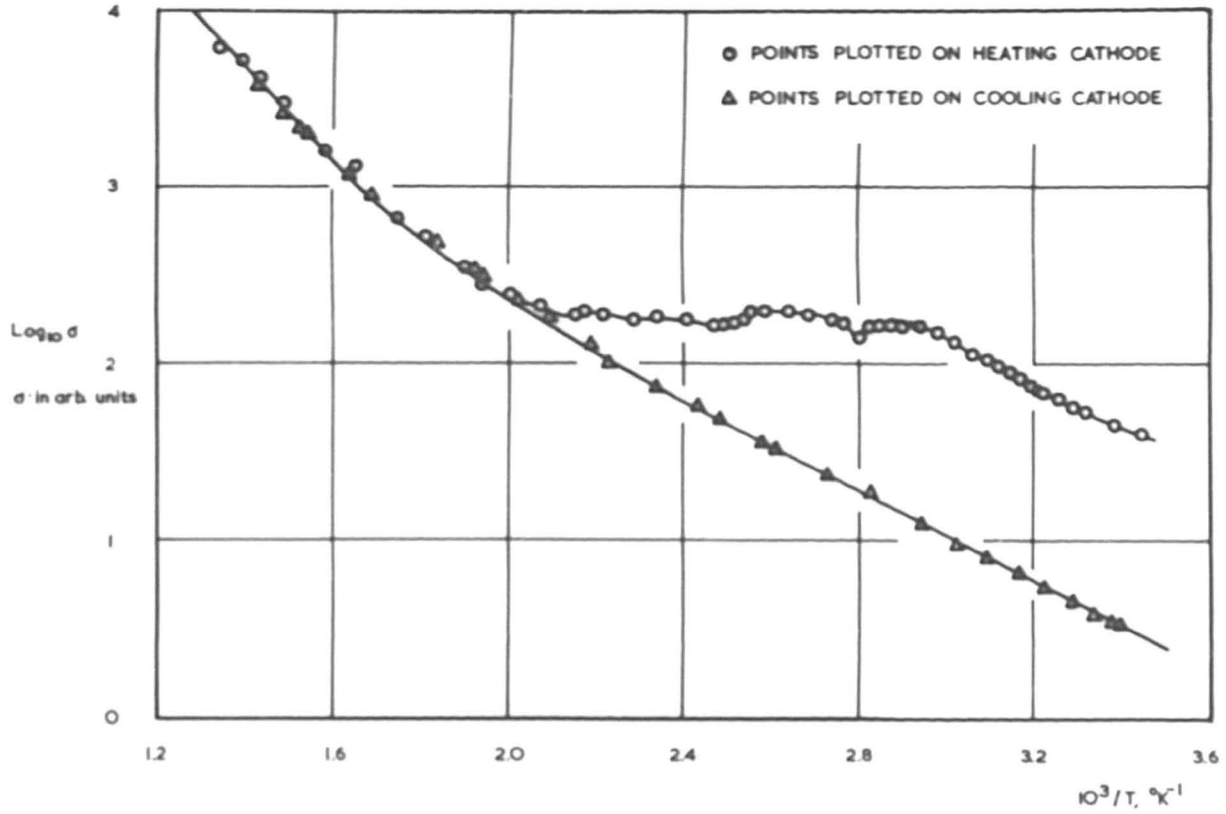

FIG.AI.3. HYPOTHESIS OF THERMAL RELEASE OF TRAPPED ELECTRONS

FIG. AI. 3.2. RATE OF HEATING

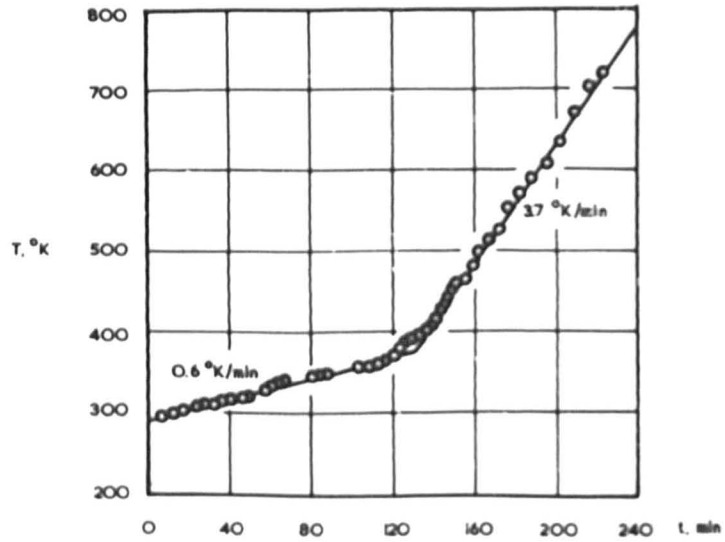

FIG. AL3.3. RELEASE OF TRAPPED ELECTRONS

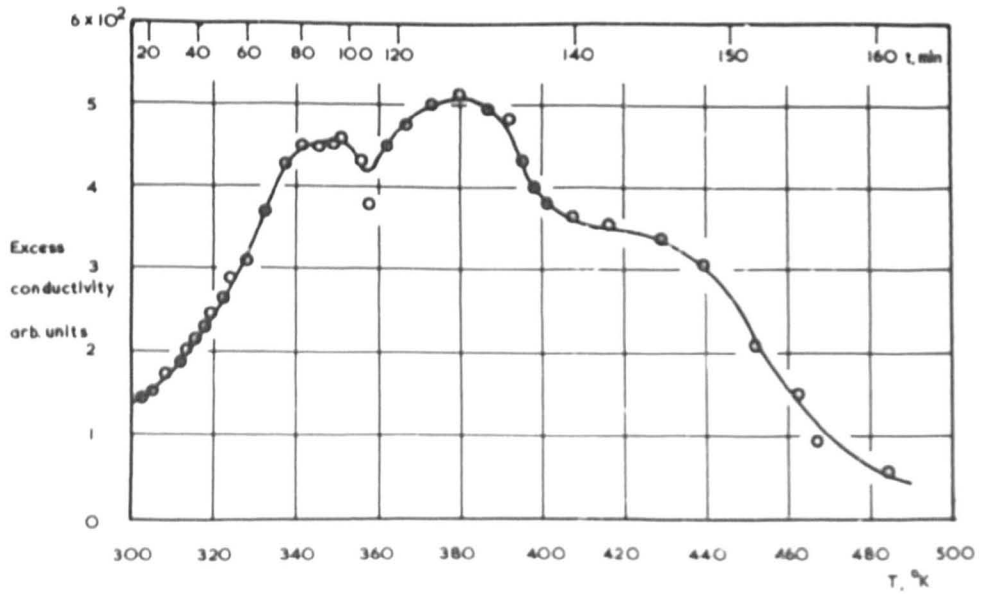

current. This explanation may account for the form of the log σ versus 1/T plots after ultra-violet illumination. The room temperature variation of conductivity after ultra-violet illumination can be explained by supposing the trapped electrons to be released slowly by thermal transitions at room temperature.

Fig. A1.3.1 shows a determination of log σ versus 1/T for BaO PC 1 140 hours after a further 90 minutes' illumination with light from the mercury arc. Many more points were taken during the warming of the cathode in an attempt to determine the form of the curve more accurately, and an attempt was made to keep the rate of heating constant. This was not, however, possible, and two different rates of heating, about 0.6 ^{o}K/min between 290 and 360 ^{o}K and 3.7 ^{o}K/min between 400 and 750 ^{o}K were obtained from the graph of temperature versus time (Fig. A1.3.2). The conductivity results obtained on warming the cathode from room temperature (upper curve) are compared with those obtained on cooling (lower curve). On the hypothesis of the thermal release of trapped electrons, assuming that all the trapped electrons are released by warming to 750 ^{o}K, the conductivity due to the thermal release at any particular temperature can be deduced by subtracting the lower curve from the upper. This has been

done in Fig. A1.3.3, and although very little reliance can be placed on the exact form of the curve it does serve to show that most of the trapped electrons have been released by the time the cathode has reached a temperature of about 500 ^{o}K. The type of curve is very similar to those obtained for thermoluminescent glow curves for phosphors (e.g. 108, 71) and it has been suggested (30) that a study of the form of the relation between conductivity and temperature can give information as to the location of trapping levels, although the theory has only been worked out for steady-state conditions and is, even in this case, extremely complicated.

An interesting parallelism between exo-electron emission and thermoluminescence has been pointed out by Grunberg (73) in a review article. Some of the trapped electrons, which on thermal release serve to enhance the conductivity current, might also be expected to be emitted from the surface of the specimen. This exo-electron emission has been detected in simultaneous determinations with the thermoluminescent effect (108) and the temperature variations of thermoluminescence and exo-electron emission can be correlated. Exo-electron emission, however, generally yields small currents which are measurable only with the assistance of an electron multiplier (105). The

possibility of such emission taking place with irradiated barium oxide cathodes may well be worthy of investigation.

A1.3. Possibility of enhanced dark conductivity in calcium oxide

A similar effect has not yet been observed in calcium oxide cathodes after irradiation with the ultra-violet. Before dark conductivity becomes measurable with the present electrometer, even an activated calcium oxide cathode must be heated to about 500 ^{o}K. At this temperature it is probable that most of any electrons trapped would already have been released, but a definite statement on this suggestion depends, of course, on the distribution of trapping levels.

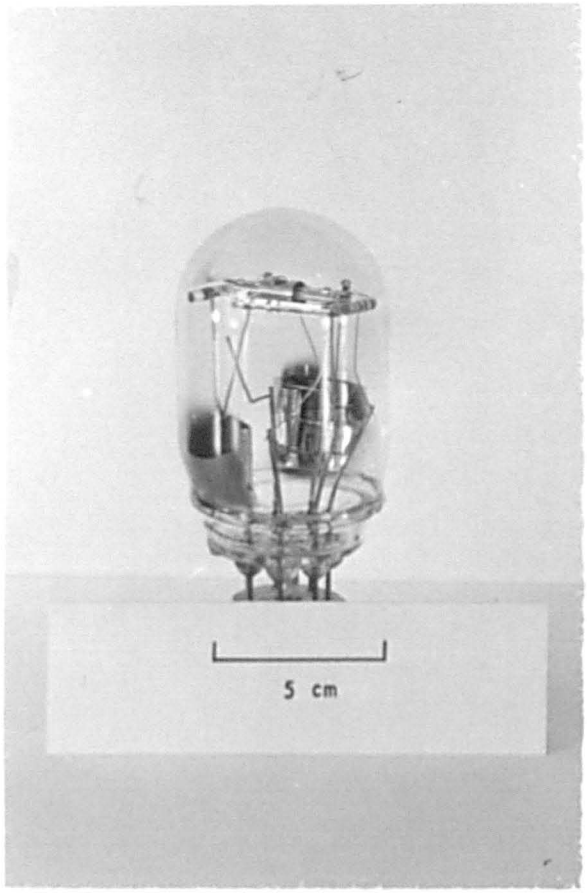
5 cm

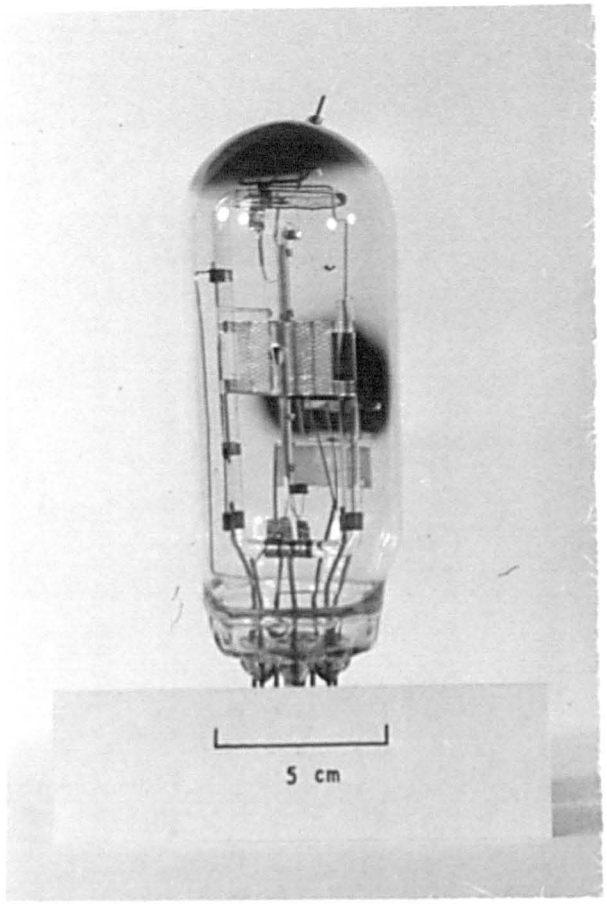
5 cm

Fig. A2.1 (opposite) Typical tube of the CaO PC series (CaO PC 7)

The diode assembly, mounted in its glass frame, is placed vertically in the tube. The ceramic probe support tubes can be seen attached to the right-hand side of the nickel cathode base. A poisoning filament covered with a paste of barium peroxide is visible just in front of the anode window. In CaO PC 7,8 and 9 the tungsten thermocouple lead leaves the envelope via a tungsten seal at the top of the tube.

Fig. A2.2 (opposite) Typical tube of the CaO M series (CaO M 4)

The diode assembly is mounted perpendicular to the axis of the envelope. A later tube in this series (CaO M 6) has a modified anode assembly to reduce illumination of the probe supports (Sec. 8.3).

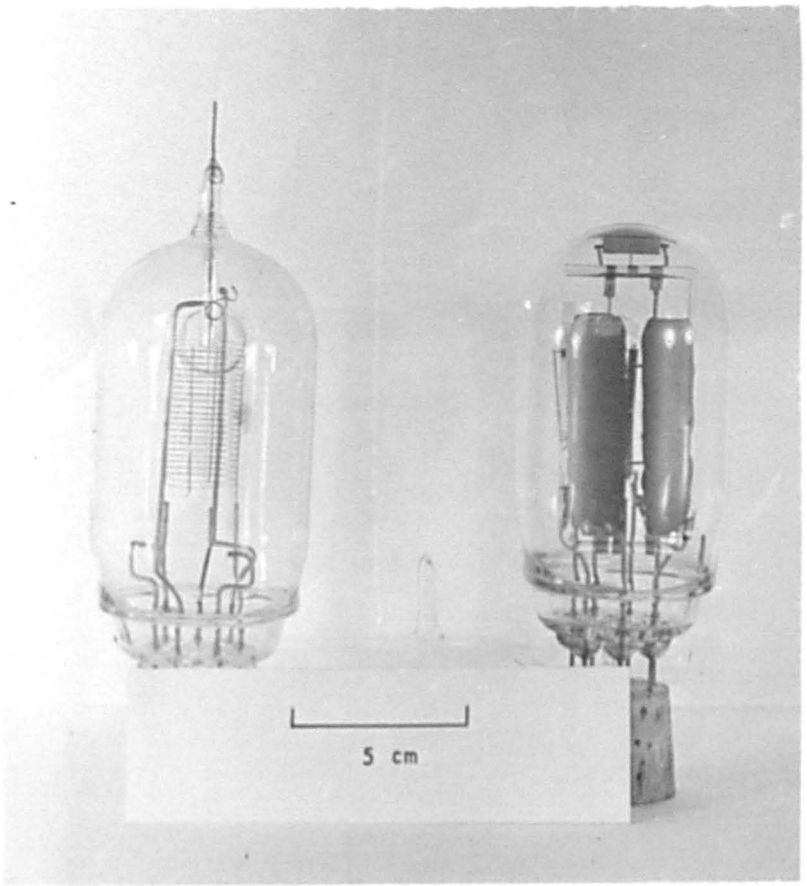
5 cm

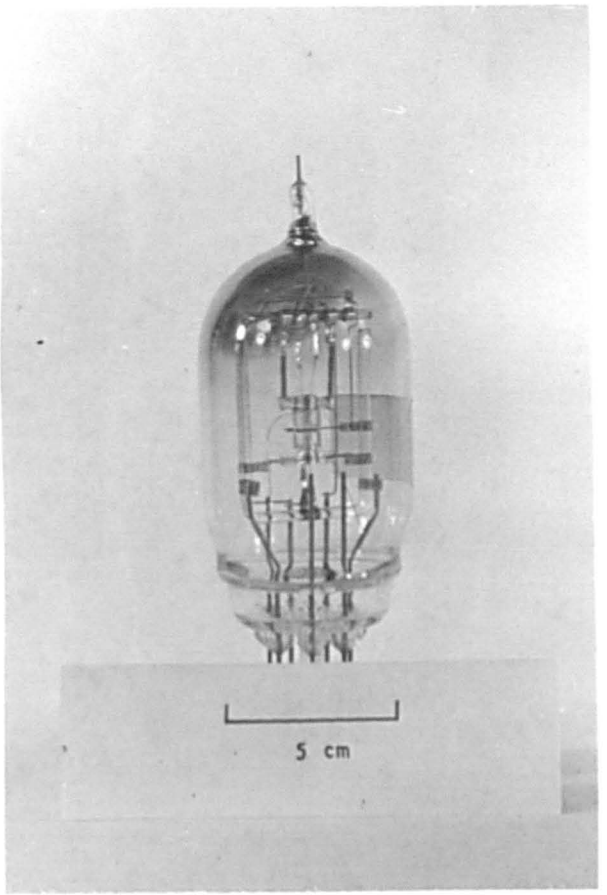
5 cm

Fig. A2.3 (opposite) Typical tube of the CaO TC series (CaO TC 5)

The calcium oxide sample is situated between the two nickel button cathodes at the centre of the tube. Each cathode is provided with an independent heater and thermocouple, and the upper cathode can slide in vertical guides, being spring-loaded in contact with the lower cathode.

Fig. A2.4 (opposite) Evaporated film tube with pressure gauge (CaO F 6)

The evaporated film tube (right) and Bayard-Alpert pressure gauge are connected by side-arms to a common pumping manifold, just visible in the background of the photograph. In the experimental tube the nickel shutter is open and the calcium oxide coated cathode is partly visible through the gap between the Aquadag electrodes on the envelope. In the pressure gauge, the collector is a fine tungsten wire connected to a tungsten seal at the top of the envelope and mounted along the axis of the cylindrical molybdenum grid. The tungsten filament which acts as a cathode is just visible in front of the grid.

Appendix 2 Experimental tubes

The various types of experimental tube constructed for use in the present programme of research are listed in this Appendix. The nomenclature adopted has been referred to in Sec. 6.3.

Series (1)	Type (2)	Reference (3)	Remarks (4)
CaO PC 1 - 11	Probe diode	Sec. 5.3.1	Cathode base along axis of envelope. 7,8,9 include oxygen filament
CaO M 1 - 6	Probe diode	Sec. 8.2.2	Short cathode, perpendicular to axis of envelope
CaO M 7	Magneto-resistive tube	Sec. 8.2.2	Ceramic based conductivity tube
CaO TC 1 - 5	Sandwich diode	Sec. 6.4	For measurements of thermoelectric power and electrical conductivity
CaO D 1	Double diode	Sec. 6.3.3	For comparison of calcium carbonate suspensions
CaO X 1	Thermionic diode		Similar to PC series, but without probe
CaO X 2	Magnetic velocity analyser	Sec. 7.3.4	

(1)	(2)	(3)	(4)
CaO R 1 - 2	Retarding potential tube	Sec. 7.3.4	
CaO F 1 - 6	Evaporated film tube	Sec. 9.3.1	For measurements of electrical conductivity and photoconductivity. 6 includes pressure gauge
CaO F 7 - 8	Evaporated film tube	Sec. 9.3.6	For measurements of optical absorption
BaO PC 1	Probe diode	App. 1	
BaO M 1	Probe diode	Sec. 8.4	
W-Ni T 1 - 12	Thermocouple comparison tube	Sec. 5.4	

The B.D.H. calcium carbonate suspension was used for all calcium oxide coated cathodes except CaO PC 1 - 4, for which the G.E.C. suspension was used (Sec. 6.3.3).

Appendix 3 Experimental errors

A3.1. Introduction

It is all too common in the oxide cathode literature to find results for work functions and activation energies quoted without any mention of the probable error in the determination. In a subject where many investigations take the form of the determination and comparison of activation energies from a number of cathodes in similar activation states, such a neglect is reprehensible. In this Appendix the probable errors in the more important thermionic, electrical and photoelectric experiments carried out in the present work are discussed.

A3.2. Thermionic emission and electrical conductivity experiments

Every determination of a Richardson line or of a conductivity plot has been accompanied by the calculation of a least-squares line, and the error in the gradient of this line is computed from the deviations of the experimental points from the line. Factors which may combine to cause the scatter of the points about the line include the instability of currents in the experimental tube and the instability of the current-measuring instrument. The former factor is minimised as far as possible by studying

thermionic emission in the region of low anode voltages to reduce poisoning effects due to the bombardment of the anode. The latter factor can be reduced by running the electrometer continuously; the instability and zero drift of the instrument is always greatest during the period immediately after switching on.

There exists the possibility of what may appear to be an important systematic error in the measurement of cathode temperature. The comparison of a number of tungsten-nickel thermocouples with chromel-alumel couples has been referred to in Sec. 5.4. It was found in this comparison that the tungsten-nickel calibration curve is not strictly reproducible from couple to couple, the calibration curve of Fig. 5.6 representing the mean of twelve determinations. Obviously, if there is doubt in the value of the cathode temperature T as determined by the thermocouple, the Richardson and conductivity plots will also be in error. Table A3.1 (p. 242) shows the mean deviations of the temperatures obtained from the twelve comparison thermocouples at a number of temperatures, and shows how these deviations are likely to affect the values of $\log_{10} i_o/T^2$ and $10^3/T$ employed in the Richardson plots.

Although the mean deviation rises considerably with increasing indicated temperature, the corresponding

Table A3.1

Deviations in Richardson plot quantities arising from deviations in cathode temperature measurements

Thermo-e.m.f., mV	Mean temp., T °K	Mean deviation ΔT °K	$\log_{10} 1/T^2$	$10^3/T$, $°K^{-1}$
0.5	300	1	$\bar{5}.046 \pm .003$	$3.33 \pm .01$
3.1	400	4	$\bar{5}.796 \pm .009$	$2.50 \pm .02$
6.3	500	7	$\bar{6}.602 \pm .012$	$2.00 \pm .03$
9.5	600	8	$\bar{6}.444 \pm .012$	$1.67 \pm .02$
12.8	700	10	$\bar{6}.310 \pm .013$	$1.43 \pm .02$
16.7	800	13	$\bar{6}.194 \pm .014$	$1.25 \pm .02$
21.1	900	15	$\bar{6}.092 \pm .015$	$1.11 \pm .02$
26.1	1000	18	$\bar{6}.000 \pm .015$	$1.00 \pm .02$

deviations in log $1/T^2$ and $10^3/T$ are nearly constant over the whole of the range of interest (the limits of most determinations in the present work are 500 and 1000 °K). In fact, the error in $10^3/T$ will be considerably more important than the error in log $1/T^2$, as the temperature variation of the logarithm of the emission current is very much greater than that of log $1/T^2$. For a thermocouple which reads consistently high or low, the constancy of the error in $10^3/T$ means that the Richardson or conductivity plot merely suffers a translation in the direction of the

$10^3/T$ axis, and the gradients of the plots will only be affected to a very small extent.

A further systematic error may become apparent at high temperatures. Due to the fall of temperature across the cathode coating, the thermocouple does not indicate the true temperature of the oxide but a higher temperature. Fig. 6.3.4 shows that at 900 ^oK in a typical cathode the thermoelectric e.m.f. between probe and cathode base is about 10 mV: for a thermoelectric power of 2.5 mV $^oK^{-1}$ (Sec. 6.4) this represents a temperature drop of about 4 ^oK. At higher temperatures, the e.m.f. becomes greater, often rising to as much as 20 mV at 1000 ^oK. At higher temperatures the thermoelectric power is less, and this e.m.f. would represent a temperature drop of about 10 ^oK. The probable error due to this fall of temperature is thus practically negligible at temperatures up to about 850 ^oK, but the fairly rapid increase in the temperature drop above 900 ^oK means that the error in $10^3/T$ is not constant over the range of $10^3/T$, and may cause a slight curvature in Richardson lines and conductivity plots at temperatures above 850 ^oK. As the actual temperature is always less than the indicated temperature (the temperature used in calculations) the calculated values of $10^3/T$ are less than they should be and the curve will show a slight upwards

concavity at high temperatures. Such a curvature is often observed both in Richardson and in conductivity plots, and has been ascribed to the space-charge effect in the cathode pores (Sec. 2.4)(48); but it would appear that the fall of temperature across the cathode coating and the corresponding error in temperature measurement may at least be a contributory factor.

It should be noted that the curvature due to this error is in the opposite sense to that discussed in the calculation of the second-order Richardson plot (Sec. 6.3.5). This second-order curvature, ascribed to a temperature-dependent change in the cathode work function, cannot be dismissed as being due to errors in the measurement of temperature.

A3.3. Photoelectric experiments

Of particular interest in this discussion is the probable error in the determination of individual points in spectral sensitivity curves.

Due to the dispersion of the optical system (Sec. 5.6) a band of photon energies about 0.04 eV wide at the red end of the spectrum and about 0.06 eV wide at the violet end is transmitted at each indicated photon energy. This, of necessity, reduces the resolution of the method.

Further errors may arise in the measurement of photoelectric emission and photoconductivity currents. As in the case of thermionic emission, these may originate either in the experimental tube or in the electrometer. It appears that fluctuating photocurrents are of much less importance than instability in the electrometer, and in order to check the rate of zero drift and give an estimate of the probable error, several measurements of the photocurrent are taken at each photon energy. With small photocurrents ($\sim 10^{-12}$ A) the probable error in an individual photocurrent reading is less than 5 %; for larger photocurrents, the probable error is considerably less.

The process of calibrating the envelope of the experimental tube for absorption due to evaporated materials may introduce an error in the determination of the relative intensity of illumination versus wavelength curve, but as the 53 CV photocell is used photocurrents are much larger (ranging from about 10^{-11} to 10^{-8} A) and errors will be relatively small.

The important error in photoelectric determinations is thus in the actual measurement of the photocurrent. The estimated total probable error is about 5 % of the sensitivity per unit incident intensity at each wavelength for a weakly photosensitive cathode and is rather less for

the more photosensitive cathodes. The dispersion of the system leads to an average error of about 2 % of the photon energy at each experimental point. There is thus little doubt that the structure observed at about 2.6 eV in spectral sensitivity curves is a real feature of the photoelectric behaviour of calcium oxide coated cathodes.

List of Symbols

a	fraction of incident radiation absorbed
A	Richardson emission constant = $\frac{4\pi m^* k^2 e}{h^3}$ = 120 amp cm^{-2} deg^{-2}
A^*	Empirical Richardson emission constant
B	Fowler emission constant = $W^{1/2} e \frac{2\pi m^* k}{h^{3/2}}$
e	electronic charge
E	electric field intensity
E_g	separation of conduction band from filled band on thermal energy scheme
E_g'	separation of conduction band from filled band on optical energy scheme
E_o	energy of bottom of conduction band
ΔE	depth of impurity level below conduction band on thermal energy scheme
$\Delta E'$	depth of impurity level below conduction band on optical energy scheme
h	Planck's constant
H	magnetic field
i	thermionic emission current
i_a	thermionic emission current in accelerating field; anode current
i_o	zero-field thermionic emission current

i_{pc} photoconductivity current

i_{pc_o} photoconductivity current in zero magnetic field

i_{pc_H} photoconductivity current in magnetic field H

I_{pc} photoconductivity current per unit incident intensity

i_{ph} external photoelectric emission current

i_{ph_o} zero-field external photoelectric emission current

I_{ph} external photoelectric emission current per unit incident intensity

j thermionic emission current density

j_o zero-field thermionic emission current density

j_r thermionic emission current density in retarding field region

j_a thermionic emission current density in accelerating field region

j_{sp} thermionic emission current density in space-charge limited region

J intensity of illumination

k Boltzmann's constant

l_o electron mean free path

m^* effective mass of electron

n_b density of impurity levels

n_f density of electrons in conduction band

Q internal work function

r fraction of incident radiation reflected

t fraction of incident radiation transmitted

T absolute temperature

T_c colour temperature

u mean electron velocity

V voltage; potential

V_a anode potential

V_e vertical component of earth's magnetic field

V_{ic} potential drop through cathode coating and interface

$\Delta V/\Delta T$ thermoelectric power

w statistical weight of states in the conduction band

W_i Fermi level

ϵ optical dielectric constant

ϵ_0 static dielectric constant

λ wavelength of radiation

λ_{th} threshold wavelength (Moss's criterion)

μ chemical potential (commonly called Fermi level) of semiconductor

ρ mean reflection coefficient for electrons at emitting surface

σ	electrical conductivity
σ_c	true semiconduction component of conductivity of cathode coating
σ_p	pore conduction component of conductivity of cathode coating
σ_s	specific conductivity
σ_o	conductivity in zero magnetic field
σ_H	conductivity in magnetic field H
ν	frequency of radiation
ν_o	photoelectric threshold frequency for photo-emission from metals
ϕ	total thermionic work function
ϕ_a	anode work function
ϕ_c	cathode work function
ϕ_{c_1}	cathode work function by first order Richardson analysis
ϕ_{c_2}	cathode work function by second order Richardson analysis
ϕ_{ph}	photoelectric work function
ϕ'_{arb}	arbitrary photoelectric threshold
$\phi'_{arb_{pc}}$	arbitrary threshold for photoconductivity
ϕ'_F	Fowler photoelectric work function
χ	external work function or electron affinity
χ'	optical external work function

List of Figures

6.3.3 Corrected current - voltage characteristics for dark conductivity - CaO PC 6^2

6.3.4 Dark conductivity current - voltage characteristics showing thermoelectric e.m.f. - CaO PC 6^4

6.4 Relation between log A* and ϕ

6.5 Comparison of G.E.C. and B.D.H. carbonate suspensions

6.6. Temperature variation of c.p.d. for CaO diodes

6.7.1 Thermionic emission characteristics - CaO PC 5^4

6.7.2 Richardson plot for thermionic emission - CaO PC 5^4

6.7.3 Temperature variation of c.p.d. - CaO PC 5^4

6.7.4 First and second order Richardson plots - CaO PC 5^4

6.7.5 Temperature variation of the cathode work function - CaO PC 5^4

6.8 External work function - CaO PC 5^2

6.9.1 Thermoelectric e.m.f. versus temperature difference characteristics - CaO TC 2^1

6.9.2 Thermoelectric power and electrical conductivity - CaO TC 2^1

6.9.3 Electrical conductivity in sandwich diodes - CaO TC 4^1

7.1 Photoelectric emission from CaO: white light current - voltage characteristic - CaO PC 5^5

7.2.1 Intensity of illumination as a function of wavelength - CaO PC 6^3

7.2.2,3 Spectral sensitivity of photoelectric emission from CaO - CaO PC 6^3

7.3.1,2 Spectral sensitivity of photoelectric emission from CaO - CaO PC $^{2-5}$

7.4.1,2,3 Spectral sensitivity of photoelectric emission from CaO - CaO PC 8^2, 9^4, 10^1;,X 1

7.5 Photoelectric work function by complete photoemission - CaO PC 1^1

7.6 Temperature variation of photoemission - CaO PC 5^2

7.7 Schematic arrangement of magnetic velocity analysis tube

7.8 Energy distribution of thermionic electrons - CaO X 2

7.9 Schematic arrangement of retarding potential tube

7.10.1,2,3 Photoconductivity in CaO cathodes: current - voltage characteristics

7.11.1,2 Spectral sensitivity of positive and negative photoconductivity currents - CaO PC 9^4

7.12.1,2 Spectral sensitivity of photoconductivity in CaO - CaO PC 5^{2-5}

7.13.1,2 Photocurrent - illumination relationship for photoconductivity currents - CaO PC 5^{2}

7.14.1,2 Temperature variation of photoconductivity currents - CaO PC 5^{3}

7.15.1,2 Temperature variation of current due to apparent photovoltaic e.m.f - CaO PC 5^{3}, 5^{6}

7.16.1,2 CaO cathode coloration: optical absorption of blue and white cathodes - CaO PC 1

7.17 Relation between photoelectric emission and photoconductivity - CaO PC 5^{5}

8.1.1,2,3 Recovery of photoemission and photoconductivity after oxygen poisoning - CaO PC 7^{1}, 9^{2}, 9^{3}

8.2.1,2 Electromagnet: relation between magnet current and magnetic field - 6.5 cm and 21 cm gaps

8.3.1,2 Magnetoresistive effect in dark conductivity - CaO M 5^{2}

8.3.3,4 Magnetoresistive effect in dark conductivity after Forman (64) and Metson (122)

8.4.1,2 Temperature variation of the dark magnetoresistive effect - CaO PC 5^{7}, M 5^{3}

8.4.3 Temperature variation of the dark magnetoresistive effect in BaO (after Metson (122))

Bibliography

1. General References

1 Eisenstein, A. "Oxide coated cathodes", Advances in electronics, 1, 1, 1948

2 Friedenstein, M., Martin, S.L., and Munday, G.L. "The mechanism of the thermionic emission from oxide-coated cathodes", Rep. Progr. Phys., 11, 298, 1948

3 Garlick, G.F.J. "Photoconductivity", Encyclopedia of Physics (ed. S. Flügge), Vol. 19, Berlin, 1956

4 Herrmann, G. and Wagener, S. "The oxide coated cathode", 2 vols., London, 1951

5 Hughes, A.L. and DuBridge, L.A. "Photoelectric phenomena", New York, 1932

6 Moss, T.S. "Photoconductivity in the elements", London, 1952

7 Moss, T.S. "Optical properties of semi-conductors", London, 1959

8 Mott, N.F. and Gurney, R.W. "Electronic processes in ionic crystals", 2nd ed., Oxford, 1953

9 Nottingham, W.B. "Thermionic emission", Encyclopedia of Physics (ed. S. Flügge), Vol. 21, Berlin, 1956

10 Weissler, G.L. "Photoelectric emission from solids", Encyclopedia of Physics (ed. S. Flügge), Vol. 21, Berlin, 1956

11 Wright, D.A. Brit. J. appl. Phys., 9, 205, 1958

2. Detailed References

12 Aldrich, L.T. Phys. Rev., 81, 320, 1951

13 American Institute of Physics Handbook, New York, 1957, 6, 79

14 Alpert, D. J. appl. Phys., 24, 860, 1953

15 Apker, L., Taft, E. and Dickey, J. Phys. Rev., 74, 1462, 1949

16 Apker, L., Taft, E. and Dickey, J. Phys. Rev., 84, 508, 1951

17 Arnold, H.D. and Ives, H.E. Phys. Rev., 19, 415, 1922

18 Barton, H.A. Phys. Rev., 26, 360, 1925

19 Bachman, C.H. and Carnahan, C.W. Proc. Inst. Radio Engrs, 26, 529, 1938

20 Becker, J.A. Phys. Rev., 34, 1323, 1929

21 Becker, J.A. and Sears, R.W. Phys. Rev., 38, 2193, 1931

22 Becker, J.A. Trans. Electrochem. Soc., 59, 207, 1931

23 Becker, J.A. Rev. mod. Phys., 7, 95, 1935

24 Berger, C.E. Phys. Rev., 34, 1566, 1929

25 Bever, R.S. and Sproull, R.L. Phys. Rev., 83, 801, 1951

26 Biguenet, C. Vide, 5, 831, 1950

27 Blewett, J.P. and Jones, E.I. Phys. Rev., 50, 464, 1936

28 Blewett, J.P. Phys. Rev., 55, 713, 1939

29 Blewett, J.P. J. appl. Phys., 10, 668, 1939

30 Broser, I. and Broser-Warminsky, R. Brit. J. appl. Phys., Suppl. 4, 90, 1954

31 Cardwell, A.B. Phys. Rev., 76, 125, 1949

32 Carroll, P.E. and Coomes, E.A. Phys. Rev., 85, 399, 1950

33 Carroll, P.E. Phys. Rev., 104, 660, 1956

34 Case, T.W. Phys. Rev., 17, 398, 1921

35 Champeix, R. Ann. Radioelect., 1, 208, 1946

36 Child, C.D. Phys. Rev., 32, 492, 1911

37 Coomes, E.A. J. appl. Phys., 17, 647, 1946

38 Crew, W.H. Phys. Rev., 28, 1265, 1926

39 Daglish, H.N. G.P.O. Research Station Thermionics Group Memo. RB2/58, 1959

40 Darbyshire, J.A. Proc. Phys. Soc. (London), 50, 964, 1938

41 Dash, W.C. Phys. Rev., 92, 68, 1953

42 Deb, S. Indian J. Phys., 25, 197, 1951

43 Debiesse, J. and Champeix, R. Vide, 4, 545, 1949

44 Dember, H. Phys. Z., 32, 554, 1931

45 Detels, F. Jb. d. drahtl. Telegr. u. Teleph. 30, 10, 52, 1927

46 DeVore, H.B. and Dewdney, J.W. Phys. Rev., 83, 805, 1951

47 DeVore, H.B. R.C.A. Rev., 13, 453, 1952

48 Dewsberry, R. M.Sc. Thesis, University of Birmingham, 1960

49 Dickey, J. and Taft, E. Phys. Rev., 80, 308, 1950

50 Dolloff, R.T. J. appl. Phys., 27, 1418, 1956

51 DuBridge, L.A. Phys. Rev., 31, 236, 1928; 32, 961, 1928

52 Dueker, J.E. and Hensley, E.B. Bull. Amer. Phys. Soc. II, 2, 271, 1957

53 Einstein, A. Ann. Phys. (Leipzig), 17, 132, 1905; 20, 199, 1906

54 Eisenstein, A. Phys. Rev., 71, 473, 1947

55 Eisenstein, A. Phys. Rev., 72, 531, 1947

56 Espe, W. Wiss. Veroff. Siemens-Werken, 5, 29, 1927; 5, 46, 1927

57 Ewles, J. Proc. Roy. Soc. A, 167, 34, 1938

58 Ewles, J. and Lee, N. J. Electrochem. Soc., 100, 399, 1953

59 Fan, H.Y. J. appl. Phys., 14, 552, 1943

60 Fan, H.Y. Phys. Rev., 92, 1424, 1953

61 Fan, H.Y. Rep. Progr. Phys., 19, 107, 1956

62 Feaster, G.R. J. appl. Phys., 20, 415, 1949

63 Fineman, A. and Eisenstein, A. J. appl. Phys., 17, 663, 1946

64 Forman, R. Phys. Rev., 96, 1479, 1954

65 Fowler, R.H. Phys. Rev., 38, 45, 1931

66 Fowler, R.H. "Statistical Mechanics", London 1936

67 Gehrts, A. Z. techn. Physik, 11, 246, 1930

68 Gibbs, R.C. and Meacham, A.
Phys. Rev., 19, 415, 1922

69 Gibson, A.F. Proc. Phys. Soc. (London) B, 64, 603, 1951

70 Glascock, H.H. and Hensley, E.B.
Bull. Amer. Phys. Soc. II, 2, 271, 1957

71 Gourge, H.F. and Hanle, W.
Acta Phys. Austriaca, 10, 427, 1957

72 Grattidge, W. and Shepherd, A.A.
Proc. Phys. Soc. (London) B, 67, 177, 1954

73 Grunberg, L. Brit. J. appl. Phys., 9, 85, 19[illegible]

74 Handbook of Chemistry and Physics, 39th ed., Cleveland, Ohio

75 Hannay, N.B., McNair, D. and White, A.H.
J. appl. Phys., 20, 669, 1949

76 Hatsopoulous, G.M. and Kaye, J.
J. appl. Phys., 29, 1124, 1958

77 Heinze, W. and Wagener, S.
Z. techn. Physik, 17, 645, 1936
20, 16, 1939

78 Hensley, E.B. J. appl. Phys., 23, 1122, 1952

79 Hensley, E.B. Report of the M.I.T. 15th Annual Conference on Physical Electronics, 1955, p. 18

80 Hensley, E.B. J. appl. Phys., 27, 286, 1956

81 Herring, C. and Nichols, M.H. Rev. mod. Phys., 21, 185, 1949

82 Herrmann, G. Z. phys. Chem., B, 35, 298, 1937

83 Higginson, G.S. Ph.D. Thesis, University of Birmingham, 1957

84 Higginson, G.S. Brit. J. appl. Phys., 8, 148, 1957

85 Higginson, G.S. Brit. J. appl. Phys., 9, 106, 1958

86 Højendahl, K. K. Danske. Vidensk. Selsk., mat-fys. Medd., 16, 2, 1938

87 Hopkins, B.J. Ph.D. Thesis, University of Birmingham, 1958

88 Hopkins, B.J. and Vick, F.A. Brit. J. appl. Phys., 9, 257, 1958

89 Hopkins, B.J. Brit. J. appl. Phys., 11, 124, 1960

90 Hopkins, B.J. Private communication

91 Horton, F. Phil. Mag., 11, 505, 1906

92 Huber, H. Thesis, University of Berlin, 1941

93 Huber, H. and Wagener, S. Z. techn. Physik, 23, 1, 1942

94 Hung, C.S. J. appl. Phys., 21, 37, 1950

95 Huxford, W.S. Phys. Rev., 38, 379, 1931

96 Isensee, H. Z. phys. Chem., B, 35, 309, 1937

97 Jamison, N.C. and Cashman, R.J. Phys. Rev., 50, 624, 1936

98 Jansen, C.G.J., Loosjes, R., van Zelst, J.J.Z. and Elings, G.A. Vide, 9, 135, 1954

99 Jentzsch, F. Ann. Phys. (Leipzig), 27, 129, 1908

100 Kane, E.O. J. appl. Phys., 22, 1214, 1951

101 Kawamura, H. J. Phys. Soc. Japan, 3, 301, 1948

102 Kestelyn-Loebenstein, A. Vide, 9, 148, 1954

103 Kobayishi, A. and Kawaji, S. J. Phys. Soc. Japan, 10, 270, 1955

104 Koster, G.F. and Slater, J.C. Phys. Rev., 96, 1208, 1954

105 Kramer, J. "Der metallische Zustand", Gottingen, 1950

106 Kramer, J. Z. Phys., 129, 34, 1951; 133, 629, 1952

107 Langmuir, I. Phys. Rev., 2, 450, 1913

108 Lepper, J. Z. Naturforsch., 10a, 47, 1955

109 Levinstein, H. Proceedings of the Atlantic City Conference on Photoconductivity, 1954, p. 601

110 Liben, I. Phys. Rev., 51, 642, 1937

111 Loosjes, R. and Vink, H.J. Philips Res. Rep., 4, 449, 1949

112 Lovett, C.M. Proc. Phys. Soc.(London) B, 67, 387, 1954

113 Lowry, E.F. Phys. Rev., 35, 1367, 1930

114 McNary, B.D. O.N.R. Technical Report No. 8, 1951; Phys. Rev., 81, 631, 1951

115 Mahlman, G.W. J. appl. Phys., 20, 197, 1949

116 Mee, C.H.B. M.Sc. Thesis, University of Birmingham, 1958

117 Melnick, D. Thesis, University of Pennsylvania, 1954

118 Merritt, E. Phys. Rev., 17, 525, 1921

119 Metson, G.H. Proc. Phys. Soc. (London) B, 62, 589, 1949

120 Metson, G.H. Vacuum, 1, 283, 1951

121 Metson, G.H. Proc. Instn. Elect. Engrs., 99, 69, 1952

122 Metson, G.H.; Metson, G.H. and Macartney, E. Instn. Elect. Engrs. Monographs 221 R, 243 R, 268 R, 269 R, 1957; 289 R, 317 R, 1958; 347 E, 1959; 357 E, 1960

123 Metson, G.H. Private communication

124 Moore, G.E., Wooten, L.A. and Morrison, J. J. appl. Phys., 26, 8, 1955

125 Morgulis, N. J. Phys., USSR, 11, 67, 1947

126 Morgulis, N. and Morchuk, P.M. Ukrain. Fiz. Zh., 2, 379, 1957

127 Morrison, S.R. Proceedings of the Philadelphia Conference on the Physics of Semiconductor Surfaces, 1956, p. 165

128 Mott, N.F. Proc. Roy. Soc. A, 171, 27, 1939

129 Mullard Technical Handbook, 4, 351-2

130 Muto, T. and Yamashita, J. J. Phys. Soc. Japan, 2, 187, 1947

131 Mutter, W.E. Phys. Rev., 72, 531, 1947

132 Nakai, J., Inuishi, Y. and Tsung-Che, Y.
J. Phys. Soc. Japan, 10, 437, 1955

133 Narita, S. J. Phys. Soc. Japan, 9, 22, 1954

134 Nergaard, L. R.C.A. Rev., 13, 664, 1952

135 Newbury, K. Phys. Rev., 34, 1418, 1929

136 Newbury, K. and Lemery, F.
J. Opt. Soc. Amer., 21, 276, 1931

137 Nisibori, E., Kawamura, H. and Hirano, K.
Proc. Phys.-Math. Soc. Japan, 23, 37, 1941

138 Noga, K. and Kawamura, S.
J. Phys. Soc. Japan, 7, 287, 1952

139 Noga, K. and Nakamura, K.
J. Phys. Soc. Japan, 9, 435, 1954

140 Okumura, K. Phys. Rev., 96, 1704, 1954

141 Ortusi, J. Vide, 9, 100, 1954

142 Paulisch, A. Z. angew. Physik, 9, 412, 1957

143 Penning, F.M. Physica, 4, 21, 1937

144 Philipp, H.R. Phys. Rev., 107, 687, 1957

145 Plumlee, R.H. J. appl. Phys., 27, 659, 1956

146 Pohl, R.W. Proc. Phys. Soc. (London), 49 (extra part), 3, 1937

147 Prescott, C.H. and Morrison, J. J. Amer. Chem. Soc., 60, 3047, 1938

148 Ramadanoff, D. Phys. Rev., 37, 884, 1931

149 Randall, J.T. and Wilkins, M.H.F. Proc. Roy. Soc. A, 184, 366, 1945

150 Richardson, O.W. "The emission of electrons from hot bodies", London, 1921

151 Rittner, E.S. Science, Lancaster, Pa. 111, 685, 1950

152 Rittner, E.S. Philips Res. Rep., 8, 161, 1953

153 Rooksby, H.P. Nature (London), 159, 609, 1947

154 Rose, A. R.C.A. Rev., 12, 362, 1951

155 Rose, A. Proceedings of the Atlantic City Conference on Photoconductivity, 1954, p. 3

156 Roy, S.C. Proc. Roy. Soc. A, 112, 599, 1926

157 Runciman, W.A. Brit. J. appl. Phys., Suppl. 4, 78, 1955

158 Sakamoto, M. Vide, 9, 109, 1954

159 Schaefer, H. and Walcher, W. Z. Phys., 121, 679, 1943

160 Schlichter, W. Ph.D. Dissertation, University of Gottingen, 1915

161 Schottky, W. Ann. Phys. (Leipzig), 44, 1011, 1914

162 Schottky, W. "Das freie Elektron in Physik und Technik", Berlin, 1940, p. 48

163 Schottky, W. Z. Phys., 118, 539, 1942

164 Schulze, R. Z. Phys., 92, 212, 1934

165 Schwarz, E. Nature (London), 162, 614, 1949

166 Shepherd, A.A. Brit. J. appl. Phys., 4, 70, 1953

167 Sloane, R.H. and Watt, C.S. Proc. Phys. Soc. (London), 61, 217, 1948

168 Sosnowski, L., Starkiewiscz, M. and Simpson, O. Nature (London), 159, 818, 1947

169 Spanner, H.J. Ann. Phys. (Leipzig), 75, 609, 1924

170 Sparks, I.L. and Philipp, H.R. J. appl. Phys., 24, 453, 1949

171 Sproull, R.L. Phys. Rev., 67, 166, 1945

172 Sproull, R.L. Bull. Amer. Phys. Soc. I, 24, 17, 1949

173 Sproull, R.L., Dash, W.C., Tyler, W.W. and Moore, A.R.
Rev. Sci. Inst., 22, 410, 1951

174 Sproull, R.L., Bever, R.S. and Libowitz, G.
Phys. Rev., 92, 77, 1953

175 Stout, V.L. Phys. Rev., 89, 310, 1953

176 Suhrmann, R. Z. Phys., 33, 63, 1925

177 Taft, E. and Apker, L. Bull. Amer. Phys. Soc. II, 3, 47, 1958

178 Takazawa, K. and Tomotika, T.
J. Phys. Soc. Japan, 9, 996, 1954

179 Tomlinson, T.B. J. appl. Phys., 25, 720, 1954

180 Tyler, W.W. Phys. Rev., 76, 179, 1949

181 Tyler, W.W. Phys. Rev., 76, 1887, 1949

182 Tyler, W.W. and Sproull, R.L.
Phys. Rev., 83, 548, 1951

183 Veenemans, C.F. Nederl. Tijdschr. Naturkunde, 10, 1, 1943

184 Vick, F.A. and Walley, C.A.
Proc. Phys. Soc. (London) B, 67, 169, 1954

185 Vink, H.J. Thesis, University of Leiden, 1948

186 Webster, H.F. and Beggs, J.E.
Bull. Amer. Phys. Soc. II, 2, 266, 1958

187 Webster, H.F. J. appl. Phys., 30, 488, 1959

188 Wehnelt, A. Ann. Phys. (Leipzig), 14, 425, 1904

189 Wilson, M.A. Proc. Roy. Soc. A, 134, 277, 1931

190 Wilson, V.C. J. appl. Phys., 30, 475, 1959

191 Wooten, L.A. Phys. Rev., 69, 248, 1946

192 Wooten, L.A., Ruehle, A.E. and Moore, G.E.
J. appl. Phys., 26, 44, 1955

193 Wright, D.A. Proc. Roy. Soc. A, 190, 394, 1947

194 Wright, D.A. Proc. Phys. Soc. (London), 60, 13, 1948; 60, 22, 1948

195 Wright, D.A. Brit. J. appl. Phys., 1, 150, 1950

196 Wright, D.A. Phys. Rev., 82, 574, 1951

197 Wright, D.A. and Woods, J.
Proc. Phys. Soc. (London) B, 65, 134, 1952

198 Yamaka, E. J. appl. Phys., 23, 937, 1952

199 Young, J.R. J. appl. Phys., 23, 1129, 1952

200 Zollweg, R.J. Phys. Rev., 97, 288, 1955

201 Zollweg, R.J. Phys. Rev., 111, 113, 1958

Acknowledgments

I wish to express my thanks to the following :

Dr. F.A. Vick, Director of the Atomic Energy Research Establishment, Harwell, and formerly Professor of Physics in the University College of North Staffordshire, who directed the work, for his continued advice and encouragement;

Professor D.J.E. Ingram, for the provision of laboratory facilities; and

my colleagues of the Physics Department, University College of North Staffordshire, for helpful advice and discussion.

The Siemens-Edison-Swan Company, Ltd., have made a generous gift of valve bases and envelopes.